

# Development of a Novel Electrophotographic Additive Layer Manufacturing Machine

Matthew James Benning

Submitted for the Award of Doctor of Philosophy

School of Mechanical and Systems Engineering

University of Newcastle upon Tyne

October 2011

# Abstract

---

The aim of this research was to develop a low-cost, desktop Additive Layer Manufacturing (ALM) system. A review of commercial ALM systems, a number of which are also called 3D printers, has been undertaken with the intention of identifying a suitable technology to embody within a system demonstrating low-cost and desktop characteristics. The review resulted in a commercially unexploited powder deposition technology, electrophotography, being identified. The significant barriers to implementation of this technology were the limitation of build height in the Z-axis due to electric field depletion and the formation of part material fringing due to the non-uniform electric field present at the boundaries of printed artefacts.

Initial trials were undertaken using a laser printing system to determine the printing characteristics of low-cost sacrificial and recyclable materials such as Mica, flour and sugar as well as an engineering polymer, Nylon 12. Mixed results were seen due to the large distribution of particle sizes and their tribocharging characteristics. The identified limiting phenomena were recreated and analysed in order to develop possible solutions, and further testing on the electrostatic behaviour and print acceptance of substrate transfer materials was undertaken with standard styrene co-polymer based toner. Consolidation techniques were investigated and powder layer transfer mechanisms were trialled, culminating in the development of the novel thermal transfer system, eliminating both the build height phenomena and artefact fringing issues. Development of a complete prototype system was undertaken, producing a compact desktop system with novel process architecture. The system functioned through the electrostatic deposition of a polymeric thermoplastic material onto the surface of a registered PTFE transfer substrate. The powder image present on the transfer substrate, was brought into close proximity to a build platform, where the powder layer was heated, consolidated and mechanically transferred using a single moving mechanism. Later concepts describe the novel continuous printing process, exhibiting high productivity while maintaining accuracy and resolution.

This work demonstrates a significant step forwards in the apparatus for use in an electrophotographic ALM system. In doing so, solutions to fundamental electrostatic transfer problems, and a clear route for the further development of a commercial electrophotography ALM process have been demonstrated. The system conceptualised, designed and produced within this research holds much novel value and provides a basis and direction for further development.

This work is dedicated to my late Nanna,

# Mrs Anita Benning

1937 – 2010

Anita spent many, many hours of my school summer holidays trying to teach me how to spell – While this was clearly time spent in vain, her confidence inspiring support never waned.



# Acknowledgments

---

I am indebted to the hands off guidance of my supervisor Professor Kenny Dalgarno who gave me the opportunity to explore and discover engineering in a way that I would have otherwise been oblivious to.

I am honour-bound to express my gratitude to the guys on the shop floor who helped me convert my designs into reality, Jamie Hodgson, Brian Stoker, Nicky Dafter, Steve Charlton, Mike Foster and the School Superintendent Ken Madden.

I am appreciative of the Duraform PE material donated to the research by Andrew Marsden of Leeds University.

I am eternally grateful to my gorgeous fiancée, Claire Garrett, who has supported me, not only financially throughout my write- up, but also morally. Despite working long hours, Claire has selflessly ensured I have been kept fed, watered and adorned with clean socks.

My sincere thanks go to Simon Gregory who not only introduced me to the Scottish Whisky Society, but also undertook the arduous task of proof reading this thesis.

I am thankful to my parents Elaine and Nigel Benning for showing restraint and avoided asking about 'the write-up'. But also appreciative of the moral support they have given me over the course of my PhD and life so far.

Finally I would like to show my gratitude for Inca and Rjukan, two black Labradors who have made the course of my PhD that little bit more pleasurable.

# Contents

---

1.1 Research Aims and Objectives .....	5
1.3 Thesis Structure.....	3
2.1 Fundamentals.....	4
2.2 Types of ALM System .....	9
2.2.1 Powder Based Systems.....	9
2.2.2 Solid Based Systems .....	14
2.2.3 Liquid Based Systems .....	19
2.3 Support Structures .....	27
2.4 Benchmark Systems .....	29
2.4.1 The Desktop Benchmark .....	31
2.5 A Review of Desktop ALM Systems Technology .....	32
2.5.7 Desktop Development Potential .....	35
2.6 The Principles of Electrophotography.....	38
2.7 Electrophotographic ALM Research.....	66
2.7.1 Research Work by A.V. Kumar at the University of Florida .....	66
2.7.2 Research Work by Cormier, North Carolina State University .....	74
2.7.3 Research Work by Wimpenny and Banerjee De Montfort University.....	76
2.8 Electrophotographic ALM Patents .....	82
2.8.1 Bynum 1992 - Automated Manufacturing System Using Thin Sections .....	82

2.8.2 Penn 1997 - System, Method & Process for Fabrication of 3-Dimensional Objects by a Static Electrostatic Imaging and Lamination Device .....	83
2.8.3 Kumar 2000 - Solid Freeform Fabrication Using Powder Deposition .....	84
2.8.4 Grenda 2001- Apparatus of Fabricating 3 Dimensional Objects by Means of Electrophotography, Ionography or a Similar Process.....	87
2.8.5 Kamada, Kato 2000 - Electrophotographic Apparatus.....	88
2.8.6 Zimmer, et al, 2002 - Device for Applying Decors and/or Characters on Glass, Glass Ceramics and Ceramic Products. ....	88
2.8.7 Liu, Jang 2002, 2004 - Layer Manufacturing Using Electrostatic Imaging and Lamination .....	89
2.8.8 Wimpenny, Banerjee 2008 - Electrostatic Printing Method and its Use in Rapid Prototyping.....	91
2.8.9 Discussion and Conclusion of the Patent Survey .....	92
2.9 A Review of Technologies Relevant to the Thermal Contact Fusing .....	96
2.10 Literature Survey Conclusions.....	101
3.0 Introduction .....	106
3.0.1 Experimental Objectives.....	106
3.1 A Physical Understanding of Electrophotography .....	107
3.1.1 Reverse Engineering: The Implementation of Electrophotographic Deposition .....	107
3.1.2 Printing Trials.....	115
3.1.3 Electrostatic Transfer .....	117
3.2 Concept Development .....	127

3.2.1 Transfer Belt Printing.....	128
3.2.2 Mechanical Layer Transfer .....	136
3.3 The Concept .....	146
3.3.1 Transfer Belt System.....	147
3.3.2 Consolidation Roller .....	158
3.3.3 Electronic Control Systems.....	159
3.4 Prototype Functional Specification .....	160
3.4.1 System Characteristics.....	160
3.4.2 The Deposition System’s Functional specification .....	162
3.4.3 The Consolidation System’s Functional Specification .....	163
3.4.4 The Z-axis System’s Functional Specification. ....	166
3.4.5 The Control System’s Functional Specification. ....	167
4.0 Introduction .....	169
4.1 Design Methodology .....	169
4.2 The Proposed Machine Layout .....	173
4.2.1 Final Layout .....	175
4.3 The Design of the Deposition Unit .....	176
4.3.1 Donor Printing Engine .....	176
4.4 The Consolidation Unit.....	177
4.4.1 The Consolidation Assembly .....	178
4.4.2 The Transfer Belt .....	185

4.4.3 The Consolidation Frame Assembly .....	186
4.4.4 Consolidation System Testing .....	190
4.5 The Z – Axis.....	191
4.5.1 Functional Testing .....	192
4.6 The Control System .....	193
4.6.1 Electronic Design .....	193
4.6.2 Firmware Programming.....	197
4.7 POC Prototype Final Assembly .....	207
5.1 Experiment Set 1: Belt Velocity and System Setup.....	209
5.1.1 Experiment 1.1: Belt Setup.....	209
5.1.2 Experiment 1.2: Z-Axis Setup .....	211
5.2 Experiment Set 2: Consolidation Assembly Setup .....	212
5.3 Experiment Set 3: Fringe Analysis .....	213
5.3.1 Substrate Testing.....	214
5.4 Experiment Set 4: Z-Axis Height Limitation .....	215
5.5 Further Testing.....	218
6.1 Prototype Performance.....	222
6.2 Sub-System Novelty.....	234
Appendix A: The Design of a Fully Adjustable Deposition System .....	257
A.1 The Rollers.....	258
A.2 Construction .....	261

A.3 Testing .....	262
A.4 Results .....	263
Appendix B: Firmware Test Programming .....	264
Appendix C: Control Programs .....	267
C.1 Bipolar Consolidation Roller and Print Engine Motor Controller Program .....	278
C.2 Unipolar Controller Program .....	280
Appendix D: List of Abbreviations .....	282

# Nomenclature

---

$\alpha$ = Linear Expansion Coefficient	$(m. m^{-1}K)$
$a$ = Electrode Radius	$(m)$
$\beta$ = Calibration Constant	$(K)$
$C$ = Capacitance	$(F)$
$c$ = Heat Capacity	$(JK^{-1})$
$D$ = Toner Diameter	$(m)$
$d$ = Photoconductor to Developer Roll Spacing	$(m)$
$d_1$ = Electrode Gap	$(m)$
$D_T$ = Average Diameter of Toner Particles	$(m)$
$\delta Q$ = Energy Needed to Melt a Given Mass of Material	$(W)$
$\delta L$ = Thermal Expansion	$(m)$
$E$ = Electric Field	$(Vm^{-1})$
$E_c$ = Critical Electric Field Strength	$(Vm^{-1})$
$E_{ave}$ = Average Electric Field	$(Vm^{-1})$
$E_f$ = Electric Field Strength in New Toner Layer	$(Vm^{-1})$
$E_{in}$ = Thermal Power Input	$(W)$
$E_{max}$ = Maximum Electric Field Strength	$(Vm^{-1})$
$E_p$ = Electric Field Strength in Printed Layers	$(Vm^{-1})$
$\epsilon_0$ = Permeability of Free Space	$(Fm^{-1})$
$\epsilon_s$ = Dielectric Permeability of Photoreceptor Layer	$(Fm^{-1})$

$F_e$ = Force Exerted on Toner Particles	(Nm)
$G_t$ = Transfer Geometry	(m)
$G_{LX}$ = Geometry of a Layer in the X Direction	(m)
$G_{LY}$ = Geometry of a Layer in the Y Direction	(m)
$G_{LZ}$ = Geometry of a Layer in the Z Direction	(m)
$h$ = Height Above Sea Level	(m)
$K_d$ = Dielectric Constant of Developer OPC Gap	(N/A)
$K_f$ = Dielectric Constant of Freshly Printed Layer	(N/A)
$K_p$ = Dielectric Constant of Previously Printed Layers	(N/A)
$K_s$ = Dielectric Constant of OPC	(N/A)
$l$ = Layer Thickness Present on the Developer Roll	(m)
$L_0$ = Length of Pipe	(m)
$L_t$ = Layer Thickness Following Consolidation	(m)
$m$ = Mass	(kg)
$P$ = Printed Layer Thickness	(m)
$P_p$ = Charge per Unit Volume in Printed Layer	(Cm <sup>-3</sup> )
$P_p$ = Charge per Unit Volume in Fresh Toner Layer	(Cm <sup>-3</sup> )
$P_s$ = System Productivity	(m <sup>3</sup> s <sup>-1</sup> )
$Q$ = Charge	(C)
$R$ = Carrier particle Radius	(m)
$R_1$ = Resistance at $T_{Ref}$	( $\Omega$ )



$R_{\text{Ref}}$ = Reference Temperature	(K)
$\rho$ = Material Density	( $kgm^{-3}$ )
$S$ = OPC Layer Thickness	(m)
$\sigma$ = Charge Density	( $Cm^{-3}$ )
$\zeta$ = Relative Air Density Factor	(N/A)
$\sigma_b$ = Charge per Unit Area of Build Platform / New Layer Interface	( $Cm^{-2}$ )
$T$ = Temperature	(K)
$t_a$ = Ambient Temperature	(K)
$t_c$ = Time to Consolidate	(s)
$t_g$ = Glass Transition Temperature	(K)
$t_m$ = Melting Temperature	(K)
$t_p$ = Time to Print	(s)
$T_{\text{Ref}}$ = Reference Temperature	(K)
$t_t$ = Time to Transfer Image From Deposition to Consolidation	(s)
$V$ = Voltage	(V)
$V_0$ = Potential Present on the Photoconductor	(s)
$V_b$ = Velocity of Belt	( $ms^{-1}$ )
$V_c$ = Consolidation Velocity	( $ms^{-1}$ )
$v_L$ = Layer volume	( $m^3$ )
$V_p$ = Print Velocity	( $ms^{-1}$ )
$x$ = Layer Displacement from Build Platform	(m)

# Chapter 1: Introduction

---

Additive Layer Manufacturing (ALM) is a collective term encompassing a range of systems that produce artefacts through the sequential deposition of layers. As far back as the 1890's, primitive forms of ALM were being utilised to produce topographical relief maps (Blanthier, 1892). Over a century later, from the late 1980's to well into the early 21<sup>st</sup> century and with the advantage of automated Computer Aided Design (CAD) based layer development systems; ALM took on the three distinct manufacturing embodiments of Rapid Prototyping (RP), Rapid Tooling (RT) and Rapid Manufacturing (RM) (Chua et al, 2010). All three of the embodiments inherited the 'Rapid' prefix, as a ratification of the system's low lead times, rather than a statement of their productivity. RP was the first use of the commercial ALM systems, producing pre-production prototypes (Hull, 1986). As RP evolved, functional prototypes were commonly being produced, and as machine technology and prototype mechanical properties developed further, the way was paved for RT and RM (Ferreira et al, 2006). As the awareness and popularity of ALM grew, and with the ever more prolific use of three dimensional CAD software, a trend of using prototypes far earlier in the development cycle began. This increased use of prototypes was seen to improve design collaboration and reduced errors before tooling and production. A limiting factor however, was the initial outlay and significant running costs of traditional ALM systems. In the latter part of the first decade of the 21<sup>st</sup> century, as the demand for systems with smaller footprints and lower costs increased, a new generation of ALM system was developed. This range of systems referred to as 3D printers, due to their desktop form factor, offered design offices, small business and even home users the chance to exploit the Free Form Fabrication potential of ALM (Wohlers, 2010). The current 3D printer markets, and the systems offered within them, are still in their infancy. While there are a number of 3D printers available, the range of small, user-friendly systems is limited. Machines are being advertised by manufacturers as being 'Desktop Systems', despite dimensions and weights reminiscent of their industrial precursors and some even processing toxic photopolymer chemicals, is not uncommon (Objet30, Objet, Israel; V-Flash, 3D Systems, USA). The function of this research was to

demonstrate a novel ALM concept, by developing a truly desktop 3D printer capable of forming artefacts with all the functional, aesthetic, and productive benefits of high-end systems, within a desktop form. The research objectives were achieved through the review and benchmarking of commercial ALM systems, the testing of multiple concepts and the generation of a proof of concept prototype.

Electrophotographic deposition, most commonly embodied within 2D desktop laser printing engines and photocopiers, was the technology chosen to develop into a novel desktop 3D printer. This work was based on the concept that a common laser printing engine could be utilised to deposit sequential powder layers on to one another, as opposed to printing images on to multiple paper substrates. A 3D printer, based on a laser printing, engine is distinct from other technologies, as it is able to be implemented at low-cost while combining high resolution, geometric accuracy and productivity. The potential application of a laser printing engine forming the basis of an ALM, system had previously been recognised by a number of researchers. However, two distinct barriers to the implementation of the electrostatic deposition technology: artefact fringing and Z-build height limitations were noted and no workable solutions offered. (Bynum, 1992; Grender, 2001; Kumar, 1999, 2000; Kumar and Dutta, 2003, 2004; Kumar et al, 2004; Kumar and Zhang, 1999; Cormier et al, 2000, 2002; Banerjee, 2006, 2008; Wimpenny and Banerjee 2008; Wimpenny et al, 2009; Jones et al, 2010). Following the identification of a developable technology the aim of this work shifted to overcome the identified technological limitations.

### **1.1 Research Aims and Objectives**

The aim of this research was to develop a novel desktop ALM machine concept based on a selected technology, generate a machine design and produce a proof of concept (POC) prototype to demonstrate the concept validity. The work presented within this thesis was governed by two proposals. The first; *'A technology can be identified for development and integration to form a low-cost desktop ALM system capable of rapidly producing accurate artefacts from engineering materials'*, generated the context for the literature review and resulted in the formation of four objectives:

- i. Research current ALM technologies to provide benchmark targets, representative of state-of-the-art ALM systems, which could be used to develop a new system.
- ii. Identify a suitable technology to take forward to develop into a truly desktop ALM system, exhibiting the characteristics of high resolution, high productivity and low-cost.
- iii. Identify former research papers and patents on the identified technology, highlighting methods and known limitations.
- iv. Based on the information gathered, conclude as to the best way forwards.

The second assumption; *'An electrophotographic deposition system of the kind found in a modern laser printer can be utilised to produce a low-cost, high definition, high productivity, additive layer manufacturing system. More specifically, a Desktop Three Dimensional Printer prototype can be produced, which demonstrates no electrostatic build limits in the Z-axis and is capable of producing artefacts without fringing.'* was developed following the literature survey and the identification of electrophotography as a possible ALM technology. This proposal provided a direction for the experimental element of this work and produced four experimental objectives:

- i. Produce a prototype system with the ability to create simple laminate artefacts.
- ii. Develop an electronic and firmware control system to facilitate the development of current and future objectives.
- iii. Develop and demonstrate a solution to the fringing effect by producing an artefact consisting of a plurality of layers without exhibiting fringe build up.
- iv. Develop and demonstrate a solution to the Z-axis height limitation by producing an artefact of over 3mm in build height

The work presented within this thesis identifies electrophotography as a candidate for ALM development, eliminates the hardware barriers identified in former research and provides a robust foundation upon which to base the next phase of development of a low-cost, high definition, truly desktop, three dimensional ALM system.

### 1.3 Thesis Structure

The structure of the thesis is shown, Table 1.1, with a brief description of the chapters. Additionally a flow diagram of the research methodology is presented in Figure 1.0.

Chapter	Work Undertaken	Analysis	Description	Objective
2	Literature Review	- Review of Commercial 3D Printers - Benchmarking of State-of-the-Art ALM - Generation of a Design Brief	The identification of a potential technology for development and the construction of a design brief based on a review of former relevant research and patents.	To identify a suitable technology in line with the research proposal and to develop a syllabus by which a Novel desktop system could be produced.
3	Concept Development	- Articulation of a development proposal - Former Research Benchmarking - Concept Testing - Belt & Electrostatic Testing - Formation of a Functional Specification	The testing of former concepts to benchmark previously encountered photoelectrostatic limitations. The Implementation of a number of concept ideas within test rigs to determine their suitability for a POC prototype system.	To initially define a development proposal to test concepts against in order to generate a functional specification, facilitating the generation of solutions to former problems.
4	Development of a POC Prototype design	- Consolidation Unit Design - Deposition Unit Design - Belt Transfer Assembly Design - Control Hardware Design - Microcontroller Firmware Design - Motion System Programming	Based on the functional specification, the development and production of a POC prototypes components and software culminating in assembly, functional testing and assembly development.	To design, produce, functionality test and develop an autonomous POC prototype capable of being tested with respect to the research proposals. Ensuring the system produced supported future machine development.
5	Testing of POC Prototype	- Produce Multiple Layer Artefacts - Produce Artefacts Without Fringing - Produce Artefact Over 3mm in Build Height	Trial the POC prototype in order to produce artefacts to satisfy the objectives and the proposals. To demonstrate no fringing and limitless build height with respective artefacts of 20 and 700 layers.	The testing of the POC prototype against the specification to determine support for the development proposal
6	Discussion	- Discussion of the Concept and Design - Discussion of the Results and Objectives	-	-
7	Conclusion	- Draw Conclusions to the Work	-	-
8	Further Work	- Discuss Further Work	-	-

Table 1.1 The structure of this thesis and a brief explanation of the chapter functions within the research.

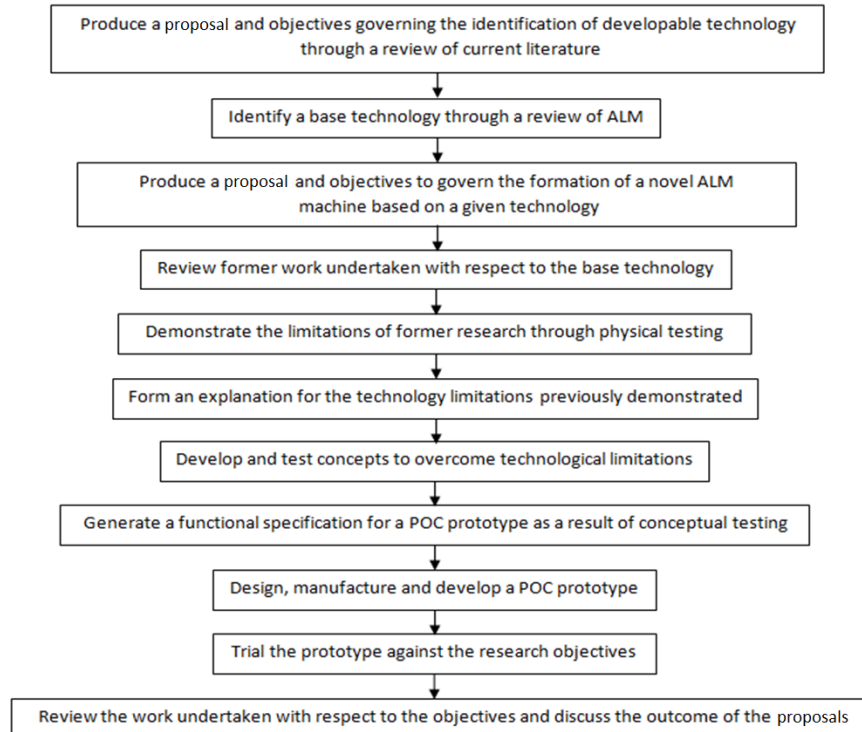


Figure 1.0 A flow diagram illustrating the research methodology adopted over the course of this research.

## Chapter 2: Literature Survey

---

This literature survey introduces the area of research from which this project arose and demonstrates the foundations on which the work has been carried out. It is intended that the following chapter be used as a basis from which to derive the rationale for the work, review current literature, and serve as a platform from which to develop discussion in subsequent chapters. There are many current and historic ALM processes offering a diverse set of material, productivity, resolution, size, post-process, and cost based factors. The first part of this chapter will look at the origins of polymer based ALM, discussing its holistic evolution and the fundamental concepts behind the commercial systems. The focus will then shift towards the discussion of bench mark systems, culminating in a review of current 3D printer technologies and their suitability for further development. The final part of this chapter will discuss the use of electrophotography based technology for the development of a novel ALM system, referencing the laser printer embodiment, commercial / formally-commercial systems, notable research and electrophotographic patents. The chapter concludes with a design brief for the development of a novel desktop ALM system based on the findings of this survey.

### **2.1 Fundamentals**

ALM systems create three dimensional artefacts through the systematic addition of material, in the form of layers, to gradually form an artefact. ALM systems characteristically process a single build material of either polymer, metal or ceramic and in some cases employ a second material, usually a water soluble polymer, as a support material. Ongoing research includes the functional mixing, or grading, of multiple materials to produce artefacts exhibiting a wide range of physical and mechanical properties (Dalgarno 2001; Giulioni et al, 2005; Li et al, 2006). In a typical ALM process, a 3D model is needed. The geometry is generally converted into a stereolithographic (STL) format file, the de facto standard for the data input of ALM system. An STL is an approximation of the surface of a 3D model, made up of multiple facets (usually triangles) whose vertices are ordered to indicate which side of the

triangle contains the volume (Yan and Gu, 1996). An example of STL generation can be seen in Figure 2.1.

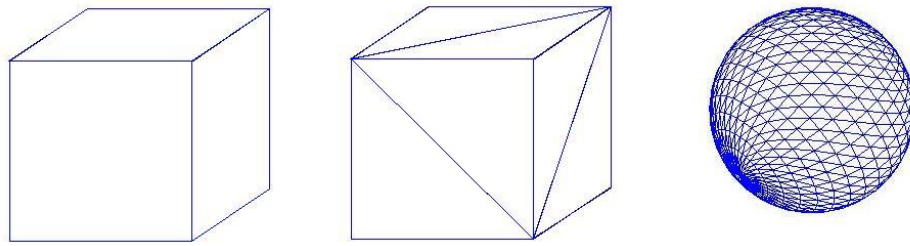


Figure 2.1 from left to right, showing a solid body, an STL version of the solid body constructed using only triangles, and a more complex body made entirely of triangles representative of an STL file output.

The intended function of the STL format is to describe the surface of an artefact within a file of limited size, the format however has its limitations; the resultant three dimensional geometries formed from STL data tend to have a poor surface finish due to the resulting surface triangulation and contain no colour or material data. In an effort to overcome these and other limitations, the international standards organisation, ASTM International, in May 2011 introduced a new file format called the Additive Manufacturing Format (AMF). The format was developed to build additional functionality into the STL format and like the STL, the AMF surfaces were formed with triangles. However, unlike STLs the AMF triangles can consist of curved edges (Fig. 2.2) to better represent the surfaces of an object (ASTM, 2011).

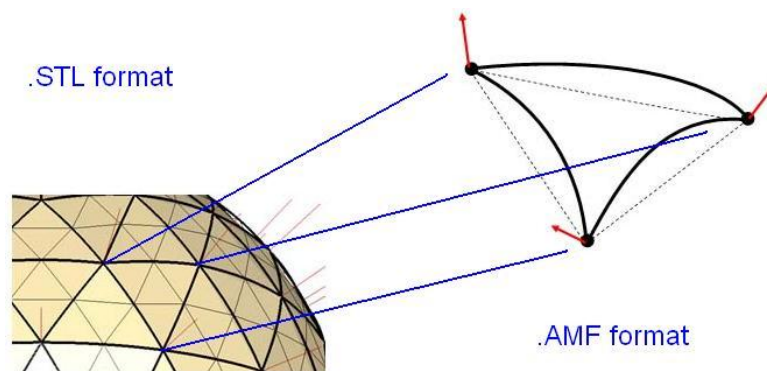
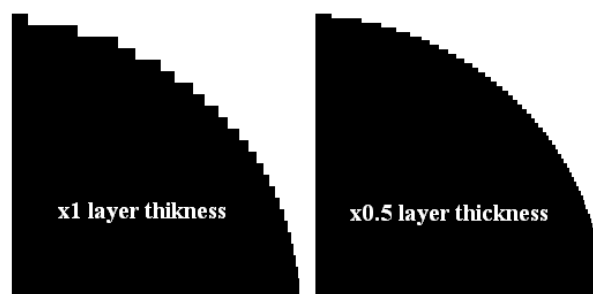


Figure 2.2 A representation of the three dimensional curved edges of an AMF file format, replacing the four, two dimensional triangles of an STL file. The resultant AMF represented curvature is significantly more accurate. (ASTM, 2011)

A converted CAD file, whether in STL or AMF format, is optimally orientated with respect to the build time, material properties, surface finish, or support structure. The data is then intersected with slicing planes to produce multiple piece wise linear contours, describing each layer of the artefact (Choi and Kwok, 2002). The layers, dependent upon the ALM process, can range in thickness from 0.025 – 1mm. Generally, a thin layer is necessary for artefacts exhibiting complex surfaces to achieve accurate reproductions without exhibiting stepping. Stepping, an example of which is shown in Figure 2.3, is a surface finish phenomenon which is a function of the radius of curvature of artefacts geometry and the layer thickness with which it was built.



**Figure 2.3** The stepping effect exhibited by ALM built artefacts.

ALM is in direct contrast to conventional manufacturing processes, such as milling or turning, where material is removed from a billet, effectively sculpting a three dimensional artefact from a volume of raw material. Many ALM processes were initially only able to produce artefacts of limited mechanical strength and as such, were predominantly used for prototyping (Chockalingam et al, 2006). However, as this prototyping technique was fully digitised, producing artefacts of even the most complex geometries straight from CAD data, it was soon realised that the concept significantly sped up the iterative design process, reducing lead times and thus coined the name Rapid Prototyping (RP). Rapid Prototyping remains the most common application for ALM technology. A number of systems however, have developed from RP to the stage where they can deliver artefacts with usable mechanical and physical properties. Depending on their application, these refined ALM technologies can produce low volume production runs or intricate manufacturing tooling, and are often referred to as Rapid Manufacturing (RM) and Rapid Tooling (RT) respectively



(Dalgarno, 2001). More recently a number of ALM processes have evolved into lower cost systems combining reliability, robustness, and user friendly technologies, within smaller foot prints. These new systems are positioned within the small office/design unit, education and even home user markets, offered to the consumer as '3D Printers'. Although 3D printers are of significantly lower cost than high end ALM systems, to both buy and maintain, many remain in the thousands / tens of thousands of pounds and out of the reach of many would-be ALM users (Wohlers, 2010).

### *Summary of the ALM Market*

As of 2009 the estimated ALM market was just less than one billion pounds and expected to increase at around 25% per year, as the use of ALM penetrated new markets. The market for artefacts manufactured by ALM is split across nearly every manufacturing sector, from visual aids to the direct manufacturing of artefacts, with form fit prototypes being the preferred use. Stratasys USA are The current market leaders, in terms of number of units sold, and producing ALM systems from £9k to £157k. It is however, the lower cost machines which generate the majority of these sales (Wohler, 2010). According to the Wohlers Report (2010), the ALM industry's self reporting annual audit, there is an interest in ALM in 70 different countries. This interest is growing and is attributed to the increasing number of ways in which manufacturing organisations are applying ALM, driving demand for improved systems. Figure 2.4 illustrates the growth of the ALM industry from its conception to 2007. As with any manufacturing industry there is the need for high end specialist machines which are of high cost but sell in relatively low volumes. If the printing industry is taken as an example, there are a number of manufacturers producing high end specialist printers for the printing of specific items such as books, magazines and textiles. The number of sales for these items is low when compared to the sales volumes of desktop printers, designed to be low-cost and versatile. The same can be said for the ALM market, with Electron Beam Melting (EBM) fulfilling the high end of the market and FDM / extrusion meeting the demands for the majority of users. Just as dot-matrix printers were replaced with printers of higher resolution and

functionality, such as inkjet and laser printers, the current low-cost ALM technologies will also be replaced with superior systems.

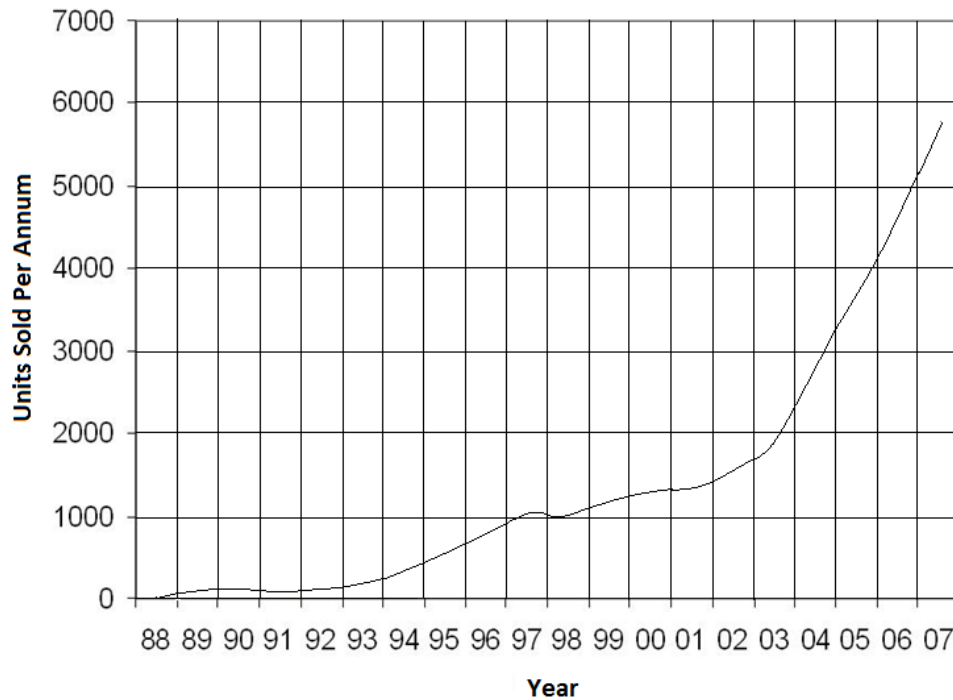


Figure 2.4 The popularity of ALM as a function of units sold per year. (Data taken from the Wohlers Report, 2008)

The ‘desktop user’, defined here as a small business; design office; education or home user, is being attracted to the market with the improvements in artefact aesthetics, material properties, system accuracy and machine productivity. Whereas, larger industry, although also concerned with these properties is additionally interested in materials diversity, production capabilities, and machine repeatability (Dimitrov et al, 2006). The low-cost market is starting to flourish with the ever increasing number of low-cost ALM systems available. The opportunity to produce a low-cost system of high accuracy, productivity and artefact material properties is more apparent than ever and will continue to be an opportunity as long as a viable, low-cost, solution remains un-commercialised.

## 2.2 Types of ALM System

As of 2010 there were 24 commercial ALM technologies offering a number of functions to different user groups and a significant number of research processes (Wohlers 2010). Most of these systems can be characterised as liquid, solid, powder or gas with reference to the physical state of their pre-process build materials. Gas based ALM systems such as those designed to produce diamond or carbon nanotubes (Bondi et al, 2006) are referenced here for completeness, but will not be discussed further, as their inherent system is incompatible with low-cost integration.

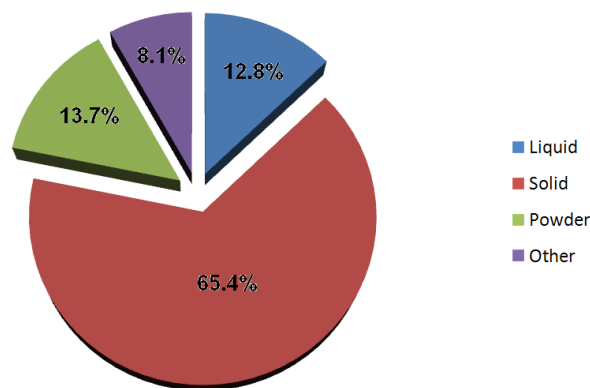


Figure 2.5 The percentage share of the characteristic system types in 2009 (Wohler, 2010)

The chart in Figure 2.5 shows the percentage market share for each of the primary ALM characteristics which are discussed further in the following sections. Systems intended for metal products will not be referenced due, to the incompatibility with the scope of this work. It is recognized that the most important techniques in terms of ALM market popularity are Fused Deposition Modelling (FDM), Stereolithography (SL), Selective Laser Sintering (SLS), and 3 Dimensional Printing (3DP) (Seitz et al, 2005). The following sections will analyse these systems while also discussing the general characteristics of the different ALM technologies available.

### 2.2.1 Powder Based Systems

The market share for powder based ALM systems has reduced significantly since early 2000, due primarily to the success of low-cost solid extrusion based systems such as Stratasys's FDM (Wohler, 2010). The range of powder based systems designed to process polymers is small. These systems are instead the favoured technology for

metal processing with companies such as MTT, 3D Systems, Phenix Systems, Concept Laser, EOS, Realizer, Arcam, Optomec, et al, all producing metal powder processing systems.

### *Direct Melting or Sintering*

Although the physical mechanisms behind the melting and sintering of conglomerate powders differs, the overall thermal input and processing techniques are similar (Kruth et al, 2005). There are a number of processes that use lasers to consolidate powder material by selectively scanning a powder bed (3D Systems' sPro, EOS' Formiga & EOSint, Aspect Inc's SEMPlice, Beijing Longyan's Af, Wuhan Binhu Mech. & Elec.'s HRP). Following the consolidation of a layer through vector by vector laser processing, the entire powder bed is incremented one layer thickness down. A new layer of powder is then spread across the build platform either by a doctor blade or counter rotating roller, enabling the next layer to be consolidated. SLS produced by 3D systems, is a widely implemented powder sintering process that was developed at the University of Texas and patented in 1989 (Deckard, 1989). SLS systems tend to be some of the most costly of all the ALM systems ranging from \$350k – \$850k (Wohler, 2010). Despite the high cost however, the artefact material properties can be close to those of the injection moulding process. Some users of SLS claim that on average the artefacts produced, for example of Nylon 12, are 82% the tensile strength of Nylon 12 in its pre processed form (Lasersintering.com, 2011). An additional benefit of SLS is that it can process the majority of thermoplastic materials which can conceivably be powdered. The process of SLS is reliant on the use of a high powered laser, typically up to 200W (sPro 230, 3D Systems, USA) and as such is unlikely to be of use within a desktop system while the cost and size of such lasers remains high. Larger artefacts created by the SLS system need post-process cool down cycles to allow an artefact to return to room temperature without generating thermally induced stress. For example, some SLS processed wax artefacts require a standard twelve hour cool down (Pham and Gault, 1998). Post-processed artefacts are porous and so, in some cases, need additional post-process infilltrants added to achieve the full density.

In summary, direct melting or sintering systems offer market leading material diversity and properties. They do however, tend to be large, have significant power requirements and need industrial cooling apparatuses, all of which are uncharacteristic of a desktop system.

### *Adhesive Binding*

Some powder processes employ two dimensional inkjet printer derived technologies to selectively introduce binder resins into a powder bed ( Z-printer, Z-Corporation, USA; Three Dimensional Printer series, VoxelJet, Germany). The process starts with a powder bed which is printed upon in the geometry of an artefact's cross section. The binder penetrates the powder bed and in addition to binding the proximal powder, binds the newly formed layer geometry to the previous. Following binding, the powder bed is indexed down one layer thickness allowing a new layer to be spread across the build platform with a roller or doctor blade. The foundations for inkjet based ALM arose from technology originally developed for the recording of electric telegraph communications, which used electrostatic forces to control the release of ink droplets on to paper (Thomson, 1867). Throughout the mid 1900's a number of inkjet concepts were investigated, resulting in the generation of two technology streams, continuous jet printing (CJP) and drop on demand (DOD) inkjet (Elmqvist, 1951). The most revolutionary property of the inkjet technology was that it was non-impact, unlike the typewriters and printing presses of the day.

### *Drop On Demand Printing*

During the 1950's, 60's and early 70's, four different types of DOD inkjet head were developed: electrostatic, piezoelectric, thermal, and electric induction. The two systems most commonly used today are the piezoelectric and thermal ink deposition. In general, the DOD system comprises of an ink reservoir, attached to an ink chamber, which in turn is connected to an ejection nozzle. The chamber consists of a small volume which incorporates either a piezoelectric crystal or heater (Menzel, 2009). A discussion of the function of both the piezoelectric and thermal DOD heads are respectively described below:

### *Piezoelectric DOD*

Ink is drawn into the chamber, by the negative pressure induced by the ink meniscus at the nozzle aperture, from the main reservoir. When a drop is required, the ink deposition control system delivers a high frequency charge to the piezoelectric crystal within the chamber, thus producing a pressure wave which ejects an ink droplet from the nozzle onto the substrate. Ink is then drawn back to fill the chamber as previously described, ready for the next drop. Commonly there are from 32 to 512 nozzles arranged in an array to increase productivity (Creagh and Frost, 2011)

### *Thermal DOD*

In common with piezoelectric DOD, the ink collects in a chamber from the reservoir due to the negative pressure induced by the ink's meniscus at the nozzle, but also through the low pressure produced by the collapse and condensation of an ink vapour bubble. When a drop is required, the ink deposition control system energises a heater within the ink chamber, vaporising surrounding ink, creating a vapour bubble which displaces a droplet out of the nozzle onto the substrate. The ink bubble formed within the chamber then condenses, reducing in volume, creating a low pressure which along with the meniscus, draws ink into the chamber as previously described (Creagh and Frost, 2011). Although thermal DOD printing heads are cheaper than piezoelectric DODs, as they do not use costly piezoelectric materials, they do need volatile inks to enable bubble formation however which limits their application. Piezoelectric DOD heads on the other hand can use many types of inks with a number of pigments, lending themselves to 3DP binders and other materials (Yun et al, 2009). DOD jet systems are small, with nozzle sizes typically ranging from 50 $\mu$ m to 200 $\mu$ m in diameter. As a result larger numbers can be combined within a single head which has proven useful for use in low-cost ALM systems. DOD droplet production is typically restricted to around 3kHz to 10kHz due to flow characteristics of the ink/binder, as at high speed cavitation can occur in the ink chamber resulting in 'miss fire' (Sachsa and Vezzetti, 2005).

### *Continuous Jet Printing*

In 1951 Siemens introduced the first CJP head. The system functioned based on the Plateau-Rayleigh instability theory which describes how a stream of falling fluid through a less dense medium tends to break up into a small stream of droplets due to the fluid's surface tension (Sachsa and Vezzetti, 2005). Within a CJP head there is a constant flow of ink through a fine aperture, creating a small stream of droplets. The droplets pass through a charging cell where they gain a bias charge and are then passed through a deflector cell. The deflector cell controls the trajectory of the droplets, selectively placing them on the powder bed or deflecting them into a 'catching system' which stops any binder coming into contact with the substrate. The deflector cell utilises an analogue signal to allow a raster effect for greater binder droplet density (Houbena et al, 2009). Many ink droplet streams, charge/deflector cells and collection systems are arranged on one head to give greater printing productivity. However due to their relative size and complexity it is not possible to include the same number of ink apertures within the same footprint as a DOD system. The most efficient aspect of this technology is the increased droplet generation rates that can range from 60 kHz to 1 MHz and working temperatures up to 350°C (Houbena et al, 2009). However, the use of catching systems can lead to crystallisation of binders in ALM, restricting or even blocking recovery ducts leading to unwanted binder placement.

The most common ALM use of the inkjet technology is within 3DP, as used in Z-Corporations Three Dimensional Printers, and was developed in the late 1980's before being patented by Massachusetts Institute of Technology (MIT) in 1989. 3DP demonstrates a number of advantages over competitive ALM systems in the form of superior productivity, five to ten times that of all other techniques, and the ability to build full colour artefacts (Zcorp.com, 2011). 3DP's superior productivity has been a leading factor in the increased productivity of many companies producing prototypes and tooling for industry, resulting in artefacts being produced in days rather than weeks (Sachsa and Vezzetti, 2005). MIT licences its 3DP technology to six companies, ExtrudeHone, Soligen, Specific Surface Corporation, TDK Corporation, Therics and Z

Corporation for development in their individual fields. The key to 3DP's superior productivity is its relatively thick layers of up to 0.203mm. Z-corp.'s high-end embodiment of MIT's 3DP technology incorporates several thermal DOD printing heads. This allows it to print an array of coloured binders into the powder bed to produce coloured models. The materials for this type of ALM process are relatively inexpensive and non toxic, e.g. plaster powder and water soluble resin binder, with unbound powder providing support to overhanging structures. Owing to the mass production of inkjet technology, 3DP can offer a high productivity ALM platform at relatively low-cost (Zcorp.com, 2009). The major disadvantage of this type of system is the generation of artefacts with poor mechanical properties. Artefacts can be post-process infiltrated with epoxies to strengthen them; however, this significantly increases production time and may require hazardous materials (ITW, 2006). The surface finish of artefacts produced by this kind of system can be limited due to binder unintentionally leaching into the neighbouring powder. The further development of inkjet technology within powder based ALM systems will be reliant on the generation of new material/binder combinations with improved mechanical properties, not the generation of new hardware solutions.

### ***2.2.2 Solid Based Systems***

As of 2010, solid based systems have been shown to be significantly more popular than the sum of the other system categories. This was primarily down to the popularity of polymer extrusion based ALM. Of the 65.4% market share claimed by solid based ALM systems, 86.9% consisted of polymer extrusion technology, 57.6% of the entire market share (Wohlers, 2010).

#### *Extrusion of Thermoplastics*

From 2002, the most popular ALM technology in terms of unit sales was that of polymer extrusion. An extrusion based ALM system is currently the least expensive ALM technology on the market, a fact which is responsible in part, to the technology's high volume sales (RapMan 3.1, Bits from Bytes, UK). In the majority of extrusion systems, the process starts with a thermoplastic polymer or wax filament. The filament is fed into a heated nozzle where it is partially melted (Gebhardt, 2003). Layer



deposition occurs when further filament material is introduced into the heated nozzle displacing the partially molten material. The displaced material is extruded from an aperture in the nozzle and deposited onto a build platform. The extruded material is deposited in the geometry of an artefact layer through the deposition of the inner and outer contours. The resultant void is then filled with a dense raster or a material saving honeycomb structure. The motion of the head, relative to the build platform, is either directly controlled by an X-Y stage and a Z-axis build platform, or by an X-Y build platform and a Z-mounted head. The X-Y mounted head being the preferred option due to a lower moving mass with less internal machine volume required. The most popular extrusion based ALM system, in terms of installed units, is FDM and is the best selling ALM system with a 32% share of the entire market. FDM was developed in the late 1980's (Crump, 1992<sub>a</sub>, 1992<sub>b</sub>) and was commercialised by Stratasys in 1990. FDM was the first solid based extrusion ALM system, depositing fine filaments of thermoplastic material to construct 3D artefacts. As the artefacts created by FDM are not supported in a powder bed, an additional explicit water soluble thermoplastic is deposited during a build to support delicate structures, overhanging geometry, or dislocated features. For this reason, FDM objects must be post-processed for several hours by soaking in a sodium hydroxide solution to remove support structures. However, due to the large filament nature of FDM, many overhanging features of up to 45° need no supporting structure (Ahn et al, 2002). FDM is one of the slower ALM processes and has historically had low resolution. Improvements have been seen with the new Stratasys Dimension Elite FDM but the process retains the limitation of filament resolution (Dimension Elite, Stratasys, USA). As with other extrusion ALM systems, FDM's layer resolution and therefore resultant surface finish in the Z direction is limited by the lack of tessellation between sequential filament deposits. The overwhelming benefit of FDM, to which it owes its success, is the process's ability to produce functional artefacts within a low-cost system. The price of Dimension Uprint, a personal printer, is currently around £10K, which is low-cost when compared to other systems on the market. Table 2.1 compares thermoplastic extrusion based systems illustrating the low-cost aspect of the technology. Figures 2.6, 2.7, 2.8 and 2.9

show pictures of example artefacts produced by the systems shown in Table 2.1, demonstrating low-cost at the expense of surface finish.

Company	Machine	Form	Cost £	Footprint mm	weight kg	Build volume mm	Layer thickness mm	Productivity mm <sup>3</sup> /min
Maker Bot Industries	<i>Thing-O-Matic</i>	Kit	793	300 x 300 x	5	110 x 110 x	0.3 - 1mm	1000
Bits from Bytes	<i>BFB 3000</i>	Assembled	1,995	580 x 520 x 520	31	320 x 300 x 200	0.1 mm	900
Dimension	<i>Uprint</i>	Assembled	9,090	635 x 660 x 800	76	203 x 152 x 152	0.254	273
	<i>HP DesignJet 3D</i>	Assembled	10,300	660 x 660 x 762	59	203 x 152 x 152	0.254	273
Bot Mill	<i>Glider 3.0</i>	Assembled	851	508 x 406 x 356	7	203 x 203 x 140	0.51	260

Table 2.1 The relative properties of five popular FDM or FDM type ALM processes



Figure 2.6 An example of a part made from Maker Bot Industries' Thing-O-Matic.

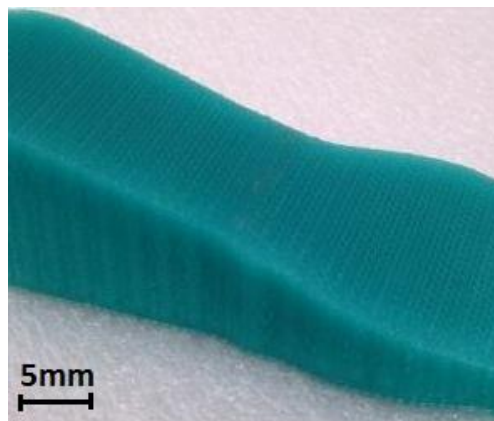


Figure 2.7 An example of a part made from the Bits from Bytes BFB3000. (BitsfromBytes.com, 2011)



**Figure 2.8** An example of a part made from the Dimension's Uprint and HP DeskJet. (Amtekcompany.com 2011)



**Figure 2.9** An example of a part made from the BotMill Glider 3.0 (Commercialisation of Rep Rap's open source Mendel) (BotMill.com, 2011)

The four systems illustrated are for example only and are not the vast range of makes and models available. They are however, a representative group of systems with profound physical and operational differences. Other 'FDM type' systems are usually a derivative or combination of the example machines. The benefits of the extrusion technology are compact size, low power consumption and a vast array of thermoplastic materials. The mechanical properties of an artefact differ from system to system but are generally good in the X/Y but are limited in the Z direction (Ahn et al, 2002). A major drawback to the extrusion system is its vector by vector processing of an extrusion head, resulting in poor productivity and exhibiting some of the lowest productivity to resolution ratios on the market. The application of the FDM type technology into a desktop system has been embodied in several machines: RapMan by Bits from Bytes (UK), Thing-O-Matic by MakerBot Industries (USA), and Glider 3.0 by BotMill (USA). All the systems however, exhibit the same poor productivity and

surface finish of Stratasys's original system. Due to the aforementioned issues of filament deposition and vector by vector processing, it is unlikely that the FDM process would be suitable for a desktop system requiring a high productivity and good surface finish.

### *Inkjetting*

Solid based ALM systems, utilising inkjet technology, function in a similar way to that of the extruded thermoplastic filaments in that they deposit molten polymer materials. The thermoplastic is preheated and deposited through heat affected DOD inkjet printing nozzles. The nozzles use localised heating, of a thermoplastic within a chamber, to create a pressure differential, ejecting 50 micron molten thermoplastic droplets at up to 200°C at a rate of 10,000 droplets per second (Yan and Gu, 1996), forming a layer of typically between 12.7 and 150 microns in thickness (Solid-scape.com, 2011). A print head on an Inkjetting system contains many hundreds of print orifices working together to print large areas in one pass, however, multiple head reciprocations may still have to be undertaken depending on the geometry of the built artefact. While the print heads in this type of system are not the standard 2D printer DOD heads as used in the powder/binder systems, the advantage of inkjet based ALM systems in general is the implementation of a high resolution and a widely understood concept. The limitations of the solid Inkjetting technology are the relatively costly materials and, more significantly, the poor reliability. If a single print orifice out of the many hundreds within a head becomes damaged or stops operating, the entire print head may need replacing at a cost of several thousand pounds. The solid Inkjet technology is currently utilised by Solidscape's 3D printer range, and was previously utilised by 3D systems under the name of 'ThermoJet'.

### *Lamination*

Lamination takes a material in sheet form and bonds the entire sheet to the build surface, before cutting out an artefact's layer geometry (SD300, Cubic Technologies, USA and Matrix 300, Mcor, Ireland). The system needs no additional support structures as the unwanted material provides support for the artefact throughout the build process. Systems use cutting apparatus ranging from CO<sub>2</sub> lasers to tungsten

blades and common materials include paper, PVC and metal foils (Grenda, 2009). The layers are adhesively joined: by heat activated adhesives pre-applied to the sheet and selectively deposited glues, or through ultrasonic welding and then milled to shape (White, 2003). Lamination is the oldest form of layer manufacturing (Blanther, 1892) and as such is arguably the simplest. The lamination technology was granted a patent in 1991 (Kinzie, 1991) before being licensed and sub-licensed to Helisys, Cubic Technologies, Kira, Solidimension and 3Dsystems (Grenda, 2009). Helisys was the first company to develop a commercial system which it called Laminated Object Manufacturing (LOM) (Feygin, 1988) before being superseded by Cubic Technologies. The advantages of the system are it is relatively low-cost, its utilisation of widely available sheet materials such as paper, and its ability to produce artefacts which can be sanded and finished. Disadvantages of the lamination ALM process include: the risk of fire from laser cutting of the laminate material, a large amount of wastage due to the cutting of excess material, poor Z-axis resolution, limited interlayer bonding strength, and in some cases the hydroscopic nature of the laminate materials which can warp and delaminate much like wood. In general, the lamination process can work with any material which is able to be produced in sheet form and has the ability to be cut and bonded.

### ***2.2.3 Liquid Based Systems***

Although liquid systems made up only 12.8% of the market in 2009, it is generally considered that they are among some of the most accurate of all the ALM systems. Their relatively small market share is due to the higher machine, materials and servicing costs, over that of some of the solid based systems. In addition there are limitations to the construction materials' mechanical properties and their selection (Wohlers, 2010).

#### *Stereolithographic Photocurable Resin Systems*

During the development of the inkjet printing technologies in the mid 20<sup>th</sup> Century, a number of major chemical companies such as DuPont, W.R. Grace and Celanese were developing photopolymer materials which were able to be converted from liquid to solid by application of light energy. These new materials were primarily developed for

the manufacture of printing plates, while PPG developed electron beam and UV curing for photopolymers for curing coatings for wood and composites (Cahill, 2011). The vast majority of liquid based ALM systems, currently on the market, produce artefacts from photocurable organic monomer resins. These are photopolymerised by exposure to light radiation, in the ultraviolet (UV) spectral range, and are commonly known as Stereolithographic systems. The monomers, usually epoxy; vinyl ester or acrylate resins with few or no crosslinks, are mixed with suitable photo inhibitors. Upon exposure to UV, spontaneous polymerisation occurs, in the course of which liquid monomer transforms into solid cured polymer (Gebhardt, 2003). There are two principles by which the photopolymerisation process is harnessed within an ALM system; either through the selective deposition of monomer layers followed by UV curing (e.g. PolyJet by Object Geometries, Israel; ProJet by 3D Systems, USA), or the selective curing of the surface of a resin bath with respect to a specific geometry of an artefact's cross section (e.g. Stereo Lithographic Apparatus (SLA) by 3D systems, USA; ZBuilder by Z-Corporation, USA). In the first instance the energy necessary to initiate polymerisation is gained through the indiscriminate exposure of an entire layer to UV radiation. This is opposed to the second instance where curing is initiated either through exposure to a high intensity scanning UV source such as a laser or through the entire cross sectional exposure from a UV source through a photo-mask or Digital Micro-mirror Device (DMD) / Digital Light Processor (DLP). The layer forming mechanism differs from one photopolymer liquid process to another but, in general, the newly polymerised layer cross section is indexed down, relative to the build direction, to allow the next layer to be deposited or to enable a film of monomer, equal in thickness to one artefact layer, to form between the build surface and UV source. A number of photocurable liquid systems index down into a vat of monomer resin where an automated wiper or resin vacuum blade levels the surface of the vat ready for the next layer to be exposed (Merot et al, 2006). One of the limitations to the layer thickness resolution is the surface tension of the photosensitive resin which tends to "tear" if spread too thinly (Gebhardt, 2003). A solution to this problem, adopted by a number of systems, is to form an artefact layer between the build

surface and a transparent glass/PTFE/silicone laminate plate (e.g. ZBuilder Ultra, ZCorporation, USA; EnvisionTEC Ultra, EnvisionTEC, Israel; V-Flash, 3D Systems, USA; Perfactory, EnvisionTEC, Germany). Stereolithography Apparatus (SLA) patented in 1986 by C. Hull of 3D systems (Hull, 1986), is the most notable of all the liquid based systems. SLA was the first commercial available ALM system, and in the early years following its launch in 1987, saw more installations of SLA units than any other process until 1996 when Stratasys overtook with its 'Dimension' FDM system (Jacobs, 1992; Schindel and Kruth, 2003 Wohlers, 2010). Following the introduction of other ALM technologies, SLA machines, made by 3D systems, were considered among the most accurate ALM systems on the market (Yan and Gu, 1996). Early 3D Systems machines functioned with a single UV laser beam and a vat of Photocurable resin producing artefacts of high accuracy and regularly within 0.1% of the overall artefact dimensions. Figure 2.10 is the annotated drawing of the first SLA as submitted by Charles Hull in his 1986 SLA patent. Supports in the SLA systems were made from the same photocurable resin as the main artefact but were optimised to be snapped off in a post-process. Further developments resulted in the maturity of multibeam scanning (Ikuta et al, 1996<sub>a</sub>, 1996<sub>b</sub>) and multi colour single material systems (Im et al, 2002). The development of micro Stereolithography demonstrated the possible resolution SLA was able to achieve. The electron microscope capture in Figure 2.11 shows the ability of SLA to produce superior artefact detail to that of any other commercial ALM system (Ikuta et al, 2008) In general, systems based on photopolymerisation of a liquid resin in an office environment may present a health risk and would not sit within the parameters of a desktop process (Prinz et al, 1997<sub>a</sub>). To overcome this, a number of system producers have brought out SL based 'desktop' personal modellers, using the same inkjet technology as two dimensional printers (PolyJet by Objet, Israel; ProJet by 3DSystems, USA). These systems are able to deposit very fine layers resulting in accurate artefacts exhibiting superior surface finish.

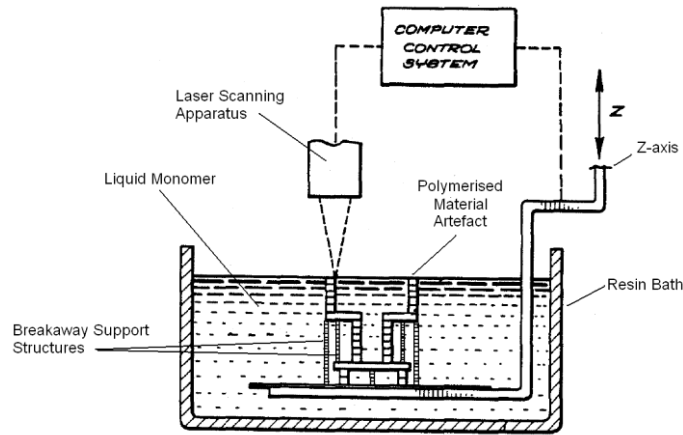


Figure 2.10 The classic SLA system as submitted in 1986 by C. Hull as part of a patent application (Hull, 1986).

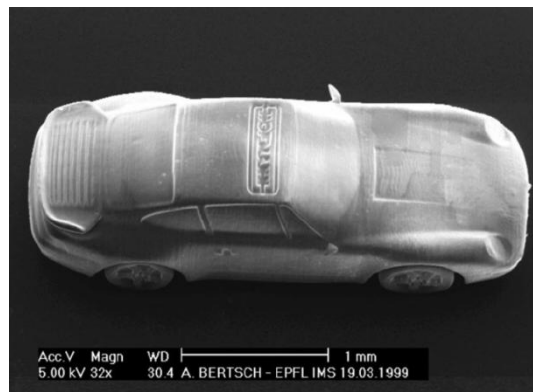


Figure 2.11 A micro scale artefact produced through micro SLA, demonstrating the process’s ability to produce market leading surface finish and accuracy (Limaye and Rosen, 2007).

Table 2.3 illustrates some of the number of different SL based systems on the market, highlighting the stark difference in cost between the ‘high end’ SLA process and some of the smaller SL processes. Figures 2.12, 2.13, 2.14 and 2.15 show the exceptional surface finishes achievable with the Photopolymerisation technologies, with Figure 2.17 highlighting the difference between a Dimension FDM (Stratasys, USA) produced artefact and an Objet PolyJet SL produced artefact.

Company	Machine	Form	Cost £	Footprint mm	weight kg	Build volume mm	Layer thickness mm	Power Req.	Light Source
Objet	Objet30 / Alaris30	3D Printer	35k	830 x 620 x 590	93	294 x 193 x 149	0.028	0.8kW	UV Lamp
3D Systems	Ipro 9000 XL	Industrial	490k	2120 x 2200 x 2280	2404	1500 x 750 x 550	0.05	12kW	Laser
3D Systems	V Flash	3D Printer	9k	66x69x78	66	228 x 171 x 203	0.1	0.7kW	Projector
3D Systems	Projet SD3000	3D Printer	37k	737 x 1257 x 1504	254	298 x 185 x 203	0.025	2.4kW	UV Lamp
Z-Corporation	Zbuilder Ultra	3D Printer	21k	71x78x180	163	260 x 160 x 190	0.05	1.4kW	Projector
CMET	Rapid Meister 3000	Industrial	305k	1020 x 2045 x 2050	1400	610 x 610 x 500	0.05	4kW	Laser

Table 2.2 The relative properties of six photopolymer based processes.



Table 2.2 shows that the more expensive systems tend to employ lasers, and have significantly higher power consumptions. Desktop systems are unlikely to employ lasers due to their power requirements, size and servicing costs. The VFlash is the least expensive system of the six systems shown and is also the most compact, but has one of the lowest z-axis resolutions exemplified by the comparably large layer thickness. The Vflash and the Zbuilder have the lowest material costs of around  $\text{£}0.37/\text{cm}^3$  and  $\text{£}0.30/\text{cm}^3$  respectively; however, they also have the least material selection (Zcorp.com, 2011; Printin3D.com, 2011). The cost variation between the high end ALM and the 3D printer is substantial, even though the highest resolution systems are of 3D printer price. This is primarily because of the materials' and systems' cost. As an example the iPro 6000 produced By 3D Systems is able to produce artefacts weighing up to 150kg, needing a substantially stronger mechanical system than a system producing artefacts of 1-2kg max. The z-axis resolution on very large artefacts such as car bumper prototypes is less apparent than that of wax investment casting jewellery patterns. For this reason the smaller systems, building smaller artefacts, require higher Z-Axis resolutions. In addition to resolution differences, larger machines producing large artefacts more slowly but a larger layer thickness helps overcome this issue.

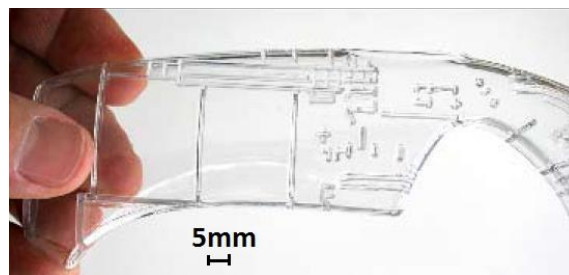


Figure 2.12 An example of a part made by 3Dsystems iPro 3000 SLA system (Dynacept.com, 2011)



Figure 2.13 An example of a part made by Objet's Objet30 Polyjet system (Dynacept.com, 2011)



Figure 2.14 An example of a part made by 3Dsystems' Vflash film transfer system (Printin3d.com, 2011)

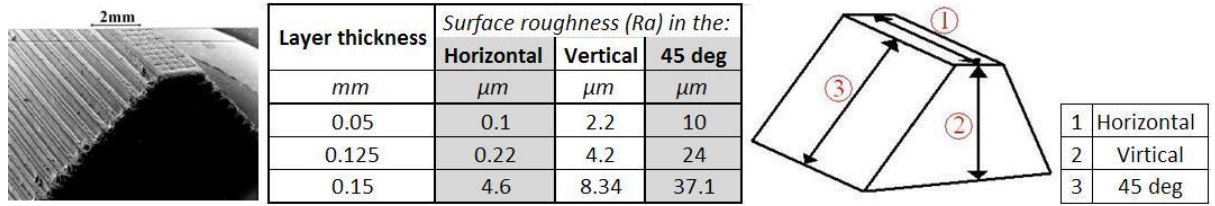


Figure 2.15 An example of a part made by 3Dsystems' SD3000 Projet system (Printin3d.com, 2011)



Figure 2.16 A comparison of Objet's Objet30 Polyjet produced artefact (left) and with the same artefact produced by Stratasys' Uprint FDM system (right) (3dscanningservices.net, 2011)

Daneshmand, Ahmadi, Nadooshan, and Aghanajafi (2007) explored the relationship between layer thickness and surface roughness in an SLA system. The Table 2.3 shows the comparative horizontal, vertical and cross pulled surface roughness due to variable layer thickness. The figures in 2.17 show the scanning electron microscope (SEM) image of a test sample and a schematic of where the surface roughness average measurements were taken.



**Table 2.3:** Surface roughness measurements taken from an SLA artefact built from 0.05, 0.125 and 0.15mm layer thicknesses. **Figure 2.17:** left: an SEM picture of the measured artefact (Daneshmand et al, 2007). Right: A schematic showing the locations of the measurements.

Some SL systems have been developed to produce multi-coloured artefacts from a single polymer material, working on the principle that under certain UV exposure conditions, resins were able to be coloured (Im et al, 2002). With the advent of Polyjet technology from Objet, not only are multicoloured SL products feasible but now even multi photoreactive material artefacts are possible. There are a number of advantages to the photopolymer based systems including the feasibility of extremely high resolution, the reuse of un-polymerised material, the ability to drain enclosed geometries and the range of finishing techniques that can be applied to a post-processed artefact. With the decreasing price of digital media projectors with the ability to form high resolution light images, the potential to create a compact, low-cost, ALM machine using photocurable polymers is apparent. However, photoreactive liquids quite often have a shelf life, can be toxic, difficult to handle, require solvent cleaning and often UV post curing, all of which would be unsuitable for a desktop system.

*Other Liquid Based Systems*

While photocurable resin based systems are currently the only commercial liquid based ALM systems on the market, there are two research systems worth noting for completeness. Following their introduction, these systems will not be discussed further within this survey as they are not in keeping with the spirit of the research due to their process complexity and/or their artefact properties.

*Water*

Water is a low-cost, environmentally friendly and safe to handle material which forms the bases of an ALM solidification process developed by Dr. Ming Leu of the University

of Missouri-Rolla (Leu et al, 2000). Rapid Freeze Prototyping (RFP) is primarily a water extrusion process which deposits liquid water in the form of water droplets or a continuous stream on to the surface of a cooled platform, in an environment typically maintained at  $-20^{\circ}\text{C}$ . In addition to water, the system can deposit a solution of sugar water, which is used as a support material for overhanging geometries, before being removed at around  $-5^{\circ}\text{C}$  to leave the frozen water structure behind. An advantage to the RFP ALM system is that water is an abundant low-cost, non toxic material which can rapidly form a structure. Increased productivity can be obtained through forming inner and outer contour surfaces and back-filling the resulting void with a stream of water (Leu et al, 2000). Once produced however, the artefact must be maintained at a temperature of less than or equal to  $0^{\circ}\text{C}$  or the artefact will return to liquid. This limitation means that, in order to produce an artefact which can be handled at common room temperatures, extra processing must be undertaken. These processes could be in the form of endothermic chemical casting, or the formation of an investment casting mould that does not require elevated temperatures in its production or produced such an environment during curing. A water freezing based system, despite its advantages, would not be suitable for a low-cost desktop system due to the need for maintained low temperatures.

### *Electrolytic*

Electrochemical deposition, more commonly known as electroplating, is a technology well known for the surface coating of substrates with thin metallic layers. A near commercial ALM system exploiting this common process was developed by the University of Southern California and referred to as Electrochemical Fabrication (EFAB) (Cohen et al, 1999). The system uses a proprietary technology, called Instant Masking, to produce microelectromechanical systems intended to form artefacts that are otherwise impossible to produce on a micro scale (isi.edu, 2011). The process is time consuming and requires up to eight steps from start to finish. A dielectric mask is deposited onto a conductive substrate before having a support material deposited on top (Fig. 2.18a). The build material is blanket deposited across the surface of the build platform (Fig. 2.18b). The surface is planarized to give a flat surface ready for the next

mask (Fig. 2.18c). The support structure layer is deposited, the build material blanket deposited and the surface planarized (Figs. 2.18d, e, f), this process is then repeated to leave a complete artefact inclusive of support (Fig. 2.18g). The support material is then etch removed to leave the desired structure (Fig. 2.18h).

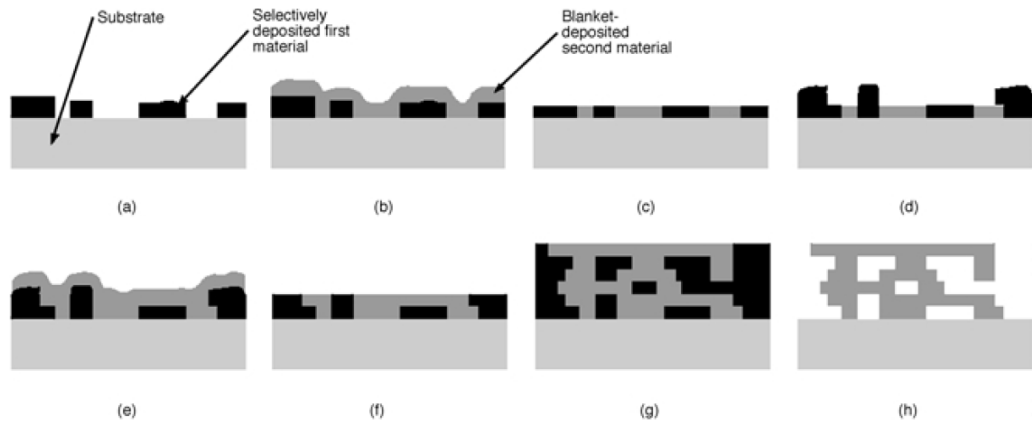


Figure 2.18 The stages of production of an artefact produced by EFAB (Cohen, 2001)

### 2.3 Support Structures

Regardless of the technology, all ALM systems need some sort of support structure to enable the unrestricted formation of complex geometries. There are two types of generic support structure, complementary support (Fig 2.19a) and explicit support (Fig 2.19b).

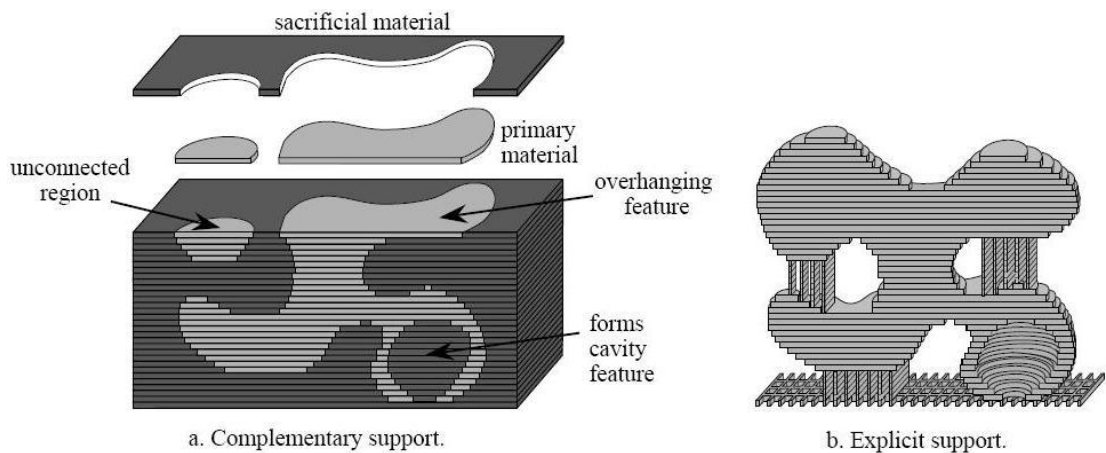


Figure 2.19a: A representation of the complementary support structure of an ALM system. 2.19b: A representation of the explicit support structure of an ALM system (Prinz et al, 1997<sub>b</sub>)

### *Complementary Support Structures*

Complementary support can consist of a primary material and a secondary sacrificial material or bonded material supported by unbound material, with the majority of commercial systems opting for the latter complementary support (E.g. 3DP, SLS, LOM). Both solid and powder based technologies use complementary support systems either by selectively consolidating powder within a powder bed, or through the successive deposition of laminate layers which have been cut and glued together in layer specific regions. PolyJet (Objet, Israel) a liquid based systems, uses the complementary support structures, depositing a UV curable water-soluble support wax which is removed in a post-process. In general, liquid based systems such as SL do not use complementary support. In many cases, due to the support structure being unattached to the artefact, no post-process de-burring or melting is needed; the artefact is simply removed from the powder bed or released from its surrounding laminates. The major disadvantage of this support system however, is apparent when considering systems which use a non recyclable sacrificial support material. These processes generate material wastage and require additional post-processing.

### *Explicit Support Structures*

In processes that are unable to provide complementary support, due to single material constraints or the cost of a non-recyclable support material, explicit support structures are used. These structures can either be manufactured from the primary build material or can be produced from a secondary material with differing physical properties. Usually a water soluble or thermally less stable material is used (FDM). In the first instance where an explicit support is generated from the primary material, such as in many photopolymer based ALM systems, the structures are designed to snap away or are embrittled with prolonged UV exposure (E.g. Zbuilder, Z-Corporation, USA). Sacrificial support material is usually designed to be dissolved in a warm solvent solution, which is often made up of water and sodium hydroxide. The advantages of explicit over complementary support are clear when used in conjunction with a non-recyclable sacrificial support material, as less waste is produced. Explicit support also provides a mechanism for support in liquid mono-material systems where

complementary support is unworkable. The most prominent limitation of using explicit support structures is the necessity for post-process removal. In some cases the drawn out process of support material removal can leave visible marking to the detriment of an artefact's surface finish.

### *Support Method Conclusions*

Embodied within a low-cost desktop ALM system, any support structures would need to be cost effective and be able to be rapidly removed without the need for additional processing equipment. The use of a complementary support structure, built with recyclable primary or secondary materials, has clear advantages of waste limitation and surface finish over that of explicit support - the caveat being that the support material has to be recyclable and easily removable. Failing the implementation of recyclable support material, the lower cost option is the use of explicit supports with the ever present limitation of laborious post-process support material removal.

## **2.4 Benchmark Systems**

The conceptualisation of a novel system required the benchmarking of a number of ALM variables which could dictate any future product's position within the ALM market. Within this research, a variable demonstrated by a benchmark system was looked upon as a target as much as a functionality baseline. For ALM equipment, it is generally recognised that the primary drivers for development are: lower equipment cost, lower maintenance costs, greater accuracy, improved surface finish, and higher productivity; however, the relative importance of these factors does vary depending on the target market (Prinz et al, 1997<sub>a</sub>; Levy et al, 2003). The benchmark systems and development variables considered most important for the benchmarking of a novel, low-cost, desktop ALM system were:

**FDM a Cost Benchmark** – The introduction of lower cost systems from manufacturers such as: Fab@Home (USA), Bits from Bytes (UK) and MakerBot Industries (USA), has seen the popularity and public awareness of ALM in the form of 3D printers grow exponentially over recent years (Wohler, 2010). A cost benchmark exemplifies a system that exhibits not only a low-cost outlay, but also represents low-cost materials,

service and running. FDM was chosen as a cost benchmark not just for the success of Stratasys's products but for the large array of ALM systems, both open source and commercial, which have entered the market using thermoplastic extrusion technology.

**SL a Resolution Benchmark** – An inherent characteristic of any ALM system is the stepping effect whether visible on a macro or micro scale. As the surface finish is mostly influenced by the prominence of stepping, a benchmark ALM system must provide a high Z-axis resolution resulting in an aesthetic artefact surface. The SL process was selected as a resolution benchmark due to its market leading high accuracy and high Z-axis resolution. A high resolution example of SL is Objet's PolyJet (Israel) which has a layer thickness down to 0.028mm.

**SLS a Mechanical Properties Benchmark** – The ability to free form highly customised objects at relatively high speed compared to conventional machining processes is an attribute possessed by the majority of current commercial ALM systems (Hon, 2007). However, few of those systems possess the ability to produce robust functional artefacts. An artefact built by a benchmark system should exhibit build material properties close to those of conventional manufacturing techniques such as injection moulding. SLS by 3D Systems (USA) was selected as a benchmark for mechanical properties because of the large number of materials it is able to process, while offering some of the most robust polymer artefacts of any ALM system.

**3DP a Productivity Benchmark** – ALM systems are known for being relatively unproductive when compared to scaled moulding technologies or the production of simple geometries by modern Computer Numerically Controlled (CNC) machinery (Hon, 2007). System manufacturers continually strive to improve upon productivity without infringing on resolution. A benchmark system should be known in the industry as setting the standard for productivity and should be used as a baseline from which to improve. 3DP from Z-Corporation (USA) was chosen as a productivity benchmark due to its market leading productivity. Data provided by Z-Corporation provides a build speed of their mid range Z450 printer of 24mm per hour in the Z-axis for a build area



of 200 x 250mm. The resultant maximum volumetric productivity is therefore around 0.0012m<sup>3</sup>/hour.

### 2.4.1 The Desktop Benchmark

In order to properly consider the design of a novel desktop system it was necessary to produce a desktop standard stating dimensions, utility needs and mass. A mid to high range computer desk, from a large retailer (IKEA, UK), was selected as the desk standard, the standard Table allowing a maximum working load of 60kg (not including its own weight and other desktop devices). To allow a desk user to retain desk space for standard office equipment (monitor, keyboard, mouse, etc), the ALM system's footprint was restricted to a maximum of 1/3 the area of the standard desk. The electricity supply to a UK household appliance is limited to around 3kW due to a 13amp plug fuse. The mass of a desktop system was chosen to be 2/3 of the maximum load permissible on the standard Table to, again, allow for standard desktop equipment. The diagram in Figure 2.20 illustrates the parameters and restrictions, while Table 2.4 formally presents the 'desktop' physical standard as adopted within this research.

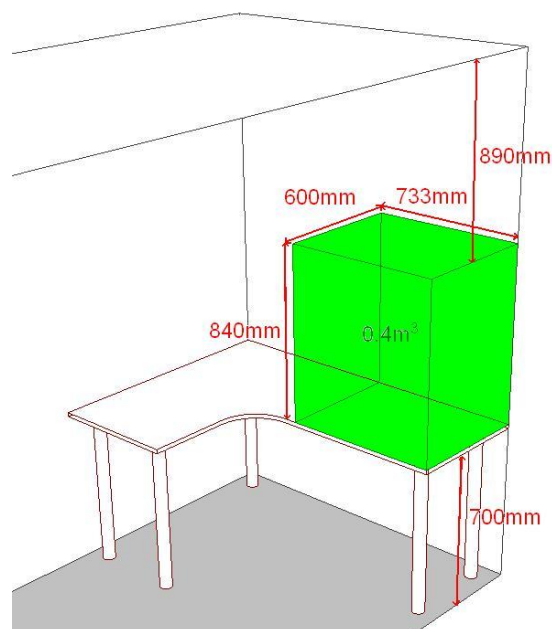


Figure 2.20 The desktop standard dimensions, in an average height room and upon an average computer table.

Standard 'Desktop' Properties	
Maximum Dimensions (L x D x H)	733 x 600 x 840
Maximum Mass	40kg
Maximum Power Consumption	3000 Watts
Process Materials	Non Toxic
Utility Required	Single Phase Electric Only

**Table 2.4** The standard properties of a desktop ALM system as used by the author when referring to a desktop system within this thesis.

## 2.5 A Review of Desktop ALM Systems Technology

Regardless of manufacturers' advertisements, there are actually very few true desktop ALM systems on the market. Many systems pertaining to 'desktop' systems are either far too large / heavy to be installed on a desktop or the additional systems required to produce artefacts, such as post curing ovens or heated washers, require additional desktop space. While these systems may not be 'desktop' they are significantly smaller in size than high end ALM systems. This, combined with lower cost, has meant they are, as a group of systems, commonly referred to as 3D printers. The following brief review will compare a number of the more popular 3D printer systems, with a view to identifying a technology with the scope to develop into a true desktop system. The systems reviewed are presented in Table 2.5.

- *SD300Pro*

SD300Pro (Solido, Israel), a LOM system, claimed to be the first to develop a desktop 3D printer. In agreement with this, the comparison Table 2.5 shows the SD300Pro to be significantly more desktop friendly than its competitors. The system however, ranks last of the six systems reviewed with the factors of materials cost (expressed in the Table as 'Part Cost'), post-processing time and robustness all playing a key role in its poor ranking. Reviewers complained of a number of issues with the Solido system including: delamination of built artefacts, inability to reuse unused material in the machine and service contracts which bound users to purchase a significant number of expensive material packs over a two year period. There are a number of other lamination ALM systems on the market such as the larger Matrix 300 manufactured by Mcor Technologies, a £20k system based on paper lamination. With all the systems

discussed sharing the limitation of material wastage. An LOM system based on a small footprint and a relatively inexpensive build material such as paper may be acceptable to the desktop ALM market, but the limited resolution and functional properties of paper remain issues. It would seem unlikely that the LOM system can be further developed to provide a novel solution to a high quality low-cost desktop system. In Jan 2011, Solido ceased trading.

- *ZBuilder Ultra*

In May 2010 Z-Corporation (USA) launched a new liquid photopolymer based system, the Zbuilder Ultra, based on EnvisionTec's Ultra technology. The Zbuilder can produce accurate, aesthetic artefacts but despite Z-Corp's advertising literature, assuring a built artefact with similar mechanical properties to that of injection moulded Acrylonitrile Butadiene Styrene (ABS), the resultant artefact mechanical properties are poor. An additional limitation with the system's material is its UV instability, which sees a part become increasingly brittle with exposure to sunlight or other UV source. The system is ranked joint first out of the six systems reviewed, standing out as a cost effective means of producing high accuracy artefacts, with good productivity and an aesthetic finish. However, if you consider its size and the toxic properties of the photopolymer in its monomer state, the system is far from an ideal desktop solution. As a low-cost ALM system installed in a workshop or small business, the Zprinter would provide an ideal form fit prototype modeller. However, for use as a desktop system the technology is incompatible. A number of companies such as 3D Systems and Objet have integrated their toxic monomer within a cartridge to minimize the likelihood of exposure to the material in its un-polymerised state. Due to the use of a monomer bath it is unlikely this technology could adopt a similar approach. In conclusion, despite the clear cost/accuracy benefits of the Zbuilder over its competitors, it would seem unlikely that the system could be developed in such a way that it would be suitable for a desktop ALM system.

- *ZPrinter 310 Plus*

This is Z-Corporation's (USA) base monochrome model. The Zprinter 310 plus comes fifth in the ranking primarily due to the poor mechanical strength and aesthetic

qualities of the artefacts it produces. The use of disposable, inexpensive inkjet heads allows the cost of the system to remain relatively low, although, considering the mass produced technology implemented, the retail price is significantly higher than would be expected. There would be scope to develop a lower-cost 3DP based system in a desktop footprint but the focus would be on the generation of materials and binders with usable mechanical properties as opposed to the generation of new hardware.

- *VFlash*

The V Flash (3D Systems, USA) is another photopolymer liquid based ALM system. Despite its poor accuracy, it is ranked third primarily due to its small desktop footprint and relatively low-cost. The V Flash, however, is a system that needs both post-process UV exposure in a suitable UV light box, and then further ultrasonic washing. This additional equipment increases the system's combined footprint from a large desktop to the area of several desktops. When the artefacts are removed from the V flash they are still moist with potentially toxic monomer resin. The V Flash builds artefacts 'upside down', when considering the function of conventional ALM systems. The build platform is placed into a thin layer of photopolymer, present on the surface of a transparent film. The film, in turn, is positioned upon a digital light projection unit which selectively exposes the photopolymer layer from the underside, thus selectively polymerising the resin. The system uses explicit supports which form part of the model. These supports must be removed in an additional post-process, leaving the V Flash with the longest post-processing activity out of the six systems reviewed. Owing to the material and post-processing this system would be unsuitable for development as a Desktop 3D printer within the scope of this research.

- *Dimension Uprint / HP Design Jet 3D*

Dimension Uprint (Stratasys, USA), a solid FDM based system, is also supplied by Hewlett-Packard ((HP) USA) its Design Jet 3D. As discussed in previous sections, FDM is the best selling ALM system due to new low-cost FDM type technologies. Stratasys, regardless of the new competition, are the best selling ALM technology company, a fact which no doubt influenced their deal to supply HP. The Uprint is its introductory system and is meant to represent affordable functional modelling. The Uprint is the

highest ranked system due to its ability to provide rounded accuracy, surface finish and excellent mechanical properties for a reasonable price. The thermoplastic extrusion type technology is currently under development by a number of manufacturers, aiming to produce a robust desktop system, and as such is not a suitable technology with which to base the development of a novel desktop system.

- *Objet30 / Alaris30*

The objet30 also sold as the Alaris30 by Objet (Israel), is a liquid photopolymer system called Poly Jet, using the same technology as two dimensional printers and Z-Corp's 3DP. The system was the most expensive of the six reviewed and was joint third primarily because of this. The Objet30's layer resolution is the highest of the six, giving it the best overall surface finish and accuracy. The Objet range offers a multi-material printer which is the only system with this ability in this product class. The support structure is explicit and consists of a different material to the artefact, allowing it to be washed off in a post-process, and is non-recyclable. As the material is fully cured in the machine itself, no post-processing UV exposure is necessary. In addition, the materials are contained within sealed cartridges thus minimising the likelihood of exposure to potentially toxic unpolymerised material. The Objet30 is already close to being a true desktop printer. The system would need to reduce in weight and in overall dimensions, but the fundamental limitation to this type of systems implementation is the expense of build materials and their limited selection.

### ***2.5.7 Desktop Development Potential***

The comparison Table 2.5 illustrates, among other things, the size of the current commercial 3D printers. Of the six systems reviewed, none were within the desktop specification and only one, the SD300Pro, had a mass within 5kg of the maximum 40kg specified. Fifty percent of the ALM systems reviewed were photopolymer based. The ease of processing a liquid to form thin layers, in addition to the high resolution light projection systems commonly available, allow high resolution systems to be developed at relatively low-cost. The concept of using a compact light projector and a small build volume to produce a desktop SL system would be viable if, a range of cost effective, non-toxic photopolymer materials with a range of material properties were available.

In common with potential SL development, 3DP holds the potential to be integrated at low-cost within a desktop system but is let down by unsuitable materials. It was clear that there were no commercial ALM system technologies which held the development potential to create a desktop system, or the technologies with potential were currently under development and so held no novel value. To move forwards a new technology with the potential to underpin a desktop ALM system had to be identified. It was observed that while a number of systems used two dimensional inkjet printing technology, no commercial systems had ever adopted laser printing technology for the direct formation of polymer artefacts. Electrophotography, the technology commonly embodied within photocopiers and desktop 2D laser printers, was viewed as a suitable technology for the development of a desktop ALM system as it was compact, light weight, nontoxic, productive, and had the potential to employ a wide variety of materials.

Commercial Desktop ALM / Three Dimensional Printer Comparison																				
System	Manufacturer	Technology	1 = Most Desirable for Desktop System													Overall Ranking				
			System Cost	Running cost	Part Cost	Mass (kg)	Dimensions (cm)	Productivity Exc. Post Process	Productivity Inc. Post Process	Layer Thickness	Surface Finish	Accuracy	Robustness	Points	Rank					
<i>Zbuilder Ultra / EnvisionTec</i>	Z Corporation	DLP SL**	£21k	5	£4.50	3	3	163	6	71x78x180	6	2	2	0.1	2	2	2	36	1	
<i>Dimension Uprint / HP Design</i>	Stratasys	FDM	£10k	3	£3.5k	1	2	76	3	64x66x80	3	6	5	0.25	6	3	3	1	36	1
<i>V Flash</i>	3D Systems	Film transfer	£9k	2	£3.5k	1	4	66	2	66x69x78	4	3	3	0.1	2	5	6	4	37	3
<i>Objet30 / Alaris30</i>	Objet	PolyJet	£35k	6	£12.3k	6	5	93	4	83x62x59	2	4	4	0.028	1	1	1	3	37	3
<i>Zprinter 310 Plus</i>	Z Corporation	Inkjet	£18k	4	£7k	5	1	115	5	74x86x109	5	1	1	0.1	2	6	5	6	41	5
<i>SD300PRO</i>	Solido	LOM***	£2k	1	£5.7k*	4	6	45	1	47x77x42	1	5	6	0.17	5	4	4	5	42	6

\* Service contract for 2 years. 24 build packs must be purchased in the first 2 years @ £370 each

\*\* Digital Light Projection Stereolithography

\*\*\*Laminate object manufactureing

Table 2.5 A comparison of six of the most popular commercial desk top / three dimensional printers on the market with weighted variable preference. Data acquired from multiple sources – system suppliers and manufacturers, (Wohlers, 2010; Grimm, 2010)

## 2.6 The Principles of Electrophotography

With the benefits of the electrophotographic process, as touched on in the previous section, it was difficult to understand why the promising technology had never been implemented within a commercial ALM system. The remainder of this review will investigate the electrophotographic process, discover its limitations and determine a brief from which to develop the 2D technology into a functional desktop 3D system. Electrophotography is the process by which a latent electrostatic image is defined on the surface of a photoconductive substrate through the selective exposure of said substrate to light radiation. The latent electrostatic image is developed with a fine powder toner before being transferred and fused to a substrate (Carlson, 1942). The process, now commonly implemented in two dimensional desktop printers, offers many key advantages for layered manufacturing applications including high speed (up to 1000 pages per minute), excellent resolution (up to 2400dpi) and layer thickness from 5- 50  $\mu\text{m}$  (Wimpenny et al, 2009).

### *Electrostatic ALM Systems*

While there are no commercial systems, historic or current, that have employed electrophotography as a basis for the direct deposition of powder onto a build platform. The use of indirect electrostatic deposition as a binder and in the formation of sinter masks has been commercially explored with varying degrees of success.

### *Paper Lamination Technology*

Kira's (Japan) Paper Lamination Technology (PLT) was a system based on Kinzie's licensed technology (Kinzie, 1991). It was an improvement over the standard LOM processes as it used a knife to cut sheet laminates instead of a laser. This meant the machine could be of lower cost and there was less chance of the machine catching fire as was known in some former machines (Hague and Reeves, 2000). Kira used the electrophotographic system to selectively print toner onto paper where, once placed on the build stack, it would be heat fused to the previous layer using the toner as a binder. Kira sold 18 systems worldwide up until 1995 when it reduced its supply capabilities and concentrated on supplying the Japanese market (Grenda, 2009).



### *Solid Ground Curing*

Solid Ground Curing (SGC) was patented by Pomerantz et al. of Scitex Corporation Ltd (Israel) in 1990, before being licensed to Cubital Inc (Israel), for commercial development. The system cured a photopolymer into a single layer through an ultraviolet mask. The mask was generated on the surface of a glass sheet, through an electrophotographic deposition process. The glass sheet was then cleaned and reprinted upon for each layer. The system size was large and had the ability to produce large models but was fundamentally let down by its complexity, resulting in poor reliability and slow sales (Grenda, 2009).

### *Selective Mask Sintering*

Selective Mask Sintering (SMS) was patented in 2003 and was initially commercialised by Speed Part RP (Germany) (Larsson, 2003). SMS then went to Sintermask GmbH (Germany), which was taken over by FIT GmbH (Germany) in 2008. FIT continued to develop the technology, said to be both much faster and much less expensive than selective laser sintering which it resembles (Grenda, 2009). The process selectively exposes a polymer powder bed with IR radiation by means of a high resolution temporary mask. The mask was created on a transparent plate using an electrophotographic process. The temporary mask is produced using a thermally stable material which does not melt or adhere to the surface of the mask plate during IR exposure. FIT introduced its ZORRO machine in 2010, but machine sales have been slow (Additive3d.com, 2011; Wohler, 2010). The formation of the IR mask demonstrates the ability of electrophotography to deposit materials other than low melt toners.

### *Desktop Factory*

Desktop Factory ((DTF) USA) formed in 2004, was one of the first true desktop ALM system concepts, promising low initial outlay combined with low build material costs. The DTF functioned on the same selective sintering concept as SLS but instead of employing a laser, the system used a focused halogen bulb to sinter each layer (desktopfactory.com, 2009) While the system was not an electrophotographic based technology, it did use electrostatic forces to deposit a repeatable thickness of powder

layers from a drum onto the build surface. There was a large amount of publicity around the development of the system with Idea Labs, the development company, said to have had more than 200 deposits of \$500 for the first production machines. However in 2009, DTF announced it no longer had the funding it needed to carry on developing the system and was subsequently sold to 3D systems before any production units were produced (Idealab.com, 2009)

### *The Application of Electrophotography in Modern Printing*

Electrophotography is the technology that underpins the operation of virtually all office copiers and laser printers. It is based on many diverse phenomena employing many properties of matter, these include but are not limited to:

- i. **Surface Charging:** Gaseous ionization and induction
- ii. **Image Formation:** Photo-generation and charge transport through disordered solid-state materials
- iii. **Particle Charging:** Triboelectrical charge generation
- iv. **Development and Transfer:** mechanical, electrostatic, and magnetic forces to detach particles
- v. **Fusing:** The application and transfer of heat and/or pressure

In addition, it relies on a precise balance of thermorheological, chemical, and mechanical properties of large area films and small particles (Pai and Springett, 1993). In 1938 Chester Carlson discovered that a zinc plate with cast amorphous sulphur could be electrostatically charged in the absence of light and then selectively discharged using a UV light source. This latent image could then be physically realised through development with a fine lycopodium powder (Carlson, 1942). Carlson went on to patent his findings in 1942 under the title of 'Electrophotography'. This patent would later form the basis from which modern laser printer technology was developed. In 1944 the US Army and the Haloid Company, later to be named Xerox Corporation, funded research into Carlson's concept with the end result being the

formation of the dry printing (Xerography) process known today (Allan, 2001). Early Xerox systems functioned as photocopiers with images being developed from the reflected light of the image to be copied. It wasn't until 1969 that an engineer at Xerox, Gary Starkweather, attached a laser imaging system to a photocopier and produced the first laser printer. Following this, a laser printer called 'Electronic Alto Research Character Generator Scanned Laser Output Terminal' (EARS) was developed and completed in 1971. A network integrated system was completed in the following year boasting two pages per second at 300dpi resolution. In 1976 IBM introduced its IBM 3800 laser printer, capable of printing 20,000 lines per minute. Xerox's first commercial laser printer, the 9700, did not come until 1977. These systems were initially large and expensive. Xerox's systems cost around \$17K and were the size of a small office. It was not until the 1980's that prices and sizes started to reduce. In 1984, Hewlett-Packard introduced its first LaserJet printer featuring 300DPI resolution for \$3,600, followed by the first colour laser printer in 1993 by QMS for \$12.5k (Reilly, 2003). Modern desktop laser printers are significantly lower cost starting at below £100 for a colour version (Dell.com, 2011). The speed of the desktop laser printer can range from 8 to 24 pages per minute (ppm) with resolutions from 300 to 600 dpi. Industrial laser printers however, can print up to 1000 ppm, with a resolution of 2400 dpi (Banerjee and Wimpenny, 2006). Each laser printer has its own specific characteristic duty cycle, resolution, printing speed, first-page-out-time, colour resolution, paper handling and image transfer mechanism. However the general function of any laser printer is the same.

### *The Laser Printer*

The laser process begins with the creation of a charge pattern formed from image data on a photoconducting surface. Charged, pigmented, thermoplastic particles called toner (dry ink), are attracted selectively to the charge pattern, developing it. The toner image is then transferred to paper and fixed by softening and fusing the toner to the paper (Pai and Springett, 1993). A diagram showing the basic lay-out of a generic laser printer can be seen in Figure 2.21.

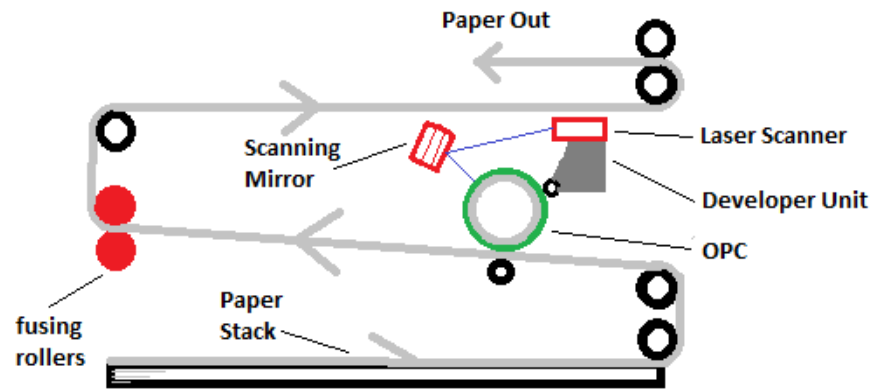


Figure 2.21 A generic printer highlighting the paper path from tray to exit.

The laser printing process executes the following steps to complete one printing cycle (Chen and Chiu, 2001);

- i. **Data** - Receive and process print data.
- ii. **Charge** - Apply a charge to the organic photoconductor (OPC).
- iii. **Expose** - Selectively discharge OPC with light energy.
- iv. **Develop** - Apply toner to the electrostatic image present on the drum.
- v. **Transfer** - Apply developed toner image to paper substrate.
- vi. **Fuse** - Apply heat and pressure to fix the toner to the substrate.

The concept of electrophotography is only possible through the interaction of charged bodies, in this case roller/substrate surfaces and toner powders. Many physical interactions within the systems are brief and on a micro-scale and are dependent on interactions at material surfaces (Pai and Springett, 1993). The migration of charged toner particles and their deposition upon a substrate is described by

$$F_e = QE \tag{2.1}$$

where  $F_e$  is the force exerted on the toner particles,  $Q$  is the charge on the toner particles, and  $E$  is the electric field acting on the toner particles. Image formation is

determined by the variation of force  $\delta F$  of the force  $F_e$  as experienced by the powder particles across the photoconductor and can be described in the first order

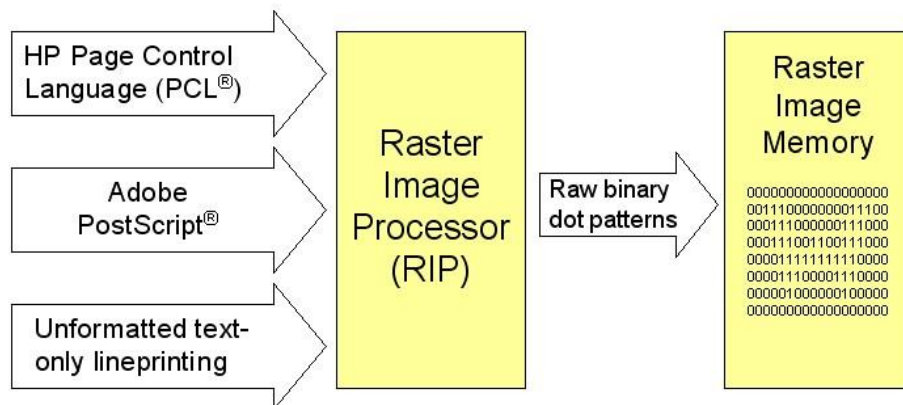
$$\delta F = Q\delta E + E\delta Q \tag{2.2}$$

where  $\delta E$  is the variation in electric field influencing the toner particle and  $\delta Q$  is the variation in charge on the toner particles. The term  $Q\delta E$  from equation 2.2 describes the electrophotographic system as used in modern laser printers, where the charge on the toner particles  $Q$  remains constant and an image is formed through the spatial variation in electric field  $\delta E$ . The electric field pattern reproduces the subject image and the particles of constant charge collect to form a real image with respect to the force  $\delta F$ . The equation also suggests that the imaging is possible when the electric field  $E$  is constant and the charge on the particles is varied. While imaging methods such as photoelectrophoresis (Tulagin, 1969) based on the  $E\delta Q$  term have been developed, they are not within the scope of this review. The following sections will study the six process steps previously discussed and highlight how they are generally implemented within a laser printing system.

#### *Print Data Processing*

A printer control system consists of one or more processors working together to control the printers functions, as well as assimilate data for printing. In addition to processing power, a laser printer needs a substantial amount of memory to enable an entire page of print data to be stored in a printable format for printing (Rodney, 2005). On submission of a document, the laser printer control system 'handshakes' with the user's personal computer through USB, parallel, Ethernet or wirelessly, and accepts data in the form of a print syntax describing a page layout. The controller processes the data into a laser raster sequence and saves the raster to memory before commencing printing. There are many printer syntaxes including, Microsoft XML Page Specification (XPS) HP Printer Command Language (PCL), Adobe Postscript (PS), or Advanced Function Printing (AFP). The machine specific printer driver installed on the host PC is responsible for the correct syntax transmission.

When compared to an inkjet printer, a laser printer control system contains a large memory bank. The large amount of memory is needed to ensure a continuous flow of print information to the printing engine during printing, as the printing system is highly synchronised and cannot tolerate asynchronous data. The print memory utilised by a raster image processor (RIP) splits the PC submitted data down into predefined fonts for text, or gray scale areas for pictures, and creates a digital array describing the desired laser output, as illustrated in Figure 2.22.



**Figure 2.22** An illustration of the raster image processor inputting data submitted from a host computer and outputting binary pattern data.

Laser printer resolution is nominally described by the abbreviation dpi (dots per inch) (Cormier et al, 2002). A low-end printer will resolve to around 600dpi<sup>2</sup>. It takes 3.96million bytes or 3.78MB of memory to store a standard A4 page of raster information at a resolution of 600x600 DPI. The printing engine (including toner cartridge), the fuser assembly and the paper feed are all driven from one motor, which allows low-cost geared synchronisation of the mechanical system (Chen and Chiu, 2001). A stepper motor is most commonly used due to the low-cost control benefits such as feedback, speed control and high torque at low speed. The feed can and often does run without a sheet of paper loaded into the system to allow the cleaning of the printing drum (Samsung, 2001).

### *Charge*

Following data compilation, the first step in the printing process is to charge a photo receptor, often referred to as an Organic Photoconductor. A bias charge can be applied to the surface of the OPC in a number of ways and is commonly achieved through corona discharge or contact with a charge roller (Drake, 2003; Waters and Stark, 1975).

### *Corona*

Corona discharge is formed when the non-uniform electric field between two electrodes separated in air approaches  $3\text{MVm}^{-1}$  (Hughes, 1997). Within a laser printer, the phenomena is usually generated using a fine wire at a high potential with respect to a surrounding shield. Both positive and negative biased wires can create corona, however, their ionisation mechanisms differ significantly (Moore, 2007).

### *Positive Corona*

Electrons and negative ions in the surrounding air are drawn to the wire, causing secondary ionization, consisting of electrons and positive and negative ions in the vicinity of the wire. Positive ions, consisting primarily of hydrated protons  $(\text{H}_2\text{O})_n\text{H}^+$  are repelled from the plasma surrounding the wire and are driven by the electric field to the corona shield and photoconductor (Pai and Springett, 1993).

### *Negative Corona*

Electrons are emitted from the wire and ionize air. The electrons attach to molecules so that the charge deposited is ionic, dominated by hydrated  $(\text{CO}_3)^-$  (Pai and Springett, 1993).

In both cases, light is given off in the form of plasma, which is formed through the excitement of nitrogen and oxygen atoms within the air. Products of corona discharge include, but are not limited to; ozone, oxides of nitrogen and ammonia (Moore, 1997)

### *Scorotron*

When a more uniform or an absolute limit charge is required on the surface of an OPC, a charged metal grid is placed between a corona discharge device and the surface.

This type of assembly is commonly referred to as a scorotron (Hayne, 1976). The grid is given a charge equal to that of the intended charge on the surface of the OPC. During operation, ions are attracted through the grid until the charge on the OPC equals that of the grid, at which point ions are no longer attracted to the surface of the OPC and instead are attracted to the grid (Pai and Springett, 1993).

### *Charge Roller*

A charge roller consists of a semi-insulating roller with a conductive metallic core in contact with a photoconductor. A charge is injected into the roller through the core and charge transfer is achieved through air breakdown within the nip between the roller and OPC (Chen and Tse, 2005). A diagram of an OPC charge roller can be seen in Figure 2.23.

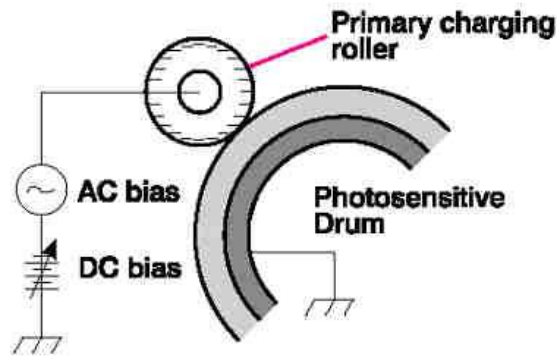


Figure 2.23 A charge roller and OPC.

### *Expose*

The exposure of an OPC within a laser printer with raster data is most commonly achieved through exposure to laser or LED light (Tateish and Hoshino, 1984). A laser printer's imaging engine is used to selectively discharge the surface of a charged OPC resulting in a latent electrostatic image in the geometry of the intended subject.

### *Imaging engine*

Despite the advances of low-cost, high speed LED technology, laser printing systems still remain popular as they can offer superior print quality and resolution (Dell, 2011). While an LED engine consists of a staggered array of LEDs, each representing a pixel



and thus limiting the resolution, a laser engine uses a scanned modulated laser capable of far higher independent pixel exposure. A laser scanning unit (LSU), houses a number of components as seen in Figure 2.24. The major components being a laser diode usually in the IR spectrum (Tateishi and Hoshino, 1984), focusing optics, a rotating polygon mirror mounted on a brushless DC motor (Chen and Chiu, 2001), a photo transistor and an  $f\theta$  beam conditioning lens (Park, 1997).

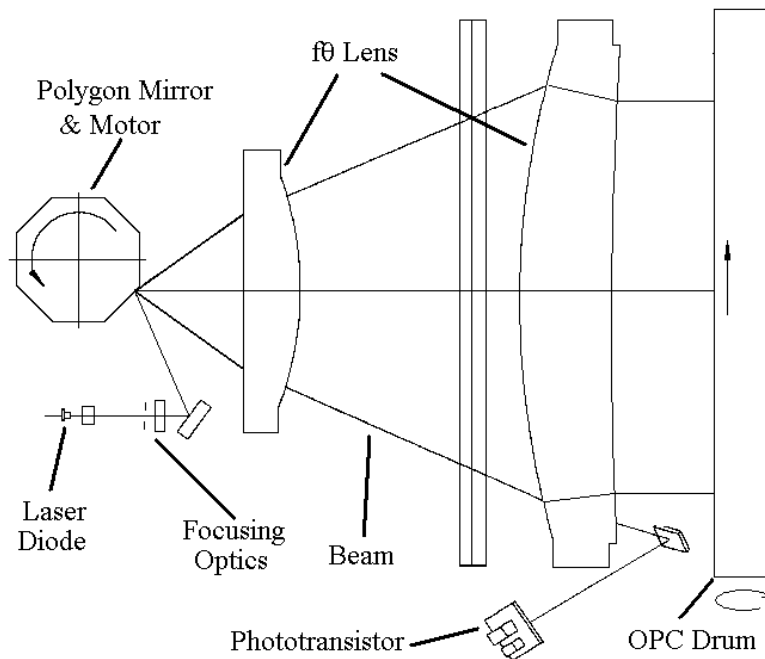


Figure 2.24 The internal parts of a laser scanning unit within a laser printer

The LSU laser, usually a monochromatic laser diode with a wave length of 780nm, is focused onto a polygon mirror while being modulated in accordance with the binary data held in the raster image memory. The polygon mirror can form a square, hexagon, or octagon which, when rotated, rapidly scans the laser beam on to the surface of the OPC. A polygon mirror is used to increase the scan speed of the laser, relative to the motors speed, by a factor equal to the number of mirrored facets. E.g. a six sided polygon mirror would have twice the scan speed of a three sided one. Typically the mirrors have six sides but larger numbers are possible for higher speed printing (Kim, 2005). The process of rastering the laser beam axially across the OPC is commonly known as main scanning, as opposed to cross scanning which is the name given to the trace of the laser beam as the OPC rotates.

As the polygon mirror scans the laser beam across the OPC, the distance the laser beam travels changes. That is to say, the light path from the central focal point, the centre of the OPC, is significantly shorter than that of the light path when the beam is at its extremities. This phenomenon has the greatest effect on the focus of the laser spot on the surface of the OPC. For sharp images the laser spot must be in focus along the full length of its scan. An LSU usually employs two  $f\theta$  lenses, (the name  $f\theta$  referencing the relationship between its focal length  $f$  and the beam incident angle  $\theta$ ). The  $f\theta$  lenses work together to ensure that the laser spot remains focused on the OPC, Additionally the  $f\theta$  lenses can be toric to help account for any inaccuracies within the polygon mirror (Park, 1997). At the extent of the laser's sweep there is a form of light sensor, usually a photo transistor, which detects the laser's presence as it passes. This is subsequently converted into an electrical pulse, commonly known as a synchronous signal. This signal is used by the control system to match the start of a data line with the modulation of the laser (Park, 1997).

### *OPC*

The OPC is the primary imaging component of a laser printer system which is selectively exposed by the LSU to form a latent electrostatic image. OPCs can be in the form of a belt or drum, with a drum being the most common in monochrome systems, due to their relatively low manufacturing costs. In its basic form, the OPC is a drum covered with a layer of organic material which is an insulator in the absence of light whilst being a conductor in the presence of light. OPC's, an example of which can be seen in Figure 2.25, comes in a number of colours and sizes, with the colour indicative of the material used to create the charge generation layer (Nakamura, 2006).



Figure 2.25 A picture of two OPC rollers with different OPC coatings.

**OPC Physical Characteristics**

OPC technology has evolved significantly, from experimental cast amorphous sulphur, into two characteristic technologies of positive charge and negative charge coatings. Modern OPCs most commonly utilise a negative charge (Nakamura, 2006).

**Negative Charge OPCs**

From innermost to outermost layer, negative charge OPCs typically consist of an aluminium substrate, undercoat (or "blocking") layer (UCL), charge generation layer (CGL), and charge transport layer (CTL) (Fig. 2.26) (Morita et al, 2007).

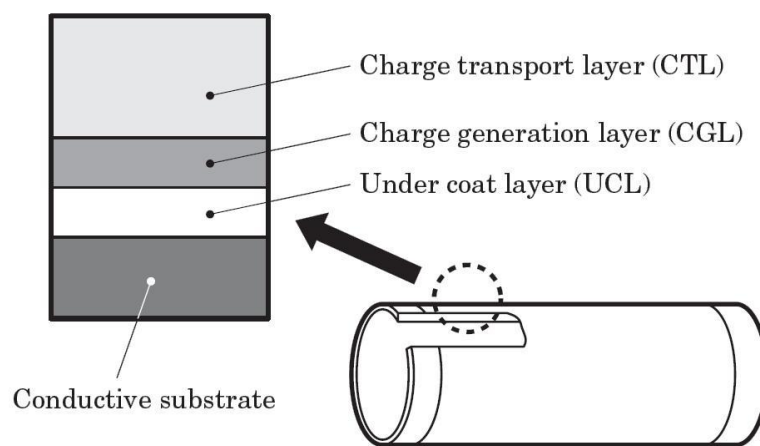


Figure 2.26 The composite layers of an OPC manufactured to accept negative charge (Morita et al, 2007)

**The Aluminium Substrate** does not play an active role in the electro-photographic process. Its primary function is to provide structural and mechanical support, and an electrical path to ground. Any conductive material can be used as the substrate but for rollers, aluminium is commonly used because of its low mass, preferential cost, machinability, and wide availability.

**The Undercoat Layer (UCL)** consists primarily of a binder resin for the purposes of blocking positive charges and preventing interference of the exposure light. Typical materials are metal oxides including anodising of the substrate with a polyamide, polyester or melamine coating (Nakamura, 2006)

**The Charge Generation Layer (CGL)** is a thin layer typically ranging from 0.1 to 1.0  $\mu\text{m}$  in thickness. This creates a positive and negative charge on exposure to photons from

the imaging source. The negative charge travels through the UCL to the substrate, while the positive charge moves to the charge transport layer. The light-sensitivity of the CGL is a critical factor in OPC performance, and can be a limiting factor for the copy speed at which an OPC can function effectively. Common charge generation materials consist of Phthalocyanine, Azo, with Polyvinylacetate, or polyketal, and other photosensitivity enhancing and anti-ageing material additives (Morita et al, 2007).

**The Charge Transport Layer (CTL)** – Is typically between 20 to 30  $\mu\text{m}$  thick and consists of an electron hole transport material such as arylamine or benzidine, combined within a protective film of polycarbonate or polyester. The function of this layer is to transport the positive charge generated in the CGL to the surface of the OPC in order to neutralise the negative charge present. A constituent material of the CTL is a hard wearing polymer resin. This is required due to its continuous contact with toner, developer, paper, the drum cleaning apparatus, ozone, and other potentially abrasive and/or contaminating agents. Consequently the CTL wear characteristics, such as durability and abrasion-resistance, are critical factors in the potential life of an OPC drum. A Figure describing the action of the layers can be seen in Figure 2.27 (Nakamura, 2006).

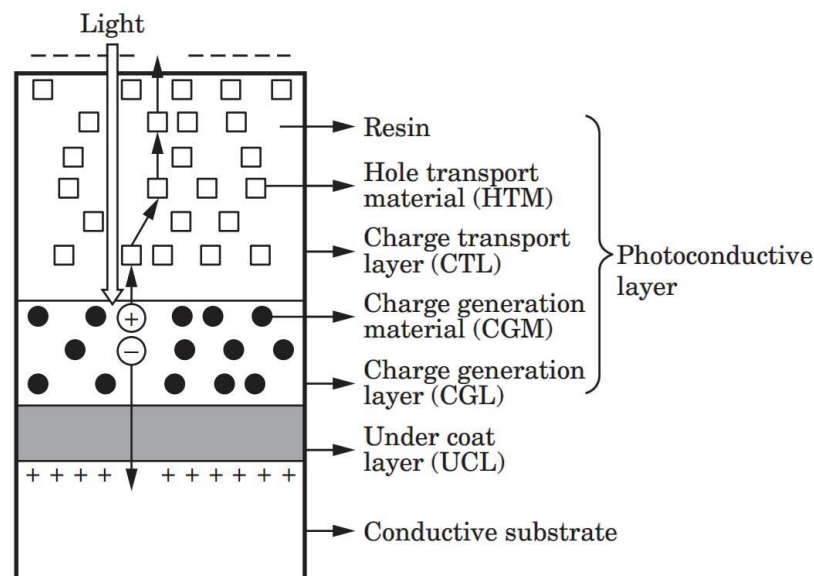


Figure 2.27 The effect of incident light on the layers of a negatively charged OPC (Nakamura, 2006)

**Positive Charge OPCs**

While most OPCs are manufactured to be negatively charged there are also a small number of manufacturers such as Mita and Fuji who produce positive charge OPCs. This type of process is less popular due to the drum only having one charging layer and is more susceptible to wear as a result. A positive charge (Fig. 2.28) or ‘Monolayer’ OPCs are similar to a negative charge OPC in that they consist of a conductive substrate and UCL however, unlike the negative charge OPCs, the positive charge OPCs combine the CGL and CTL into a single layer. Since this single layer determines all the electrical and physical characteristics of the coating (including charge acceptance, photosensitivity, and wear-resistance) there is a tendency to wear more quickly than negatively charged OPC’s. As light and charge of the OPC do not have to pass through a separate CTL layer, the positively charged OPC can produce a higher resolution image in addition to the system architecture producing less ozone. (Narita and Obinata, 2011).

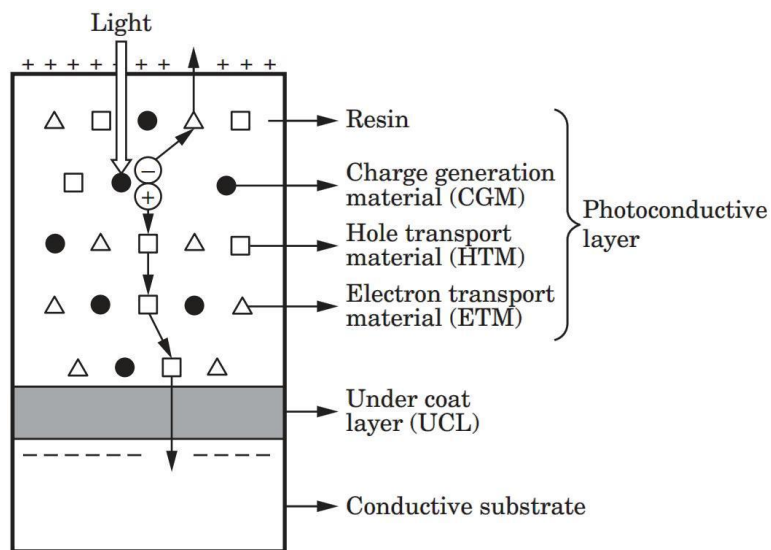


Figure 2.28 A positively charged OPC showing the combined CGL and CTL (Nakamura, 2006).

**General OPC Characteristics**

The material chosen to form an OPC must meet several criteria (Pai and Springett, 1993):

- (1) The OPC film should accept and hold charge prior to exposure and then maintain the charge pattern formed during exposure until development has

taken place. Fundamentally, this means that the rate of charge loss in the absence of light dark discharge must be minimized.

- (2) The photoreceptor must efficiency photogenerate, and therefore photodischarge effectively, at the wavelength of the laser or LED imaging unit (for example, 660 - 680 nm for LED arrays).
- (3) The photogenerated charge must propagate to the surface of the OPC in a fraction of the time between exposure and development. This factor constrains both OPC design and to a certain extent maximum printer productivity.
- (4) The values of charged, partially discharged and residual voltages must be repeatable during multiple exposures. A condition termed "cycle-up" results from a build-up of residual voltage caused by accumulation of trapped charge. A condition termed "cycle-down" results from increased dark discharge with repetitive use. Charge trapping is caused by certain impurities. This places stringent requirements on purity, typically  $\leq 1$  ppb.
- (5) The OPC materials must be sufficiently stable to perform in a chemically reactive corona environment containing ozone, oxides of nitrogen, water, and other effluents as well as to withstand wear and abrasion by repeated development and cleaning processes.

There are three important characteristics of an OPC material, charge acceptance, dark decay and photodischarge:

- i. **Charge acceptance** is the ability of the OPC to accept charge on its surface, which is proportional to CTL thickness (Nakamura, 2006).
- ii. **Dark decay** is the leakage of charge from the OPC in the absence of light over time. This is an important factor which dictates the minimum speed at which an OPC can operate (Tateishi and Hoshino, 1984). The plot in Figure 2.29 illustrates the dark decay phenomena and shows that prolonged process time has a negative effect on the surface potential.
- iii. **Photodischarge** is an indication of the time it takes to discharge a portion of the photoconductor after a charge has been generated by exposure to

light energy. This factor represents the highest speed an OPC can operate (Scharfe, 1984).

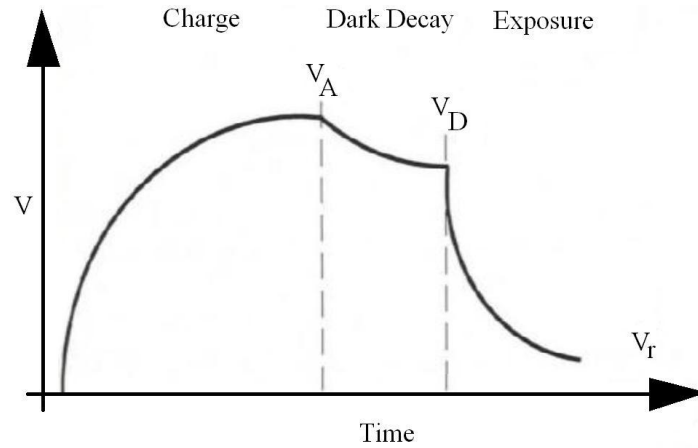


Figure 2.29 The potential difference on a photoconductor surface with respect to time, during charging, dark decay and exposure (Scharfe, 1984).

In an ideal case where an OPC exhibits no dark decay, the potential  $V$  across its surface is related to the charge density  $\sigma$  and is given by

$$\sigma = CV = \frac{\epsilon_s}{s} V \quad (2.3)$$

where  $C$  is the geometrical capacitance per unit area of the device and  $\epsilon_s$  is the dielectric permittivity of the photoreceptor layer of thickness  $s$ . To further:

$$\epsilon_s = K_s \epsilon_0 \quad (2.4)$$

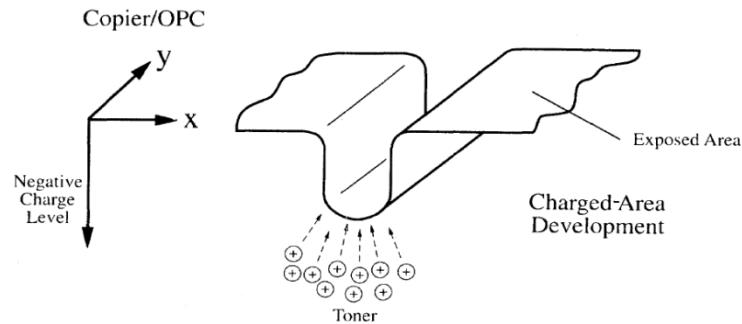
where  $K_s$  is the dielectric constant of the photoreceptor material and  $\epsilon_0$  is the permittivity of free space.

### *Develop*

The process of applying toner to the latent electrostatic image present upon the OPC following exposure is referred to as 'developing'. There are two main developing mechanisms, Charged Area Development (CAD) and Discharged-Area Development (DAD) utilised by either mono component or dual component development methods.

*Charged-Area Development*

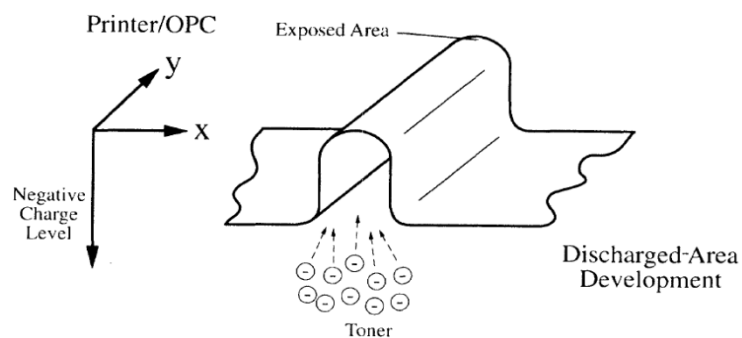
CAD requires a toner to be charged to a polarity opposite to that of the OPC. The charged toner is attracted to the portions of the OPC which remain unexposed. A graphical representation of CAD can be seen in Figure 2.30.



**Figure 2.30** A representation of the charged-area development (CAD) on a negative charge OPC. The toner particles are positively charged and are attracted to the unexposed portions of the OPC (Morita et al, 2007)

*Discharged-Area Development (DAD)*

DAD requires toner to be charged to the same potential as the OPC. The charged toner is attracted to the portions of the OPC which are exposed during exposure. DAD was primarily employed in the early years of laser printing to minimise the effects of heating through large areas of laser exposure as seen in CAD. Modern solid state diodes have all but eliminated this problem, but many laser printing systems retain the DAD architecture (Morita et al, 2007). A graphical representation of DAD can be seen in Figure 2.31.



**Figure 2.31** A representation of the discharged-area development (DAD) on a negative charge OPC. The toner particles are negatively charged and are attracted to the exposed portions of the OPC (Morita et al, 2007)





### *Powder Cloud Development*

A toner powder cloud is formed between the developer roller and the OPC with the use of either an alternating current multiplexed onto a high DC potential or air turbulence. The powder cloud allows charged toner particles to come into close proximity to the charged image present on the OPC, the image is then selectively developed through electrostatic attraction. This system relies on the tribocharging of toner within the powder cloud. Fine powders were traditionally used which allowed high resolution development but was notoriously hard to control due to high charge distributions within the powder cloud. Powder cloud development is now rarely used (Pai and Springett, 1993).

### *Contact Development*

A toner material is tribocharged within the cartridge housing through forced agitation and dynamic contact with a doctor blade (Banerjee and Wimpenny, 2006). The charged powder adheres to a charged developer roller and is brought into contact with the photo receptor where development takes place. As this process allows smaller and lighter developing systems, when compared to other methods, it is often employed within desktop printers (Pai and Springett, 1993; Samsung, 2001).

### *Dual Component Toner Development*

In contrast to the single component development system previously discussed, a dual component system employs additional carrier particles to which charged toner readily adheres. The carrier particles are a number of orders of magnitude larger than the toner and often acquire in the region of  $10^3$  toner particles per carrier (Thourson, 1972). There are two notable systems which employ dual component development, magnetic brush and cascade.

### *Magnetic Brush Development*

The general concept of magnetic brush development is the magnetic formation of brush like strands which emanate from the developer roller. The developer roller is a stator with an internally revolving magnet that pulls the toner strands with it as it turns. The brush comes into close proximity to the Charged OPC, attracting the toner

from the carrier particles to develop its latent image. There are two types of brush development, insulative (IMB) and conductive (CMB) (Folkins, 1988). Insulative development involves carrier particles that are coated with an insulating layer so that electrical contact between adjacent particles is excluded, whereas conductive brush development allows electrical contact between carrier particles. The latter was developed after the former and facilitated thicker printed layers due to the electrostatic field being transmitted further in to a developing brush by the conductive particles (Folkins, 1988).

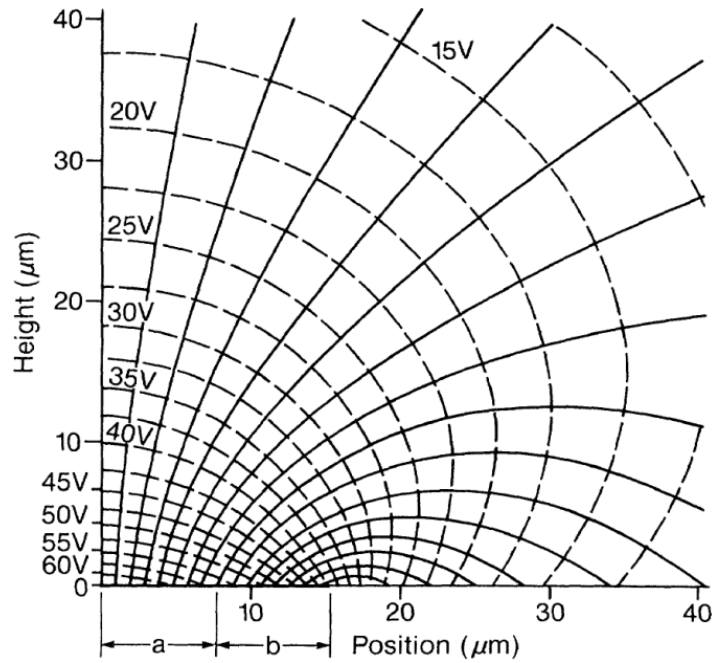
### *Cascade Development*

Cascade development utilises carrier particles to retain toner in much the same way as brush development, but the carrier particles are not chosen for their ferrous properties, rather their mass. Glass or steel carrier particles are often used as a massive particle to 'cascade' toner over the surface of a charged OPC surface. The toner is pulled from the carrier particles by the latent OPC image and the carrier particles are re-circulated. Due to powder handling issues and electric field formation, this system is rarely implemented but can form thick layers particularly on edges and lines when implemented (Thourson, 1972).

### *Development Fields*

The electric field present above a photoreceptor determines how the toner particles interact with the OPC and consequently dictate the geometry of a developed image. A surface charge created during exposure, does not necessarily create a significant electric field above the OPC. Instead, large 'solid' exposed areas retain most of their charge within the OPC layer, with only the outer edges inducing a field above the OPC surface. This phenomenon results in the development of only the fringes of a solid area, where the image boundaries abruptly change polarity (Pai and Springett, 1993). A field plot is presented in Figure 2.33 which describes the electric field on a fine printed line of 30 $\mu$ m in diameter (Neugebauer 1969; Pai and Springett, 1993). The field strength is highest where the field lines are at their most dense, highlighting the increased field formation at the edge of the line. Thourson illustrates the stark differences between solid area and line field in terms of the OPC field configuration,

OPC field strength and the resultant developed images in the absence of a development electrode, in Figure 2.34 (Thourson, 1972).



2.33 The Field pattern above a 30 micron printed line, the line represented is assumed to be of infinite length and the  $x,y,z$  origin assumed to pass through the centre of the line, thus the resultant plot is one half of the line in the  $x$  direction and symmetrical about the  $y$  axis. The  $Y$  axis represents displacement above the OPC (Neugebauer, 1969; Pai and Springett, 1993)

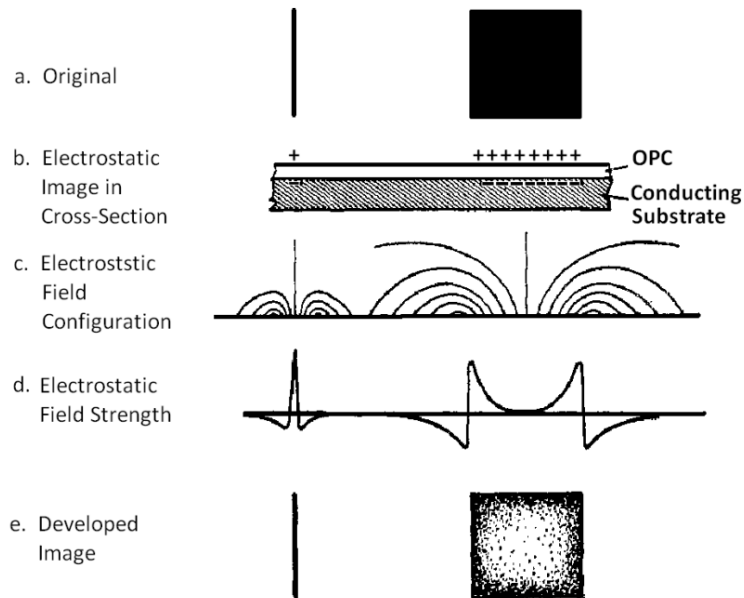
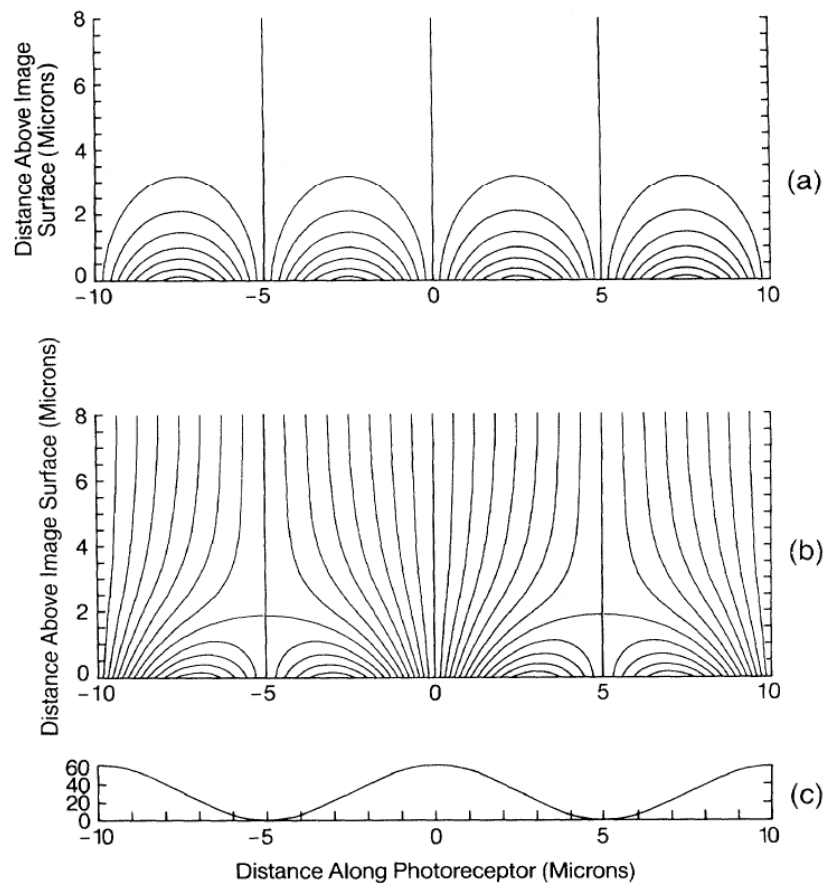


Figure 2.34 The electrostatic fringing effect generated by weak electric fields in the centre of solid black areas during electrophotographic development in the absence of a development electrode (after Thourson, 1972).

A partial solution to this problem is to place a charged development electrode in close proximity to the OPC and thereby influencing the electric field present in the centre of the image. This provides a more uniform field above the OPC, as the field lines emanating from the surface charge are shared equally between the OPC layer and space above the OPC (Scharfe, 1984; Pai and Springett, 1993). To illustrate this point Figure 2.35 illustrates a sinusoidal (line) charge pattern (2.35c) on the surface of an OPC and demonstrates the resultant field lines with (2.35b) and without (2.35a) a developing electrode. Note in the absence of a development electrode, the field lines protrude only three microns from the OPC surface and are of a higher density at the edges of the charge lines. Whereas in the presence of an electrode placed 100  $\mu\text{m}$  from the surface of the OPC, the field lines are of a more uniform density across the charge line and protrude more than 8  $\mu\text{m}$  from the OPC surface.



**Figure 2.35** Field flux lines above a photoreceptor surface charge with a sinusoidal charge pattern of 100 lines per  $\text{mm} \sim \lambda = 10 \mu\text{m}$  (a) Field flux lines in the absence of an electrode. (b) Field flux lines in the presence of a developer electrode (Pai and Springett, 1993).

Both the voltage and the spacing of the developer electrode dictate its effectiveness. Ideally the electrode would be at the same distance from the surface of the OPC as the dielectric thickness of the OPC layer and have the same voltage applied to it as to the OPC substrate. In reality however, the proximity of the developer electrode to the OPC is limited by the thickness of the toner layer or the necessary air gap needed for a given development process. Pai and Springett (1993) gave the examples of IMB and CMB development where the development electrode was the magnetic developer roller supplying the toner to the OPC. The developer rollers were typically mounted 1500  $\mu\text{m}$  from the surface of the OPC. The OPCs were typically 30  $\mu\text{m}$  in thickness with a dielectric constant of around 3. The carrier particles were assumed to be 150  $\mu\text{m}$  in diameter and in an IMB system assumed to have a dielectric constant of 6. When the carrier particles were insulated the average electric field,  $E_{ave}$ , at the air gap was given by

$$E_{ave} = \frac{V_o}{s/K_s + d/K_d} \quad (2.5)$$

Where  $s/K_s$  is the dielectric thickness of the photoconductor,  $d/K_d$  is the dielectric thickness of the photoconductor to developer roll spacing, and  $V_o$  is the initial potential on the photoconductor which is relative to the surface charge density given by equation 2.3. As the dielectric thickness of the developer electrode spacing is significantly greater than that of the OPC dielectric thickness the term  $d/K_d$  has a significant influence on the resultant average electric field. If the case of a CMB system is considered, the average dielectric thickness between OPC and developer electrode is significantly reduced. Pai and Springett assumed the dielectric thickness of the air gap between OPC and developer was equal to the toner diameter  $D$  plus a fraction ( $\sim 1/2$ ) of a carrier particles radius  $R$ . The average value of the electric field for a conducting developer can be given by

$$E_{ave} = \frac{V_o}{s/K_s + (D + R/2)} \quad (2.6)$$

As  $D + R/2 \ll d/K_d$ , the CMD developer system significantly increases the electric field above the OPC. The significance of the difference is apparent when considering that the fringe fields are essentially unaffected by the developer electrode proximity, therefore the closer the developer electrode is to the OPC, the greater the solid area development efficiency (Pai and Springett, 1993). The observed result is that IMB is better for developing line images such as letters, while CMD is better for developing solid areas (Thourson, 1972). In-depth modelling of a three layer OPC system has been performed by Kao (1973).

### *Toner*

As discussed there are two main developing methods and there are two main types of toner, single component and dual component. Dual component toners consist of small polymer toner particles typically of a median 8 micron diameter (Nakamura and Kutsuwada, 1989) dispersed within ferrous particles of significantly larger size, typically 150 microns. Single component toners can be further classified as resistive magnetic (as used in Hewlett Packard (USA) and Canon (Japan) systems) and resistive non-magnetic (used in Lexmark (USA) systems) (Banerjee and Wimpenny, 2006). For resistive magnetic toners, mixing the thermoplastic polymer with magnetic iron oxide makes the toner itself magnetic. This eliminated the need for dual component carrier bead transport in magnetic-brush development (Pai and Springett, 1993). Resistive non-magnetic toner is of similar composition as the small toner particles present within dual component toners. Two SEM micrographs in figures 2.36a and 2.36b show a single mono-component toner particle and a carrier particle from a dual component toner with attracted toner particles, respectively. Toners are typically formed from styrene co-polymers i.e. acrylates, methacrylates and butadienes with additives such as; colorants, charge control agents, flow control agents, and wax. However, dual component and magnetic mono-component toners have additional ferrous additives (Banerjee and Wimpenny, 2006). Single component toner is most common in desktop printers as it tends to be smaller and lighter due to their ability to function without heavy magnets, and can be deposited in finer layers (Pai and Springett, 1993)

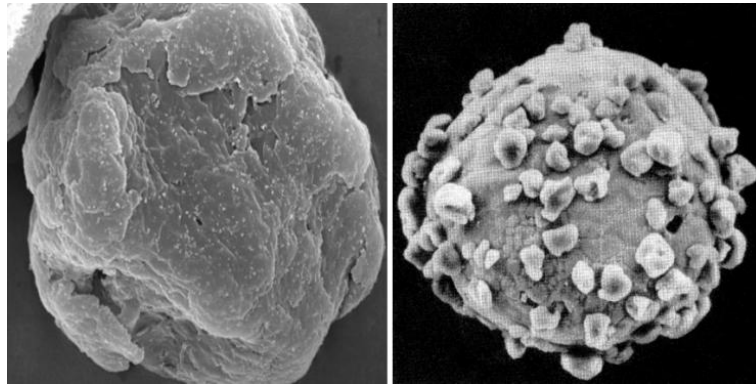


Figure 3.36a (Left) An SEM micrograph of a standard mono component toner particle (Wimpenny et al, 2009), b (right) An SEM picture of a dual component carrier particle with electrostatically adhered toner particles (Pai and Springett, 1993)

There are a number of thermal, mechanical and electrical properties a toner must exhibit in order to facilitate printing (Scharfe, 1984)

- **Thermal properties**

- ***The glass transition temperature*** ( $T_g$ ), the temperature at which the toner particles soften.
- ***Molten viscosity***, the viscosity of the toner after melting, used to predict flow characteristics during fusing.
- ***Thermal stability***, to ensure the toner does not break down when exposed to heat.

- **Electrical properties**

- ***Dielectric strength***, to determine the charge acceptance characteristics of a toner.
- ***Turboelectric response***, necessary to understand the charge generating characteristics of a material.
- ***Toner polarity***, needed to ensure image development.



- **Mechanical properties**
  - **Coefficient of friction**, the developing system has a number of moving parts and tone friction must be taken into consideration.
  - **Hardness**, abrasive materials can damage the developing system
  - **Dimensions**, of the particles are important for charge calculation and along with hardness, should be controlled to reduce abrasion. A Typical toner particle's diameter is 5 – 10 microns with a narrow distribution needed (Nakamura and Kutsuwada, 1989)
  - **Impact strength** is important for the pulverising manufacturing process.

The majority of the charge, present on a toner particle while developing, is produced through tribological charging and is a key element to the electrophotographic process. There are two types of additive used to control many of the above factors, internal and external additives.

- **Internal Additives** – Additives such as charge control agents (CCA) are internal additives, as they are introduced into the formulation for the toner material prior to particle manufacture. A CCA is used to control the polarity of the charge that the toner will take after tribological charging.
- **External Additives** – Additives such as flow control agents (FCA) pigments and waxes are external additives, as they are introduced to the toner particles as a surface coating. An FCA is a material which stops the toner from binding together and sticking to the surface of the OPC during operation.

A number of researchers have looked into developing printable materials. Trials have seen the experimentation with materials such as; HDPE, PVA, LDPE, PP, Somos 201 (an elastomeric material for SLS produced by 3D Systems (USA)) and a soluble acrylic material (Cormier et al, 2002; Banerjee and Wimpenny, 2006, 2008; Wimpenny et al, 2009). Much of the work undertaken by Banerjee and Wimpenny has been to develop new polymer materials for electrophotographic printing (Jones et al, 2010).

### **Toner charging**

The toner charge to mass ratio ( $Q/M$ ) determines the amount of toner developed and toner with a charge of the wrong polarity is known to degrade image quality (Schein, 1999). During the printing/copying process the toner powder gains charge, this can be achieved in several ways; the most widely used method being tribological charging, where by toner particles accumulate a positive or negative charge through tribological contact with an intermediate developer roller, carrier particle or doctor blade (Scharfe, 1984). The accumulated charge,  $Q$ , is a function of the capacitance,  $C$ , between the voltage,  $V$ , across the toner and charge medium

$$Q = CV \tag{2.7}$$

The resultant force  $F$ , on the particle after charging, in an electric field,  $E$ , of roller or substrate is expressed by

$$F = QE \tag{2.8}$$

In general, in the case of a solid, the charge transfer generally increases with contact area, contact roughness and velocity (Kaiser, 2006). Despite the importance of the toner charge properties, its optimisation remains empirical, with its consequent large development costs in terms of time and testing (Schein, 1999). The triboelectrical series, an example of which is shown in Table 2.37, is used as an indicator to predict the resultant bias charge after mechanical contact. The materials to the left (top) of the series tend to acquire a positive charge through loss of electrons, while materials to the right (bottom) of the series tend to acquire a negative charge through the acquisition of electrons. It is widely understood that the turboelectric series should not be used with a high degree of confidence, but should be referenced as a guide only.



Figure 2.37 An example of a turboelectric series (Iuga et al, 2005)

### *Image Transfer*

Following the powder development of an image onto the surface of an OPC, the image is transferred to a substrate or transfer belt. This transfer is facilitated through the use of either corona charging or roller charging of the substrate, or roller transfer. The charge present on the surface of the transfer substrate is of the opposite polarity to that of the toner image. The electrostatic force overcomes the adhesive force between toner and OPC and transfers the image onto the substrate (Yang and Hartmann, 1976). To optimise transfer, the correct charge-to-mass ratio must be used. In toners with a large distribution of particle size, smaller toner particles require a higher electric field to release from the OPC, resulting in transfer efficiencies down as low as 80% to 85% (Pai and Springett, 1993). This phenomenon can be overcome to a certain extent, by the use of pressure in addition to the electric field during image transfer.

### *Fusing*

There are principally five methods of fusing a toner image to a substrate: Cold pressure, Hot roll, Radiant Flash and Vapour.

**Cold fusing** uses high pressure between two rollers to force a soft toner to flow into a substrate, cold fusing methods are known for their high productivity.

**Hot roll** fusing systems are by far the most commonly used of all the fusing methods in desktop printers today (Hudson, 1963; Elter, 1984; Urban et al, 1987; Sugihara et al, 2000; Byung et al, 2008). The system uses low melt, low viscosity toners and a heated roller to fuse the powder image. Although not as productive as cold pressure fusing it is of lower cost to implement.

**Radiant heating** is often implemented through IR sources such as halogen lamps to indiscriminately heat the entire substrate, thereby thermally fusing toner and

substrate (Wimpenny et al, 2009). Flash fusing uses high intensity discharge flash lamps such as xenon flash tubes to expose the surface of a substrate to high energy fluxes. Both the radiant and flash type fusing methods work best with IR absorbing toners (dark colours) and are implemented most prominently in industrial systems due to the high cost of implementation (Pai and Springett, 1993).

**Vapour fusing** uses toner solvents to chemically 'thin' a toner allowing it to flow into a substrate. The solvents are volatile and evaporate following fusing. This system is rarely used but is useful when fixing toners that are pressure or thermally sensitive (Scharfe, 1984).

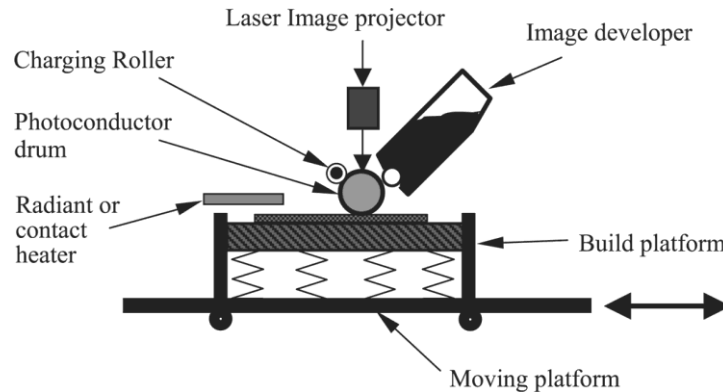
## **2.7 Electrophotographic ALM Research**

Three institutions have led the development of electrophotographic ALM systems. The available data on each of the research groups, innovations and relative ongoing research will be discussed next.

### ***2.7.1 Research Work by A.V. Kumar at the University of Florida***

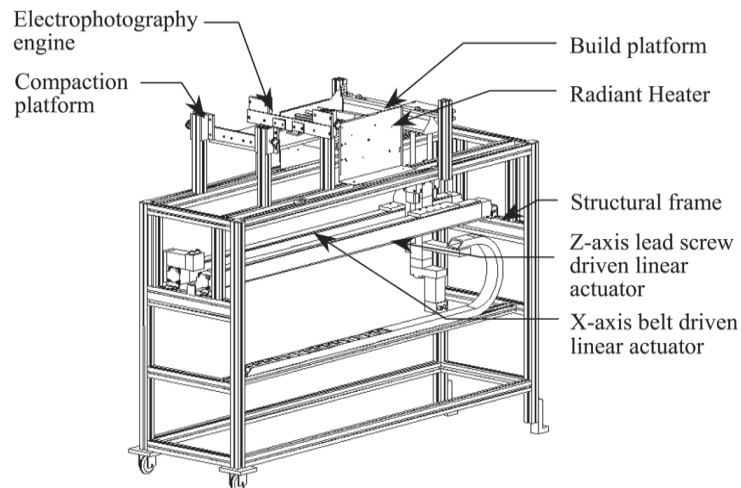
Professor Ashok Kumar of the University of Florida has led a research group developing electrophotographic ALM systems since the late nineties (Kumar, 1999; Kumar and Zhang 1999; Kumar and Dutta, 2003, 2004; Kumar et al, 2004). Their work was filed in a provisional patent in 1997 and following a market survey carried out in 1998 by the University of Florida's technology licensing office, a full patent was filed (Kumar, 1999, 2000). In the initial stages of the research, a test bed was constructed based around the electrophotographic imaging system of a Canon printer with 600 DPI resolution (Kumar and Dutta, 2003). Kumar's research was conducted using the standard toner of the Canon electrophotography unit which functioned on a two component toner system. The composition of the toner was an iron oxide carrier particle with a styrene/2-ethylhexylacrylate/butylmethacrylate/methyl methacrylate base polymer with an average particle size of 5 microns (Kumar, 1999; Kumar and Zhang, 1999). Initially the system was manual, but was later converted to use a two axes standalone controller (DMC 1200, Galil, USA) to control the movements of a build platform. The underside of the Canon printer was removed to expose the OPC roller, allowing the

build platform to pass beneath it to collect a deposited artefact layer before moving to be consolidated.



**Figure 2.38 Kumar's first electrophotographic ALM system embodiment containing a reciprocating build platform and a radiant consolidation heater (Kumar and Dutta, 2003).**

Kumar's initial embodiment, a schematic of which can be seen in Figure 2.38, describes a system working on the principal of direct deposition of toner from an OPC drum onto the surface of a build platform, which was heated to 180 – 200°C using a radiant heater (Kumar and Dutta, 2003, 2004). The resultant design for the test bed can be seen in Figure 2.39.



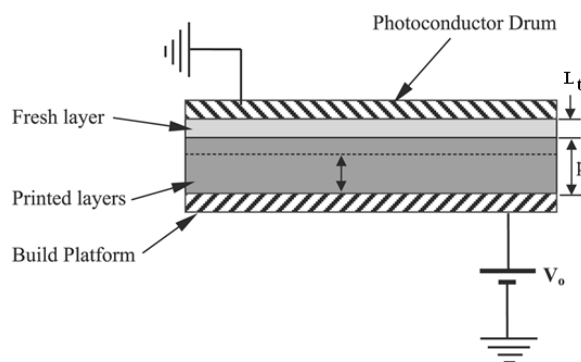
**Figure 2.39 Kumar's initial electrophotographic test bed (Kumar and Dutta, 2004)**

Initial tests were undertaken in a semi automated fashion where a layer would be printed onto the build platform, moved to fuse under a radiant heater, from which the z axis would be manually brought into contact with a compaction plate to ensure

complete consolidation. This sequence could then be manually restarted to print another layer (Kumar and Zhang, 1999; Kumar, 1999). The testing concluded with a number of findings:

### *Layer thickness*

In order to aid the transfer of the negatively charged toner from the OPC to build platform, the build platform was charged with a 1kV positive potential. This high voltage created a large electric field which subsequently ensured that the first few layers to be deposited upon the build platform were thick at around 5 – 10  $\mu\text{m}$ . After 20-30 prints the volume and therefore the layer thickness of the powder being deposited dropped sharply, resulting in printing ceasing to occur altogether after 40 to 45 prints (Kumar and Dutta, 2003). Kumar identified that the electric field experienced by the OPC was reducing exponentially as the artefact height increased. This was due to the insulating nature of the toner used. Kumar demonstrated that the field strength could be computed using a simplified model show in Figure 2.40 where the curvature of the photoconductor drum was neglected due to its large radius of curvature in comparison to the fine layer of powder present upon it. The parallel plates were assumed to be of infinite dimensions so that there were no fringe effects and so the field between the plates could be assumed to be uniform (Kumar and Dutta, 2003).



**Figure 2.40 Kumar's free body diagram defining the physical properties of use in his field strength analyses (Kumar, and Dutta, 2003).**

Assuming that a DC voltage  $V_0$  is applied to the build platform and the photoconductor is grounded, the electric field in the printed layers at a distance  $x$  from the build platform can be computed using Gauss's law,

$$E_p = \frac{\sigma_b + \rho_p x}{K_p \varepsilon_0} \quad (2.9)$$

From equation 2.9,  $\sigma_b$  is the charge per unit area at the interface of the build platform and the previously printed layers,  $\rho_p$  is the charge per unit volume in the printed toner layers,  $K_p$  is the relative permittivity of the printed layers of powder, and  $\varepsilon_0$  is the permittivity of free space. Similarly, the electric field in the fresh toner layer on the photoconductor surface is,

$$E_f = \frac{\sigma_b + \rho_p p + \rho_f (x - p)}{K_f \varepsilon_0} \quad (2.10)$$

where,  $\rho_f$  is the charge per unit volume in the fresh toner layer and  $K_f$  is the relative permittivity of the fresh toner layer. The voltage drop from the build platform to the photoconductor can be expressed as:

$$V_0 = \int_0^p E_p dx + \int_p^{p+L_t} E_f dx \quad (2.11)$$

$$V_0 = \frac{\sigma_b p}{K_p \varepsilon_0} + \frac{\rho_p p^2}{2K_p \varepsilon_0} + \frac{\sigma_b L_t}{K_f \varepsilon_0} + \frac{\rho_p p L_t}{K_f \varepsilon_0} + \frac{\rho_f L_t^2}{2K_f \varepsilon_0} \quad (2.12)$$

Solving for  $\sigma_b$  and substituting into and simplifying the electric field at the interface of the printed toner layers, the fresh toner layer is obtained as:

$$E_f = \frac{K_p}{K_f p + K_p L_t} \left[ V_0 + \frac{\rho_p p^2}{2\varepsilon_0 K_p} - \frac{\rho_f L_t^2}{2\varepsilon_0 K_f} \right] \quad (2.13)$$

As the print height  $p$  increases, the field strength  $E_f$  decreases. Figure 2.43 shows a plot of  $E_f$  as a function of  $p$  using the following values for the other parameters:

$V_0=1,000$  V,  $\varepsilon_0=8.85 \times 10^{-12}$  F/m,  $\rho_p=0$ ,  $\rho_f=-2.26$  C/m<sup>3</sup>,  $L_t=2 \times 10^{-5}$  m,  $K_f=K_p=3$ .

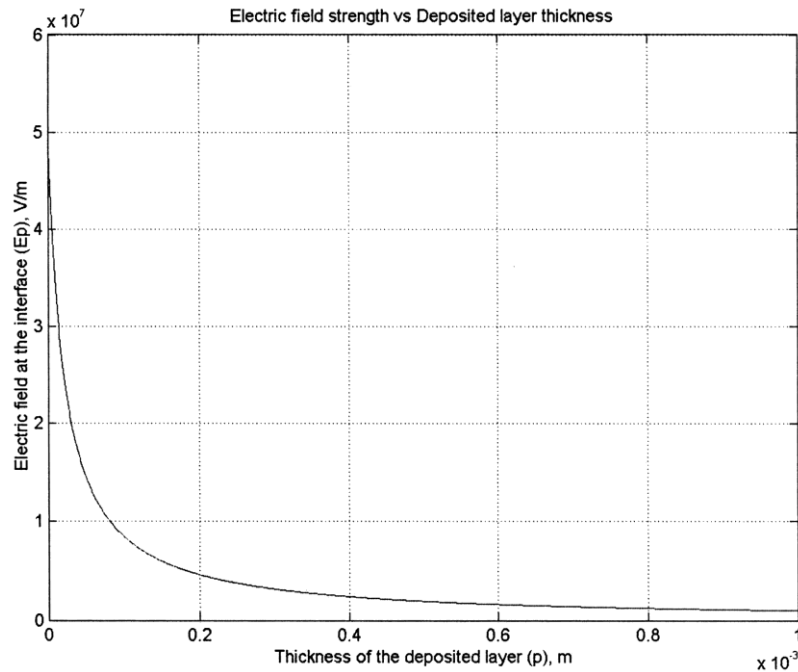


Figure 2.41 A plot of the field strength versus print height as modelled by (Kumar and Dutta, 2003).

The plot shown in Figure 2.41 shows that the field strength at the surface of a printed part reduces significantly as each progressive layer displaces it further from the build platform, the field source. Kumar suggested that the field degradation would not occur if conductive powders were used. He hypothesised that the reduction in the field strength in insulating powders could be overcome by applying a charge to the surface of the build platform via a charge applicator, allowing printing over one millimetre in height (Kumar, 1999).

### *Print Quality*

The build platform's velocity with respect to the radiant heater was controlled precisely to ensure that the powder was fully fused (Kumar et al, 2004). This method was found to produce inaccurate prints, due to the delay between IR sintering and compaction. This was because the powder had cooled and solidified, inhibiting the compaction process and resulting in an uneven surface (Kumar and Dutta, 2003). Kumar noted that on the larger of the printed artefacts, the edges or boundaries of the artefact grew faster than in the inner surface. It was concluded that the phenomenon occurred due to the non-uniform field at the boundaries of the printed image, resulting in a stronger electrostatic attraction force, and so a higher powder deposition



at the edges. A solution discussed was to use multiple materials to prevent the fringing occurring on the artefact surface (Kumar and Dutta, 2003). This however did not take into consideration that the fringing effect may well form during layer development on the OPC.

### *Test Bed MKII*

Kumar's research team took into consideration the findings of the initial trials and produced a second test bed, as shown in Figure 2.42. The developed test bed design abandoned the radiant heater and was replaced by a mica strip heater that was directly attached to the compaction platform (Kumar et al, 2004). The compaction plate was heated to 180°C and kept at this temperature during operation. Kumar found that by directly heating the compaction plate, more accurate control over the fusing temperature was possible and furthermore during the compaction any unevenness in the printed image was flattened out (Kumar and Dutta, 2003). Unsurprisingly, it was noted that simply pushing down the fringes with a heated compaction plate led to artefact bulging and distortion, as the excess material was displaced (Kumar et al, 2004). However the use of the heated compaction plate allowed the surface of the fused material to dissipate its residual charge due to the presence of current flow in the toner at its fusing temperature. This was found to be an advantage as residual charge on previously printed powder layers was reduced and therefore thicker layers could be deposited (Kumar and Dutta, 2003).

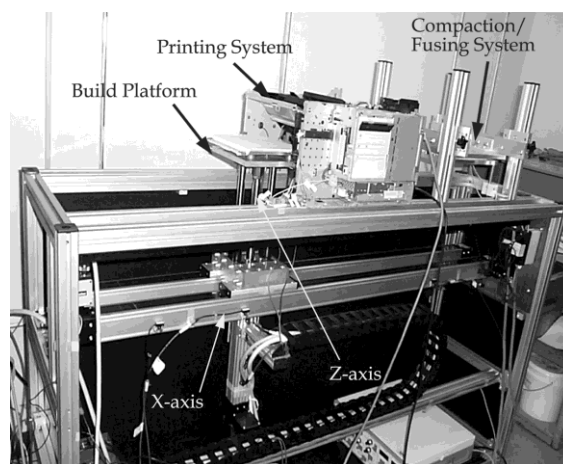


Figure 2.42 Kumar's second ALM test bed with additional mica fuser/compactor (Kumar and Dutta, 2003).

The second test bed also incorporated a means to charge the top surface of the build platform to allow printing higher than one millimetre. Kumar found that following preliminary attempts at charging the top layer, using a charge roller revealed an additional problem. During printing, the photoconductor drum came into contact with the charged surface of the build platform and acquired its positive charge. Subsequently, the charging unit was unable to uniformly charge the photoconductor as the latent charge acquired from the build platform neutralised the charge roller's potential. These neutralised areas of the photoconductor picked up powder from the image developer resulting in unwanted background printing (Kumar et al, 2004). It was hypothesised that to solve this problem it may have been necessary to employ an intermediate metallic transfer roller to allow the photoconductor drum to first print on a transfer roller and then subsequently transfer the powder to the build platform. Further tests demonstrated that using the surface charging technique, the artefact height increased up to 3mm after printing 575 layers using this charging mechanism but substantial fringing was still apparent (Kumar et al, 2004). In further testing Kumar employed the printed toner as a binder (Kumar et al, 2004). Testing involved the printing of toner powder onto an electrically conductive metallic powder bed. It was found that due to the conductive nature of the powder bed, the individual powder particles would charge and discharge rapidly by jumping between build platform and transfer roller. A ceramic powder and toner binder were then compressed and heated, with the intention that the toner would melt and wick into the powder bed acting as a binder and consolidating selected regions of the powder bed. It was found that although the powder cloud was reduced, it did not eliminate an additional effect of reverse printing from powder bed to transfer roller (Kumar et al, 2004). Kumar's research team developed a Java slicing program to produce the required artefact layer geometries and a C++ program to control the printing process (Kumar and Dutta, 2003). Kumar stated that the test bed was capable of printing up to 12 times a minute but, as the platform needed to be moved under a compaction platform for fusing, it was not possible to print continuously. The final test bed design could print approximately five times per minute at an average layer thickness of 20 microns, comparable to a build rate of 100 microns per minute, significantly slower than many

commercial ALM systems (Kumar and Dutta, 2003). It was suggested that the rate could be improved by optimising the fusing time and platform velocity. In addition, it was suggested that a larger powder particle size could be used, however this could have led to lower print resolution (Kumar et al, 2004).

From Kumar's research it was possible to draw the following conclusions:

- The voltage applied to the platform and the print gap between photoconductor, the compression pressure, the fusing time and fusing temperature all played roles in the quality of resultant printing and final artefact.
- The full productive potential of the electrophotographic process was not exploited within Kumar's research, nor was it shown to be a research objective. The use of a stop start printing process, with printing, heating and consolidation machine elements individually embodied, would have been unable to take full advantage of the productivity potential of the electrophotography process.
- It was shown that the thickest layers and the sharpest powder images were achieved with no print gap and 1kV potential difference between OPC and build platform while ensuring the velocity of the platform matched the tangential velocity of the OPC.
- While fringing was identified, no solution was demonstrated. Kumar suggested that the problem could be overcome by printing both a support material and an artefact material on to the bed simultaneously. While this may reduce the effect of fringing during transfer it does not address the issue of fringing occurring during layer development on the OPC.
- The maximum artefact height formed within the work was 3mm. The artefacts showed significant distortion in the form of fringing and bulging due to the heat plate displacing the additional fringe material.

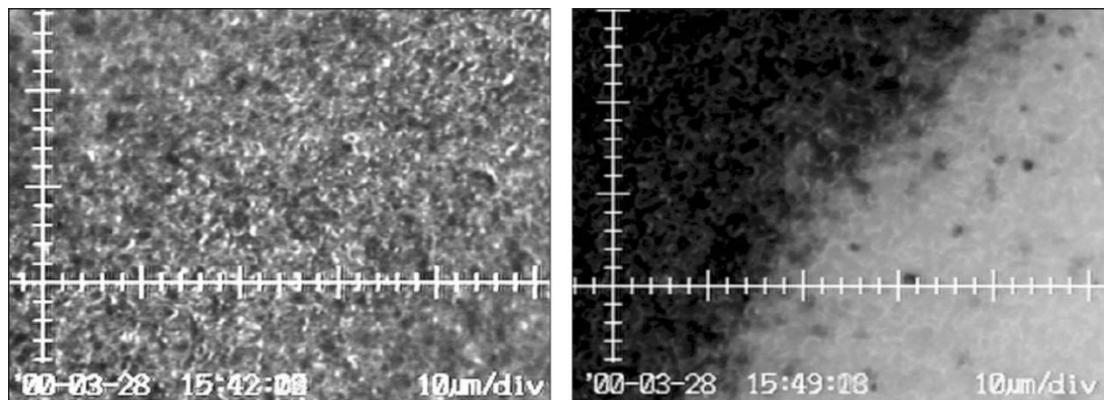
### ***2.7.2 Research Work by Cormier, North Carolina State University***

Professor Denis Cormier of North Carolina State University, in common with other researchers, Bynum (1992), Penn (1997), Kumar (1999) and Zhang (Kumar, Zhang, 1999) realised the potential of the laser printing system for use in an ALM system. Cormier collaborated with Dr Harvey West of the same institution and Professor James Taylor of the Rochester Institute of Technology, to explore the feasibility of using electrophotography to produce 3D artefacts (Cormier et al, 2002). Research initially focused on the formation of a broad concept, named '3D Laser Printing', in which selectively coloured objects were formed through the deposition of multiple layers containing a plurality of coloured polymeric materials. Printing experiments were undertaken with a HP LaserJet 4500 with the standard four, cyan, magenta, yellow and black, toner system. A polyvinyl-alcohol (PVOH) was passed through the printing system a number of times, building an artefact of 30 layers in height with an average layer thickness of 8.35 $\mu$ m (Cormier et al, 2000, 2002). Following printing, the PVOH substrate was dissolved in water to leave a 30 layer artefact. Cormier et al, were particularly interested in the colouration of 3D artefacts and found that with multiple coloured layer prints, the luminescent of a printed colour decreased. It was hypothesised that the coloured toner material was translucent and needed a white back ground in order to reflect light. This hypothesis was shown to be correct following the multiple deposition of white toner with a coloured ultimate layer (Cormier et al; 2000). In the same paper it was noted that, when investigated under a microscope, the density of monochrome areas was significantly lower than a dual colour boundary (figure 2.43). While no explanation was given for this within the paper there are possible explanations:

- i. The microscope study of the colour boundaries focused on the boundaries of two independently developed images. These two images both had significant fringe development and so when a small section was viewed under a microscope it was assumed that the high boundary densities were common across the whole image. Conversely, the monochrome image was viewed in

the centre of the image where the development forces are at their weakest and would therefore be less dense than the developed fringe.

- ii. The printer manufacturers assume that colour prints are intended to be pictures, and therefore, set the printer to increase the developer layer thickness to provide higher quality picture prints. Conversely, a monochrome print may be assumed to be text and so a thinner developer layer thickness is adopted to save toner materials.



**Figure 2.43** Left: The centre of a solid area of a monochrome print . Right: A black/yellow toner interface exhibiting a higher density than the monochrome image (Cormier et al, 2000)

The artefacts produced with standard toner were found to be brittle (Cormier et al, 2000). While the material is known to be brittle, this may also have been a factor of the printer's paper routing system. Cormier et al (2002) trailed a 10µm HDPE powder, noting that the LaserJet 4500 printed the powder without any difficulty, although no artefacts were reported to have been formed. Subsequent trials by Banerjee and Wimpenny (2006) failed to recreate the printing results using virgin HDPE powder but, when surface coated with 1-2% (by weight) of flow control additive, could generate deposition albeit of limited density. It was concluded that the HDPE used by Cormier et al must have had additional additives unknown to Cormier (Banerjee and Wimpenny, 2006). While there is no evidence of a system being produced, Cormier et al (2000) did propose that a system producing layers of an average of 8.35µm in thickness could generate a productivity of 7.014mm/hr vertical build rate. The resolution was also discussed concluding that while a 600 dpi and 1200 dpi system could produce a minimum feature size of 0.042mm and 0.021mm respectively, it was

in fact the machine capabilities which would limit possible resolution. Cormier et al, developed a broad concept which proposed to produce multicoloured artefacts through an electrophotographic ALM system. A number of hypotheses were tested including, most notably, the successful printing of HDPE; a result which to this day has only been partially recreated (Banerjee and Wimpenny, 2006). No discussion of fringe formation or Z-axis height limitation was formally entered into, most likely down to the fact that only preliminary experimentation had been undertaken and these limitations had not been identified. Fringe formation was a likely factor in an observation of a dual colour toner interface, but was not identified as such by Cormier. Future work on an automated test rig was discussed but no further publications were found referencing progress (Cormier et al, 2000, 2002).

### ***2.7.3 Research Work by Wimpenny and Banerjee De Montfort University***

Research into electrophotographic ALM at De Montfort University was headed by Professor David Wimpenny from 2004 onwards (Banerjee and Wimpenny, 2006, 2008; Wimpenny and Banerjee, 2008; Wimpenny et al 2009; Jones et al, 2010) The research was initially funded under a four and a half year, EU integrated project, called "Custom-Fit" (Wimpenny et al, 2009). The project was intended to develop new systems and materials for the production of individual customised products. The majority of the papers published by Wimpenny et al, discuss the development of Electrophotographic compatible engineering materials (Banerjee and Wimpenny, 2006, 2008; Wimpenny et al, 2009). In addition to materials development, Wimpenny and Banerjee submitted a patent highlighting hardware development undertaken at De Montfort University (GB patent 2446/386, World patent 2008/096105) which will be discussed in a forthcoming section of this review. In the first paper available, the work at De Montfort (Banerjee and Wimpenny, 2006) discussed former work demonstrating a Z-height limitation of 1-2mm (Kumar and Dutta, 2003), although it is apparent that the largest artefact actually produced in Kumar's work was 3mm in the Z-axis (Kumar and Dutta, 2004). The printing of HEDP in former research was referenced (Cormier et al, 2002) and was studied by Wimpenny et al as a baseline for further development with other engineering materials; polypropylene (PP), low density

polyethylene (LDPE), polyvinyl acetate (PVA) and a Polybutylene Terephthalate (PBT) derivative Somos 201. Initial testing with a standard magnetic toner and a HP LaserJet 4 printing system showed the standard styrene acrylic co-polymer based toner to be unsuitable for the layer manufacturing of artefacts, due to surface cracking of a plurality of deposited and fused layers (Banerjee and Wimpenny, 2006). Little information was given to the procedure by which this experiment was carried out. It would seem likely that if a substrate had been passed through a printer numerous times, in order to deposit 10 layers, surface cracking would be seen in many materials due to fatigue imposed by multiple paper routing rollers. 'Off the shelf' polymeric materials were put through a number of grinding trials. Pulverisation trials were conducted with HDPE, PP, and standard toner. A 10  $\mu\text{m}$  upper dimension limit was used to determine the effectiveness of the trials. 20% and 45% of the engineering polymers were  $\leq 10 \mu\text{m}$  whereas 80% of the standard toner was within tolerance following grinding (Banerjee and Wimpenny, 2006). This result demonstrated the brittle characteristics of the standard toner. A number of other grinding methods were trialled with engineering polymers, which also demonstrated poor grinding efficiency. A second grinding trial with a brittle material, P400 (a water soluble acrylic used for FDM support), was undertaken. Results showed that 30% of the powder produced was under the 20  $\mu\text{m}$  upper size limit after two hours of grinding. Following further grinding trials with a more efficient mill, a 60% of  $\leq 20 \mu\text{m}$  yield was achieved (Banerjee and Wimpenny, 2008). Following poor milling and grinding results, research focused on the development of toner materials from 'off the shelf' HDPE, LDPE and PP polymer powders, produced chemically (Banerjee and Wimpenny, 2006). 1-2% fumed silica (by weight) was used as a CCA and FCA as it produced a negative particle with low caking characteristics (Wimpenny et al, 2009). The trial analysed the rotational speed and geometry of the mixing apparatus in an effort to optimise coating. A 'paddle type' blade geometry was found to give a better mixing efficiency than the 'shear type' mixing blades. It was also shown that using this mixing approach, the surface of polymer particles could be evenly coated with the required additives (Banerjee and Wimpenny, 2006) The resultant coated powders plus additional prepared P400 were printed using the mono component HP LaserJet 4 and a dual

component Ricoh 7000 laser printer. The HP LaserJet4 print trials showed that while HDPE, LDPE and PP could all be printed with FCA and CCA, the resultant prints were of poor quality and density. The ability of the LaserJet 4 to print with the nonmagnetic polymers was surprising as it was assumed the printer needed a magnetic toner (Banerjee and Wimpenny, 2006). Printing with the Ricoh 7000 was undertaken with coated P400 (10%) and a blend of ferrite carrier particles (90%). The results showed that the P400 printed well but within the printed areas there were patches of less dense deposits. This was attributed to the P400 powder toner not adhering adequately to the surface of the carrier particles during processing. It was hypothesised that this may be a factor of the carrier particles' geometry (Banerjee and Wimpenny, 2008). It would also seem probable that the charge to mass ratio of the P400 particles was too low. This could have been increased through the use of P400 particles with a smaller diameter, leading to carrier particles retaining a greater number of P400 particles. Following the successful printing of a number of polymer powders, research turned to the effects of IR sintering and the amounts of FCA and CCA on the resultant strength of moulded artefacts (Banerjee and Wimpenny 2008; Wimpenny et al, 2009). The powders were compacted into moulds and sintered with IR radiation for differing lengths of time and heater displacement. Tensile test specimens of 100mm in length and 2mm in thickness were produced in Somos 201 and P400 materials, with 0%, 0.3% and 0.6% FCA coatings by weight. While no mechanical results were given for the P400, it was noted that the material did sinter with a small amount of shrinkage (Banerjee and Wimpenny, 2008). A full factorial experiment was undertaken with the Somos 201 to determine the significance of the factors; fusing time/temperature, % FCA coating by weight and Somos 201 particle size. The resultant significance of the effects can be seen in Figure 2.44, demonstrating that particle size had the largest effect on artefact strength with FCA the second most significant factor (Wimpenny et al, 2009). It was found that the longer the sinter time, the higher the peak stress (ultimate tensile stress (UTS)) and the higher the powder diameter or FCA content, the lower the UTS. While it was concluded that the factors of FCA and particle size had a significant influence on potential electrophotographic materials, the trials only analysed one FCA, one material, and one potential ALM fusing method.



While it was suggested that radiant IR was the most likely fusing apparatus to be used within an electrophotographic ALM system (Wimpenny et al, 2009), there are a number of other fusing systems which have been overlooked by this work.

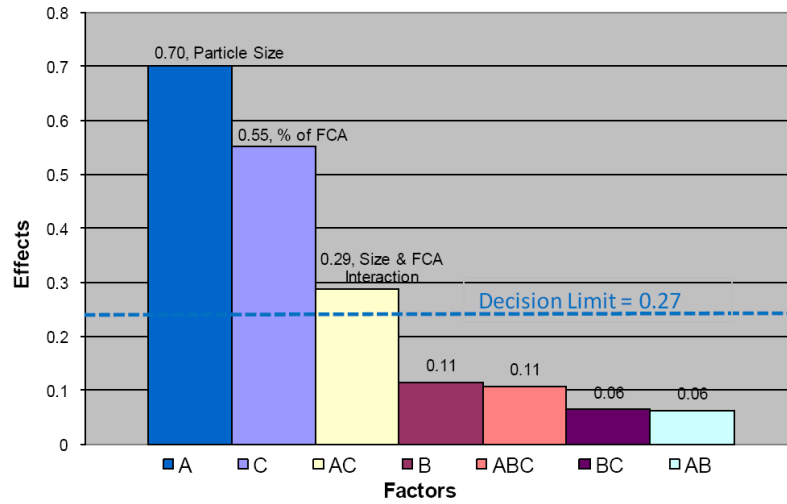


Figure 2.44 A Pareto Chart of Design of Experiments (DOE) Effects (Wimpenny et al, 2009)

An ALM system based on Wimpenny and Banerjee’s 2008 patent was used to create multilayer dog bone test specimens from 50 layers of Somos 201 with 0.5% silica additive. The specimens were printed using a large prototype Selective Laser Printing (SLP) machine developed in partnership with MTT Technologies (Figure 2.45). The system printed the samples to 0.78mm thickness through the dual component deposition and fusing with IR radiation (Jones et al, 2010). While the number of layers per sample was not explicitly disclosed, the average layer thickness was given as 11 to 12  $\mu\text{m}$ , resulting in a layer count of between 65 and 80 layers. The specimens were tensile tested and showed an average elongation at failure of 513%, which was claimed to be similar to conventional injection moulded samples, although no comparison was given. No other tensile properties were disclosed. Jones et al (2010) hypothesised that the mechanical properties of the specimens could be increased if oxidation during sintering was inhibited. The effects of printing in a vacuum of between 101.3 kPa and 2.4 kPa, and inert atmospheres of argon and nitrogen were investigated.



Figure 2.45 SLP Development Rig (Jones et al, 2010)

An HP LaserJet 1200 was used for the experiments and printed standard toner in the ASTM 2036-05 test pattern. Results in air showed that print density deteriorated with increased vacuum until 33.6kPa, after which deposition ceased. Humidity was also investigated as a variable of print quality, but was shown to have no significant effect at vacuum pressures. Testing in a nitrogen atmosphere showed only slight print density decay, whereas tests performed in argon resulted in no deposition. It was assumed that the vacuum reduced the availability of an ion source resulting in poor printing efficiency. Jones et al were surprised to find that printing took place in nitrogen as stable negative ions were rarely formed, while argon with similar ionization potential allowed no deposition to take place. An experiment was undertaken to investigate the print process whilst operating in a vacuum. A print cycle was started and then halted mid print and the OPC investigated. Results showed that the OPC remained undeveloped below 33.6 kPa. While the results showed that a vacuum and atmospheres of nitrogen and argon reduced print density or stopped deposition all together, no tests were run to evaluate print density at elevated pressures. During vacuum testing, while the OPC was checked for a developed image; the developer roller was not checked for layer formation, nor the rollers checked for correct working voltages. Whilst it was concluded that the vacuum had resulted in a reduction in ionisation potential (Jones et al, 2010), the paper did not elaborate to where ions may be needed in the HP LaserJet 1200, nor did it allude to the OPC charging device, which may have been significant.

The work by Wimpenny and Banerjee at De Montfort University has shown that:

- HDPE can be successfully printed using a magnetic component laser printer given the right size distribution and surface coatings in partial agreement with Cormier 2002 (Banerjee and Wimpenny, 2006).
- Five thermoplastic materials HDPE, LDPE, PP, Somos 201, and P400, have been shown to be a feasible future toner powder, following further testing and development (Banerjee and Wimpenny, 2006; Wimpenny and Banerjee, 2008)
- Surface coating by fused silica is required to print virgin polymers but the silica content must be controlled as it has a significant effect on the tensile strength of an IR or oven sintered Somos 201 artefact.
- The potential to combine the necessary additives by surface coating, through carefully controlled mixing, is possible under the correct conditions.
- The particle size of IR sintered Somos 201 artefacts has a significant effect on the resultant tensile strength of an artefact. With larger particles resulting in a lower UTS than smaller particles.
- Thermoplastic engineering polymers such as HDPE, LDPE and PP yield high particle size distributions using conventional milling techniques due to their poor milling efficiency.

The toner material research conducted at De Montfort shows an exciting array of possible materials viable for use in an electrostatic ALM system and although further work needs to be undertaken, the mechanical property data showed promise. The work sets out a good benchmark for further materials development such as FCA, particle size and fusing method. The mechanical apparatus designed to test the toners, as with Kumar, did not reflect the productivity potential of the electrophotographic printing system, as a stop/start routine was adopted. The papers failed to address the issues of fringing and Z-axis build height limitation as seen in previous works (Kumar and Dutta, 2003, 2004). The unusual thickness of test samples (0.78mm) (Jones et al,

2010) and not the 2mm as seen in previous papers (Banerjee and Wimpenny 2008; Wimpenny et al, 2009) suggests that Z-height might still have been an issue.

## 2.8 Electrophotographic ALM Patents

There are numerous patents based on electrophotographic printing and a significant number of patents referencing the use of electrostatics for powder control. The following section reviews those patents which explicitly discuss the use of electrophotography for use within an ALM system, or hold a significant step in technological understanding to warrant discussion. The printing of metal powders, in such patents as Karlsen (2007), although a significant feat, will not be discussed as it does not fit within the scope of this research as set out previously.

### 2.8.1 Bynum 1992 - Automated Manufacturing System Using Thin Sections

Bynum's application in 1989 was by no means the first submission of an ALM patent; (Swanson, 1977, 1980; Swanson et al, 1978, 1981; Hull, 1986) but his patent was first to reference an ALM system, based on the principal technology of electrophotographic printing. The patent disclosed a number of embodiments but most notable was the system in Figure 2.46.

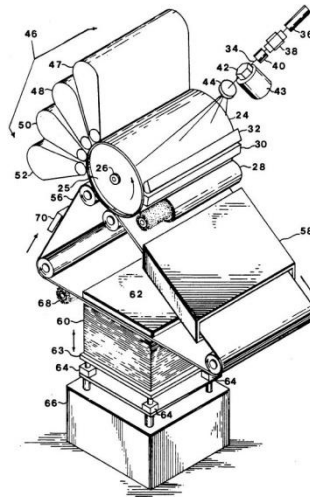


Figure 2.46 An electrophotographic ALM embodiment as proposed by Bynum (1992).

The proposed system employed a single OPC drum in contact with a means of applying a surface charge, an image forming apparatus, a number of material developers and a

transfer belt. It was suggested that the OPC be charged via corona after which any number of electromagnetic energy sources could be used to produce the latent image on its surface through selective discharge. Following the formation of the latent image, the OPC would come into contact with a powder hopper where the latent image would be developed. The cycle of charging and selectively discharging would then continue until all the desired materials had been deposited on to the OPC's surface. A charged support medium, suggested to be a Teflon belt, would then receive the plural material image, transferring it to a tackification assembly. A number of tackification methods were suggested including external heat, solvent vapour or induced heating. Following tackification, the powder image would then be transferred by the support medium to a build platform where it would be consolidated through contact with the build surface and a backing plate. A notable innovation was the suggestion of distributing metal flakes within the deposited image upon the support belt and then using inductance to tackify the entire layer. It is conceivable that the concept of only tackifying the layer present on the belt and not the top surface of the build platform may have resulted in poor adhesion. No further information or results on the implementation of any of the technology offered in Bynum's patent was uncovered during the course of this literature survey. The patent sets out the fundamentals for forthcoming patents and although apparently commercially unsuccessful, the concepts of belt transfer, interlayer plural material deposition, and tackification were all an invaluable baseline from which to develop subsequent systems.

### ***2.8.2 Penn 1997 - System, Method & Process for Fabrication of 3-Dimensional Objects by a Static Electrostatic Imaging and Lamination Device***

Penn's patent application in 1994, which failed to reference Bynum's patent issued in 1992, consisted of a number of embodiments with his preferred shown in Figure 2.47. The system uses a transfer belt suggested to be 'transparency' or Milar, which employed a number of imaging and developing assemblies along its length, producing laminate layers containing multiple materials. A key innovation in Penn's submission was the use of a dielectric belt as a latent image retainer, transposed through the use

of ionography. The latent image present on the belt was then developed with any number of materials but with the support material suggested to be a soluble wax substance such as Polyethylene Glycol. The resultant multi-powder image, continuously moving upon the endless belt, was tackified and then applied to the surface of the moving build platform in registration with the belt. The thermal energy for tackification was gained from contact with a stationary platen or roller.

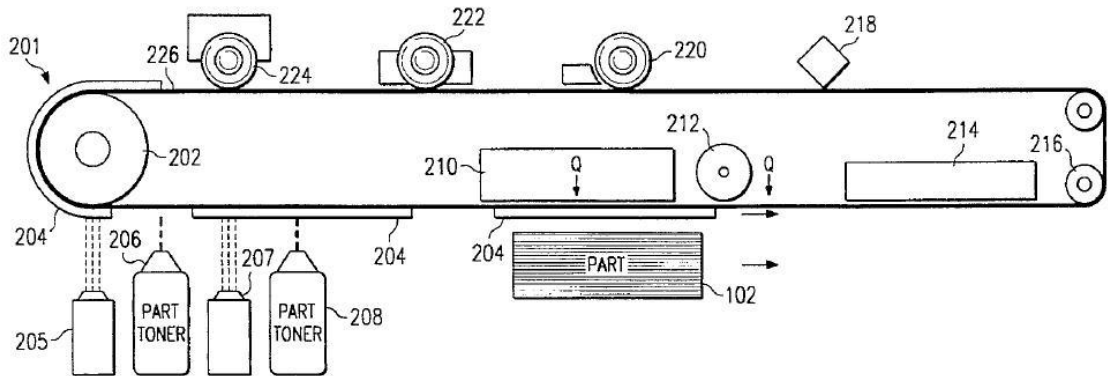


Figure 2.47 Penn's preferred embodiment of an electrostatic ALM device (Penn, 1997)

The use of an ionography type imager to form an image directly on the belt was a clear technological step, as it allowed the application of a number of new layers which could be overlapped with current layers without disturbing them. The control of the ion flow to form the image is a non-standard device and so would probably have been an issue during development. In common with Bynum's patent, the platen and belt were both moving and as such precise registration of both moving elements may have been an issue. It is noted that Penn highlights the need for at least two materials, a build and a support material, in order for the system to function. The use of low melt / soluble materials was a previously known art which Penn adopted to provide a means of removing support materials.

### **2.8.3 Kumar 2000 - Solid Freeform Fabrication Using Powder Deposition**

Kumar's patent, filed in 1998, was as a result of the work undertaken at the University of Florida as discussed in the previous chapter. The principal mechanical assemblies of Kumar's embodiments are remarkably similar to those of the two patents previously discussed. Kumar's preferred embodiment (Fig 2.48), and in common with Bynum and

Penn, consists of a transfer/support belt, an imaging means, several material deposition units, a Z-axis build platform and the necessary belt cleaning and charging apparatus.

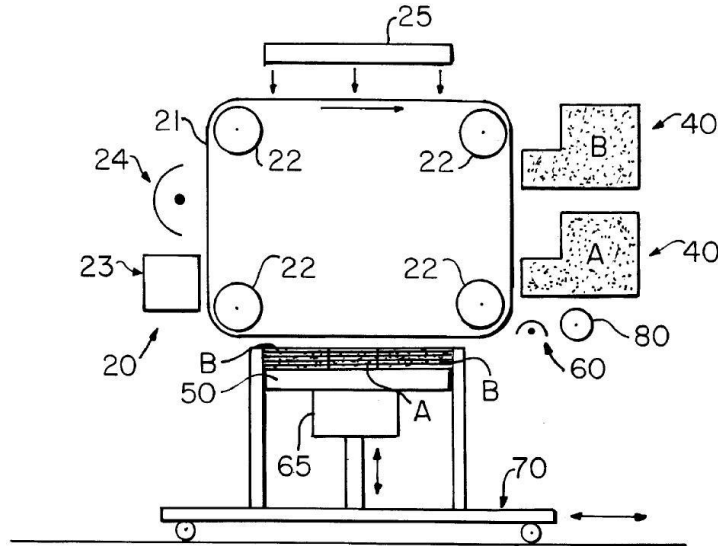


Figure 2.48 Kumar's preferred embodiment of an electrostatic ALM device (Kumar, 2000).

In contrast to previous arts, Kumar employed an OPC coated transfer belt which took a latent image by means of selective laser/LED discharge imaging apparatus. The image would then be powder developed and transferred to the build platform. Selected areas of individual layers could be comprised of individual materials, or a grade thereof, by successive latent images being developed by different powder developer units and then transferred to the build platform. Presumably because of the sensitivity of the OPC material to heat, Kumar suggested the use of electrostatic transfer of the powder image; present on the transfer belt; onto the build surface without the application of heat. In order to achieve this, Kumar suggests charging the build surface in one of two ways depending on the properties of the powders present upon the build platform:

- If electroconductive powder materials are present, a charge could be applied to the metal structure of the build platform itself, thus providing a charge on the surface of the build laminate stack by means of conductance.

- If electroinsulating powder materials are present, then a corona charging apparatus could be passed over the build platform, thus imparting a bias charge on the surface of the build laminate stack.

Again, in common with Bynum and Penn, the transfer of powder image from belt to platform was undertaken with synchronous motion of both elements. Following the transfer of a powder however, the build platform would pass under a corona charging means, and then under a heated compression roller to compact and impart green strength to the laminate stack prior to post-process sintering. The use of an OPC belt and the transfer of powder onto the build platform purely through electrostatic attraction was Kumar's unique selling point (USP). However research conducted since Kumar's patent has shown that the use of electrostatic charging alone is not sufficient to ensure either the complete transfer of powder layers or that back printing does not occur from powder bed to transfer belt, although imparted green strength should reduce this risk (Kumar and Dutta, 2003). Another of Kumar's embodiments (Fig 2.49) described the direct electrophotographic deposition of layer materials onto the surface of a build platform. The build platform would be in motion, passed beneath consolidation, charging and deposition systems. One of the issues raised in later patents referencing this system is the effect of charge transfer onto the OPC drums. As the electrostatic image on the surface of the OPC is attracted through an electrostatic potential between it and the build platform, it has the effect of leaving a latent electrostatic image on the surface of the OPC, hindering successive printing (Kumar and Dutta, 2003).

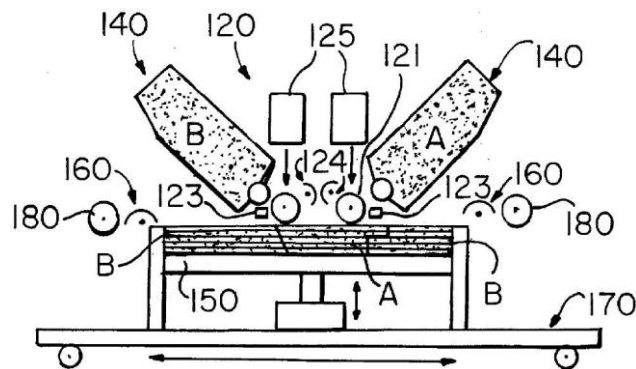


Figure 2.49 An alternative embodiment suggested by Kumar for an electrostatic ALM system (Kumar, 2000)



### 2.8.4 Grenda 2001- Apparatus of Fabricating 3 Dimensional Objects by Means of Electrophotography, Ionography or a Similar Process

As the number of patents referencing the use of electrostatic imaging within an ALM system gradually built up, the successive step changes in technology became less apparent. Grenda's patent filed in 1994 reinforced the use of ionography and tries to distance the technology from electrophotographic imaging techniques. It is also apparent that, most likely in an effort to differentiate the embodiments from previous patents, an extra intermediary belt was introduced into the system. A diagram of Grenda's preferred embodiment can be seen in Figure 2.50.

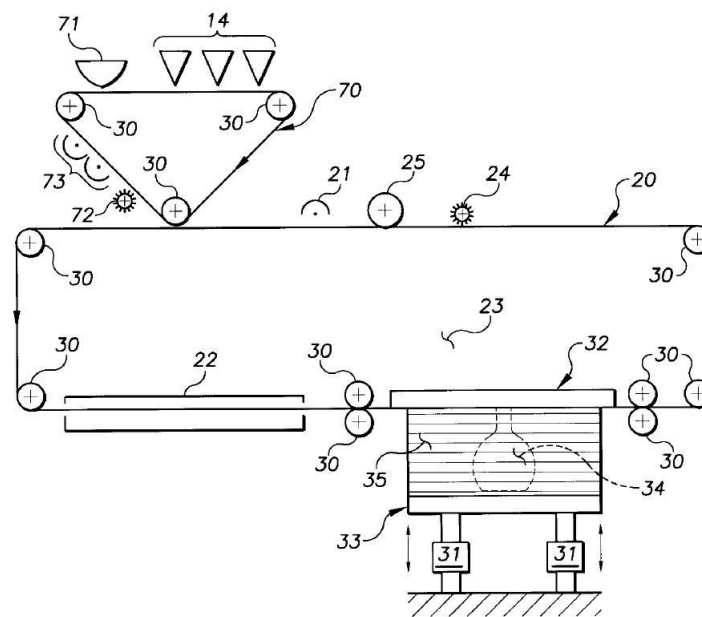


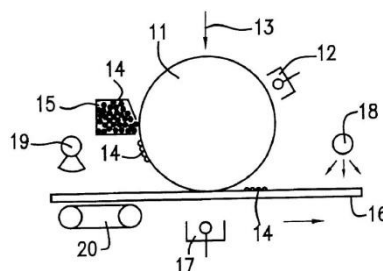
Figure 2.50 Grenda's preferred embodiment for an electrostatic based ALM system (Grenda, 2001)

The process employs a dielectric belt that revolves to produce a developed powder image through a similar process as that described in Penn's patent of 1994 (Penn, 1994). Grenda's patent deposits the powder image from the imaging belt on to the intermediary belt at which point it is transferred, tackified and consolidated as described in Bynum's patent of 1992 (Bynum, 1992). In addition to the explicit use of ionography, Grenda describes a two stage backing plate designed to consolidate laminate layers through the belt, before sliding to provide a cool surface with which to solidify the freshly consolidated layer. Although novel steps are referenced within this

patent, few seem to be of any consequence to the development of a commercial system.

### **2.8.5 Kamada, Kato 2000 - Electrophotographic Apparatus**

As discussed previously, the later patents tend to have the same functionality but with a slight difference in the system set-up to provide novelty. Kamada and Kato's electrostatic embodiment, although not strictly an ALM process, was novel in application and of specific interest within this review due to the layer alignment and consolidation techniques used. The system as shown in Figure 2.51 describes the use of an electrophotographic imaging and developing system to selectively deposit conductive material onto a ceramic substrate. The printing system employed a camera and associated software to orientate a pre-processed ceramic board so that it lined up with the printing engine for circuit track deposition. The camera assured correct alignment in the X/Y direction as well as angular alignment  $\theta$  in the horizontal plane. The powder, once deposited, was fused to the ceramic circuit board through the use of a flash lamp, as used in high-end two dimensional paper printers.



2.51 Kamada and Kato's preferred embodiment for the deposition of circuit conducting material onto a ceramic substrate (Kamada and Kato, 2000)

### **2.8.6 Zimmer, et al, 2002 - Device for Applying Decors and/or Characters on Glass, Glass Ceramics and Ceramic Products.**

In common with Kamada's et al 2000 patent, Zimmer's et al was not strictly an ALM system, but was of significant interest when considering the holistic evolution of electrophotographic ALM technology. The patent by Wimpenny (Wimpenny and Banerjee 2008), paid particular interest to this patent as it held the potential for overcoming the Z-axis limitation problem as discussed in previous chapters. The

principal in use within Zimmer's et al, patent was the use of multiple coronas mounted inside transfer and deposition rollers which not only attracted toner but also repelled it onto the surface of a substrate when necessary. The Coronas were positioned so that they imparted a bias charge on a conductive roller which, due to the potential difference between roller and toner, attracted toner from an OPC imager/ developer unit. The toner was then brought into contact with the pre corona-charge substrate to be printed upon, where transfer of toner from roller to substrate occurred. To aid the transfer of toner to the substrate, the transfer roller would be given a charge, via corona, equal to that of the toner, thus repelling it onto the surface of the substrate. The toner present on the surface of the substrate was fused into the surface of the glass.

### ***2.8.7 Liu, Jang 2002, 2004 - Layer Manufacturing Using Electrostatic Imaging and Lamination***

Until Liu and Jang's patent submission of 2001, all electrophotographic based ALM systems had used electrostatics to transport build and support materials onto a build platform where they were consolidated to form a three dimensional artefact. Liu and Jang however suggest that in one embodiment (Fig 2.52) the electrostatic system functioning with an OPC coated belt and image projection system, would transport developed powder images to a powder bed. Once made tacky, the powder image would be deposited onto the surface of the powder bed, where upon further heating, would allow the printed image to infiltrate, acting as a binder to consolidate selected areas of the powder bed. Following the consolidation/binding of a single layer, the bed would index down one layer, where a virgin layer of powder would be spread, with a perforated dispensing roller, ready for the next binder infiltration.

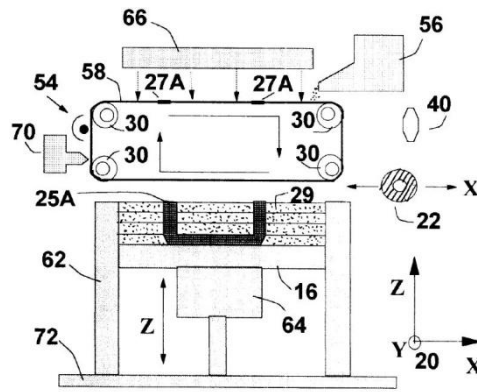


Figure 2.52 Liu and Jang’s preferred embodiment of an ALM process employing electrophotography to print binder into a powder bed (Liu and Jang, 2002)

The second embodiment employs the same process as discussed except that it uses a charge array to produce and develop a powder image. The charge array (fig 2.53) is a large capacitive array which selectively activates individual capacitive pixels in order to form an image. The pixel formation represents the cross section of an artefact which is then deposited into the powder bed by changing the polarity of the capacitive pixels to repel the attracted binder powder image.

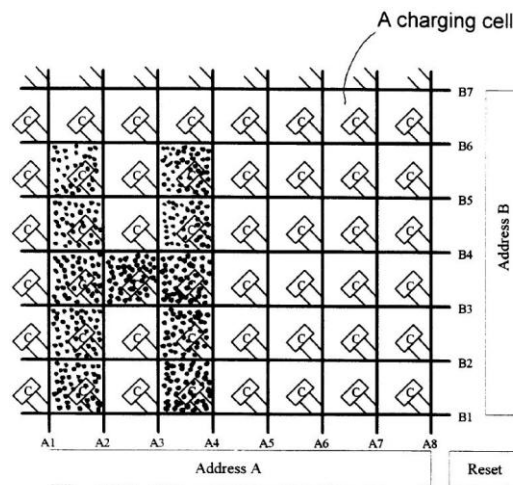


Figure 2.53 Liu and Jang’s novel capacitive charge array offered as part of an ALM process (Liu and Jang, 2004)

The novel concept of capacitive charge arrays to form powder layers demonstrates great flexibility in the powders that are able to be used within an ALM system. The exact design of an array and its function are theoretically sound but the implementation may be somewhat harder to practically achieve.

### ***2.8.8 Wimpenny, Banerjee 2008 - Electrostatic Printing Method and its Use in Rapid Prototyping***

A product of this research was a process based on the electrostatic deposition of polymer powders called Plastic Powder Printing (PPP). The process selectively deposited thermo-plastic polymer powders which were then fused with an infrared thermal source. The commercial development of the PPP process was later renamed Selective Laser Printing. Following this, much published work referenced the ongoing development of new materials for use in electrostatic printing systems (Banerjee and Wimpenny, 2006, 2008; Wimpenny et al, 2009). Wimpenny and Banerjee's filing of a world patent in 2007 is the most up to date patent with regard to the use of electrostatic printing in an ALM system. When patenting a niche technology, which for the most part has already been well patented, it is often difficult to find new innovations. With this in mind, Wimpenny and Banerjee's patent covers a large amount of work which, as noted by the patent examiner, for any one claim struggles to stand up in its own right as a technological innovation in respect to previous works. The system comprises of an electrophotographic, ionographic or magnographic imaging system which develops a real image on its surface before electrostatically transferring it onto an intermediary transfer belt. The powder image on the surface of the intermediary transfer belt is then brought into dynamic vibrational contact with a pre-heated/tackified build platform, and through the application of a repulsion charge, pressure and the aforementioned mechanical vibration, the powder image is transferred and consolidated. The dynamic mechanical force applied was that of low amplitude, ultrasound frequency, assisting the transfer and consolidation of powder. An additional sintering means was mounted close to the transfer system allowing the build powder to be deposited on the build platform which would then move into contact with the further sintering means. The patent goes on to list the possible ways that two laminate layers could conceivably be fixed together including the relevant technologies of LOM and SLS. There are a large number of further claims, the vast number of which do not belong to an exemplified embodiment, which seem to add little value to the ALM system suggested. The aided ultrasonic transfer of powders and

the hybridization of fusing technologies with the suggested ALM embodiment are of interest.

### ***2.8.9 Discussion and Conclusion of the Patent Survey***

The numerous patents showing the development of ALM systems starting in the late 1980's on to the present day have shown that, while there are number of technological concepts, there are still significant barriers to overcome before a commercial product could be produced. The tables 2.6a and 2.6b list the key claims and innovations of each of the patents discussed. Large innovative steps were seen with the first patents, and with each additional patent produced, in general, there was a dilution of overall novelty. The implications of the patents to the development of a new desktop system would not be fully understood until the conceptual testing had taken place. It is apparent that there were two areas that had not been fully disclosed:

All of the thermal consolidation means within these patents have either been, stationary with the build platform moving relative to them, or both the thermal consolidation and the build platform have been stationary in the X/Y plane and brought into contact in the Z direction. This would allow for the conceptualisation of an alternative thermal consolidation means such as a moving thermal roller.

Three out of the five direct artefact printing electrophotographic ALM patents (those that constructed artefacts using electrostatic means to deposit build materials not binders) used moving build surfaces which, in order to function accurately, have to seamlessly line up with the deposition means or risk inaccurate layer placement. It is also conceivable that models of significant mass would severely limit the speed at which the system could operate due to the inertia of the build platform. Those patents which did not employ a moving build platform instead used staggered printing, where individual layers would be printed one at a time with a pause in printing between consolidation cycles. As the laser printing system's productivity is best utilised with continuous printing, the innovation of a system with a belt accumulator is apparent. The accumulator would allow the continuous printing of layers while also facilitating the intermittent pausing of the belt for consolidation.

The use of the aforementioned points may help with the elimination of a Z-axis height limitation, and the problem of artefact fringing in previous works, by providing a mechanical transfer means between a transfer belt and build platform. The increase productivity from continuous printing could also maintain a relatively high temperature within the part built artefact thus aiding tackified transfer. It is also worth noting that all the patented processes occur in a room temperature atmosphere. In addition there is the option to elevate the surrounding atmosphere temperature local to the build platform and consolidation means, in order to aid mechanical tackified transfer.

Patent Filed / Number	Novel Claims Referencing Electrostatic Deposition	Innovative Technological Step	Status of Patent
Bynum 16/08/1989 5088047	1 The use of OPC to electrostatically form a powder image, forming a physical lamina.	Using an electromagnetic energy source to selectively discharge an OPC with the intention of creating an artefact layer from thermo plastic.	Expired
	2 The use of an intermediate support medium for the transfer of said powder lamina.	A support medium in the form of a PTFE belt used to transfer artefact layers and support material to the build surface	
	3 The use of a plurality of powders to form a physical lamina of a number of material properties.	The use of a number of powders to produce a graded artefact exhibiting a number of material properties and to provide support. The use of metallic flakes to enable inductance heating.	
	4 A method to tackify said powder lamina whilst on the support medium.	A method by which each powder layer is tackified on the surface of the support medium prior to consolidation. Tackification through thermal irradiance, solvents, or inductance.	
Penn 09/11/1994 5593531	1 The selective charging of a non photoreactive belt to form two separate images of the attraction of artefact and support layers in a single pass.	The use of a transparency or Milar continuous belt to hold an electrostatic latent charge which is developed on the belt by means of an electrostatic developer.	Current Until 2014
	2 The transfer of thermally tackified powders to the build surface via an endless belt where upon it is fused through thermal means onto a moving platen.	The use of a heat platen or roller to takify the powder present on the surface of the support medium to facilitate transfer which is effected through thermal contact.	
Kumar 11/12/1998 6066285	1 The use of a continuous photoreactive belt, with associated charging, powder deposition and cleaning points.	A belt coated with an OPC material designed to be continuously rotated while being selectively discharged to form a latent image. The image is then powder developed directly onto the surface of the belt.	Current Until 2018
	2 The use of a thermal compaction roller to impart 'green' strength into a part prior to post processing.	The use of a thermal means, specifically a "heat roller", to provide green strength to each deposited layer after deposition has taken place.	
	3 A method of artefact lamina powder image transfer via electrostatic attraction to the build platform by surface charging or conductive charging.	The use of a coroner discharge to charge the surface of a nonconductive build surface or the application of a charge to the base of the build platform for conductive builds to assist layer transfer.	

Table 2.6a The relevant claims and associated innovation of notable ALM based electrostatic patents.



Grenda 31/03/1994 6206672	1	The use of an intermediary dielectric belt, to which a latent image is applied before powder development, and propulsion of powder image on the surface of a transfer belt.	An intermediary belt was employed to produce an artefact and support material cross section before electrostatically propelling the resultant powder image on to the surface of a velocity registered transfer belt.	Lapsed
	2	The use of ionography in addition to the use of electrophotography to form a latent image on the surface of an intermediary belt.	A method by which latent images were transferred to an intermediary belt through direct ionography or indirect electrophotography and subsequently powder developed.	
	3	The use of a consolidation platen consisting of a heated side and a cool side which was to be combined, through the belt, with pressure from a solenoid.	The use of a consolidation plate with both a heated and cooled portion, allowed through transfer belt consolidation and cooling of sequential powder layers.	
Kamanda et al. 18/03/1999 6157789	1	The use of a circuit pattern forming position recognising camera, for detecting a circuit pattern forming position on a ceramic substrate.	The use of a camera to position a ceramic substrate in the X,Y and $\theta$ planes, to which a circuit forming powder would be printed.	Current Until 2019
	2	The fusing of circuit forming powders through the implementation of a flash lamp.	The electroconductive powder material is consolidated via irradiated energy obtained from a flash lamp. The details of the flash lamp, including its operation, are not disclosed within the patent	
Zimmer et al 21/08/1999 6487386	1	The use of multiple coronas to control the addition of a developed powder image to a substrate.	A number of coronas affected the transport of powder from developer roller, to intermediary and finally using a corona sharing the same charge as the powder image to repel it onto a substrate.	Current Until 2019
Liu et al. 17/01/2001 6376148 B1 6780368 B2	1	The use of electrostatic imaging to print a binder material into a powder bed.	The use of electrophotography to transfer binder into a material bed. The binder can take any dry form including photoactive polymers which are cured or fused by electromagnetic energy.	Current Until 2021
	2	The use of a capacitive array to electrostatically form a binder layer with respect to the geometry of an artefact's layer slice data.	The uses of an individually addressable capacitor array which can be either positively or negatively charged to develop a powder image and then transfer the image into a powder bed.	
Wimpenny et al. 06/02/2007 GB2446386 /WO096105	1	The transfer of a real image assisted by the forced vibration of the photoconductor carrier, preferably at ultrasonic frequencies.	The use of mechanical vibration to aid the transfer of powder images from one substrate to another.	Current Until 2027
	2	The hybridisation of the 3D electrostatic deposition system with that of a selective laser sintering ALM system.	The use of SLS technology to selectively sinter graded materials deposited by electrostatic means.	

**Table 2.6b The relevant claims and associated innovation of notable ALM based electrostatic patents.**

## **2.9 A Review of Technologies Relevant to the Thermal Contact Fusing**

Thermal consolidation of polymer powders in commercial layer manufacturing processes is achieved through focused radiation sintering, using a scanning laser or focused incandescent light source. An example of this is SLS (3D Systems, USA) and the commercially unsuccessful Desk Top Factory (3D Systems, USA) using a laser and halogen light source respectively. Simply, a focused energy spot locally heats a bed of polymer powder giving rise to the formation and growth of necks between the particles (Gusarov et al, 2003) thus creating a bound porous structure. To date there are no commercial layer manufacturing processes which employ direct contact thermal consolidation of polymer powders. This section will investigate the current literature on and surrounding direct contact thermal consolidation with a view to developing a novel consolidation system for use in desktop ALM.

### *Prior Art*

In one embodiment of LOM a 'warm' heated plate or roller is used to activate a heat sensitive adhesive laminated between sequential layers of material (Helisis, 2005). The process environment is maintained at an elevated temperature but just below that of the activation temperature of the adhesive, minimizing the contact time of any heat activation plate/roller, by reducing the energy addition needed to raise the temperature of a layer to the adhesive activation temperature. Although adhesive bonding of laminates is not in the spirit of this research, it is useful to mention as the concept of hot plates/rollers could be a transferable technology. There are several patents disclosing un-commercialised LM processes which reference the use of a heat plate to consolidate polymer powders. One such patent is that of the previously discussed Grenda (1994), where a photoelectrostatic powder deposition system employs a large heated plate to compress and consolidate powdered material. The heat plate then slides out of contact to allow a cooling plate to engage the newly consolidated material, thus speeding up the deposition process. There are many patents on the subject of heated "fixing" rollers for printing applications. One of the earliest of such patents is Frederick W. Hudson's filed in 1963 (Hudson, 1963). Hudson's patent describes the "improvements in heat fusing devices and, particularly,

to improved apparatus for the fixing of xerographic powder images” namely a heated roller. Hudson, for the first time, disclosed the concept of using a PTFE coated roller to minimise the effects of tackified toner adhesion. Previously toner would be liquefied due to contact with a heated fixing plate, adhering itself to the fixing plate where it would leave unwanted residue on further copies. Figure 2.54 details Hudson’s concept and highlights a resistive heater coil mounted inside a quartz tube.

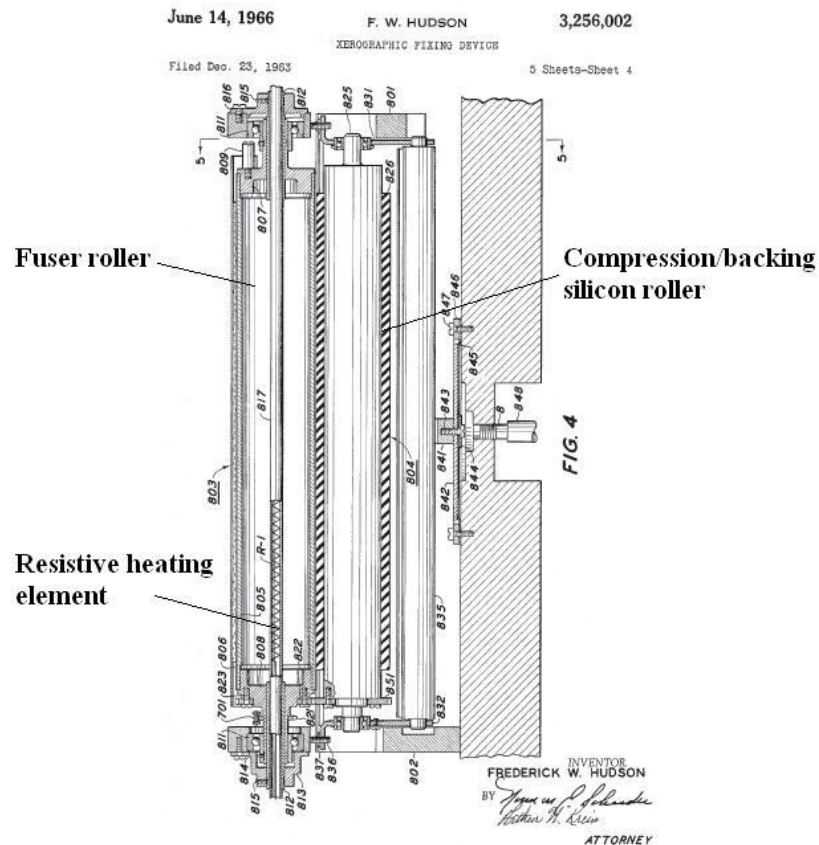


Figure 2.54 A patent illustration depicting the heat fusion roller in F.W.Hudsons patent (Hudson, 1963)

Hudson’s design was the first of the rotary fixers. Principally, there was no declared provision to neither measure nor regulate the temperature of the roller other than switching the resistive heater on or off. The fuser roller employs not only a non-stick PTFE coating but also the addition of a silicon oil to prevent tackified toner adhesion and retention. In modern printers this would be an unlikely proposition, due to oil residue left on copies and the extra consumables necessary for the printer to function.

Some years later in 1984 Elter's patent discloses a thermal control system for the monitoring and management of the heated fuser rolls for a Xerox photocopying machine (figure 2.55) (Elter, 1984).

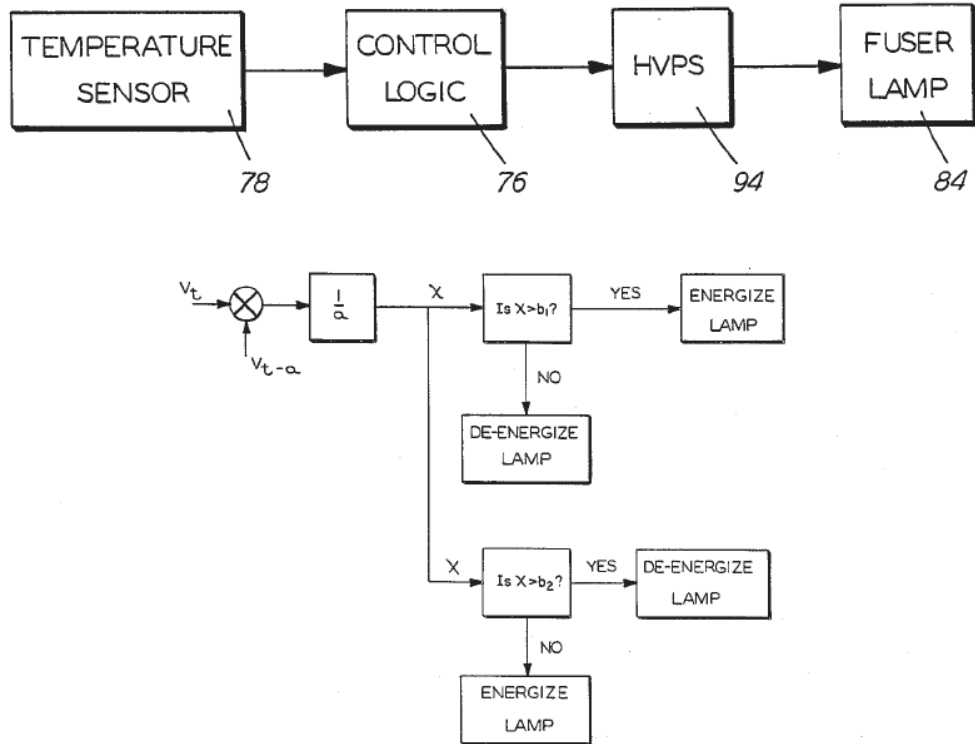


Figure 2.55 A schematic of Elter's roller temperature control system (Elter, 1984).

Along with the addition of the surface temperature control, the system employed an incandescent lamp as a heat source. This allowed the roller to be hollow and therefore of a lower mass, heated by absorbed infrared energy, as opposed to conduction as Hudson suggested. Elter's disclosed concept had all the elements necessary to make a low-cost heated roller system. Other concepts are suggested: US patent number 4,810,858, disclosed by Urban et al in 1987 introduced the idea of a fixing roller with a thin resistance heater film near the surface (Figure 2.56) (Urban et al, 1987).

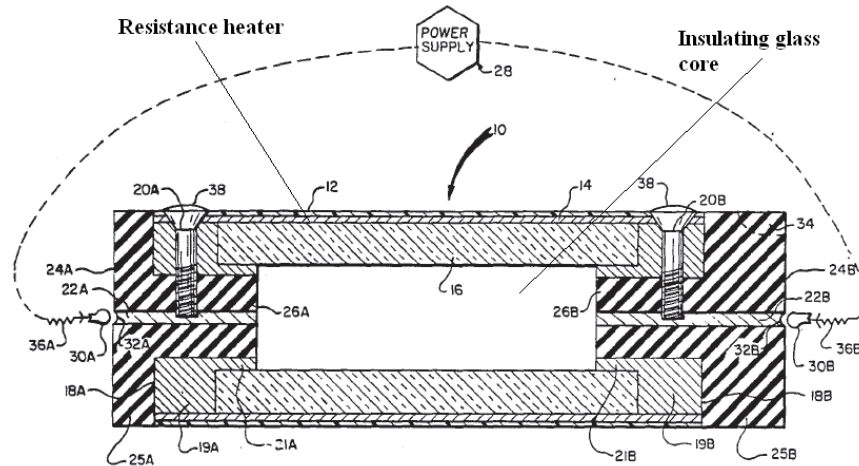


Figure 2.56 A resistance heater on the surface of a fixing roller (Urban et al, 1987)

Although the surface resistance heater may have been designed to improve efficiency, due to a lower thermal inertia as the roller was not heating up from the inside, the advantage is lost through roller complexity. The manufacturing process would have been significantly more involved and the overall performance may not have been optimised due to lack of conformal heating. Ultimately, the mass of the roller would seem to be substantially higher than that of a hollow tube with an incandescent lamp running through the centre. The idea of an incandescent lamp heated roller was taken a step further in 2000, when Sugihara et al (2000) used the principal of the original incandescent lamp and tube system but filled the lamp with highly heat conductive gas and made the roller substantially thinner. This innovation allowed for quicker warm up times and therefore greater efficiency (figure 2.55).

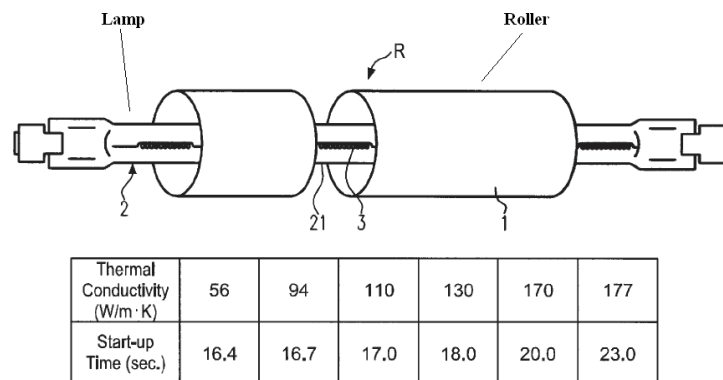


Figure 2.57 Heat roller and thermal conductivity/heat up time of fixer roller comparison chart (Sugihara, 2000)

More recently researchers have been investigating roller technology for the textile industry, where textile materials are coated with thermoplastic polymers using heated rollers. Conventional heated rollers can have surface temperature profiles up to  $10^{\circ}\text{C}$  deviations, which can cause listing in fabrics (Byung et al, 2008). The solution suggested by Byung et al is to have an oil-filled steel roller (Fig 2.56) which has independently monitored and controllable heating zones, thus insuring conformal heating and a minimal surface temperature profile (Ji et al, 2008). While this Idea may be suitable for the textile industry, for a cost effective ALM machine it may be too costly, especially as it may be the case that a deviation of  $10^{\circ}\text{C}$  across the surface of the roller has a limited impact on the consolidation of a powder layer.

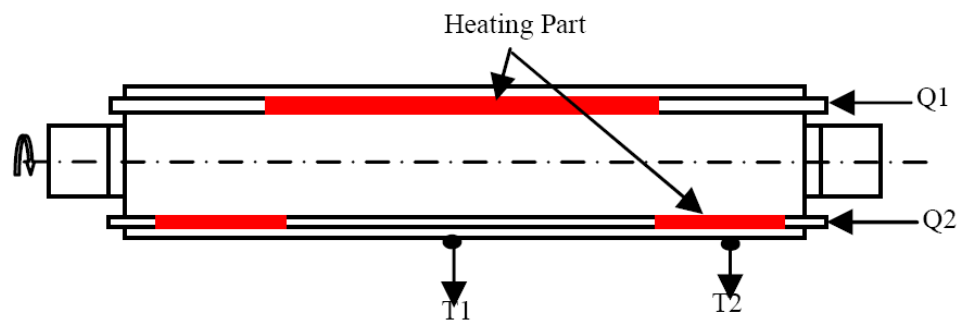


Figure 2.58 A Multizone heated roller (Byung et al, 2008)

### *Heated Rollers in ALM*

As discussed at the start of this section there is currently no direct thermal contact commercial ALM system on the market. From the literature it can be summarised that there are four main design issues:

- Means of heating, e.g. resistive contact or incandescent irradiance.
- Thermal monitoring and max temperature control, e.g. resistive temperature device (RTD), thermocouple, thermister.
- Mass and shape of the system, i.e. what shape will the consolidation apparatus take: cylindrical or flat plate?

- Thermal inertia, i.e. how long will the system take to heat up and will it offer conformal heating?

Solutions to the design problems can only be offered with further testing however the research offers a foundation from which a system specific consolidation solution, based on direct thermal contact heating, can be designed.

### **2.10 Literature Survey Conclusions.**

The conclusions drawn from this survey are offered in the form of a requirement brief which highlights the implications of existing technology on the design and conceptualisation of a new system. The purpose of the brief is to set out a general framework by which a desktop electrophotographic ALM system can be designed and by doing so highlights the research gap. This section will lead into the conceptualisation of a system, formed in the next chapter, ensuring novelty by building on the findings of this survey.

#### *Embodiment*

*Mass and Dimensions* - The review of 3D printers, so called because of their comparable size to standard 2D desktop printers, has shown that while a number of system providers claim to offer 'desktop' systems, the majority are far from desktop in dimensions and weight. The introduction to this review set out a standard by which a desktop system could be measured. It was apparent however, that the majority of 'desktop' systems reviewed did not comply. Any novel system developed within this work should be designed to comply with the formed standard as laid out in Table 2.4.

*Function* - It has been shown that the majority of ALM utilised by the current market was for form / fit prototyping. Most of the 3D printers currently available are designed for the prototype manufacturing or model making markets. The design of a new system should look to provide an ALM system for use in the prototype and model making market, while providing suitable artefact properties to enable the system to produce functional artefacts as required.



*Build Volume* - The build volumes of the smaller systems are by definition restricted by the overall volume of the system. It is generally accepted that a 3D printer provides a smaller build volume than an industrial ALM system. The build volume in a new system should represent the largest proportion of the overall machine volume possible. Build volumes of existing 3D printers such as 3D Systems' Vflash, Objet's Objet30, and Stratasys' Uprint should be used as a reference. Most desktop laser printers are designed to print upon a substrate of A4 (219x297mm) in size. It would therefore be intuitive to take advantage of the full printable area.

*Power and Utility Requirements* - Many of the industrial ALM systems require a three-phase power supply with large power ratings, for example 3D Systems' iPro 9000XL requires a 12kW supply. UK plugged appliances are restricted to around 3kW due to the current capacity of a 13 Amp fused plug. In addition to this, a number of systems need additional utilities such as water supply and access to a drain. A new system should only employ technology that allows it to function within the normal power parameters of a plugged appliance, and should not need access to any other utilities, allowing it to be installed within an office environment.

*Environment* - Historically, electrophotographic systems have been known for their high Ozone and nitrogen oxide release, resulting in unpleasant odours and the potential for environmental damage. Some industrial ALM systems require good ventilation and have cooling surfaces which require adequate air flow. A new electrophotographic system should minimise the release of corona generated products and toner based particles, while requiring no special ventilation provisions above that of a standard home, school or office setting.

### *Process*

*Productivity* - A key factor in the advertising campaigns of a number of the 3D printer manufactures is build speed, e.g. "5x-10x faster than all other technologies" (Z-Corporation's website referring to its Z-printers), "High speed printing" (Objet's online sales literature referring to its Connex system) and "2x faster than other rapid prototyping machines" (advertising literature for Envisiontec's Ultra system).



Productivity however is not just build speed; it is also dependent on the post-process time. The Z-printer produced by Z- Corporation is known for its productivity, a new system should equal or better the  $0.0012\text{m}^3/\text{hour}$  currently offered. Two dimensional printers have a 'first page out' Key Performance Indicator (KPI), a measure of the time between issuing the printer with print data and the first page of that data to be printed. As desktop systems are developed and offer higher productivities, a characterisation of systems based on this KPI may be used. Currently the Uprint FDM systems have the longest warm up period of the 3D printers of 20 minutes, while other systems such as the Zbuilder require cleaning pre and post-process. There should be minimal warm up time on a new ALM system, as a warm up time of 20 minutes in a highly productive system, could be a significant proportional increase in production time.

*Artefact Aesthetics* – Although the material properties of an artefact have been shown to be closely linked with layer thickness, a strong correlation between layer thickness and surface finish also exist. Additional variables such as layer alignment, layer dimensional accuracy and overall repeatability, also have an impact on surface quality. The leading ALM systems are able to achieve 0.1% dimensional accuracy over their build volume, a layer thickness down to 0.028mm with a corresponding surface finish down to  $0.1\mu$ ,  $2.2\mu$ ,  $10\mu\text{m}$  (Ra) in the horizontal, vertical and  $45^\circ$  (X/Z) directions respectively. The design for a new system should reference these values as a surface finish target through the control of the aforementioned variables. Both Kumar and Wimpenny discussed the limitations of electrostatic deposition in the Z-axis, with a maximum part thickness of 3mm demonstrated. Electrostatic solutions were explored, resulting in no complete solution. In addition to this, fringing occurred during electrostatic transfer due to an incoherent electric field across the build surface around the artefact edges. A new electrophotographic system should look to explore mechanical transfer to eliminate both the z-axis build limitation and the fringing phenomena.

*Materials* - While the materials and processes of 3D printers differ, there is a common representation of their artefact mechanical properties, expressed as the qualitative

'durability factor'. This inherent characterisation of 3D printers comes as artefacts produced, generally exhibit poor measurable mechanical properties such as, young's modulus, UTS and flexural modulus. At the high-end of the market, users of the 3D systems SLS machine produce artefacts with 82% of the tensile strength of the raw material. The materials that a new system should accommodate should typically exhibit comparable mechanical properties to those offered by SLS. The work by Wimpenny and Banerjee suggested that materials with comparable properties to those used in SLS could be printed. The highest resolution systems, including a number of 3D printers, use toxic photoreactive polymers. It is conceivable that for a desktop system, which would be used in the home and schools, an inherently toxic material would not be acceptable. A number of systems such as the Vflash, Objet30 and the Projet SD3000 have attempted to minimise the chances of exposure through the use of material cartridges with varying success. An electrophotographic system, using fine build powders should also aim to limit the possible exposure to build materials. The use of recyclable complementary support should be considered in the new system, whether through the deposition of unconsolidated build material or secondary support materials.

### *Usability*

A new system would be supplied to the customer pre-assembled. The system would need to be self configuring and should not require user intervention other than to replace consumables and periodic maintenance. There should be an easy to interpret user interface to warn the user of errors, low material, and build time remaining and to allow the user to execute simple commands such as error clear, pause etc. The system should accept a number of different 3D file formats, which could be compiled and converted into a single file format by secondary software.

### *Cost*

Desktop Factory created significant market hype with its proposal to introduce a true desktop printer to the market for under \$5000 (equivalent to around £3000). From the number of buyers willing to reserve one of these systems before launch, it is clear that the price was agreeable with the marketplace. It is clear from market data that

the FDM systems sell in far larger quantities than any other system. This is due to the low machine cost but also the system's ability to produce artefacts with good mechanical properties. A machine cost to artefact functionality ratio is an important factor in the popularity of a 3D printer. A new system should look to be produced for a market of between £3k and £5k, placing it below the current 3D printers but above open source / kit systems and look to exploit the cost to functionality ratio.

# Chapter 3: Concept Development

---

## 3.0 Introduction

The previous chapter concluded with a requirement brief for an electrophotographic ALM system. The brief highlighted some of the technological problems that have historically limited the integration of such technology in an ALM machine. This chapter is intended to test and analyse these problems, providing an understanding from which to develop solutions, and generate physical benchmarks for the development of a functional prototype.

### 3.0.1 Experimental Objectives

Within the introduction two proposals governed the overall aim of this work. The first proposal governed the aims of the literature review while the second; *'An electrophotographic deposition system of the kind found in a modern laser printer can be utilised to produce a low-cost, high definition, high productivity, additive layer manufacturing system. More specifically, a Desktop Three Dimensional Printer prototype can be produced, which demonstrates no electrostatic build limits in the Z-axis and is capable of producing artefacts without fringing.'* generated the following four objectives which provided a direction for the experimental work detailed within the following chapters:

- i. Produce a prototype system with the ability to create simple laminate artefacts.
- ii. Develop an electronic and firmware control system to facilitate the development of current and future objectives.
- iii. Develop and demonstrate a solution to the fringing effect by producing an artefact consisting of a plurality of layers without exhibiting fringe build up.
- iv. Develop and demonstrate a solution to the Z-axis height limitation by producing an artefact of over 3mm in build height

### **3.1 A Physical Understanding of Electrophotography**

The purpose of this section is to build on theoretical understanding gained from the literature survey. The section includes, the reverse engineering of a desktop laser printer, the trial printing of widely available powders, the demonstration of the Z-Axis build limitation and a realisation of the fringing effect.

#### ***3.1.1 Reverse Engineering: The Implementation of Electrophotographic Deposition***

Although there were a number of systems that employed electrophotographic deposition, the most common embodiment was the desktop laser printer. The laser printer embodiment exemplifies the successful implementation of electrophotography and is the lowest cost use of the imaging method. In order to understand the process, a laser printer was dismantled and the components and their interactions studied. As previously discussed, there are two types of developer system commonly employed within laser printers, single (magnetic and non-magnetic) and dual-component. A single component, non-magnetic system was selected for investigation as, although a theoretically a more complex process, the system could be used to print raw materials without the need for magnetic additives.

#### *Selection of the Subject Printer*

There were a number of manufactures producing single component laser printers, but the two printers selected for this investigation were:

- The **Dell 1100**, which when released in 2005 was the first printer to retail below \$100 and so was of interest as it reflected the low-cost aspect of the proposed ALM system.
- The **Samsung ML4500**, which, unlike many modern laser printers, with a base loading paper tray, had the classic top loading paper stack as you would expect to find in an ink jet printer. This layout lent itself to print materials testing, due to the position of the OPC relative to the paper feed.

The Table 3.1 lists the general specifications of the two printers selected for reverse engineering.

<b>Make</b>	Dell	Samsung
<b>Model</b>	1100	ML 4500
<b>Print engine manufacturer</b>	Samsung	Samsung
<b>Resolution</b>	600x600	600x600
<b>Productivity</b>	16 ppm	8ppm
<b>Interface</b>	USB	Parallel

**Table 3.1** The general specifications of the printers chosen to be the subject of reverse engineering.

### Basic Printer Operation

The Dell 1100 and the Samsung ML4500, ignoring the paper feed system, are functionally very similar. This is presumably due to their print engines both being manufactured by Samsung. Due to this similarity, the function of both printers will be discussed together, with any major differences highlighted when significant. The printers were studied under normal printing conditions to understand their operation. Several print cycles were performed and the flow diagram (Fig 3.2) was produced to represent the printer’s operational sequence.

### *The Sensor System*

There were four main parts to the laser printers, the paper feed, printing engine, fuser assembly, and safety lockout, all of which were monitored by the printer’s control unit via multiple sensors. Table 3.2 describes the individual sensors found on the printer and their function.

Sensor Group	Sensor	Type	Nominal Value	Description
<i>Paper</i>	In Tray	Binary - opto gate	1	Detects paper in tray
	In Feed	Binary - opto gate	0	Detects paper in feed
	In Fuser	Binary - opto gate	0	Detects paper in fuser
<i>Print engine</i>	Laser speed	Analogue – Hall Effect	N/A	Detects speed of laser scanning mirror
	Laser position	Binary - phototransistor	0	Detects the position of the laser during scanning
<i>Fuser</i>	Temperature	Analogue - Thermister	N/A	Monitors the fuser temperature
	Over temperature	Binary - bimetallic switch	1	Turns logic 0 in the event of an over temperature
<b>Safety</b>	Case secure	Binary - micro switch	1	Detects that all access panels are secured

**Table 3.2** Printer sensors, their brief description, their output and their basic operation

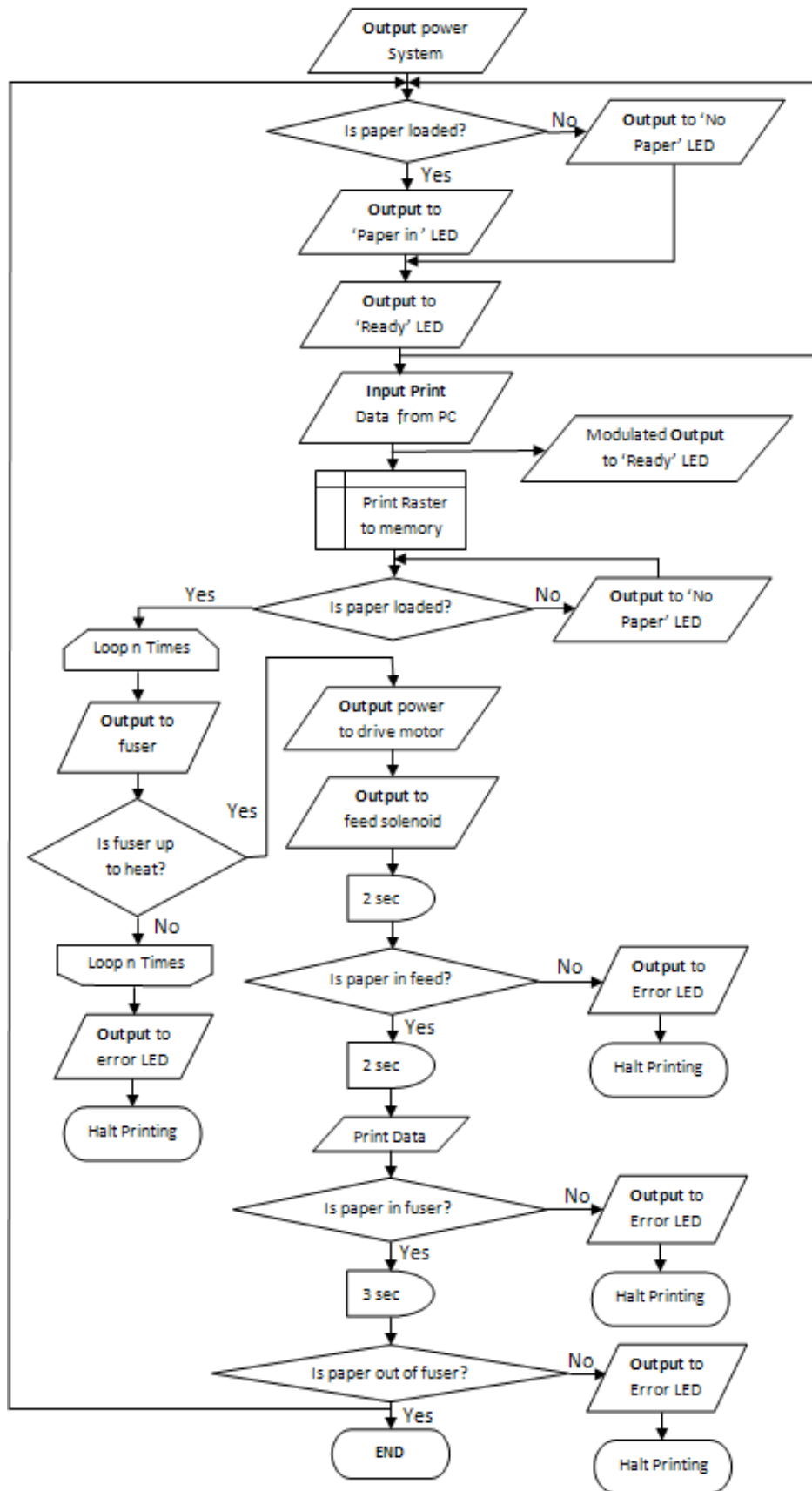


Figure 3.1 The operational sequence of the reverse engineered laser printer.

There were six types of sensor within the printing system namely; optical gate (optogate), photo transistor, Hall Effect, micro switch, thermister, and bi-metallic thermostat. A number of the sensors of key interest are discussed below:

#### *Optogate*

When actuated, the optogate sensors allowed current to sink to ground, bringing an I/O pin of the printer's microcontroller to a low logic state. The three optogates within the printer were used to track the leading and trailing edges of the printing substrate through the printer during operation. After a sensor was triggered, the printer's controller would look for the next sensor to be triggered within a given period of time. The time was predetermined based on the feed velocity and the dimensions of the printed substrate. If the sensors were triggered out of this assumed time envelope, an error flag would be raised.

#### *Thermister*

To measure the temperature of the fuser, a solid state component known as a thermister was used. A thermisters resistance is inversely proportional to its temperature, a relationship which can be approximated by;

$$R = R_{Ref} e^{\beta \left( \frac{1}{T} - \frac{1}{T_{Ref}} \right)} \quad (3.1)$$

Where T is the temperature in Kelvin,  $T_{Ref}$  is the reference temperature, usually room temperature (298 K), R is the resistance of the thermister in Ohms,  $R_{Ref}$  is the resistance at  $T_{Ref}$ ,  $\beta$  is a calibration constant dependent on the thermister's material – usually between 3000 K and 5000 K. An expression in terms of temperature can be derived

$$\frac{1}{T} = \frac{1}{R_{Ref}} + \frac{1}{\beta} [\ln(R) - \ln(R_{Ref})] \quad (3.2)$$



$$T = \frac{T_{Ref} \beta}{\beta + T_{Ref} [\ln(R) - \ln(R_{Ref})]} \quad (3.3)$$

A thermister was probably used over a thermocouple for economy, as the operational temperature range was narrow and because the measurement tolerance was low.

### The Actuator System

The printer had two primary actuators, the feed motor and the clutch solenoid, and one secondary actuator the paper load cam. The paper load cam was operated intermittently as a combination of the actuation of the two primary actuators.

#### *The Feed Motor*

The feed motor and attached gearbox drove the feed rollers and the rollers within the printer's developer unit. The motor was of unipolar stepper type and driven from a dedicated integrated circuit (IC) within the actuator PCB.

#### *The Clutch Solenoid and Paper Load Cam*

When the printing engine was ready to print, the clutch solenoid was activated by the printer control system. The resultant activation allowed a sprocket to be driven by the main drive motor, in turn operating the paper load cam, issuing the printing substrate into the system. The load solenoid was of specific interest as it indicated the moment at which the printing engine was ready to print. Following the activation of the solenoid the printers control system expected a 'paper in feed' sensor signal to be received approximately two seconds later.

### The Electronics Systems

The electronic systems of the printer were made up of six individually mounted PCBs which were interlinked with wiring looms. Each had a function of either power regulation, sensor interfacing, Data handling or actuator control.

### *Incoming Step-down Power Supply*

Mains supply entered the printer through the step down power supply PCB. The function of this supply was to rectify the incoming 230v alternating current (AC) and provide four direct current (DC) outputs, two of 24v and two of 5v. The board provided a heater field effect transistor (FET) switching circuit for the fuser assembly and incorporated an optogate sensor to flag the print substrate entering and exiting the fuser unit.

### *Main Control Board*

The main control board issued the control output for the printer. The controller was based around the Advanced RISC Machines (ARM) microprocessor architecture and was specifically designed for the control of inkjet and laser printers. In addition to power input, the control board has a number of other outputs providing a communications link between itself and peripheral boards. The main control board accepts computer communications through a parallel or universal serial bus (USB) interface and provides raster image processing and memory for the LSU.

### *High Voltage Power Supply*

To generate the high potential needed to electrostatically develop powder images, the printer employed a high voltage (HV) power supply. The HV supply received an input of 24v DC and stepped it up to several thousand volts before issuing it to the print engine roller. The measured output voltages and there designated rollers are listed in Table 3.3. The voltage of the supply and developer roller could be electronically adjusted to alter toner thickness in standard and toner save modes. The transfer roller is supplied with an intelligent high voltage which changes proportionally with the resistance between itself and the OPC. The function of this is to allow the printer to print upon substrates of differing dielectric properties while maintaining deposition density.

Name of output	Reference	Voltage
Transfer HV	Ground	+199V to +2100V *
Main HV	Transfer HV	-1550V
OPC HV	Transfer HV	-1300V
Supply/Developer HV	OPC HV	-630vV/ -530V **
* <i>Dependent on resistance between OPC/Transfer HV</i>		
** <i>Dependent on the thickness of toner layer required</i>		

**Table 3. The relative voltage outputs of the ML4500 high voltage supply unit.**

There were a number of factory preset trimming potentiometers (trim-pots) which were integrated within the HV board. These trim-pots indirectly altered the roller voltages and could be adjusted to optimise printing density.

#### *Sensor PCB*

In addition to the paper exit sensor mounted on the step down power board, there was an ancillary board which consisted of two optogate sensors. Their function was to sense the presence of paper in the paper tray and to sense the leading edge of the paper as it passed through the printing system. The latter sensor was important for determining the position of the paper and therefore, was the key sensor influencing the position of the powder image deposited onto a print substrate.

#### *User Interface*

The printer had a simple button and LED interface. The LEDs indicated; paper status, toner saver mode, printer ready and a machine error. The buttons provided the facility to; enter the printer into toner saver mode (a mode which reduces the voltage between the supply / developer roller and the OPC), print a test document, cancel printing and perform a reprint.

#### *Actuator Control Board*

The actuator control board provided the means for the printer controller to control the feed stepper motor, the clutch solenoid and the auxiliary case cooling fan. The stepper motor was controlled using a bipolar IC operating from a modulated input produced by the main control board.

### *Diagnostic Control Unit*

Samsung produced a Diagnostic Control Unit (DCU) which enabled a service technician to interface with the printer through a surface mounted (SMD) connector on the main control board. The service manual presented a Table of error codes and their corresponding definitions. The DCU also allowed the setting of a number of minor variables, such as main high voltage set point, and allowed a number of the systems to be run independently for testing.

### Conclusion

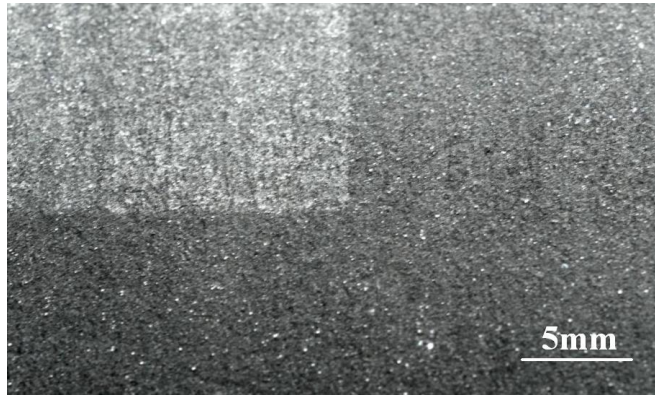
The reverse engineering of the printers demonstrated the implementation of photoelectrostatic technology. The printers studied were of non magnetic single component type, as this was deemed the more likely of the two main photoelectrostatic developer techniques to be of relevance in a future ALM system. It was observed that the printing system used a series of sensors to track the leading and tailing edges of the print substrate as it passed through the printer. The printer's control system ensured no errors had occurred during the printing process by comparing sensor triggering, relative to time, to the predicted triggering calculated based on the print velocity and substrate dimensions. A controller designed to manage the functions of an ALM prototype, through the interfacing of a donor printer's sensors, would have to produce the correct timings to emulate a sheet of paper passing through the printer. The 'paper in feed' sensor indicated the position of the leading edge of the substrate and therefore dictated when the printing engine should start depositing a powder image. It was therefore important to synchronise this sensor with the desired position of the powder image on the print substrate. Prior to the feed sensor indicating the position of the substrate, it was observed that the paper load solenoid indicated the point at which the LSU was up to speed and the print engine was ready to print. This actuator was therefore an important indicator of the printing engines state. It was observed that the fuser unit used a low-cost thermister and a bimetallic thermostat to both, maintain the fuser roller at the correct temperature and prevent it from overheating in the event of a control malfunction.

### ***3.1.2 Printing Trials***

The printing trials in this chapter have been carried out with donor parts from the Samsung ML4500 printer

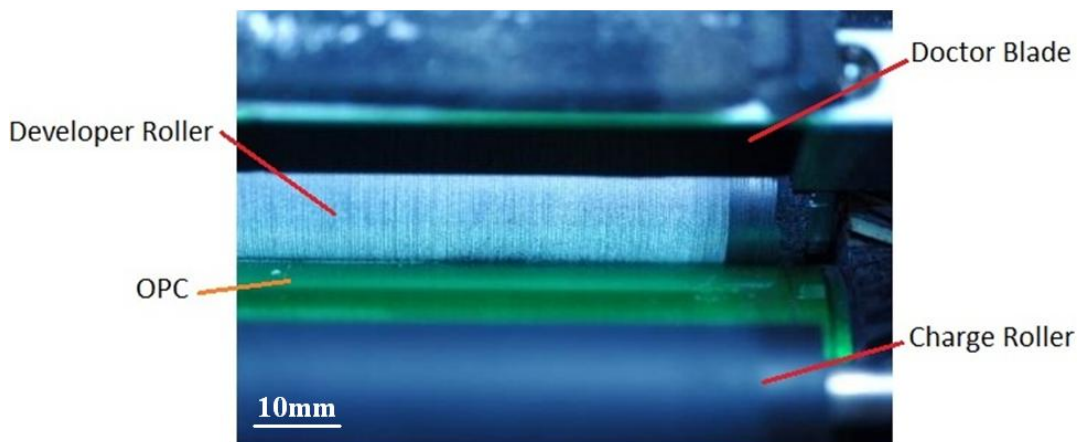
#### *Basic Materials Testing*

Due to the poor mechanical properties of the standard toner material, the suitability of the ML4500's hardware to cope with materials with differing physical properties was investigated. A number of benchmark tests were performed using standard low-cost household powders; plain white flour, Table salt (NaCl) and powdered sugar in addition to mica (PW-80) supplied by Minelco (UK) and Duraform PA a nylon 12 based material manufactured by 3D Systems (USA). Flour, sugar and salt were selected for testing as they represented three low-cost household powders commonly available that had potential as support materials. Mica was selected as it was a low-cost commonly available ceramic, with potential recyclable support material characteristics. Nylon 12 was an engineering plastic selected as it was easily obtainable in powdered form and was renowned for producing usable artefacts from the SLS process. The flour, Salt and Sugar were hand ground and sieve graded to a maximum particle size of 30  $\mu\text{m}$ . The Mica with a 45  $\mu\text{m}$  average particle diameter (Minelco, 2011) and the Duraform with an average of 58  $\mu\text{m}$  was also sieve graded to a maximum particle size of 30  $\mu\text{m}$ . Grading of the Duraform took a significant period of time to build up a large enough sample volume, as the material acquired had a particle diameter range of 25 – 92  $\mu\text{m}$  (Arptech, 2011). Each of the powders was tested individually. A laser cartridge was cleaned between trials using high pressure air and refilled with a test powder. A powder image was then printed onto a contrasting paper substrate and visually inspected. As NaCl salt, Mica and Nylon tend to acquire a positive tribocharge (Halim and Barringer, 2007; Sumawi and Barringer, 2005; Lee, 2009) it was expected that either no development, or back ground development would be seen. The results were somewhat surprising; testing showed that all the powders except the mica would print to some degree, although generally the image was a very fine layer with surrounding area contamination. The picture in Figure 3.2 shows the corner of a sugar deposit onto a black paper substrate.



**Figure 3.2** A fine sugar deposited onto a black substrate, with image contamination running across the substrate in the form of fine white spots of sugar deposit.

The nylon powder printed with the thickest layer but was significantly less dense than a standard toner deposited layer, and contained streaking where no material was deposited. These streaks were also seen on the surface of the developer roller (Fig 3.3). This suggested that there was a high distribution of nylon particle sizes, the larger of which had become lodged in the doctor blade, thus preventing a uniform coating on the surface of the developer roller and ultimately producing a poor powder image.



**Figure 3.3** Streaking on the developer roller due to a large distribution of Nylon powder particle dimensions.

The contamination of the substrate and the fine deposits of low density suggested a poor developer density, most likely due to a low powder tribocharge or a tribocharge of incorrect polarity. The flour salt and sugar were hydroscopic in comparison to standard toner, a factor which is known to have a significant effect on tribocharging efficiency (Banerjee and Wimpenny, 2008) and may have been a contributing factor in

this case. When ground, mica forms a powder with a high aspect ratio which has a high tendency to cake. It was expected that the powdered sugar would act in much the same way; however, it was noted that both the Duraform nylon and powdered sugar contained additional flow control additives to prevent caking. It may have been these additional additives that led to the increased deposition of nylon and sugar over that of the other powders tested. Ultimately the 30 $\mu$ m upper particle limit was too great for a developer unit designed for 5 -10  $\mu$ m toner and resulted in poor quality printing. It is often difficult to obtain powdered material cost effectively in the 5-10  $\mu$ m range. As an alternative, it was prudent to look at the design of a fully adjustable printing cartridge to allow-cost effective testing of a wider range of materials. As identified by Banerjee and Wimpenny (2006, 2008) FCA and CCA are also key to the development of a selection of electrophotographic materials, as most likely demonstrated with the relatively dense deposition of the sugar and nylon powders during testing. While the successful and repeatable deposition of sugar could have led to a low-cost soluble support material, for the scope of this research, no further materials testing was investigated. The design of a deposition system which was fully adjustable to facilitate future materials testing was considered during the design of the prototype system.

### ***3.1.3 Electrostatic Transfer***

Research conducted on the implementation of electrophotographic printing disclosed the problems of electrostatic powder transfer onto a build surface. This was exemplified by a limit to the build height and the fringe built up around the edges of an artefact following several deposition and consolidation cycles (Kumar and Dutta 2003, 2004; Wimpenny and Banerjee, 2008). The following sections discuss experiments undertaken to re-create these phenomena in order to create a base line from which to test possible solutions.

#### ***Build Height Limitation***

As discussed in the literature review the electrophotographic printing process requires an electrostatic charge to provide the force with which to transfer toner from OPC to substrate. In the case of a simplified ALM system, the substrate is often a previously

deposited layer upon a build platform. Within a paper printing system, the paper substrate to be printed on is quite often not directly charged to receive the powder image from the OPC, but instead is an intermediate substrate passed between the OPC and a transfer roller (Fig 3.4).

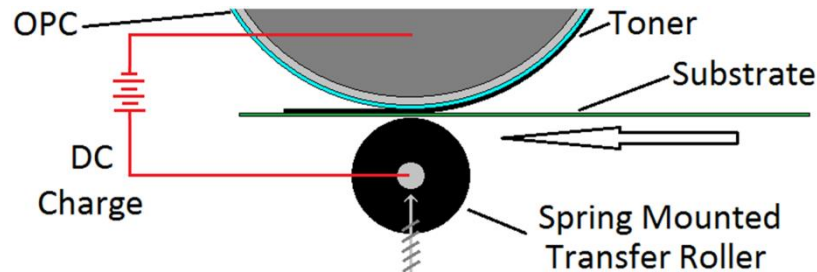


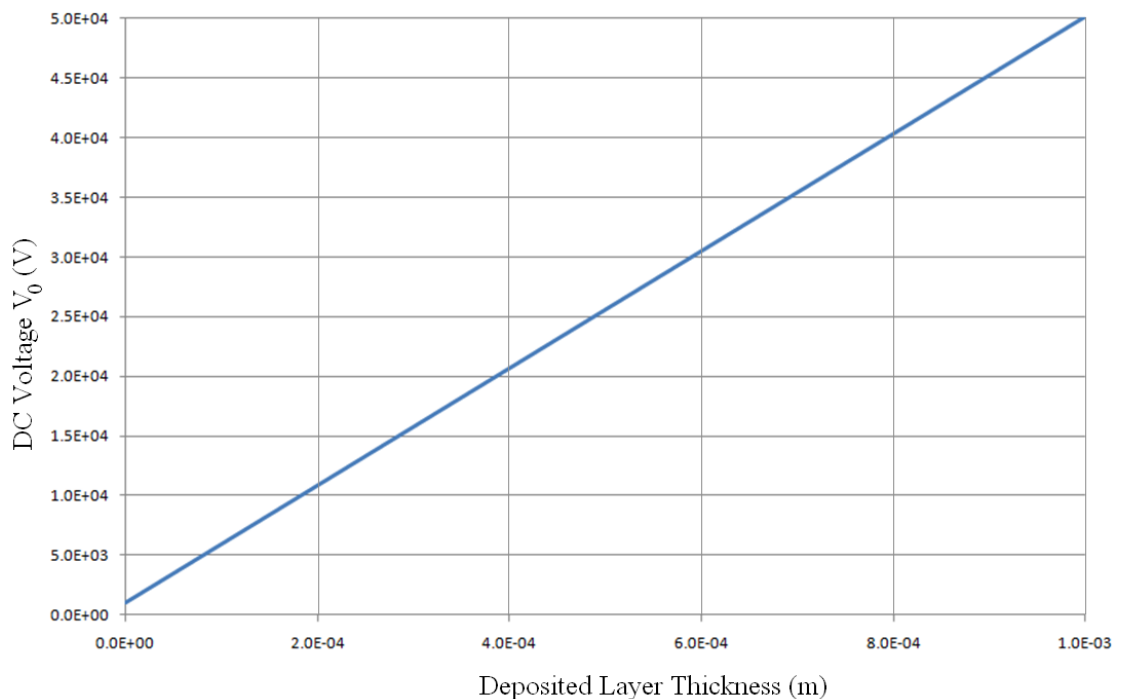
Figure 3.4 The deposition of toner onto a substrate using a transfer roller

The transfer roller creates an electric field on the surface of the paper, attracting the toner from the OPC to the charged surface. In an ALM system the transfer roller and print substrate could have been replaced by a build platform mounted on a Z-Axis. As each layer of powder material was attracted from the OPC to the build platform, the Z-axis could have been sequentially indexed down one layer thickness. Paper substrates generally ranged in thickness from 0.08-0.5mm, a printer measured the dielectric strength of a substrate it was to print upon, by measuring the resistance between the transfer roller and OPC. The printer control system would then adjust the magnitude of the DC charge, typically from around 500 to 1000 volts, to maintain the correct electric field to ensure efficient toner transfer. The ALM systems described in the literature survey however, have had a constant DC charge creating a constant electric field, which would have been seen to gradually deplete with respect to the build surface with each sequential layer deposited. Kumar and Dutta (2004) described the depletion of electric field ( $E_f$ ) due to build surface displacement with the equation 2.12. The equation described the exponential decay of the electric field at the build surface, due to its increased displacement from the field source, following sequential layer deposits. We can therefore represent the potential difference ( $V_0$ ) needed to generate an electric field as



$$V_0 = \frac{\frac{E_f}{K_p}}{K_f P + K_p d} - \frac{P_p P^2}{2\varepsilon_0 K_p} + \frac{P_f d^2}{2\varepsilon_0 K_f} \quad (3.4)$$

In order to maintain a constant electric field on the surface of the deposited material, equation 3.4 dictated that the potential difference between the OPC and build platform had to increase linearly with build thickness ( $P$ ). Figure 3.5 illustrates the linear voltage / displacement relationship, with  $V_0$  as a function of  $P$ ,  $E_f = 4.915 \times 10^7$  v/m,  $\varepsilon_0 = 8.85 \times 10^{-12}$  F/m,  $\rho_p = 0$ ,  $\rho_f = -2.26$  C/m<sup>3</sup>,  $d = 2 \times 10^{-5}$  m,  $K_f = K_p = 3$ .



**Figure 3.5** The voltage as a function of the layer build height required to maintain a constant electric field.

The relationship demonstrates that it is not suitable to incrementally increase the voltage between the OPC and build platform after each layer deposit. This would have led to a voltage approaching 5MV between OPC and build platform for a part of 100mm in height. This high voltage would have most likely resulted in the spark discharge, from build platform to OPC and surrounding objects separated by air.

An experiment was carried out with standard Styrene-acrylate copolymer based toner to investigate the height limitation due to the decaying electric field as the

displacement of the deposition surface increased from the field source. A number of multilayer images were printed onto a card/foil laminate substrate, with a 1kV build surface DC charge relative to the OPC. Consolidation was achieved in a purpose built heated press. The press, Figure 3.6, was designed with a Z- axis table (DMC 1010, Galil, USA), used to apply a predetermined pressure on the sample to be consolidated. The temperature of the overhead mica heater was controlled by a commercial proportional integral derivative (PID) controller and held at an experimentally determined 180°C. The Z-axis was manually controlled and the motion incremented in 100 encoder step counts (equivalent to 1 micron) until the micro balance upon which the sample was mounted indicated a reading of 0.5g, equivalent to a consolidating pressure of 2.3 kPa.

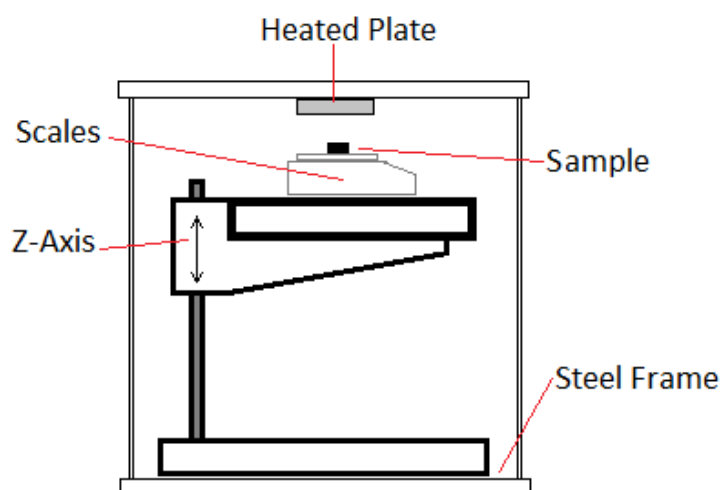


Figure 3.6 A schematic of a controlled consolidation heat press for the testing of layer thickness deposits.

The heater consisted of an aluminium back plate which had an insulating layer, a mica heater, and a surface ground stainless steel plate mounted on its underside. The stainless steel plate was PTFE coated to provide a non stick surface. The principle of the experiment was to show the drop in layer thickness due to the increased displacement of the deposition surface from the electric field, generated in the foil backing of the print substrate. The micro balance was to ensure the constant consolidation pressure of the layers as they became increasingly thinner. Although the resolution of the layer thickness reading was only one micron, an average of a tenth layer period was taken to demonstrate the relationship. The plot in Figure 3.7

demonstrates the relationship between the number of layers and the resulting layer thickness average with a period of ten. As expected the data shows an almost exponential reduction in layer thickness to zero within the ninety layers printed, and supports previous observations by Kumar and Dutta (2003). An image of the consolidated layers can be seen in Figure 3.8.

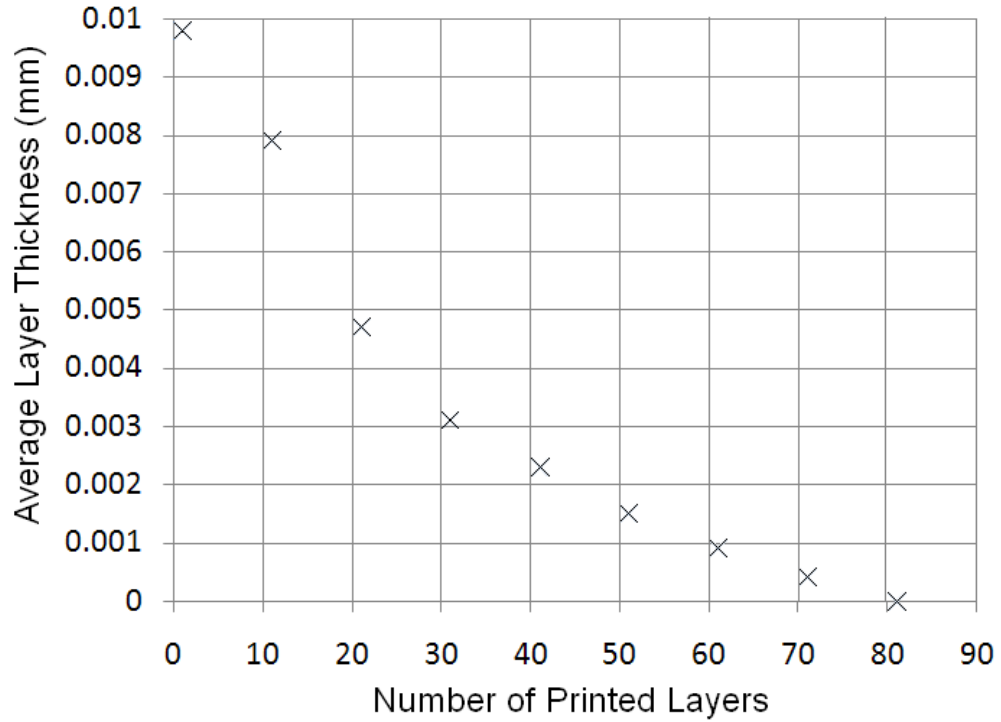


Figure 3.7 The relationship between the layer thickness and the reduction in electric field strength as a function of number of layers printed.

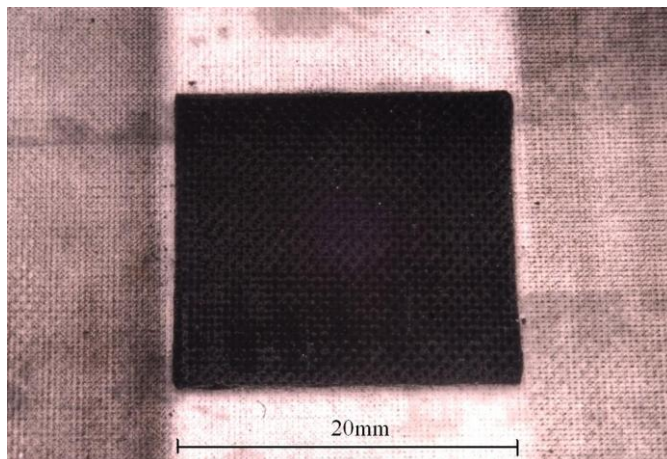


Figure 3.8 The ninety sequentially deposited and consolidated layers of a 20 x 20 x 0.3mm printed block; the surface texture was generated by the PTFE release film attached to the heated consolidation plate.

### *Surface Charging*

The second set of tests used the same test rig as in the first tests but instead of the generation of an electric field using the substrates foil backing, the top layer of the consolidated material was charged using a corona charging apparatus. The results showed a constant layer thickness of  $10 \pm 1$  micron producing a deposit of 0.889mm in height after 90 layers. However due to a build up of fringe material it was found that after only 10 layers a fringe was visible, after twenty layers an obvious fringe had developed and after fifty layers, only the edges of the powder image would be fully consolidated, leaving the centre of the deposit in a semi sintered powder form. The fringe formation after 50 layers can be seen in Figure 3.9.

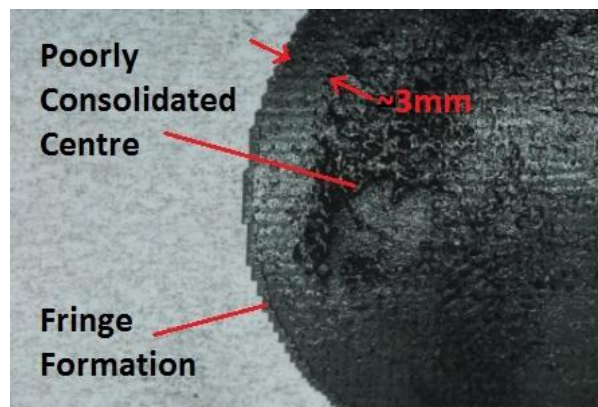
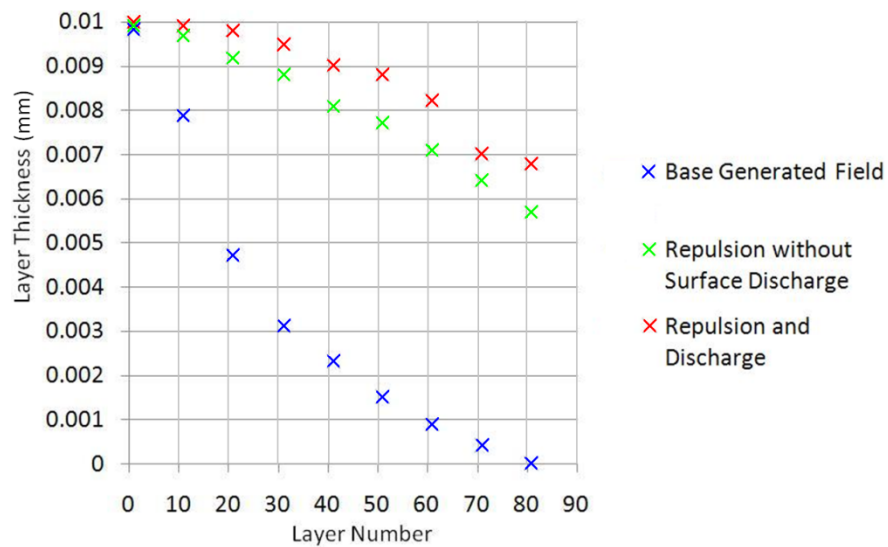


Figure 3.9 An example of fringing showing the unconsolidated internal area after 50 layers.

### *Repulsion Transfer*

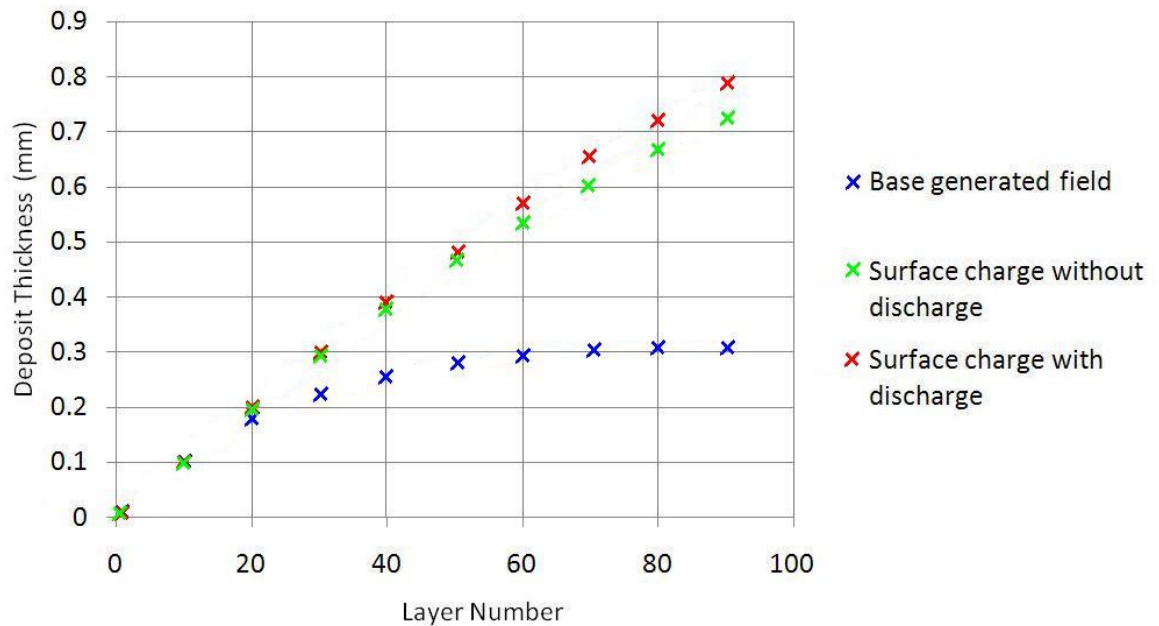
Repulsion transfer, as suggested by Wimpenny and Banerjee in their 2007 patent, as a solution to the problem of the deposition height limit, was also tested. However, it was not possible to use the previously described test apparatus to investigate this, as it was not possible to apply a repulsion force to the OPC. Instead each layer was printed upon a transfer sheet, which was then placed into a transfer jig employing a roller, with the same -1.5kV charge as the toner present upon the transfer sheet. The roller was passed over the belt surface depositing the powder onto a substrate before being consolidated as in previous tests. The transfer jig was mounted on height adjustment screws which were indexed one layer thickness higher, than the deposit thickness, as determined from the Z-axis during the consolidation of the previous layer. While an

improvement of the layer deposition thickness was seen in the initial few layers, once again the deposition rate fell as the part height increased. It was concluded that residual charges built up on the surface of previously consolidated material, resulted in the repulsion of additional layers. The test was repeated, but with the additional process of discharging the top layer of the build surface between deposits. The results showed that eliminating residual surface charge resulted in a greater powder transfer than in previous tests. However, it was noted that the layer thickness still thinned as subsequent layers were deposited. The results are presented in the plot (Fig 3.10).



**Figure 3.10** The results of the repulsion transfer experiments showing layer average thickness relative to number of layers deposited.

The data obtained from the readings of the repulsion charge experiment show a more linear curve than that of the standard, base generated field. There was a source of error in the data resulting in an uneven plot. This was due to the difficulty of ensuring the transfer rig was suitably aligned and positioned at the correct layer height. A better example of the relative effects of repulsion and standard field generation transfer can be seen in Figure 3.11, where the cumulative deposit height over the course of the ninety layers is plotted. As with other experiments conducted, where electrostatic force has been the key transfer mechanism, a fringe was clearly visible around the perimeter of a printed part.

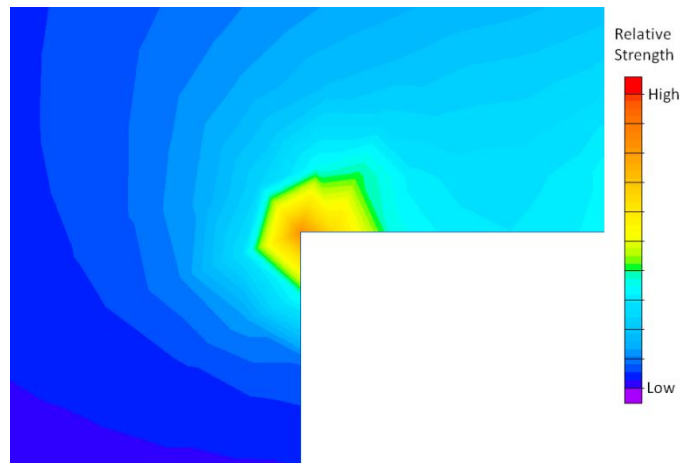


**Figure 3.11** The results of the repulsion transfer experiments expressed as deposit thickness relative to cumulative layer number

In the second experiment, where the deposition surface was discharge prior to the repulsion transfer, it was concluded that due to the presence of layer thickness decay, that the close proximity of the charged repulsion roller to the body of the deposited layer, induced a charge in the volume of the deposit. This induced charge then went on to repel sequential layers. As the volume of the deposit increased so too did its capacity to produce larger induced electric fields, thus having a greater effect on subsequent layer deposits.

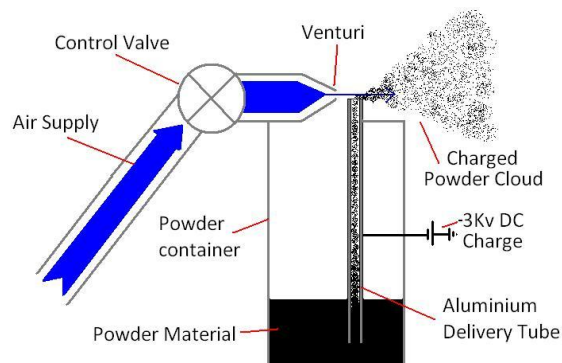
### *Fringing*

The effect of a build up of a thicker powder deposit around the periphery of an artefact, due to sequential powder deposits, was noted in the experiments previously discussed. The electric field generated at the tip of a charged sharp edged electrode is highly non-uniform. Jackson (1999) provides a numerical example of the edge effect. Jackson's problem is provided as an example in QuickField 5.8, a Finite Element Analysis (FEA) program, and produces a visual representation of the relative field intensity on the edge of a sharp geometry in a vacuum (Fig 3.12). From the model it is clear that such geometries produce significant fringe fields.



**Figure 3.12** A relative field strength FEA diagram produced in QuickField 5.8 software, showing the increased relative electric field on a cross-sectional edge of an object of with a higher surface potential relative its surroundings, within air.

In addition to the fringing seen during OPC charge development, the phenomenon of fringing during transfer occurs due to the non-uniform electric field across a charged surface providing higher electric field strength around an artefacts periphery. This increased strength went on to attract more powder during image transfer than that of the relatively uniform field distribution, present across the body of the artefact. An experiment was undertaken to visualise the effects of fringing using a dielectric substrate, in this case paper. A charge of 3kV was applied to the surface of a sheet of paper which was subsequently exposed to a charged powder cloud. The powder cloud was formed using the venturi effect and an apparatus designed for the purpose of charging the powder as it passed through a delivery tube (Fig 3.13).



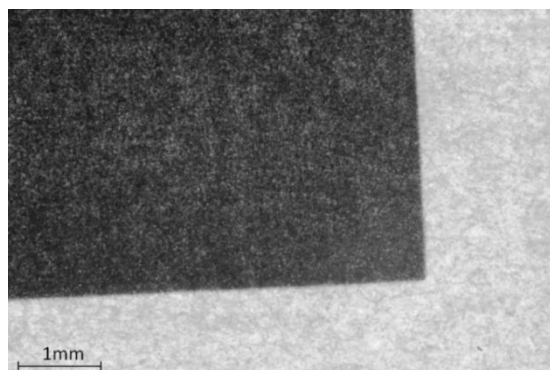
**Figure 3.13** A schematic of the apparatus designed to produce a charged powder cloud for the development of charged images.

The charged powder cloud was blown upwards and allowed to settle on the surface of the charged substrate without the influence of the air propellant. The paper was charged by passing it between two conductive rollers which imparted a uniform charge across its surface. The experiment showed an increased powder deposition around the edges of the substrate where the electric field was at its highest.



**Figure 3.14** The results of an experiment to visualise the effects of fringing due to the non-uniform electric fields on the edges of a uniformly charged substrate. The darkened edges show a higher deposit of material.

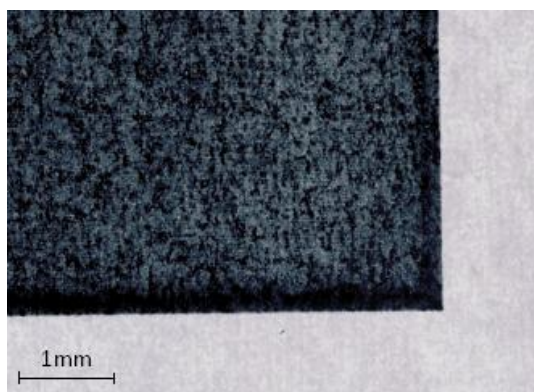
The results from the experiment in Figure 3.14 show clearly the fringing effect caused by the non-uniform electric field at the edges of the substrate, exemplified as a high powder volume deposited at the edges of the paper. Additional testing was undertaken, to investigate the development of powder images transferred directly on to a paper substrate from the OPC, to determine whether fringing also occurred at the edges of the latent electrostatic image present on the photoreceptor during development. Figure 3.15 shows the results of testing and demonstrates that fringing does not occur during initial development using the ML4500 printing system.



**Figure 3.15** A back lit image of an unconsolidated powder image printed by the Samsung ML4500 laser printer on the surface of a paper substrate showing no signs of fringing.



The absence of fringing on the ML4500 printed image was surprising considering the understanding of fringe formation gained during the literature survey. As a comparison, a magnetic developer system was trialled, the HP 2055DN with standard magnetic toner was printed using the same geometry (Fig 3.16) and the resultant image showed clear signs of fringing.



**Figure 3.16** A back lit image of a powder image on the surface of a paper substrate printed by a magnetic HP2055DN Laser printer, showing significant fringing.

The result of the development fringing testing was unexpected, as it was predicted that a latent electrostatic image present on the surface of the OPC would experience the fringing effect. However, in terms of the generation of an ALM system, which can produce parts without fringing, the fringeless OPC development of the ML4500 eliminates one of the two fringe sources, leaving only the fringing due to powder transfer to overcome.

### **3.2 Concept Development**

It was clear that the major issues of the build height limit and the fringe phenomena were both fundamentally electrostatic effects. It was also clear that the problem now lay solely in the deposition of powder layers and not the development of electrophotographic images upon the OPC. With this in mind an alternative deposition solution was sought that did not involve the electrostatic transfer of powder images. The solution investigated was of mechanical transfer, i.e. the adhesive properties of semi-molten materials and the application of pressure. The following section discusses

the testing and development of the transfer and deposition systems used to achieve this mechanical transfer.

### ***3.2.1 Transfer Belt Printing***

OPC rollers exhibit their best operational characteristics at low temperatures.

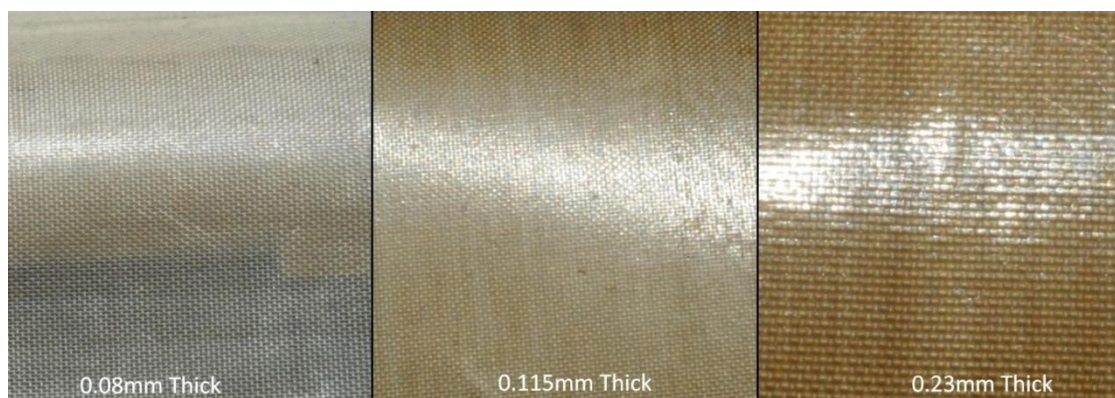
Typically, temperatures over 45°C have a significant impact on an OPC's ability to hold charge, resulting in poor image formation (Morita et al, 2007). To protect the OPC from the additional heat required for the consolidation process a transfer belt was implemented. The transfer belt characteristics were as follows:

- The ability to accept electrophotographically printed images
- Retain a powder image during transport
- Resistant to temperatures in the T<sub>g</sub> to T<sub>m</sub> region of a deposited powder (typically up to 175°C for nylon 12)
- High thermal stability
- Low surface energy and high surface finish
- Capable of being formed into a belt
- Low-cost

The list of requirements left three feasible material options. A steel belt laminated with a low surface energy polymer such as PTFE, a fibre reinforced PTFE or a fibre reinforced silicon material. Following a preliminary cost based investigation a steel belt was initially ruled out.

#### ***Fibre Reinforced PTFE Material***

A glass fibre reinforced PTFE material was selected for testing. The material was sourced in three different thicknesses of 0.08mm, 0.115mm and 0.23mm from Technical Engineering Services Ltd (UK). The difference in thickness was, in the most part, due to the thickness of the PTFE laminates and as such the thicker the laminate the better the surface finish, as less reinforcing weave was visible on the materials surface. Figure 3.17 shows the surface of the belt materials and their comparable surface finishes.



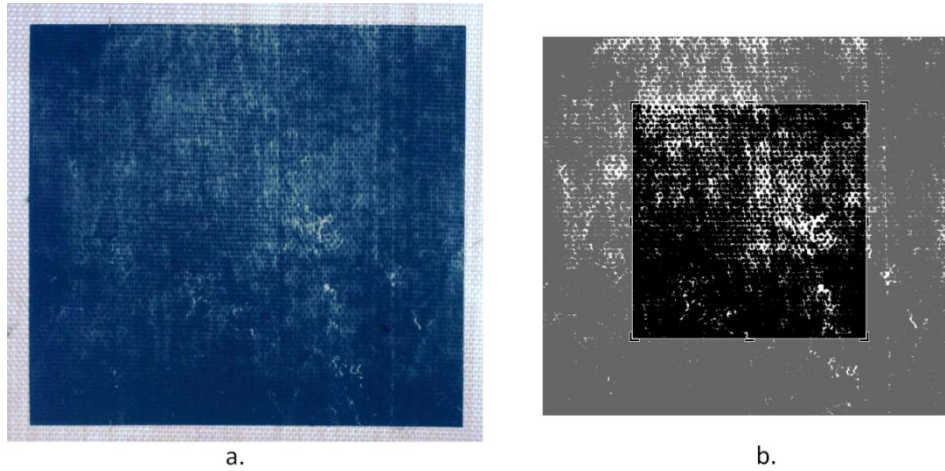
**Figure 3.17** The respective surface finishes of the glass fibre reinforced PTFE belts with the lowest surface finish 0.08mm thick material far left, the medium surface finish 0.115mm thick material in the middle and the highest surface finish 0.23mm thick material far right. All samples pictured were 150mm square.

Each of the three materials exhibited a maximum working temperature of 260°C, low coefficient of thermal expansion, and were able to be formed into belts by the manufacturer.

### *Printing Trials*

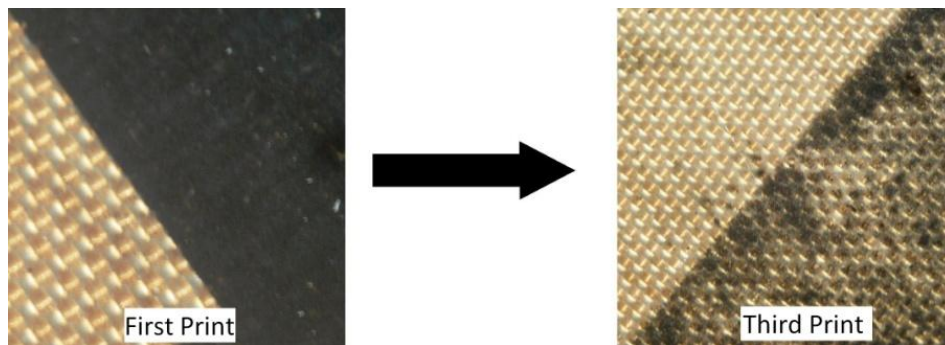
Initial trials were conducted with sample material sheets cut into A4 (297 x 210 mm) sheet size and printed upon by a standard Samsung ML4500 with standard toner. A 50 x 50 mm test square was printed on the sheets, wiped cleaned with a cloth and then reprinted upon in order to determine the materials ability to process multiple prints. The image density was measured using image processing software. A black and white scanning of the deposit at 600 x 600 dpi resolution and a low threshold of 7 to filter out the effect of belt material colour (i.e. pixels must have be 97% saturated on the 255 bit gray scale to have been recorded as black) was taken. The resultant scanned image was then cropped to a sample area of 1000 x 1000 pixels and the area measured by open source image analysis software 'ImageJ' (distributed by the National Institutes of Health, USA). The software measured a percentage white density over an area, which was then converted into a toner density for intuitive comparison. A control was tested, consisting of a 1000 x 1000 pixel sample of a 50 x 50 mm square, printed onto 80g/m<sup>2</sup> plane white paper and the range taken over 10 prints. It was found that the print density measurements had a deviation of less than 0.01%. A degradation of 0.5% in print density was set as the threshold for maximum allowable print density

reduction before 'noticeable image decay' was apparent. An illustration of the measurement process can be seen in Figure 3.18.



**Figure 3.18 (a) A photograph of a reduced density print on a 0.23mm thick PTFE belt due to multiple print and cleaning passes. (b) A black and white scanned image of the print shown in (a) with a 1000x1000pixel sample area highlighted – The resultant print density was determined to be 86.0%.**

The density of the first print on all the materials was good all exhibiting a 100% density. However, subsequent prints became less dense and reached the 0.5% degradation threshold within 2-6 prints, a phenomenon most apparent with the thicker 0.23mm belt (figure 3.19).



**Figure 3.19 Two pictures showing the results of multiple prints onto a 0.23mm thick glass fibre reinforced belt on first and third prints respectively.**

The degradation in print quality was not unexpected, the toner within a conventional mono component laser printer is electro negative and attracted to the more positive regions of an OPC during image development. Teflon is extremely electro negative, meaning as it comes in dynamic contact with other materials it will tend to amass a

negative charge. The act of cleaning the PTFE material with a dry cloth before passing the material through the printer, imparted a negative charge. This charge, being similar to that of the charge on the toner, repelled the toner back onto the surface of the OPC, resulting in poor image transfer. The thicker materials were more susceptible to the effects of tribocharging as the backing transfer roller, within the printing engine, was unable to overcome the high dielectric thickness, allowing the triboelectric charge on the surface of the material to dictate the powder transfer efficiency.

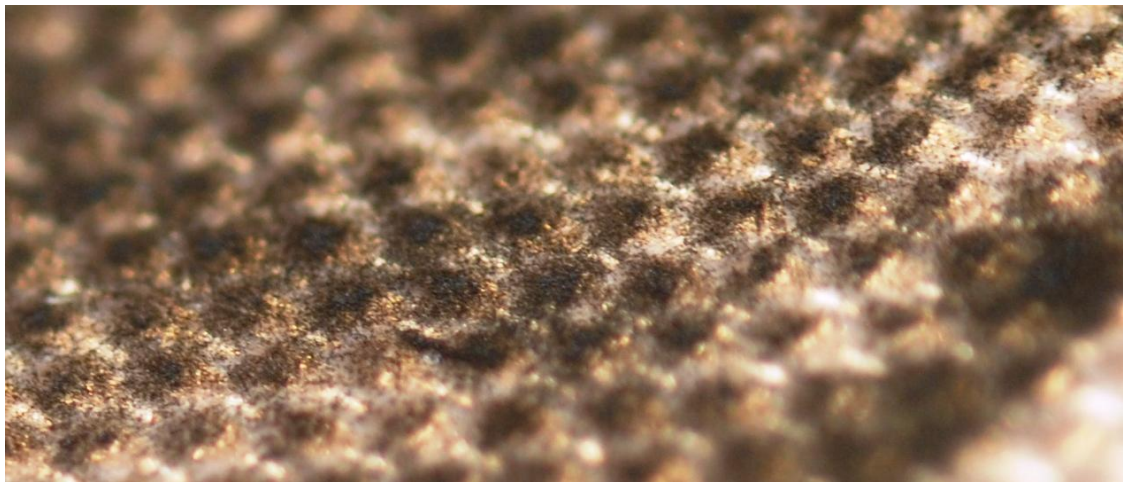
### *Passive Earthed Conductor Surface Discharge*

There were a number of ways to overcome the surface tribocharging effects of the Teflon material. The first, passing the material over an earthed conductor post cleaning was experimented with and initially showed good results. The thinner, 0.008mm thick material showed no sign of print degradation until around print 20 or following print testing of other materials. The late onset of print degradation was concluded to be as a result of a poorly earthed discharge conductor, which had slowly gained a negative charge over the period of testing. The thickest, 0.23mm, material printed a number of times but, as before, started to show signs of image degradation after only a small number of prints.

### *Active Corona Discharge*

An AC corona discharge bar was used to eliminate the charge present on the surface of the belt material following cleaning. The design of the corona discharge apparatus will be discussed in detail in the design section of this thesis. However, the corona produced an ion discharge of positive and negatively charged ions which were attracted to the charge present on the surface of the belt, thus discharging it. The experiments of printing onto the glass reinforced PTFE were repeated with the resultant printing density noted. In common with the passive discharge technique, the 0.08mm and the 0.115mm thick materials printed with a constant efficiency and continued to show no sign of image degradation after 50 prints. The 0.23mm material however, once again showed signs of image degradation (Fig 3.20).





**Figure 3.20** The surface of the 0.23mm glass fibre reinforced PTFE material with deposits of toner present only on the warp, in the weft spacing.

From the results it was clear that there was another source of electrostatic charge being generated within the thicker material, other than surface charge from dynamic contact. From the visual results it was concluded that the larger number of X/Y fibres within the thicker material rubbed against one another while the material flexed during printing. While the surface charge was eliminated by corona discharge, the internal glass fibres held charge and acted to repel toner where the fibres were closest to the materials surface. The schematic in Figure 3.21 describes the physical action of the fibres repelling the toner particles.



**Figure 3.21** A schematic of the effect seen when printing toner onto a substrate with inner tribocharged reinforcing fibres.

### *Alternative Glass fibre Reinforced PTFE Materials*

In order to overcome the tribocharging of internal fibres which could not be discharged through active or passive surface discharge, either the insulating glass fibres had to be replaced with conductive fibres such as carbon fibre or steel braid, or the PTFE material needed to conduct the electrostatic charge from the insulating glass

fibres. As the latter product already existed, a glass fibre reinforced carbon filled PTFE material, was the solution trialled. The testing was completed in a similar fashion to the previous tests, where the test material was printed on, cleaned, and then actively discharged with an AC corona. A 0.23mm thick material was tested which subsequently showed no reduction in print quality over a 50 print cycle.

*Summary of the Testing of the Glass Fibre Reinforced Belt Materials*

Table 3.4 shows the results of the belt testing, highlighting the need for the discharging of residual tribocharge on the belt surface and the internal reinforcing fibre. The thinner Glass Fibre Reinforced PTFE material was less susceptible to internal tribocharging than the thicker material, as there were fewer X/Y fibres in the warp and weft, resulting in less relative movement during material flexing. Probably the largest influence was the thickness of the PTFE dielectric on the surface of the fibre reinforcing. The thinner PTFE coatings allowed both charge migration to the surface of the PTFE belt where it was discharged by corona, and the induction charging by the transfer roller during printing.

Glass reinforced Material	Thickness	Fibres in		Prints to Noticeable Image Decay (50 Prints Max)		
		Warp	Weft	No Discharge	Passive Discharge	Active Discharge
Pure PTFE	0.08mm	180	140	6	No Decay	No Decay
Pure PTFE	0.115mm	180	140	4	30	No Decay
Pure PTFE	0.23mm	440	380	3	5	6
Carbon PTFE	0.23mm	440	380	2	N/A	No Decay

**Table 3.4 A Table showing the results from the belt material printing trials, illustrating the effect of surface and internal discharging.**

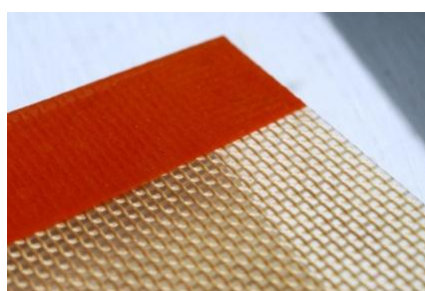
*Glass Reinforced Silicone Material*

Reinforced vulcanised silicone is commonly used as gasket materials in its thicker form and in its thinner forms used as heat sealing belts in automated packing lines due to its high thermal stability. Silicone is less electronegative than PTFE but has the limitation of being significantly more expensive. The silicon materials also tend to be thicker, and therefore held more thermal energy, which needed removing prior to cleaning or contact with the OPC. Some laser printers, commonly colour printers, use a transfer belt to form a multi-coloured image before depositing onto a paper substrate. The

belts used within laser printers often use vulcanised silicone, but are not of use in this application as they have poor thermal resistance due to the cotton internal reinforcement used.

### *Initial Print Testing*

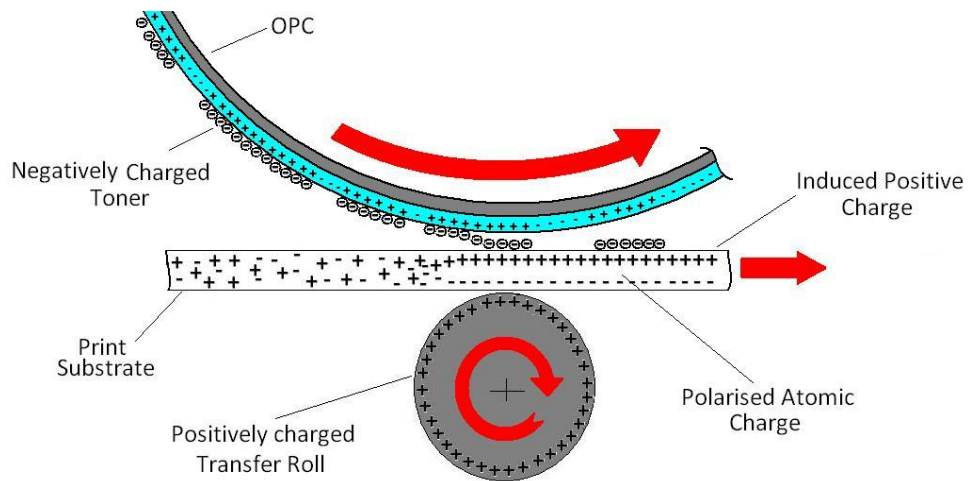
The silicon belt material was sourced from Technical Engineering Services Ltd. The material tested was 1.9mm thick, with a smooth surface finish and cut to form the dimensions of a standard A4 sheet for testing (Fig 3.22). The first print trial conducted, printed an image multiple times on to the sample material with standard printing variables as previously discussed.



**Figure 3.22** The surface finish of the glass fibre reinforced silicone sheet.

It was found that the belt was capable of retaining only a faint print, regardless of the number of times it was issued to the printer. Due to the materials thin cross sectional area of only 1.9mm thick the printers transfer roller was unable to induce a strong enough electric field on the surface of the material to overcome the attraction force between toner and OPC. The solution was to increase the voltage across the transfer roller / OPC interface, thus increasing the electric field, inducing a positive charge on the surface of the silicon material through atomic charge polarisation. The theory of inductive charging is illustrated in the schematic in Figure 3.23. The positive electric field generated by the transfer roller attracted the electrons from the silicon atoms, thus orienting themselves with the electric field. This polarisation of the atom's electrons created a negative field on the lower surface of the material and a positive field on the top surface. Although the electrons do not physically migrate through the material, they can orientate with the field, to produce weak electrostatic forces strong enough to attract the toner from the OPC.





**Figure 3.23** The physical action of induction charging of a dielectric material during Electrophotographic printing.

### *Second Printing Trial*

The transfer roll was supplied with a  $-2.6\text{kV}$  DC bias with respect to the OPC, twice that nominally supplied by the printers high voltage supply. The separation of the transfer roller and OPC had to be maintained during printing, as contact between the two rollers would have led to spark discharge and damaging to the OPC coating. Separation was maintained with two purpose machined bearing spacers. The second printing cycle generated better printing results with a clear sharp image formed on the surface of the material on the first print cycle. Attempts were made to remove the toner material from the belts surface by wiping with a cloth but the surface retained the Majority of the deposited powder. Only by washing with running water could the powder be reliably removed. Following cleaning the belt could be indefinitely printed upon.

### *Belt Material Conclusion*

The use of non conductive reinforcing fibres within the test materials led to unexpected residual charges which limited print quality after a number of prints. PTFE was the best performing material overall based on cost and function, with the thinner  $0.08\text{mm}$  and  $0.115\text{mm}$  glass reinforced materials performing best. The use of a reinforced silicon material as a transfer belt in an ALM system, while providing a superior image, was not viable due to the inability of the surface to be cleaned effectively. Further work may have demonstrated a way of effectively removing the

unconsolidated powder, but with the adequate results of the thinner reinforced PTFE material testing, further trials were not conducted. With the use of an active surface charge eliminator, the 0.08 and 0.115mm glass reinforced PTFE belts were printed upon with no noticeable image degradation up to the test cut off of 50 prints. The testing has confirmed the use of either of these two materials, with the surface finish of the 0.115mm thick material preferred.

### 3.2.2 Mechanical Layer Transfer

As previously concluded, the phenomena referred to as fringing and the physical build height limitation exhibited by the multi layer electrophotographic printing of powdered materials, was purely electrostatic in cause. For this reason, the mechanical transfer of powdered materials was investigated. Each of the three systems described within this section show the development of a concept through system schematics and test results.

#### *Heat Plate Consolidation*

Arguably the simplest of the mechanical consolidation systems investigated within this research was that of the heated plate. The system concept consisted of a, deposition engine, a transfer belt, a stationary heat plate, Z-Axis and associated running apparatus (Fig 3.24).

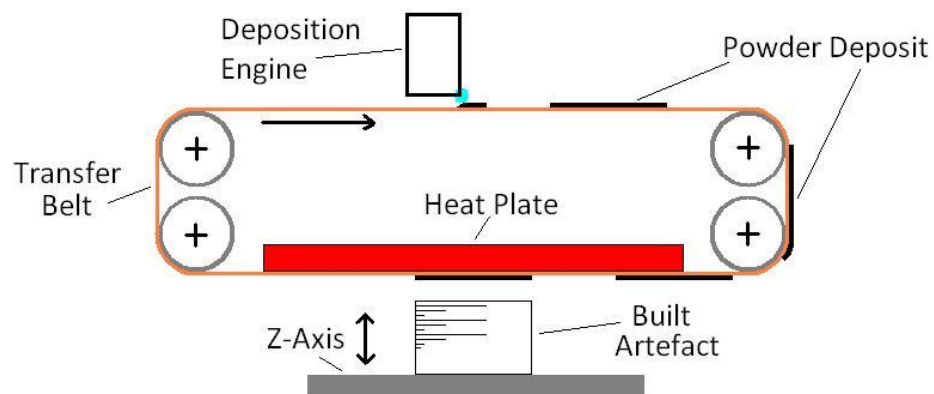


Figure 3.24 The system set up using heated plate consolidation

### Function

The principal of operation, as illustrated in Figure 3.25 was to maintain a consolidation plate at a given temperature while revolving a transfer belt upon which a powder image was deposited. As the powder image was indexed over the hot plate's surface it would start to melt, sinter and tackify. When in the correct position over the Z-axis build platform, the belt motion would stop, at which point the powder image would be fully tackified. The Z-axis would be brought into contact with the tackified powder image, and a light pressure applied to fully consolidate the image to the build surface. The Z-axis would then retract, pulling with it the freshly consolidated layer from the belt surface.

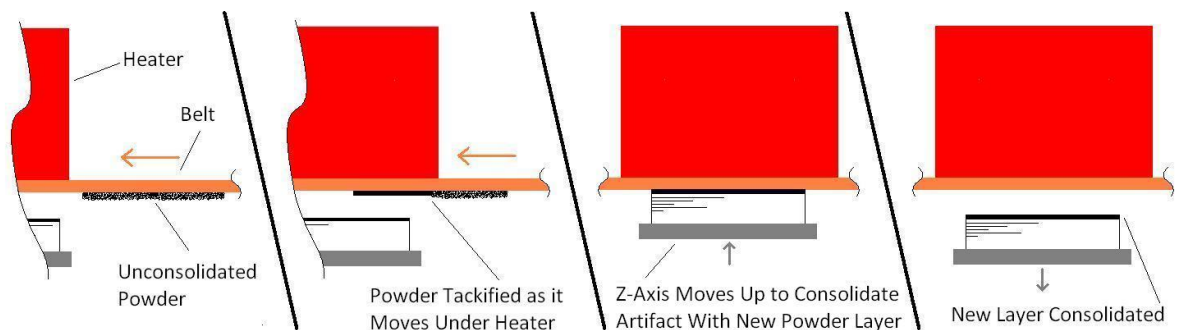


Figure 3.25 The function of the heated plate consolidation system

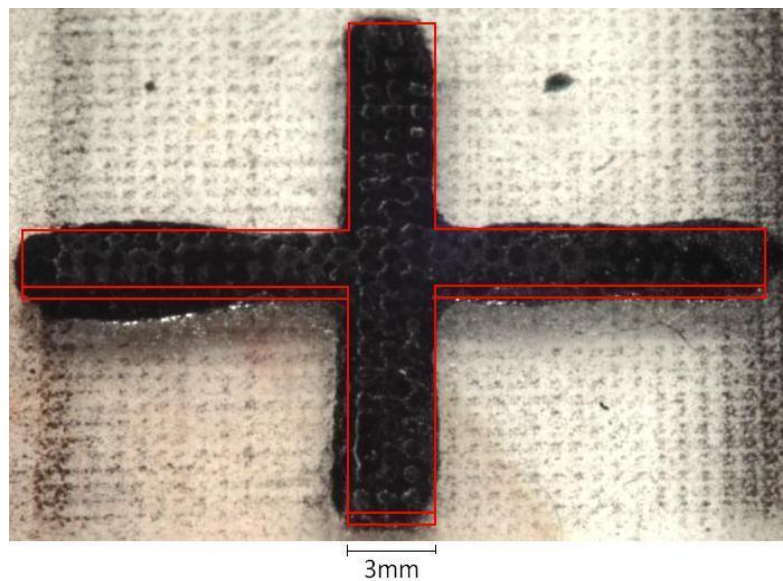
### Testing

The test rig initially designed to test the effect of layer thickness as a result of displacement from the electric field source, was adapted to consolidate images from a belt material. An A4 sized sheet of the glass reinforced PTFE material was printed upon with a cross geometry (a cross was chosen as it aided the lining up process) (Fusayasu, 2001). The belt material with the printed layer was then mounted precisely on to the surface of the mica heater plate, and the Z-axis brought into contact with the tackified powder image. A set of digital micro scales was used to ensure a constant consolidation pressure.

### Results

Initial results produced artefacts with 50 layers in a cross geometry. The consolidation of the layers was consistent but tended to remain stuck to the belt material until a

large displacement of the Z-Axis was executed, at which point the artefact and layer were released. The belt material was then held under higher tension during consolidation, to prevent sagging during post consolidation layer release. The tensioning of the belt however, did not allow the belt's back surface to come away from the heater during layer release, allowing the layer to stay tacky, and so the consolidated material was drawn from belt to build surface. When the next layer was deposited, the uneven surface was extruded and deposited to form an uneven artefact edge. The result of this can be seen in the picture in Figure 3.26, which also includes an overlay showing the intended artefact geometry. Figure 3.27 illustrates the incoherent consolidation problem which left parts of an artefacts layer consolidated on the build platform, while other parts remained on the belt. Figure 3.29 shows an enlarged image of the surface of an artefact with an area of consolidated material and an area where a number of layers had been pulled away.



**Figure 3.26** A picture with geometry overlay, of a 50 layer 0.5 x 20 x 20mm artefact, showing good consolidation but deformation and general artefact inaccuracy due to the effects of material pulling and re-deposition.

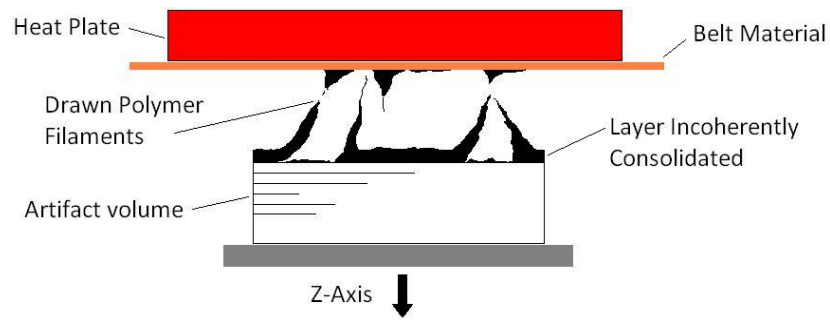


Figure 3.A 'pulled' layer due to tackified layer belt retention.

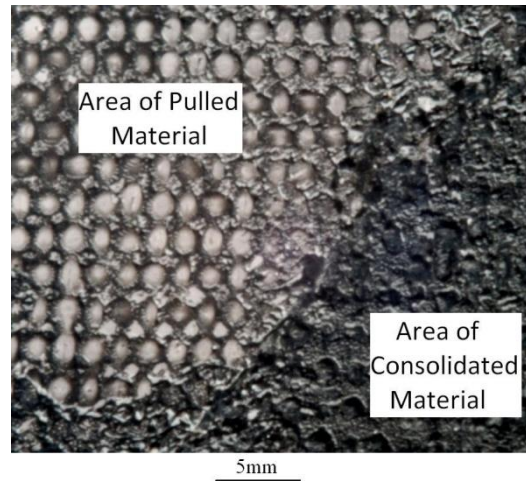


Figure 3.28 The effects of material pulling, due to tackified material retention.

*Conclusion*

The heat plate initially showed promising results due to the loose belt material allowing the layer to pull out of contact with the heat plate and thus allowed to cool while being released from the belt material. Following the increased tension of the belt material during consolidation, the belt and therefore consolidated layer was not able to be displaced from the heater. Without the heater displacement, the layer was not allowed to cool and solidify, resulting in tackified material being retained on the belt surface. Grenda (2001) proposed an embodiment employing a consolidation plate consisting of both a heating and a cooling area. This allowed a layer to be consolidated and then solidified for release. A limitation of such a device is apparent when considering the volume of a commercial system, as the consolidation plate would have to be twice the size of a single heat plate. In addition to the extra machine volume

needed, the cost of producing a cooling system and ensuring its thermal independence from the heat plate, would be an issue in a low-cost desktop system

### *Heat Blade Consolidation*

The tests conducted on the heat plate showed that once consolidated, the layer present on the belt needed time to solidify, to allow it to be released from the belt without the issue of material pulling. A solution investigated was that of a small heat plate that was moved over the surface of the layer to be consolidated in a continuous motion, tackifying and consolidating the material as it passed over before moving away to allow the consolidated layer to cool. A schematic of the system can be seen in Figure 3.29 showing the small heat plate as a curved heat blade to stop the edges of the heater snagging the belt as it moved.

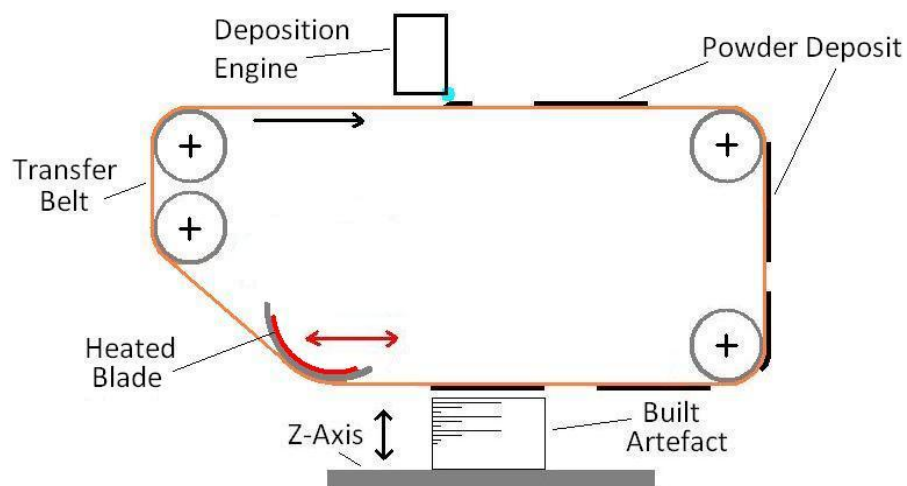


Figure 3.29 A system set up using heated blade consolidation

### *Function*

The principal of operation, as illustrated in Figure 3.30 was to maintain a consolidation blade at a given temperature while revolving a transfer belt upon which a powder image was deposited. When in the correct position over the Z-axis build platform, the belt motion would stop. The Z-axis would be positioned at the correct height for a layer to be deposited, at which point the heated blade would be moved across the build platform. As the heated blade was brought into contact with the belt portion

containing the powder image, the powder image would start to tackify through conduction. As the blade moved further it spread the newly tackified layer onto the build surface applying a small amount of pressure to consolidate. As the blade moved, it left behind it the belt and consolidated layer allowing it to cool, before the Z-Axis retracted, releasing the artefact and newly consolidated layer. The blade would then return home ready for the next layer.

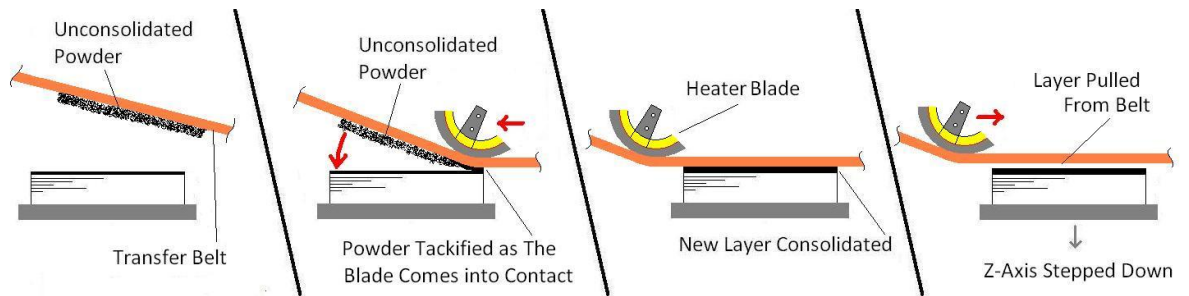


Figure 3.30 The function of the heated blade consolidation system

### Testing

A test bed was designed to provide a linear bearing mounting point for the heater blade and a clamp to mount the transfer belt material, while consolidation took place. For ease of design the heated blade was simplified to a heated roller which was constrained so that it was unable to rotate. Figure 3.32 shows both the intended CAD design and the constructed test rig.

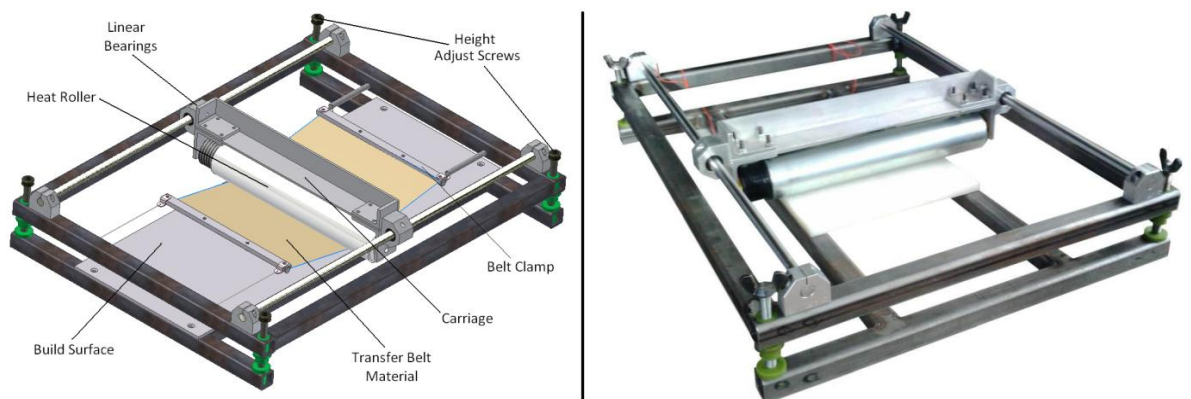


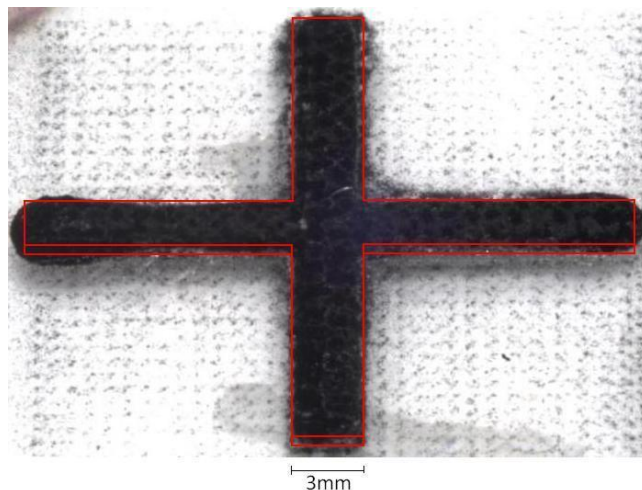
Figure 3.31 Left: A CAD render of the heat blade test rig. Right: A photograph of the test rig prior to belt mounting



As in previous tests, a powder layer image in a cross geometry was printed on to an A4 sheet of belt material. The belt was then aligned and clamped within the test rig which housed the heating blade mounted on linear bearings. The blade was run at a constant speed using a motorised lead screw, across the surface of the build surface to enable consolidation of a layer. The relative velocity at which the blade was run, was optimised through experimentation, ensuring complete consolidation. The height screws were then indexed up one layer thickness (10 microns) and subsequent layers printed.

#### *Results*

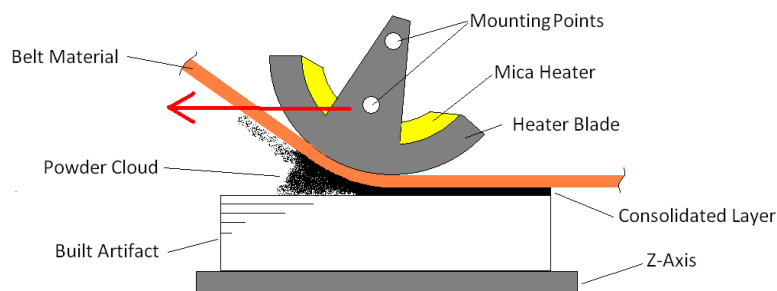
Following the consolidation of the first few layers it was clear that the heater blade was pushing material before it, producing poor images. It was assumed that the height offset was incorrect and so this was varied. At the larger offset consolidation stopped altogether as the layer present on the belt was not in contact with the build surface. A number of trials with a number of layer height offsets produced a 50 layer artefact as seen in Figure 3.32. The final layer height was that of the starting 10 micron value and the evidence of material smearing and powder cloud formation can be clearly seen within the figure 3.32.



**Figure 3.32** A picture with a geometry overlay, showing the resultant 50 layer (0.5 x 20 x 20mm) deposit consolidated with a heated blade. The occurrence of material smearing and powder cloud formation can be seen as a thickening of the geometry to the left hand side and a dark material dusting around the base of the artefact respectively.



After further investigation it was found that the cause of the smearing was not due to layer thickness irregularities but due to the formation of a powder cloud in front of the consolidation blade. As the blade moved over the belt, it produced a tribological charge. The charge generated by the PTFE was measured and found to be highly electronegative in nature ranging from -9kV to -21kV and so repelled the deposited powder as the blade ran across the build platform. A schematic of the phenomena can be seen in Figure 3.33. It was found that the belt material after consolidation would need cleaning to remove consolidated material displaced by the powder cloud.



**Figure 3.33 A schematic of the triboelectric powder cloud formation resulting in powder spreading**

### *Conclusion*

The use of a heated blade allowed the cooling of a layer post consolidation and eliminated the problem of material pulling. The system produced a powder cloud due to tribological charging which reduced the accuracy of the consolidated image. A solution may have been to electrically ground the heat blade, the tribological charging however, highlighted the presence of frictional forces which would have undoubtedly reduced the working life of a belt.

### *Heat Roller Consolidation*

The concept of the roller was to function in a similar way to the heat blade; to tackify the material while on the belt through conduction heating and then roll it on to the surface of the build platform. Figure 3.35 is a schematic illustration of the heated roller consolidation system.

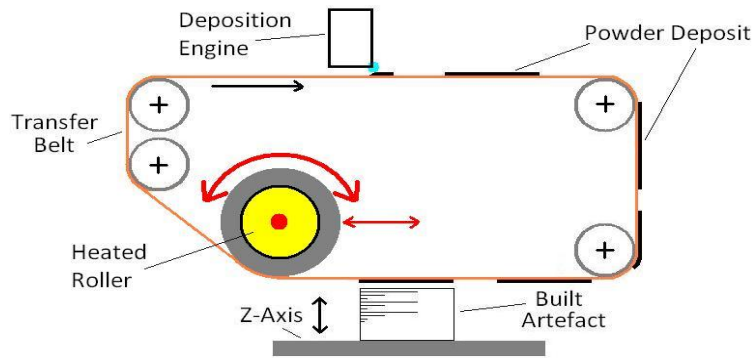


Figure 3.34 The system set up using heated roller consolidation

*Function*

The principal of operation, as illustrated in Figure 3.35, was to maintain a consolidation roller at a given temperature while revolving a transfer belt upon which a powder image was deposited. When in the correct position over the Z-axis build platform the belt motion would stop. The Z-axis would be positioned at the correct height for a layer to be deposited, at which point the heated roller moves across the build platform. As the heated roller was brought into contact with the belt portion containing the powder image, the powder image would start to tackify through conduction. As the roller moves further it would roll the newly tackified layer onto the build surface applying a small amount of pressure to consolidate. As the roller moved it would have left behind it the belt and consolidated layer allowing it to cool, before the Z-Axis retracted, releasing the artefact and newly consolidated layer. The roller would then return home ready for the next layer.

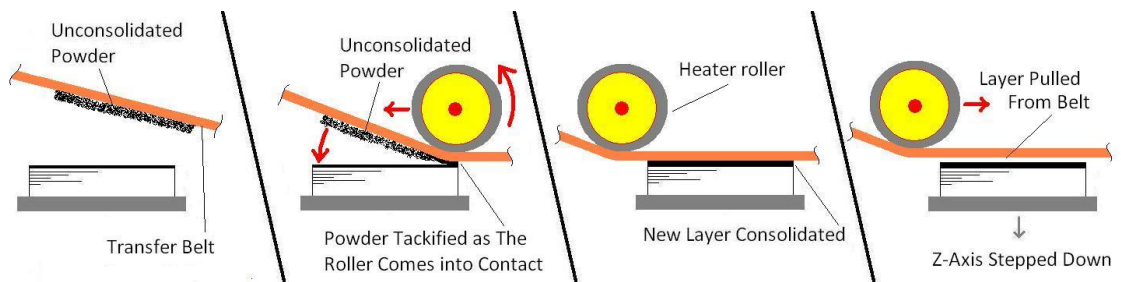


Figure 3.35 The function of the heated roller consolidation system

*Testing*

The test bed originally designed to test the heated blade was used in much the same way as it was for the blade testing. The velocity with which the roller was moved over

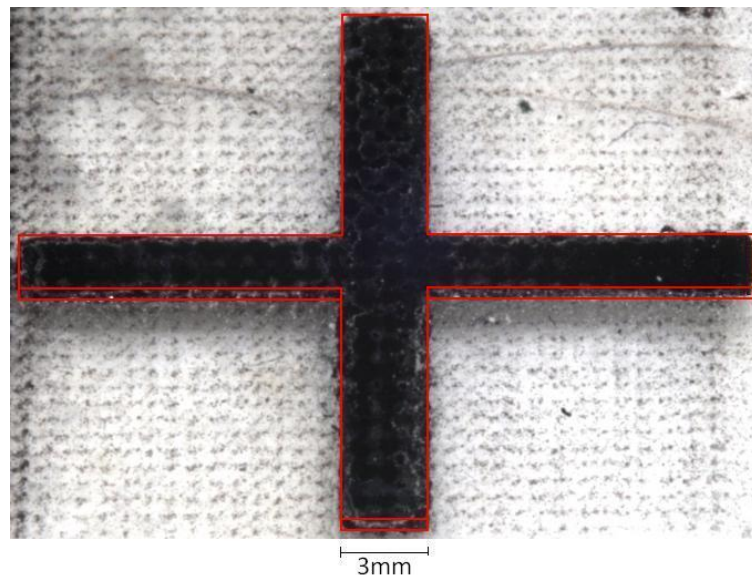
the surface of the build platform was experimented with to provide uniform consolidation.

### *Results*

The heated roller performed well, producing a well consolidated artefact after 50 layers with correctly formed geometry and no fringing as shown in figure 3.36. The z-axis limitation was not trialled at this point due to the manual factor of layer alignment printing and consolidation.

### *Conclusion*

The heated roller consolidation system has been shown to produce consistent consolidation with no image distortion or fringing after 50 prints. Although the z-axis height limitation was not manually tested, the heated roller solution showed no evidence to conclude that the Z-axis height limitation would be an ongoing issue. The final testing of this consolidation system will be discussed within the prototype testing section within this thesis.



**Figure 3.36** A picture with a geometry overlay showing the resultant 50 layer deposit consolidated with a heated Roller. The image demonstrates the ability of the roller to consolidate effectively.

### 3.3 The Concept

Following the results obtained from the experimentation discussed in the previous sections, this section will look at the formation of a system concept. The concept will be deconstructed in the conclusion of this chapter, to form a functional specification from which to create a prototype system design. Throughout the development of a new system it is necessary to have a vision of the end product. In this case the end product was a Desktop ALM system offering high productivity and high quality built artefacts. Figure 3.37 shows the ideal situation of a developed product, used within an office environment.



Figure 3.37 A visualisation of the intended implementation of a developed desktop ALM system.

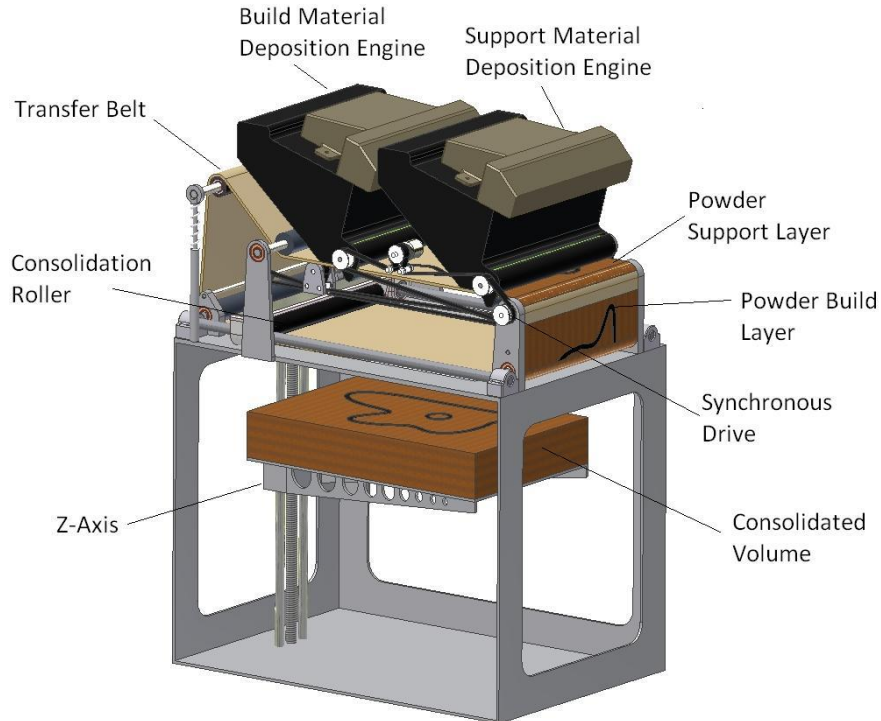


Figure 3.38 An initial system layout showing the component positions of a desktop electrophotographic ALM system.

Figure 3.38 was created as an initial system layout, showing the location, number and function of developer units, the transfer belt path without drive, Z-axis position and consolidation roller location. With the general aesthetic, environmental and system layout concepts generated, a functional specification for the generation of a prototype design could be produced.

### ***3.3.1 Transfer Belt System***

The belt system, within the proposed ALM concept, is responsible for the transport of powdered materials from deposition system to build platform. It is an intrinsic part of the holistic concept, and has a strong bearing on overall system productivity and accuracy.

#### *Productivity*

Two dimensional electrophotographic systems can have through puts of up to 200 pages per minute, equivalent to a paper velocity of around one meter per second. The literature survey highlighted the patents and previous works undertaken with respect to the implementation of Electrophotography as an ALM technology. It is apparent however, that the technologies surveyed failed to take full advantage of the possible productivity offered by the Electrophotography system. Kumar and Wimpenny opted to print onto a moving platform which was then moved to a separate consolidation apparatus. Bynum and Grenda described a system which printed on to a belt, which was stopped to consolidate above a build surface. The limitation to productivity in all former embodiments was the necessity to stop printing while each layer was consolidated. Electrophotographic printing at its most productive is a highly synchronous continuous process, which is significantly less efficient if the printing engine is paused. The key to high productivity within an electrophotographic ALM system is a solution which allows the continuous printing of layers while accommodating consolidation. Kumar and Wimpenny suggested moving the build platform relative to the transfer medium. This could be adapted to allow continuous layer printing, but with the artefact and support mass' creating limiting inertial forces during platform reciprocation. A solution offered within this research is the use of an accumulator. Figure 3.39 illustrates the design of a simple accumulator, which pays

out belt material to the deposition system while consolidation takes place, and then re-accumulates it while the next image is being shuttled into place above the build platform.

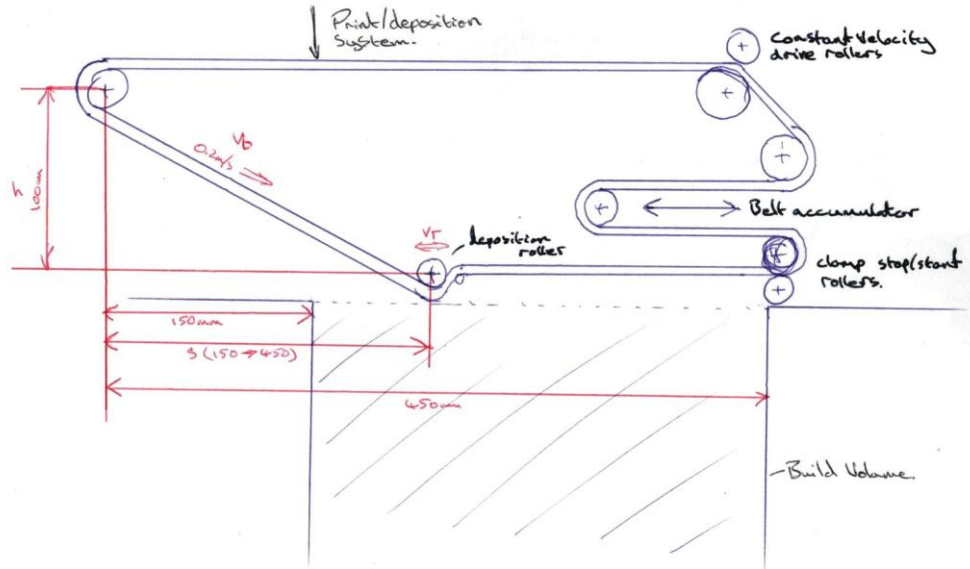
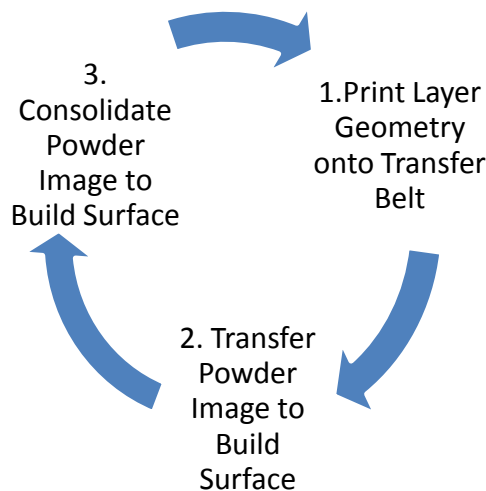


Figure 3.39 AAan accumulator system for improved productivity

*Productivity of a Belt ALM System without Accumulator*

Taking a simplified electrophotographic system as described in the schematic of Figure 3.40, where a transfer belt is printed on, the image transferred to the build platform and the image consolidated onto a build surface, the maximum system productivity can be calculated. The system fulfils a printing cycle following three physical steps as illustrated in Figure 3.41.



**Figure 3.40** The three processes undertaken by an ALM system to consolidate a layer.

The total belt length needed to produce and consolidate a single layer is represented by the maximum image geometry in the Y-axis ( $G_{Ly}$ ) plus the geometry of the layer image spacing ( $G_{Ls}$ ). The transfer geometry ( $G_t$ ) is calculated by the sum of ( $G_{Ly}$ ) + ( $G_{Ls}$ ) and represents the length the belt must move in order to line up the next image for consolidation.

Assuming an ideal system where the printing, image transfer and consolidation roller homing are all performed concurrently, the system productivity ( $P_s$ ) can be expressed as

$$P_s = \frac{V_L}{t_p + t_c} \quad (3.5)$$

Where  $t_p$  and  $t_c$  are the time taken to print and consolidate a single layer respectively. The layer volume ( $V_L$ ) can be expressed as

$$V_L = G_{Lx} \cdot G_{Ly} \cdot G_{Lz} \quad (3.6)$$

Where  $G_{Lx}$  and  $G_{Lz}$  are the geometries of the printed image layer in the X and Z axes respectively.  $t_p$  and  $t_c$  are variables with respect to layer geometry, where  $t_p$  is a function of the print engine printing velocity  $v_p$  and the  $t_c$  a function of consolidation roller velocity  $v_r$ .

$$t_p = \frac{G_t}{v_p} \quad (3.7)$$

$$t_c = \frac{G_t}{v_r} \quad (3.8)$$

And  $v_r$  being a function of roller thermal power ( $E_{in}$ ) and the energy needed to increase a layer of material from ambient temperature ( $t_a$ ) to that of its melting temperature ( $t_m$ ) considering its heat capacity ( $c$ ) and density ( $\rho$ )

$$V_r = \frac{G_{Ly}}{\frac{G_{Lx} \cdot G_{Ly} \cdot G_{Lz} \cdot \rho \cdot c \cdot (t_m - t_a)}{E_{in}}} \quad (3.9)$$

Assuming the roller thermal output and velocity stay constant and substituting equations 3.6, 3.7 and 3.8, back into equation 3.5, a complete expression for the productivity of a belt electrophotographic ALM system can be represented by

$$P_s = \frac{G_{Lx} \cdot G_{Ly} \cdot G_{Lz}}{\frac{G_{Ly} + G_{Ls}}{v_p} + \frac{G_{Ly} + G_{Ls}}{v_r}} \quad (3.10)$$

Substituting the values of  $G_{Lx} = 200\text{mm}$ ,  $G_{Lz} = 0.01\text{mm}$ ,  $G_{Ls} = 30\text{mm}$  and  $V_p$  and =  $(12/60) \cdot 297 = 59.4\text{mm/sec}$  and  $v_r = 1.25v_p$  the overall system productivity ( $P_s$ ) can be plotted (Fig 3.41) with respect to layer volume as a function of  $G_{Ly}$

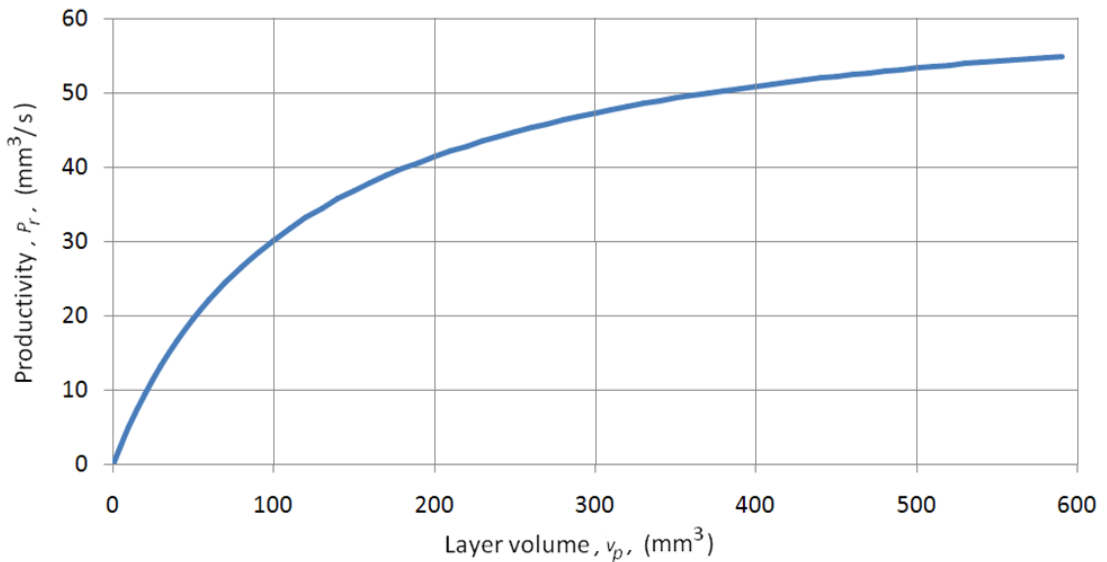
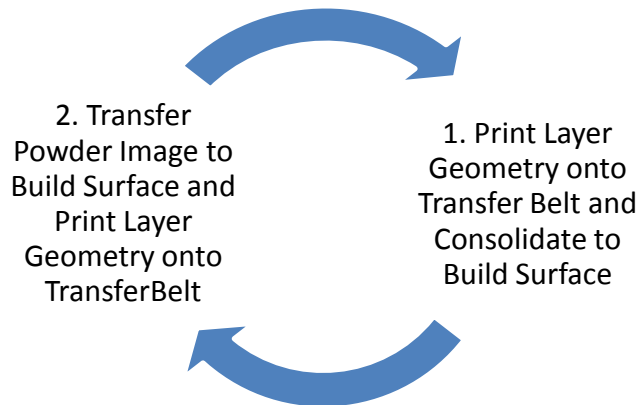


Figure 3.41 Productivity against layer volume of belt electrophotographic ALM system without an accumulator.



*Productivity of a Belt ALM System with Accumulator*

The advantage of an accumulator system was to allow the concurrent printing and consolidation on to and from a single belt. The function of the system was to collect belt material in an accumulator while the belt was being aligned for the next powder image to be consolidated. In this type of system the belt velocity  $v_b$  can vary while the print velocity  $v_p$  remains constant. There were two solutions, either  $t_p \geq t_c + t_t$  or  $t_p < t_c + t_t$  where  $t_t$  was the time to transfer an image from printer/accumulator to the correct position above the build platform. In the previously discussed belted system, without accumulator,  $t_c$  was assumed to be equal to  $t_p$ , and  $t_t$  was neglected due to its concurrency with  $t_p$ . To exploit the benefit of an accumulator,  $t_p$  must be  $t_p \geq t_c + t_t$ . In other words the printing speed should be the productivity bottle neck. As  $t_t = \frac{v_b}{G_t}$  where  $v_b$  is a variable greater than  $v_p$ , the impact of  $t_t$  on the printing speed can be reduced with the rapid transfer of a pre-printed powder image to the correct position for consolidation. The process sequence can be seen in Figure 3.42.



**Figure 3.42** The two processes undertaken by an electrophotographic ALM system using an accumulator.

Assuming  $t_p \geq t_c + t_t$  then the system productivity ( $P_s$ ) for a belt electrophotographic ALM system with an accumulator can be simply expressed as

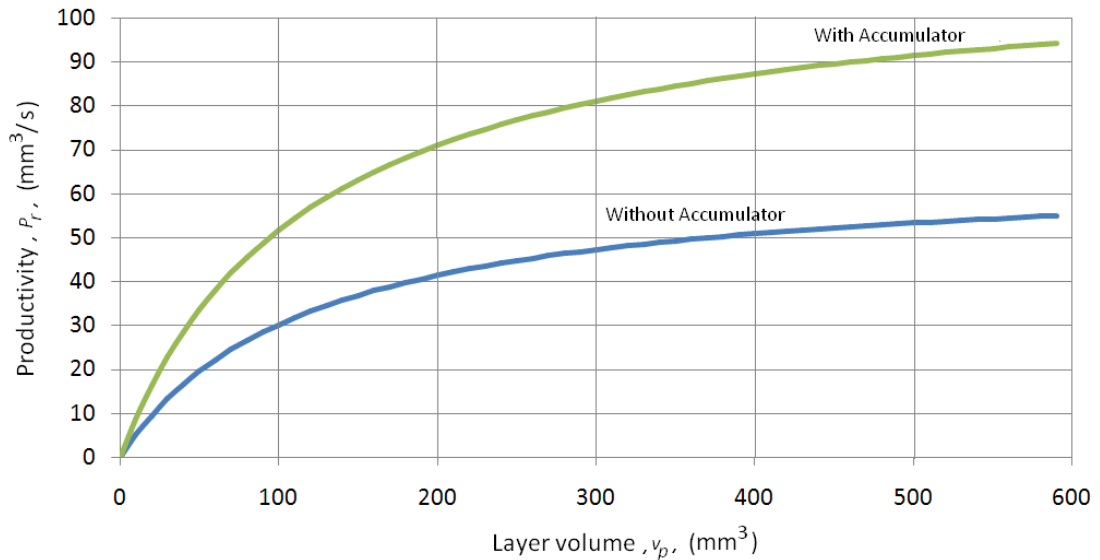
$$P_s = \frac{V_L}{t_p}$$

(3.11)

Substituting  $V_L$  and  $t_p$  from equation 3.2 and 3.3,

$$P_s = \frac{G_{Lx} \cdot G_{Ly} \cdot G_{Lz}}{\frac{G_{Ly} + G_{Ls}}{v_p}} \quad (3.12)$$

Assuming  $v_r = 1.25 v_p$  and  $v_b = 4v_p$ ,  $G_{Lx} = 200\text{mm}$ ,  $G_{Lz} = 0.01\text{mm}$ ,  $G_{Ls} = 30\text{mm}$  and  $v_p = 59.4\text{mm/sec}$ , the overall system productivity ( $P_s$ ) can be plotted with respect to layer volume as a function of  $G_{Ly}$



**Figure 3.43** A plot of the theoretical comparable productivities between an ALM system with and without an accumulator

The plot in Figure 3.44 shows the marked theoretical productive improvement with the implementation of an accumulator. The calculation demands that the total transfer and consolidation time of a single layer must not exceed the time taken to print a layer. In reality a system which provided faster printing than consolidation could still have a productive gain over an accumulator free system but the advantage may not be so marked.

### *Productivity Conclusion*

The results of the productivity estimations for maximum productivity, with and without an accumulator are dependent on a number of variables, the most significant of which was the printing time and the consolidation time. While printing time per unit area was a constant with respect to the printing engine design, consolidation time was variable. Consolidation required a minimum energy input affected by a level of thermal exposure for a given period of time. This suggested that lower consolidation times could be achieved with higher thermal exposure levels. There is a limit to this relationship due to various factors including thermal conductivity, thermal contact and point of thermal decomposition of the build material as well as belt material factors. Further empirical investigation would be necessary to determine the true nature of these factors. The full benefit of an accumulator system would have been if it were to have been combined with low-cost printing systems exhibiting low printing velocities. Significant increased efficiency through the use of an accumulator has been noted with further investigation necessary. For the development of a prototype to satisfy the objectives, a standard system without an accumulator was adopted to simplify the machine design and operation.

### *Accuracy*

A key property of the chosen belt material was its high resistance to bonding with layer powders under thermally adverse conditions. Through testing, PTFE was shown to be the optimum solution due to its thermal stability and low surface energy. The low surface energy property of PTFE however, generated a problem while relying on friction to drive the belt. It was concluded that a mechanical interlocking type of system such as a chain or band drive should be used to ensure consistent layer alignment. While the concept of having a physical interlocking belt drive was relatively straight forward the precise actuation, to enable layer line up, was less apparent. In terms of a low-cost rotary drive the only option was electric motor, DC brushed, DC brushless or Stepper motor.

### *DC Motor*

Both brushed and brushless motors provide no usable feedback on their position during operation (other than to commutate the brushless motor) and as such need a secondary feedback system such as optical encoders. Encoder feedback systems are often expensive and if combined with a brushless motor can be very costly to implement. Brushless motors are known for their high power to weight ratios, efficiency and reliability when compared to brushed type motors. The limitation being that brushless motors need high value electronic control systems.

### *Stepper Motor*

In common with brushless DC motors, a stepper motor required an electronic controller to rotate; however, the major difference was that a stepper motor could provide open loop feedback allowing relative position feedback during operation. Stepper motors were used in many laser printers as a low-cost solution for relative position sensing and velocity control. Stepper motors were unable to give absolute position feedback but could give relative position and velocity feedback with the presumption that the rotor was in sequence with its drive signal. In addition, the finite rotor positioning of a stepper motor, i.e. 200 steps per revolution and high step torque allowed the accurate and repeatable positioning of the rotor.

### *Conclusion*

The finite positioning of the stepper motor was advantageous in the transfer of deposited powder images from deposition system to build platform by simply maintaining the number of steps for every layer. DC brushless motors were of high cost and although brushed were less expensive; the integration of feedback makes cost more of an issue.

### *Belt Discharging*

Discharging of the belt material was touched on during the belt material trials indicating the active, non-contact corona discharge apparatus to be the optimum choice. Corona discharge apparatus can be expensive, produce harmful gas products such as O<sub>3</sub> and nitrogen oxide, as well as producing an unpleasant odour, all of

which are less than ideal characteristics for a desktop system. A number of tests were undertaken with commercially available passive and active static eliminators.

### *Method*

A PTFE sheet was tribocharged with a polyester fibre material and the resultant surface charge was recorded in three random areas with a surface charge meter (715, Fraser, UK). The discharge apparatuses to be tested were passed in contact or close proximity to the PTFE surface, after which the surface charge was once again measured in three places and the residual average charge recorded. Four passive discharge methods were investigated:

- Conductor electrically connected to ground (Fig 3.44)



**Figure 3.44 A passive conductor type static charge eliminator**

The principal of operation of the conductor discharge was to conduct the surface charge from the PTFE to ground through direct contact. This method is the lowest cost potential solution but can only work with the conductor in contact with the PTFE substrate.

- A Carbon fibre brush electrically connected to ground (Fig 3.45)

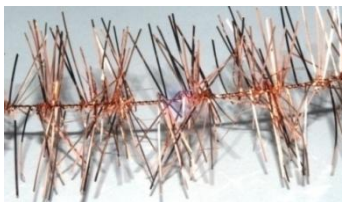


**Figure 3.45 A passive carbon fibre brush type static charge eliminator**

The operational principle of the carbon brush is to create a highly non uniform electric field at the tips of the 10micron carbon filaments, thus ionising the air, equalising the charge between brush and substrate. As the brush is tethered to ground the resultant

charge left on the surface of the PTFE substrate should theoretically be close to the ground charge 0v. The charge on the substrate will never actually reach 0v with a non contact passive system as the energy needed to discharge the surface is gained from the surface charge itself. Theoretical equilibrium is reached when the charge left on the surface of the substrate is no longer sufficient to create an electric field strong enough to ionise the surrounding air. In reality, the surface may continue to lose (or gain) charge through the effects of humidity, gas or airborne impurity movement.

- Brass tinsel electrically connected to ground (Fig 3.46)



**Figure 3.46 A passive brass tinsel type static charge eliminator**

The conductive tinsel is a technology developed before the advent of carbon fibre dischargers. The bristles of the tinsel function in much the same way as the carbon fibre brush filaments, but as the thickness of the bristles is significantly thicker than the diameter of the carbon fibre, the electric field is less non-uniform and so results are expected to be less efficient.

Two active discharge methods were investigated:

- AC charge roller (Fig 3.47)



**Figure 3.47 An active charge roller static charge eliminator**

Both active methods of discharge used alternating current (AC) as the continuously changing polarity of the electric field attracted charged ions to and from areas of non uniform charge. The roller was applied to the surface of the substrate and neutralised the residual charge.

- AC corona (Fig 3.48)

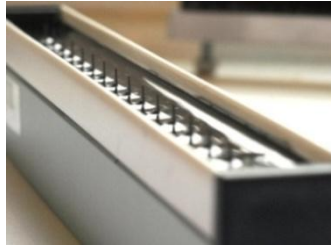


Figure 3.48 An active corona discharge static charge eliminator

The corona was generated on the tip of sharp points which created a highly non uniform electric field. The resulting stream of charged ions are attracted to oppositely attracted areas of the substrate, collectively neutralising residual charge

*Results*

The results of the testing for each of the static eliminators is shown in Table 3.5, with the active apparatus providing better results. The Non-contact carbon brush discharge performed better than contact discharge. This may be an effect of passing the brush over the surface and producing a tribological charge. The brass tinsel reduced the charge significantly, but still left a relatively large charge of -2500 volts on the substrates surface. The worst performer was the ground connected conductor which left a -5300 volt potential on the surface of the substrate. This could have been due to a number of factors with the most likely being inefficient contact and through forced contact tribological effects.

Type of anti static apparatus	Initial Surface Charge (kV)	Average Surface charge (kV)	
		Contact	Non-contact
<b>Passive</b>			
Ground Conductor	-24.6	-5.3	-
Carbon fibre Brush	-24.4	-3.1	-1.5
Brass tinsel	-24.6	-2.5	-3.5
<b>Active</b>			
AC charge roller	-24.5	0.3	-
AC Corona discharge	-24.9	-	0

Table 3.5 A Table presenting the results of trials undertaken to assess the efficiency of a number of electrostatic discharge means.

### *Conclusion*

The AC corona although expensive is the best option for complete eradication of surface charge. The next best solution would be a charge roller, which could also be employed to induction charge the belt with a positive potential if the AC current was multiplexed on top of a positive DC potential. A non contact solution would be preferred over a contact solution as a brush or roller in contact may wear and/or pick up debris from a transfer belt, thus reducing efficiency over time.

### **3.3.2 Consolidation Roller**

The literature survey reviewed five heated roller laser printer and photocopier fixing apparatus patents, each representing a step change in technology. The following section will discuss areas of design interest referencing the reviewed patents.

### *Thermal Source*

The consolidation roller needed a thermal source in order to consolidate the powder layers into the artefact geometry. The thermal system was to consist of a means of thermal energy generation and the control of the resultant surface temperature of the roller. Thermal energy could have been generated in a number of ways, Sugihara et al (2000), offers a patent which described the use of a halogen capsule with an internal resistive element. Through the reverse engineering of the printers as previously discussed, a number of the inexpensive halogen heaters were collected. Low-cost and part availability drew the conclusion that the halogen heater capsules should be used in a future prototype design. The control of the surface temperature of the consolidation roller should be maintained at a constant temperature within a few degrees. The exact allowable temperature drift would have only been apparent through testing. The system could have been modelled and a PID transfer function developed, however for the scope of this research a digital thermal controller (Cal 3200) was to be used, which derived the systems transfer functions using collected data. While more expensive than producing proprietary control hardware and software, for the purposes of the initial system prototyping, the use of a commercial controller eliminated an untested system component and associated failure mode.



### *Actuation*

Actuation of the consolidation roller involved the indirect reciprocation of the roller over the surface of the build platform. The actuation is required to be performed at a constant speed with a smooth action. A limit switch will be required at either end of the rollers travel to allow the control system to determine the rollers position. While a brushless or brushed DC motor with velocity feedback may be the best option for smooth motion. This option would require the development of system tools, hardware, software and firmware to control the rollers travel. With this in mind, the use of a stepper motor for the actuation of the roller would be most cost effective. While stepper motors are known for their stepping action, their velocity and smooth operation can be adjusted through the use of step routines. The step routines are Full step, Half step, Wave and micro step. Full step is the incremental rotation from pole to pole of the stator, producing an uneven motion but at high torque. Half step, as would be expected produces a motion which is smoother due to the apparent doubling of the number of steps per revolution. The half step phenomenon is created by energising two pole windings simultaneously between steps, pulling the rotor between poles. The half step routine produces less torque than the full step but provides a smoother operating motion. Wave is rarely used and so will not be discussed here. Micro step differs from the other step routines as it uses an analogue current signal (or digital pulse width modulation (PWM) approximation) rather than binary drive signal. Instead of switching coils to step the rotor, it gradually increases the current seen by a pole coil while reducing the current in another. The resultant motion of the rotor is smooth and regular. The torque from micro stepping can be high and high speed rotation is also possible. However, due to the need for modulated control of the individual field windings, the control hardware is relatively costly when compared to standard stepper motor controllers. The prototype should look to use a low-cost half step routine, and develop a solution through testing if necessary.

### **3.3.3 Electronic Control Systems**

The prototype was to be designed to be altered and experimented with to provide useful data. One of the key concepts was the modularisation of the control

electronics, allowing a single programmable controller to communicate with interchangeable ancillary modules, to allow multitasking and hot swapping of actuator devices. There are a number of IC controller architectures on the market including ARM's ARM, Microchip's PIC and Atmel's AVR micro controllers. Each has their advantages and disadvantages, this application required an EEPROM and to keep the circuit complexity to a minimum a PIC was chosen as the controller architecture.

### **3.4 Prototype Functional Specification**

The purpose of this specification is to generate guidelines and definitions from which designs for the individual parts of a prototype can be based. As with the preceding design chapter, the specification is broken down into four separate sections of the deposition, consolidation, Z-axis and control systems. The first section however will discuss the general system characteristics.

#### ***3.4.1 System Characteristics***

##### *Function*

The system as a whole is required to function synchronously to fulfil the requirements of the objectives.

##### *Materials*

Although a number of build materials have been tested and the results discussed, the material used within this prototype system will consist of the standard styrene copolymer toner powder. The powder exhibits the following key properties (Samsung, 2006):

- Glass transition temperature (T<sub>g</sub>): 65 – 75 deg C
- Melting temperature (T<sub>m</sub>): 80 – 90 deg C
- Average Particle size: 5 – 8 microns
- Triboelectric polarity: Highly electronegative
- Composition: (% by weight) 80 – 95 Styrene Acrylic Copolymer, 3 – 8 Carbon Black, < 5 Particle control agent.
- Single component – non magnetic

The use of secondary support materials is not within the scope of this thesis.

*Productivity*

The initial prototype will be developed to demonstrate its ability to fulfil the objectives previously set out in this thesis. As a result the productivity of the prototype is a secondary consideration. As the prototype will be of belt type with no accumulator, the productivity will be a factor of the deposition velocity, the image transfer velocity and the consolidation velocity.

*Control*

The low level control of the majority of the system will be undertaken by a donor printer’s controller (ML4500) and a number of ancillary controllers. The high-level control will be performed by a proprietary system which will be interfaced with the donor printer’s controller.

*Cost*

The prototype should be designed and constructed with the overall low-cost spirit of a desktop system in mind. Components of high cost may be used if a viable low-cost alternative could be implemented in future systems.

*Form*

The POC prototype should be true to desktop dimensions to demonstrate the technologies suitability for final integration into a desktop product. The standard desktop properties (Table 3.6) as introduced in the literature survey should be used as guidelines. Once again, larger components or subsystems can be used if a more compact low-cost solution is available for future prototypes and commercial systems.

<b>Standard 'Desktop' Properties</b>	
<b>Maximum Dimensions (L x D x H)</b>	733 x 600 x 840
<b>Maximum Mass</b>	40kg
<b>Maximum Power Consumption</b>	3000 Watts
<b>Process Materials</b>	Non Toxic
<b>Utility Required</b>	Single Phase Electric Only

Figure 3.6 A Table developed within the literature survey illustrating the key constraints of a standard ‘Desktop’ system.

### ***3.4.2 The Deposition System's Functional specification***

#### *Function*

The deposition system consists of the LSU, powdered material supply, developer rollers, OPC and transfer roller. The primary function of the system is to form dense, accurate powder images and deposit them onto a transfer substrate.

The charging of the belt substrate will be undertaken by induction charging by a transfer roller at elevated positive DC charge.

#### *Materials*

A number of the key components should be taken from a donor printer and as such the part materials are not variable. Any structures designed should be made of an easily machined material, preferably an engineering polymer. The available manufacturing routes include laser cutting, CNC milling, turning and other hand operated processes.

Materials which are designed to come into contact with electrostatically charged components should be manufactured from a non conducting material with appropriate dielectric strength.

The OPC component is sensitive to ambient light and as such any enclosures designed should ensure that they do not transmit or defuse light allowing printing interference from ambient light sources.

#### *Productivity*

The donor printer's printing engine dictates the productivity of the deposition unit. An 8ppm Samsung ML4500 laser printer was used in the majority of the materials testing and was used as a donor printer for parts for the prototype deposition system. Long term potential productivity will be assessed and discussed later in this thesis. A rapid deposition of powder materials is ultimately required.

#### *Accuracy and Resolution*

Dimensional accuracy in the X and Y is a factor of the accuracy of the initial deposited layer image, the transfer alignment and the consolidation technique. Dimensional

accuracy in the Z-direction is a factor of the layer deposition thickness and Z-axis accuracy. The X-Y resolution of the donor printer is 600 x 600 Dpi; however, no formal figures are given for printer engine accuracy in the printer literature. The layer thickness has been shown to be constant during testing with a layer resolution of 0.01mm and an accuracy of 0.01mm. Fundamentally the system must provide repeatability to allow multi layer deposition to take place.

### *Control*

The control of the deposition system will remain with the donor printer's microcontroller system. This will be interfaced with the ALM systems proprietary controller developed within this research. Interface options include the manipulation of sensors such as the paper in magazine, paper in feed, paper in fuser and case open sensors. The system must be fully synchronised with the rest of the system to facilitate accurate deposition.

### *Cost*

In terms of determining system costs the print engine is a significant factor. Items such as the OPC and LSU must be of high quality to ensure not only accurate generation of layers but a high print count expectancy.

### *Form*

The deposition systems major dimensional constitute is the powdered material supply. In this prototype the deposition system may retain the dimensions of the donor laser printer and therefore be significantly larger than would be expected from future systems. A new deposition system should look to make the development rollers, the OPC drum and the doctor blade adjustable to facilitate future research into thicker deposited layers and use of different low-cost materials.

### ***3.4.3 The Consolidation System's Functional Specification***

#### *Function*

The consolidation system consists of the layer transfer belt and its means of drive, the consolidation roller assembly, its heater, its reciprocating drive and the main body of

the prototype. The purpose of the system is to transfer loose powder images from the deposition system, accurately position them above the Z-axis build platform and consolidate them to a build surface consisting of previously consolidated material.

The consolidation system should incorporate belt conditioning such as cleaning and electrostatic discharge.

- **Belt Cleaning**, should be performed prior to belt discharge as any contact could cause tribological charging of the belt material. The cleaning apparatus may be implemented in a number of forms while ensuring no belt damage occurs. Experiments have shown that most materials will wipe from the surface of the belt with a synthetic sponge or polyurethane scraper, abrasive materials such as household polymer pan scourers should not be used.
- **Belt Discharging**, can be achieved through a number of passive means including earthed contact and proximal electrode, and active means such as charge roller or corona discharge. Due to the triboelectrical properties of the belt material, non contact discharge is preferable, with a higher discharge efficiency found with active corona discharge.

### *Materials*

The main parts of the consolidation system consist of the transfer belt, the prototype housing and consolidation roller.

- **Transfer Belt**, glass reinforced PTFE materials of under 0.115mm in thickness have been shown to be an optimal choice. Guide roller materials should look to minimise the build up of tribocharge by selecting materials which could potentially earth surface charges.
- **Prototype Housing**, is the main frame upon which the individual systems are affixed. The housing frame is needed to mount the belt rollers and the consolidation roller linear bearings. As the complete system will be compact it would be preferential for it to have transparent sides to observe the function of the system during testing. Materials such as polycarbonate or acrylic would be suitable as they would provide the necessary strength, while lending

themselves to the laser machining process available. Attention must be paid to the regions of the prototype which may be exposed to thermal energy from the consolidation roller and heat shielding may be necessary.

- **The Consolidation Roller**, should be constructed from materials which are thermally stable up to a working temperature of 200°C. The roller must consist of a highly conductive material supported by bearings and employ a coaxial halogen capsule heater. Cooling of the bearings may be necessary, but airflow across the belt surface should be avoided to ensure minimal powder disturbance. A non-stick surface coating such as PTFE may be advantageous to aid cleaning of the roller if unwanted material deposits form during use.

### *Productivity*

The productivity of the consolidation unit is a function of both the consolidation rollers velocity and the belt velocity. However, prior to further developing the system a consolidation time is required. The reverse engineered laser printer (ML4500) studied, took four seconds to fuse a sheet of toner and A4 paper and as such the consolidation roller should look to take four seconds or less to consolidate.

### *Accuracy and Resolution*

Accuracy within the consolidation system is determined by the ability of the transfer belt to position sequential layers on top of one another prior to consolidation. Assuming synchronisation of the initial printing of the image on to the belt, the belt drive is the primary alignment variable. The belt drive should consist of a cogging mechanism which allows the belt to interlock with a drive timing mechanism. The belt position feedback can be provided open or closed loop but must ensure accurate drive. A possible solution may be the use of a stepper motor and gearbox system.

### *Control*

The control of the belt drive and the consolidation roller will be undertaken by a proprietary electronic control system. The two actuators will be paired with two independent ancillary controllers which communicate with the master controller. The

ancillary controllers will allow different actuators to be substituted during testing without affecting the main controller program.

#### *Cost*

In terms of determining system costs the consolidation system is a large system with the second largest cost factor. The volume needed to house the belt and its drive, as well as the consolidation roller and its drive, is large in comparison to the other systems. In common with the rest of the system, for the first prototype, the components need not be constrained by tight budgetary requirements, but should reflect the low-cost spirit of the research while still providing a suitable subject for 'POC' testing.

#### *Form*

The dimensions of the consolidation system are a factor of the donor laser printers dimensions and the volume needed for the consolidation roller, the belt and both their drives. The prototype will be used to determine the dimensions of further prototypes.

### ***3.4.4 The Z-axis System's Functional Specification.***

#### *Function*

The primary function of the z axis is to provide an absolute height reference with which to transfer and consolidate sequential layers. The Z-axis indexes down a predetermined layer thickness to gradually create a volume into which an artefact is formed.

#### *Materials*

The Z-Axis is a vital part of all ALM systems and as such there are a wide variety of designs currently employed within commercial systems. There are many low-cost, established solutions for the z-axis apparatus and the 'POC' prototype will use a Galil DMC-1010 servo motor controlled Z-Axis available for use within the department. The materials used in the commercial system are of relatively high cost, but future systems will reflect the low-cost nature of the research.



### *Productivity*

The velocity of the Z axis is adjustable and has a sufficient velocity to have no bearing on the overall productivity of the system.

### *Accuracy and Resolution*

The required system resolution for the Z axis is 10 microns. The control system for the Z-axis used in testing had a resolution of 100 step counts per micron. Testing during set up, which will be discussed in forthcoming chapters, shows the Z-axis used to be of adequate resolution.

### *Control*

The Z-axis is to be Galil motion controlled and will be interfaced with the ALM systems proprietary controller, which will issue a command to run the pre programmed command sequence.

### *Form*

The physical dimensions of the Z-axis system used are out of the specified range for a desk top system. However, there are a large number of pre existing Z-axis designs which would fulfil the prerequisites of both size and cost which can be considered for future systems (all low ALM systems employ a Z-axis including the low-cost systems, e.g. fab@home, bits-from-bytes.)

The Z-axis Table area is 500 x 500 mm and so an adjustable Table of smaller dimensions may need to be produced for testing.

## **3.4.5 The Control System's Functional Specification.**

### *Function*

The electronic control system developed is required to be of modular construction with a programmable master controller. The function the ancillary controllers is dependent on the chosen actuators. The actuators may include Bipolar and Unipolar stepper motors, indicators, LCD displays, 240Vac switching and DC motors.

### *Materials*

A number of PCB's will have to be produced with the necessary connecting headers to create a control system. Due to the current frequencies used to drive the stepper motors, the master controller PCB should be designed to minimise the effects of interference.

### *Accuracy and Resolution*

The actuator control electronics and associated programs should be able to efficiently operate the prototypes hardware to ensure optimum accuracy. The resolution of any stepper motors used should be increased through the use of step down gearing.

### *Control*

The control of the deposition system will remain with the donor printer's microcontroller system. This will be interfaced with the ALM systems proprietary controller developed within this research. Interface options include the manipulation of sensors such as the paper in magazine, paper in feed, paper in fuser and case open sensors. The base to each control board should be a PIC microcontroller produced by Microchip and programmed in such a way that program variables are easily adjustable. The system will interface with a PC through a parallel port or USB and function from issued Bitmap or JPEG files representing artefact slices.

### *Cost*

Cost of electronics and actuator technology is always large with technologically integrated machinery, with the cost of producing one off and prototype PCB's especially high. The true cost of electronics can only be assessed and optimised in later prototypes. However the use of widely available components and low-cost hardware is a necessity.

### *Form*

As previously discussed the control system should take the form of one master controller, communicating with a number of ancillary boards. There should be an ancillary board for each of the prototype actuators. The physical dimensions of the actuators and PCB's should be as small as economically possible.

# Chapter 4: Prototype Design

---

## 4.0 Introduction

Following a review of 3D printers within the literature survey, the concept chapter tested a number of concepts and concluded with the formation of a specification for the design of a novel prototype ALM system. Using this specification as a point of reference, this chapter will detail the design and construction of a proof of concept (POC) prototype.

The design of an integrated system consisting of software, firmware and hardware demanded an understanding of multiple engineering disciplines. For the benefit of the reader, the following chapter is split into sections and subsections based around functional areas of the prototype. However in reality, the system was designed concurrently, in its entirety, as many parts of the machine were functionally linked.

## 4.1 Design Methodology

A systematic approach was applied to the development of the ALM system within this research. The proposed POC prototype was split into functional sub-systems consisting of: deposition, powder transport, layer consolidation and z-axis. The diagram, Fig 4.1, illustrates the key links and ultimately, the vast number of design constraints imposed by the interdependent sub-systems. The design development was undertaken iteratively to ensure final compatibility. The sub-system designs were developed in parallel and necessary design considerations were reviewed and incorporated continually. This approach ensured that the final prototype functioned synchronously. Figure 4.2 illustrates the cyclic nature of the proposed ALM system, while figures 4.3 and 4.4 illustrate two IDEF0 diagrams which describe both the general project flow and the more specific iterative design process respectively. The least complex of the four subsystems was designed first. At the upper end of the IDEF0 node diagram (Fig. 4.4) the sub-systems were considered for redesign a greater number of times than those towards the lower end. Designing the least complex sub-systems first, ensured that minimal time was spent iteratively incorporating the

additional constraints from the development of subsequent sub-systems. Table 4.1 shows the number of times each sub-system underwent a design iteration. Three dimensional CAD modelling played a key role in the development of the POC prototype, as it allowed sub-system interfaces to be virtually analysed and facilitated rapid design iteration. The CAD software used was Autodesk Inventor, which provided not only a three dimensional modelling facility, but allowed for the

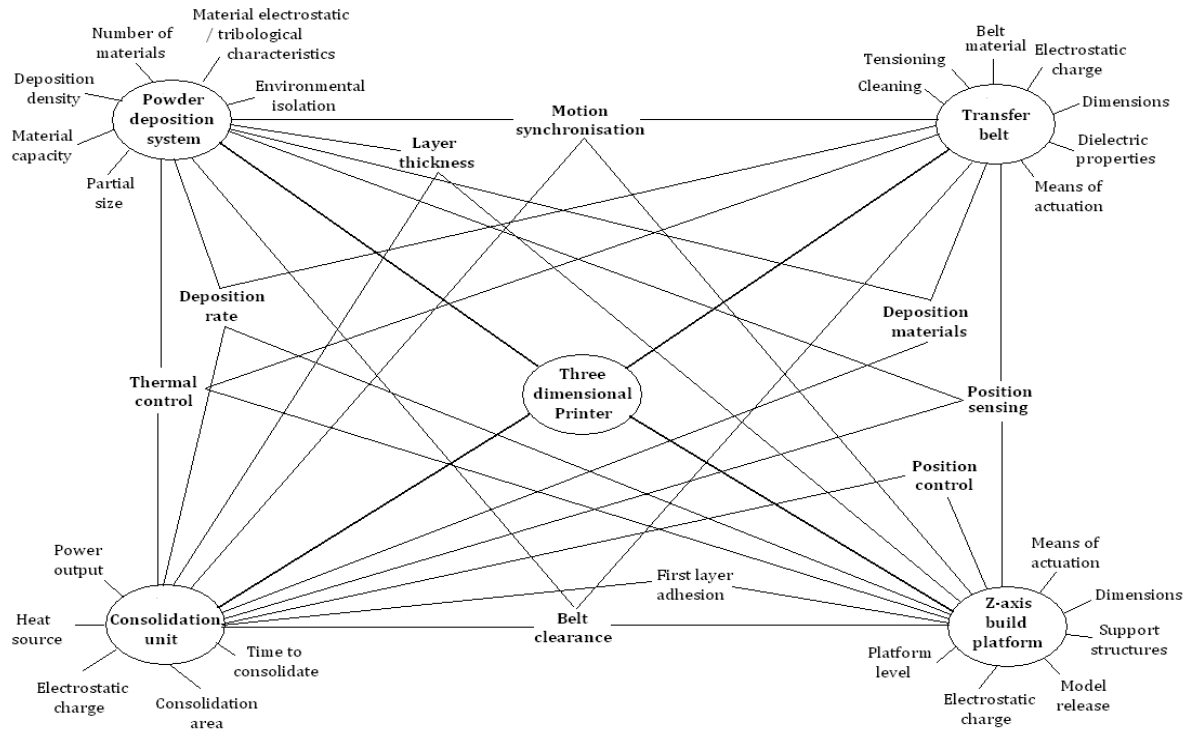
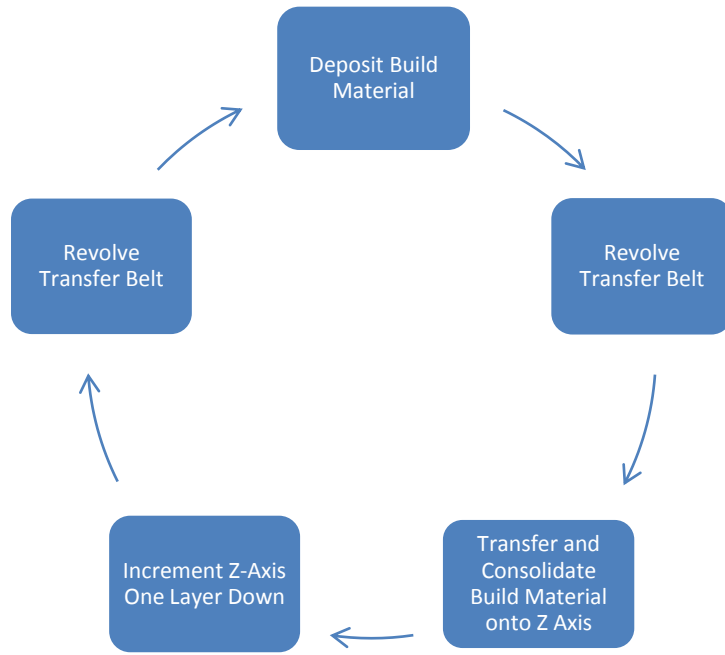


Figure 4.1 The sub-system considerations demonstrating their complex interdependencies

generation of two dimensional working drawings from which many of the parts were manufactured.

Subsystem	Design Iteration			
Z-axis	*	*	*	*
Transfer belt	*	*	*	
Consolidation unit	*	*		
Deposition unit	*			

Table 4.1 The number of respective design iterations undertaken to produce four, synchronous, sub-systems, which combined to form the POC prototype



**Figure 4.2 A Basic process cycle of the prototype ALM process**

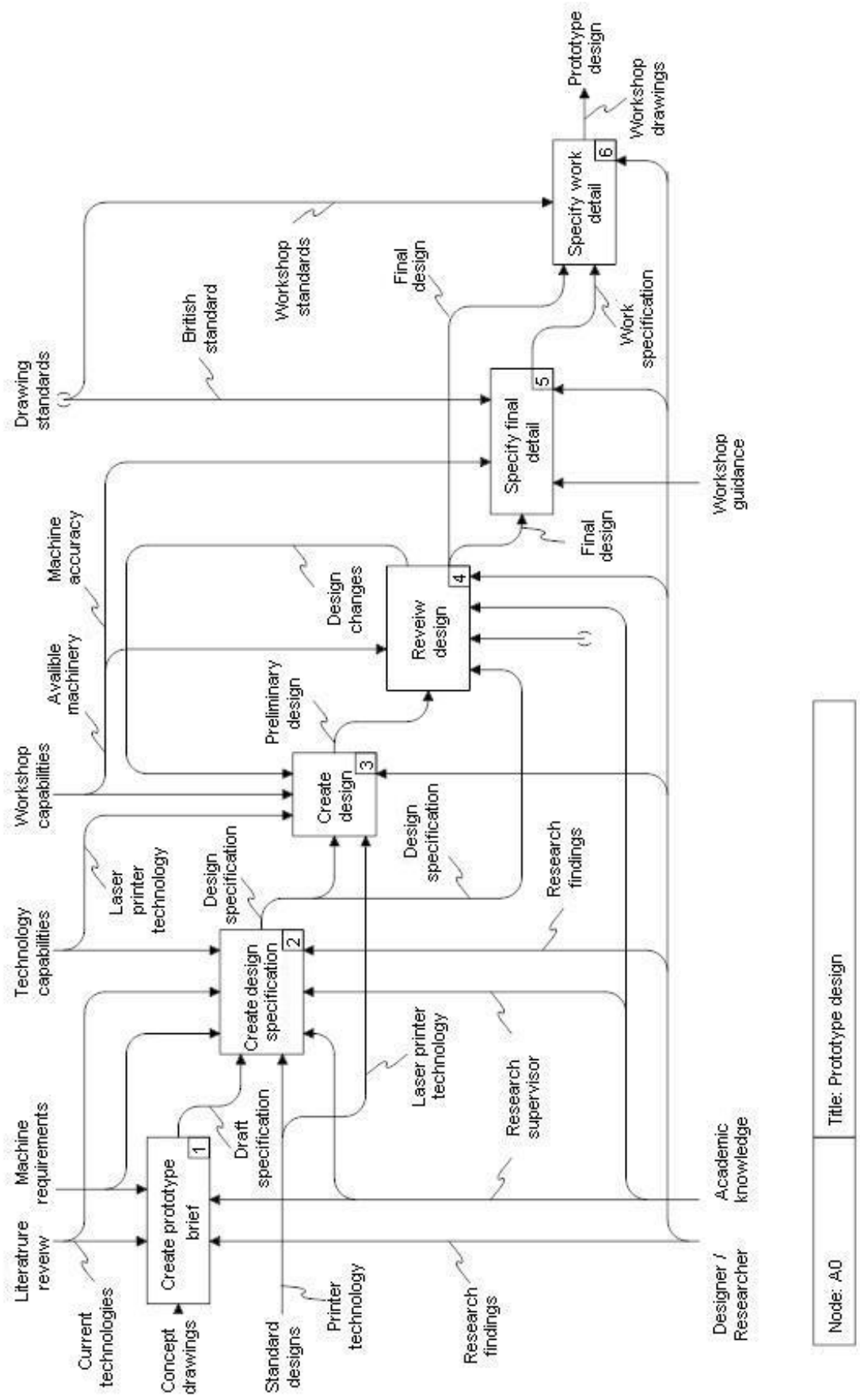
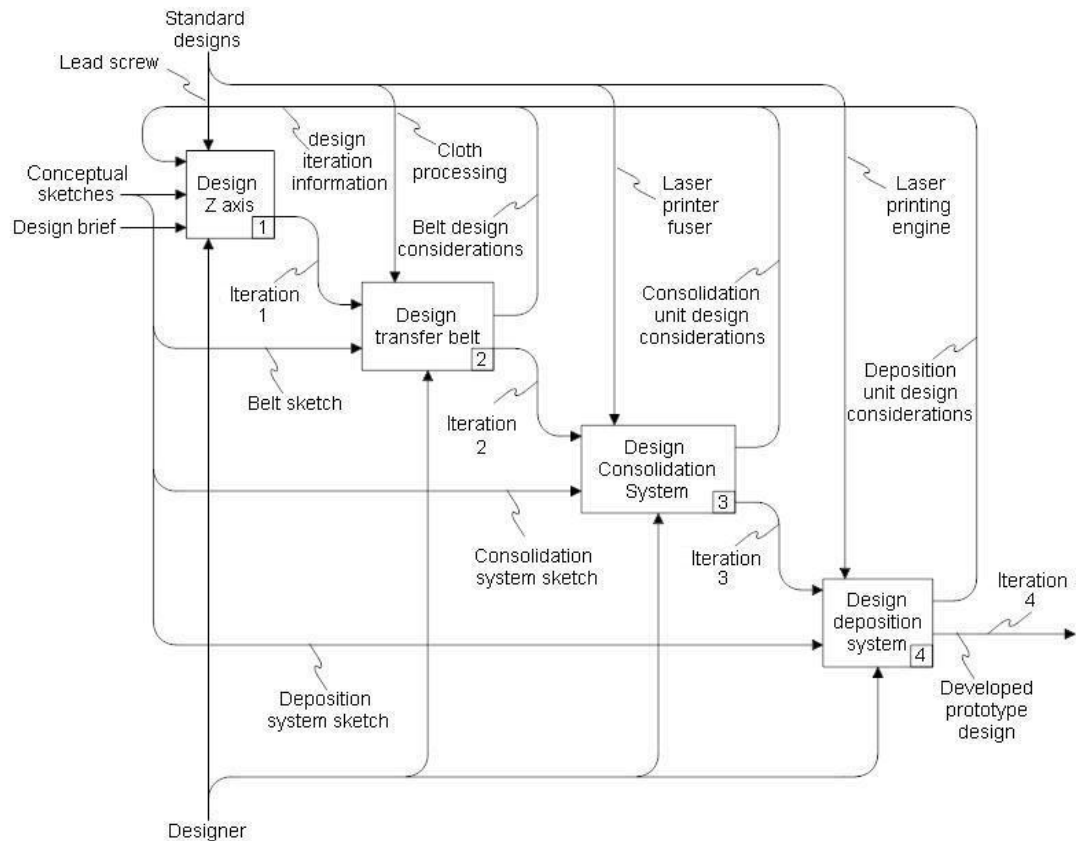


Figure 4.3 An IDEF0 diagram showing the general design flow of the ALM system

Node: A0 Title: Prototype design



Node: A03	Title: The sub-system's design iteration process
-----------	--

Figure 4.4 An IDEF0 node diagram focusing on the iterative design process within the overall design framework

## 4.2 The Proposed Machine Layout

The key design considerations for the prototype embodiment were:

- **Dimensions** - The prototype should have dimensions less than 733 x 600 x 840mm in the X, Y and Z axis respectively
- **Mass** - The prototype should have a mass less than 40kg
- **Power Consumption** - The power consumption of the prototype should be less than 3kw

The system layout was intended to give approximate relative and dimensional locations of system components. The dimensions for a number of standard parts including the proposed build volume, OPC, laser scanning engine and tractor drive

units, were used to scale the initial layout. The system layout sketch shown in Figure 4.5 highlights the relative position of the design systems which combined to produce the prototype. The overall position of the prototype's systems was constrained by a number of design suppositions, detailed as follows:

### ***The Printing Engine***

- Sensitive to orientation, powder material was to be gravity fed from a hopper.

### ***Belt Powder Transfer***

- As the belt underwent heating cycles, a belt tensioning device / simple accumulator system was needed to allow thermal expansion of the transfer belt.

### ***Heated Consolidation***

- Consolidation occurred above the z-axis.
- Consolidation was achieved using 'through belt' conduction heating by means of a heated roller.

### ***Z-Axis***

- The Z-axis was mounted below the deposition and consolidation systems and was incremented down relative to one layer thickness per layer print cycle.

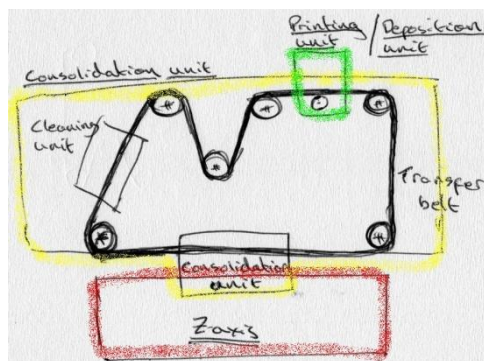


Figure 4.5 An initial system sketch identifying the design systems.

An inclusive system embodiment sketch was produced (Fig4.6) based on the design assumptions, basic process flow, the results of concept testing and the functional specification.



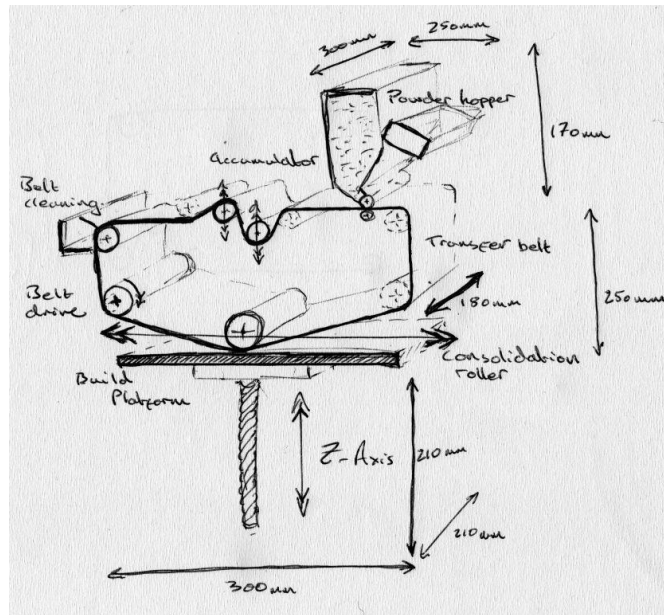


Figure 4.6 A preliminary holistic sketch incorporating known part geometries

### 4.2.1 Final Layout

Figure 4.7 depicts a CAD rendered model of the final prototype design highlighting the three key design sections, the deposition unit, the consolidation/transfer unit and the Z-axis.

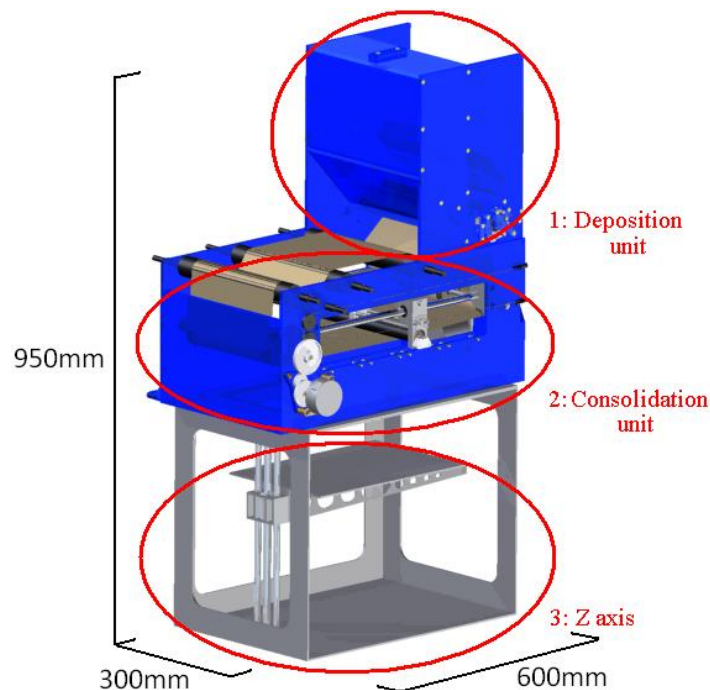


Figure 4.7 A CAD render of the final prototype highlighting three key sub-systems.

### 4.3 The Design of the Deposition Unit

The concept testing highlighted the need for a fully adjustable deposition system to allow the printing of a range of materials other than the standard toner. A design for such a unit was undertaken, tested and found in need of further setup and development. Due to the project time constraints and considering the objectives for this work it was decided that parts from a donor laser printer should be used to generate preliminary results to satisfy the objectives. The design and testing of the deposition unit is included within this thesis, appendix A.

#### 4.3.1 Donor Printing Engine

A printing engine and carcass were taken from a Samsung ML4500 printer and adapted to allow for mounting on the prototype sub structure and accept a belt substrate. A portion of the printer was removed to allow a transfer belt to pass over an adapted transfer roller as seen in a final assembly picture Figure 4.8.

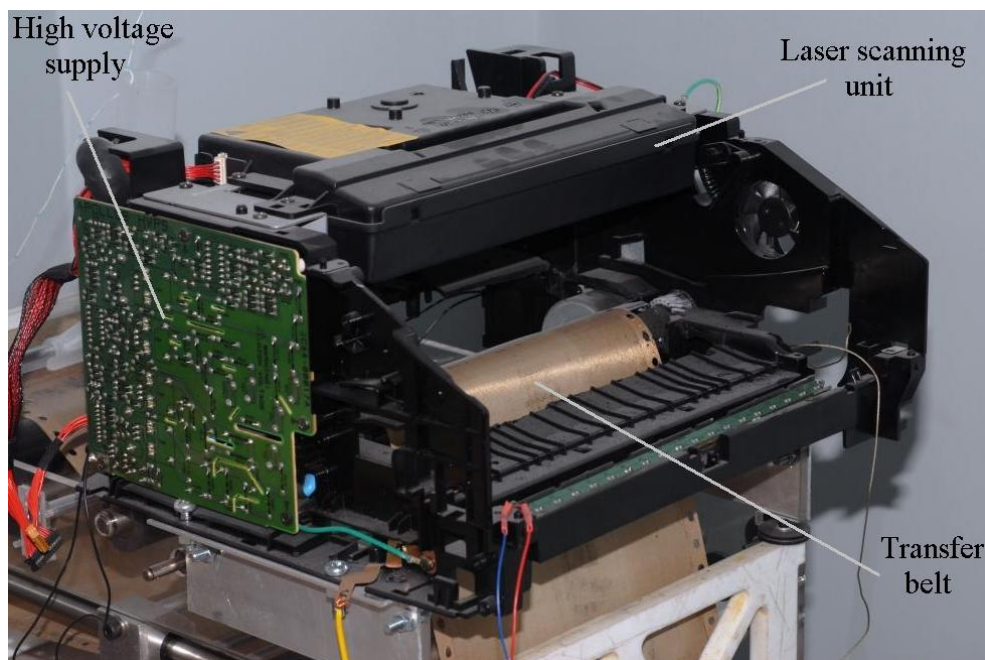


Figure 4.8 The components of the POC printing unit with material supply and developer roller removed.

#### *Image Transfer*

Although a standard printing engine was integrated within the system, a transfer assembly was commissioned for the prototype. The transfer roller bearings and spring

mounts were produced of conductive materials so that the rollers charge relative to the OPC could be optimised independently of the print engine's control system.

#### **4.4 The Consolidation Unit**

The consolidation unit (Fig 4.9) consisted of three sub systems, the image transfer assembly, the consolidation assembly, and the embodying housing structure. The functional specification for the consolidation unit set out the following key specifications for each of the sub-systems:

##### *The Housing*

- **Form** -The housing to be rigid and of transparent construction
- **Function** - Provide housing for the belt cleaning, discharge and tensioning devices, and the consolidation assembly

##### *Image Transfer Assembly*

- **Material** - To be constructed of glass reinforced PTFE material of under 0.115mm in thickness.
- **Conditioning** - Belt cleaning to be non abrasive and belt discharging best performed by corona discharge.
- **Drive** - Belt drive to match print velocity, using a physically interlocking system and positioning to be absolute.

##### *The Consolidation Assembly*

- **Function** - A reciprocating, rotating, and infra red heated roller at a maximum working temperature of 200°C
- **Productivity** - Consolidation to take four seconds

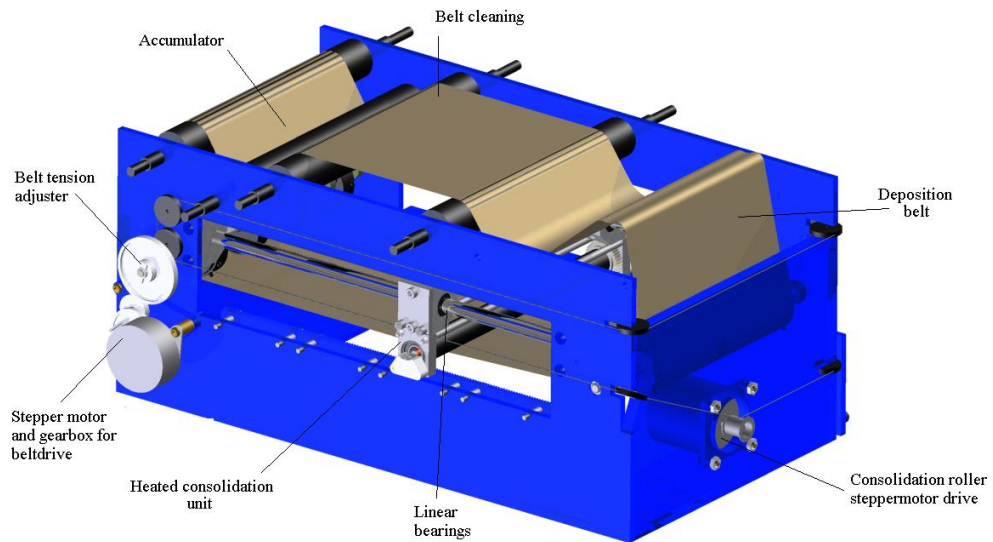


Figure 4.9 A CAD rendered diagram showing the main parts of the consolidation unit

#### ***4.4.1 The Consolidation Assembly***

At the centre of the prototype's consolidation unit was a carriage consisting of a heated cylindrical roller, constrained within bearings, mounted upon a linear bearing track. The carriage was designed to be driven at a constant velocity across the inner surface of the transfer belt, and therefore indirectly consolidated a powder layer present on the belt's outer surface. The detailed design conditions imposed on formation of the consolidation roller and carriage were:

- The necessity to be driven smoothly and at constant velocity
- To be of cost effective construction (inclusive of drive)
- The ability to provide position feedback
- To have a powerful and controllable heating means
- To be level and true across its movement

In order to produce a design which conformed to the aforementioned points, the consolidation roller and associated constraining carriage were split up into several design areas.

As previously determined, the requirement was to transfer thermal energy into the sequential powder layers thus effecting consolidation. A number of primary build material physical properties were considered during the early stages of the design process including specific heat capacity, thermal conductivity and melting temperature. In addition, consideration was given to the method by which the consolidation unit would provide the necessary thermal energy to the powder layer. The literature survey identified examples of methods by which fuser units, within laser printers, fuse toners to paper. Some of the more popular methods were RTDs, standard resistance heaters and incandescent irradiance. Within the prototype design an incandescent bulb was used (Fig 4.10), mounted coaxially within a metallic roller, providing a cost effective thermal source. Taking the specific heat capacity of a energy intensive build material, Nylon 12, and equation 4.1 and 4.2, an estimate was produced for the necessary energy input needed to raise a layer's temperature to that of its melting point ( $t_m = 180^\circ\text{C}$ ) thus nucleating the consolidation process. Neglecting losses, and assuming a value of  $1.64 \text{ J/gK}$  for the specific heat capacity and  $1\text{g/cm}^3$  material density, it was estimated that a single  $5\mu\text{m}$  layer of build material, with width and length dimensions of  $200 \times 300 \text{ mm}$  respectively, at an ambient temperature of  $20^\circ\text{C}$ , would require an input of around  $79\text{J}$  to bring the entire layer up to  $t_m$ . The design specification dictated that layer consolidation took 4 seconds. The roller would therefore need to deliver a minimum of  $20\text{J}$  per second, equivalent to  $20 \text{ Watts}$ , to establish  $t_m$  of the deposited layer at the roller's point of contact with the powder. This calculation was an estimate of the energy needed as conductive losses to the previous layers and losses to the atmosphere would have occurred. Given that an incandescent fuser lamp emits around  $90\%$  of its energy in infrared (IR) (Calwell, 2008), it was assumed that a  $450 \text{ Watt}$  fuser lamp was an adequate starting point. This allowed for a maximum of  $95\%$  loss of IR energy output in order to achieve  $t_m$ . If experimentation had shown that the thermal source was inadequate, the dwell time of the roller over the layer could have been increased.

$$\delta Q = mc\delta t \tag{4.1}$$

Substituting  $m = AL_t\rho$

$$\delta Q = AL_t\rho c\delta t \quad (4.2)$$

Where:

$\delta Q$  = Energy needed to melt a given mass of material from ambient temperature

$m$  = mass of build material

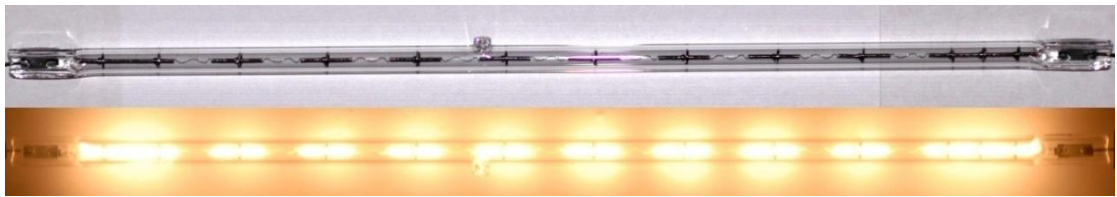
$A$  = build material area

$L_t$  = Layer thickness

$\rho$  = Density of build material

$c$  = Specific heat capacity of build material

$\delta t$  = Change in temperature from ambient to melting temperature of build material



**Figure 4.10** The 240 Volt, 450 Watt incandescent heating element chosen to heat the consolidation roller (lower picture, illuminated showing the filament hotspots).

There were many other factors to consider; the melted layer not only needed to melt and consolidate to its self but also to the build volume, requiring more energy, in addition to the thermal conductivity of the belt and powder materials. This calculation was to ensure that the heating capacity was there to accommodate early prototype testing and showed a 450 Watt thermal source to be an adequate starting point. Halogen gas filled capsules must run at temperatures exceeding 250°C to maintain efficiency and, depending on the bulb wattage and tube diameter, can reach temperatures approaching 650°C (Furfari, 2001; NEMA, 2003). The diagram in Figure 4.11 illustrates the design of the thermal source, its mountings and the mounting for the temperature control sensor.

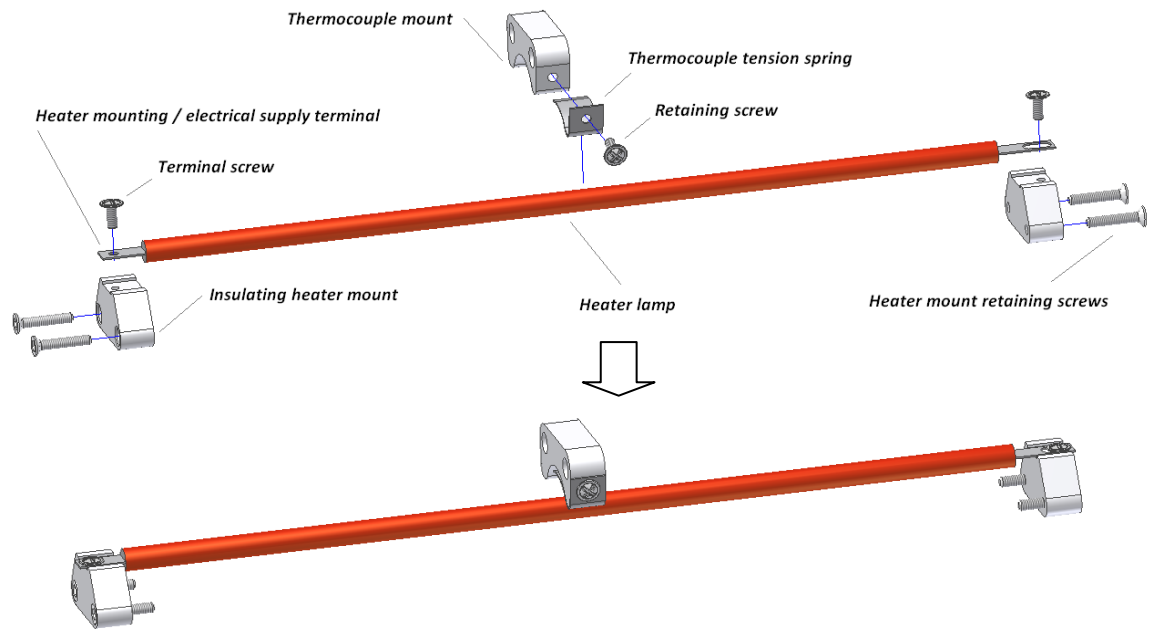


Figure 4.11 The final design of the heating components.

A commercial PID controller was used to maintain the rollers set temperature which, through functional testing, was shown to maintain a maximum working temperature of 200°C with no adverse effects to the machines structure or mechanisms.

#### *The Consolidation Roller*

Based on the requirements of the design specification, the highest temperature ( $T_{max}$ ) that the roller was expected to work at was 200°C, the force was assumed to be minimal and required a ground finish with an  $R_a$  value of around 0.1 $\mu$ m. The roller needed to heat up quickly and have a modest heat capacity to provide a thermal damper, allowing better thermal stability during layer transfer and consolidation. An increased thermal mass would also reduce a layers exposure to the hotspots seen in Figure 4.10. The roller was manufactured from aluminium because of its relatively high thermal conductivity, good machining characteristics, low mass and low-cost availability. The roller was covered with a thin PTFE coating as its low surface energy reduced the build up of bound polymer debris on the rollers surface. The bearing seat design incorporated a large axial clearance of 0.5mm, detailed in Figure 4.12, to allow the heated tube to expand and contract without distorting the carriage. The minimum necessary clearance was calculated using equation 4.3.

$$\delta L = \alpha L_0 \delta t \quad (4.3)$$

Where

$dI$  = expansion (m)

$L_o$  = length of pipe (m)

$dt$  = temperature difference ( $^{\circ}K$ )

$\alpha$  = linear expansion coefficient ( $m/m^{\circ}K$ )

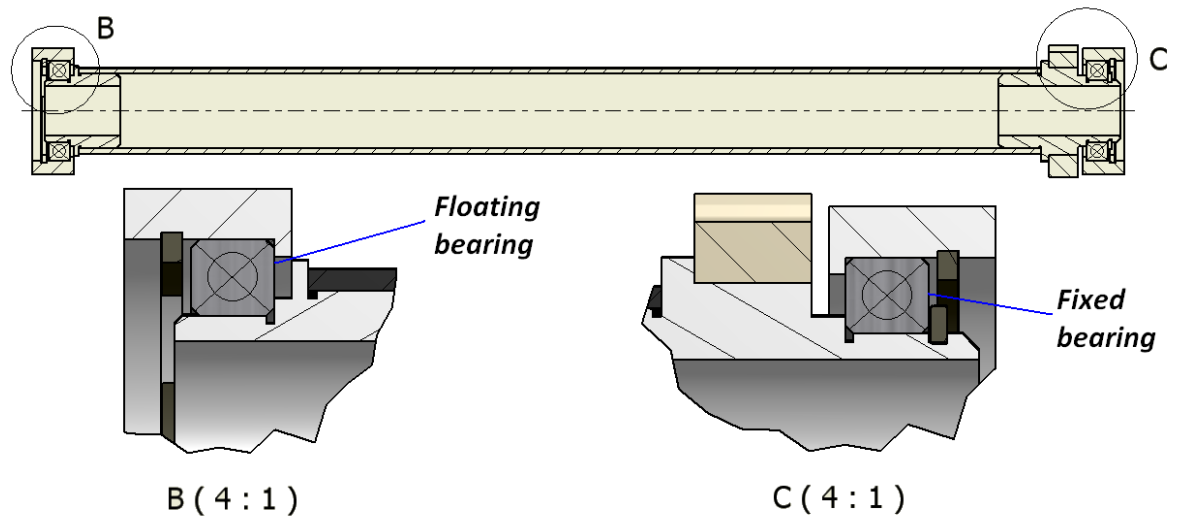


Figure 4.12. The consolidation roller's bearing mounts, with details of axial bearing play to allow for thermal expansion / contraction.

There were a number of ways to actuate the required rotation, but in order to synchronise the rotation with the reciprocating motion of the entire consolidation assembly, a rack and pinion design was adopted. Figure 4.13 shows the CAD rendered exploded and assembly diagrams of the roller's components.



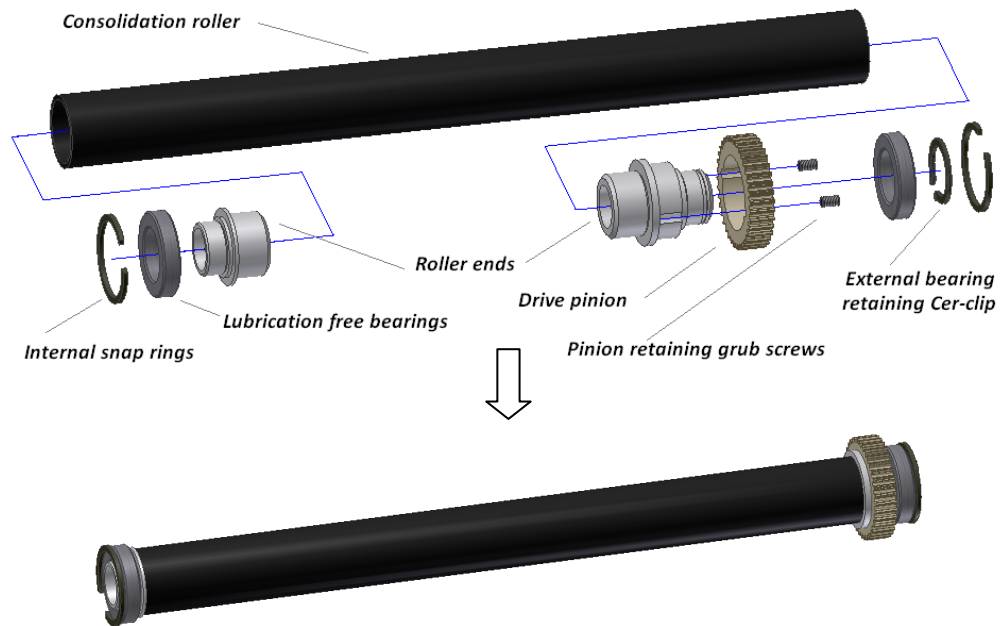


Figure 4.13. Upper: CAD explosion diagram of the heated roller assembly. Lower: a CAD assembly drawing of the heated roller.

### *The Consolidation Carriage Assembly*

The consolidation carriage provided a robust platform for mounting the consolidation roller and was intended to be an absolute dimensional height reference for each deposited layer. The structure was designed with adequate strength to maintain its shape whilst still being able to withstand the maximum working temperatures. Figure 4.14 illustrates an exploded diagram of the consolidation carriage assembly.

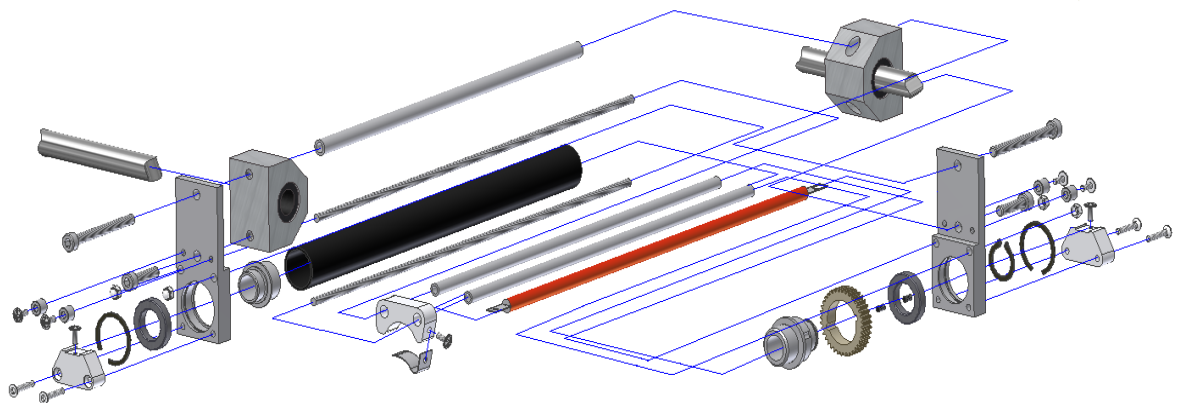
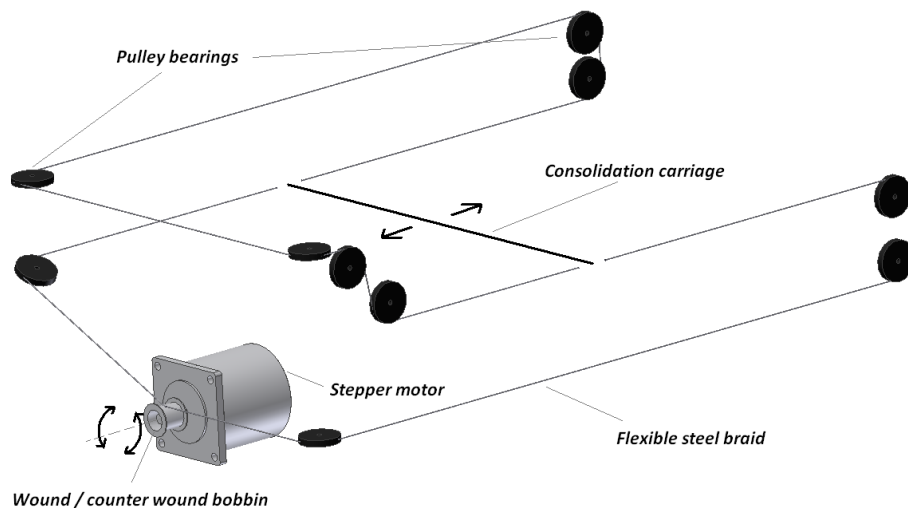


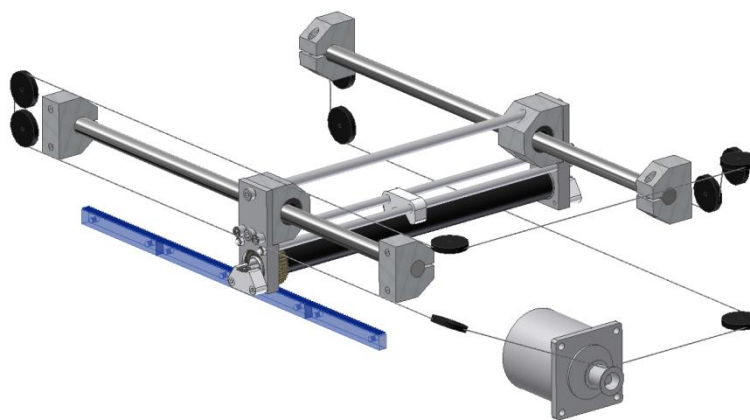
Figure 4.14 An exploded diagram of the consolidation carriage

*Linear Drive*

A controller was required to know both the position and, when in operation, the velocity of the consolidation roller. A stepper motor, a low-cost and relatively simple actuation solution, was implemented as position and speed were directly related to the controller output. A significant problem arose when trying to convert the motor's torque into a usable linear motion. The consolidation roller assembly sat within a belt and therefore an externally applied mechanical driving force could not be applied directly to its centre. Instead the linear actuating force was applied to the extents of the roller's carriage. Figure 4.15 illustrates the 'push/pull' balanced drive solution, a loop of flexible, polymer sheathed steel wire, linked each end of the consolidation unit to a bobbin mounted on the stepper motor.



**Figure 4.15** The consolidation carriage's 'push/pull' linear drive system



**Figure 4.16** The complete consolidation carriage assembly including drive

Figure 4.16 illustrates the final assembly of the consolidation unit. The unit required end of travel sensors which were incorporated within the consolidation frame assembly but are not shown in the illustration. Functional tests showed that the roller drive was able to propel the consolidation carriage at the 0.075m/second (75mm/second) necessary to consolidate a full 300mm long layer in four seconds.

### ***4.4.2 The Transfer Belt***

Based on results obtained from belt materials testing, a belt composed of glass reinforced PTFE was commissioned. A derivative of this material was widely available due to its common uses in the food industry for hot sealing and in the textile industry for fusing polymer transfers onto the surface of clothing materials. Due to the low surface energy of PTFE, it was found that achieving adequate bonding of belt seams with widely available adhesive and solvents was difficult. A solution was sought in the implementation of an alternative joining method. It was found that there were a number of standard joints used in industry to join conveyor type belts. Some such as chain or wire stitched belts were immediately discounted as the joints they produced were inflexible and could have caused damage to the rollers of the deposition system. To enable the manufacture of belts in house with no specialist equipment, a simple heat welded lap joint was chosen.

#### *Belt Testing*

The majority of the belt surface was shown to be an adequate substrate upon which to deposit powder images. The seam however, due to its increased rigidity, was found to be unusable. In addition, this section also had difficulty passing through the cleaning and deposition units. The prototype control system was programmed to avoid depositing layer material onto the seam portion of the belt, thus reducing the belt's capacity, and ultimately having a detrimental effect on the prototype's productivity.

#### *Belt Drive and Positioning*

Inspiration for the belt drive was taken from the classic dot-matrix printer paper drives, an example of which can be seen in Figure 4.17. The paper drives on these

machines were also known as ‘tractor drives’, where a number of punched holes at a regular pitch were located onto rotating sprocket wheels.

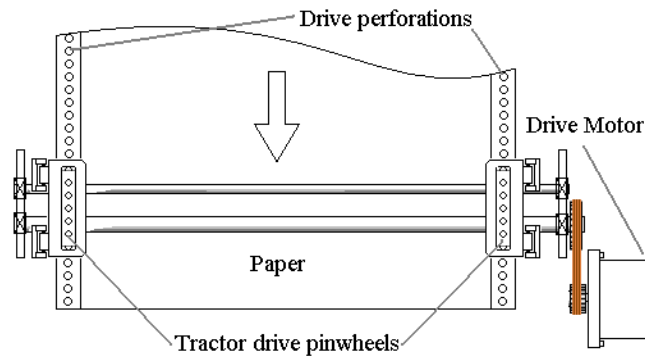


Figure 4.17 A diagram showing an example of a tractor paper drive used to drive the transfer belt

The belt edges were reinforced and a jig designed to accurately laser cut the drive holes.

#### 4.4.3 The Consolidation Frame Assembly

The final layout of the frame (Fig 4.18) was derived from the assembly of the sub-systems, however, the first prototype was designed with a large clearance between the consolidation assembly and upper belt portion. This clearance allow for convective cooling and the option for retrospective modification. The sides of the main frame were constructed from 6mm thick transparent acrylic sheet which allowed observation of the workings of the assembled POC prototype. An additional benefit of the chosen material was that it lent itself to the laser machining processes available on site.

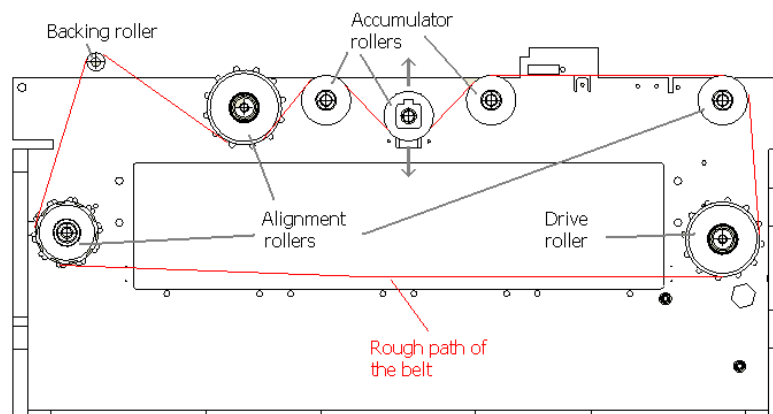
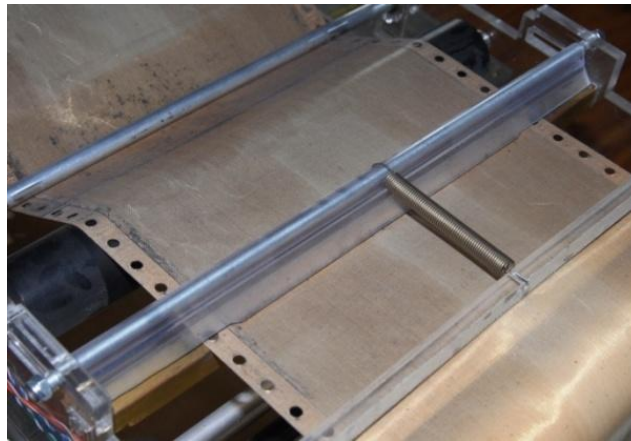


Figure 4.18 A diagram showing the position of the eight consolidation assembly rollers

### *Belt Cleaning*

It was important to keep the belt free from debris and unconsolidated material, to maintain the system's performance. Loose debris, such as unconsolidated powder, was simply removed using a polyurethane blade. The blade, due to tribological charging, gained a positive charge during use which aided material retention. In the prototype, the unconsolidated debris was removed following a part build cycle. A light spring ensured the blade remained in contact with the belt throughout the build process (Fig 4.19). However, if consolidated material remained on the surface of the belt it was significantly harder to remove whilst concurrently printing. In the prototype system, any consolidated material remaining on the belt was removed by hand following a build cycle.



**Figure 4.19** The belt cleaning blade, retention spring and belt.

### *Belt Discharging*

The active static charge eliminator was made up of high potential, sharp, pointed electrodes in close proximity to a large flat grounded electrode. The high electric field density generated by the large potential between the closely positioned electrodes, caused a corona discharge by means of the generation of a charged ion. The gap between the electrodes and the necessary potential difference to create a corona discharge was calculated.

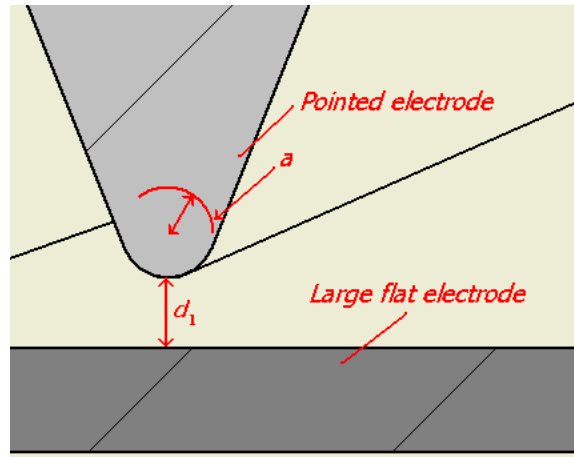


Figure 4.20 The variables considered when calculating the minimum corona discharge voltage between the two electrodes of the static charge eliminator.

The diagram in Figure 4.20 illustrates the electrode geometries and their variables. In order to induce corona discharge the electric field needed to be non uniform i.e. The radii of the pointed electrode must have been small in comparison to the electrode gap  $d$ . The empirically derived equation used to calculate the critical electric field strength ( $E_c$ ) for the onset of corona was given by Kaser (2006),

$$E_c = 3\zeta \left( 1 + \frac{0.03}{\sqrt{\zeta a}} \right) \times 10^6 \frac{\text{V}}{\text{m}} \quad (4.4)$$

$$\text{Where } \zeta = \frac{273}{273 + T} e^{-\frac{3.45 \times 10^{-2} h}{273 + T}} \quad (4.5)$$

Where  $T$  was the temperature in degrees Centigrade,  $h$  was the height above sea level in meters, and  $\zeta$  was the relative air density factor. Using the expression for maximum electric field ( $E_{max}$ ) as derived by Kaser (2006) for the geometry in Figure 4.20

$$E_{max} = \frac{V}{d_1} \left[ \frac{\frac{2d_1}{a} + 1 + \sqrt{\left(\frac{2d_1}{a} + 1\right)^2 + 8}}{4} \right] \approx \frac{V}{d} \left( 0.94 \frac{d_1}{a} + 0.8 \right) \quad (4.6)$$

the critical voltage for the onset of corona was given by

$$V_c = 3a \zeta \left(1 + \frac{0.03}{\sqrt{\zeta a}}\right) \sqrt{\frac{a+d_1}{a}} \ln \left[ \frac{a+d_1}{a} + \sqrt{\left(\frac{a+d_1}{a}\right)^2 - 1} \right] \times 10^6 \text{ V} \quad (4.7)$$

$$\approx 3a \zeta \left(1 + \frac{0.03}{\sqrt{\zeta a}}\right) \ln \left(\frac{2d_1}{a}\right) \times 10^6 \text{ V} \quad \text{if } d_1 \gg a \quad (4.8)$$

$$\text{Where } \zeta = \frac{273}{273 + T} e^{-\frac{3.45 \times 10^{-2} h}{273 + T}}$$

The plot in Figure 4.21 shows the relationship between the critical voltage and the electrode displacement. At an electrode displacement of 5 mm the critical voltage was around 4KV. The AC corona oscillated at around 50Hz and applied a mixed stream of both positive and negative ions onto the surface of the belt leaving a resultant uniform charge.

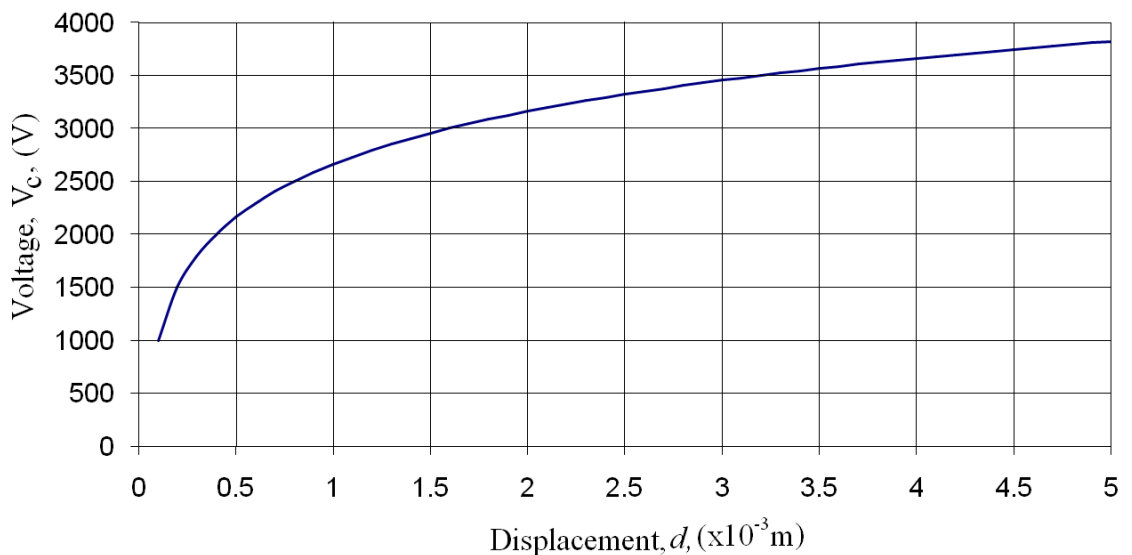


Figure 4.21 The relationship between the critical voltage of corona onset  $V_c$  against electrode displacement  $d$ .

Testing of the effectiveness of the discharge apparatus showed that at low belt velocity all the latent charge was eradicated, however, at working velocity there remained a small charge. Initial tests showed that the transfer roller was able to overcome this remaining charge.

#### 4.4.4 Consolidation System Testing

During initial testing the system performed as expected, however, one significant problem was identified, as the transfer belt adhered to the surface of the part being built and could only be released through a large displacement of the z axis. The act of pulling the part from the belt created a force throughout the entire system for which it was not designed. While the prototype system's Z-axis was robust enough to cope with the load, it was feared that the additional stress on the prototype machine would be detrimental to its operation.

#### Consolidation System Development

A solution to overcome the belt adhesion issue was to tension the transfer belt, which reduced the tendency for the belt to adhere to the build surface but did not eradicate the problem. The solution was to redesign the bearing retainers to include a set of rollers that 'peeled' the belt from the surface of the part/build platform as it passed. Figure 4.22 is a CAD illustration of the problem and the solution and Figure 4.23 is a CAD rendered model of the altered bearing retainer design.

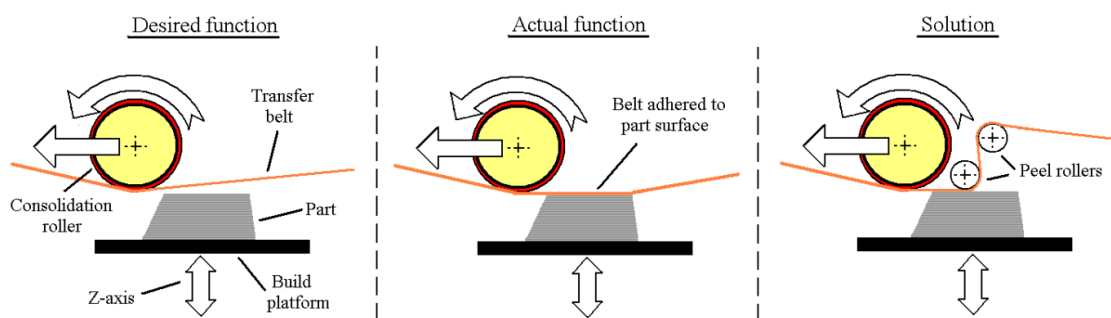


Figure 4.22 The solution to the problem of belt/part surface adhesion.



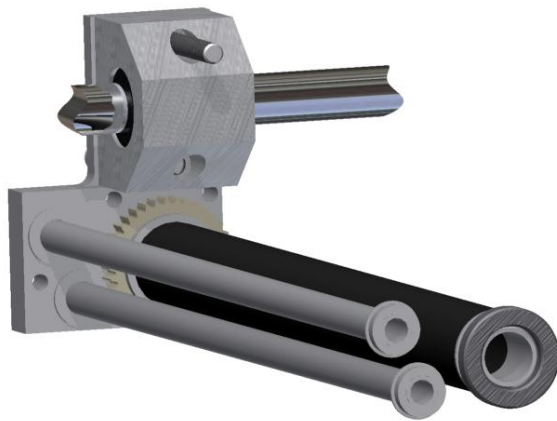


Figure 4.23 A CAD model of the redesigned consolidation carriage with parts removed to view the peel rollers.

#### 4.5 The Z - Axis

The functional specification set out a number of guide lines for the Z-axis unit with the key points being;

- **Function** – The primary function of the z axis is to provide an absolute height reference
- **Construction** – The z-axis must be rigid to allow accurate consolidation to take place
- **Resolution** – The z-axis must be able to accurately move in 10 micron steps

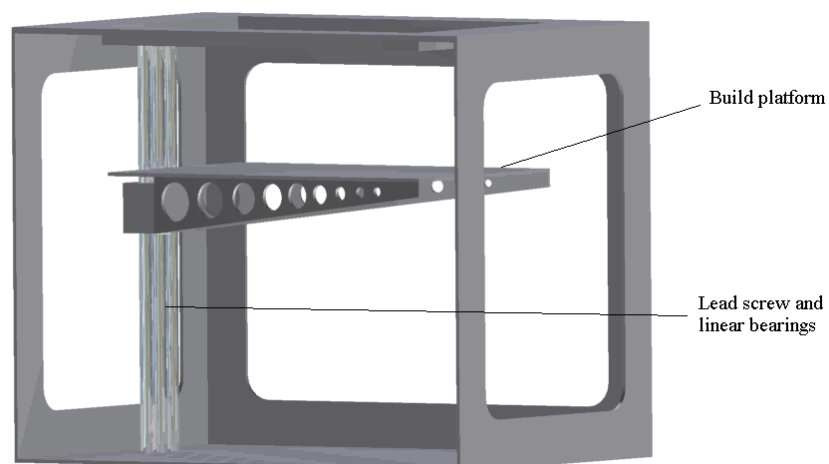


Figure 4.24 The main parts of the Z axis

The Z-axis, as CAD illustrated in Figure 4.24, was a device used to position the build surface at the correct height for the deposition of part layers. As such, the overall movement during the build process was downwards. Although initial designs were developed, the final design and construction of a Z-axis was not undertaken. Instead, a commercial Z-axis was used (A Galil DMC-1010 servo controlled system). The benefit of a commercial assembly over that of a proprietary system was that no debugging was necessary and the Z-axis performed as it should first time. While the design brief dictated that the Z-axis should be low-cost, which the commercial assembly, associated control hardware and user interface (UI) software was not. The initial system prototype needed to demonstrate the option of utilise technology which was available at low-cost, but at that stage did not have to implement it. For example, the Z-axis in the Fab@home ALM system as briefly discussed within the literature review, utilised a low-cost technology which could easily be implemented in future cost based prototypes.

### ***4.5.1 Functional Testing***

Testing was undertaken to ensure the z-axis was able to be accurately indexed in 10  $\mu\text{m}$  increments, and to determine the correct number of optical encoder counts to realise a 10  $\mu\text{m}$  displacement. A dial gauge with 1  $\mu\text{m}$  resolution was mounted on the surface of the Z-axis Table and the dial's plunger brought into contact with a horizontal beam secured above. The controller's manual indicated there were 100 encoder counts per 1  $\mu\text{m}$ . A series of tests were undertaken to determine the number of encoder counts per 10 micron step, and the backlash present in the drive lead screw. The resultant encoder count for a 10  $\mu\text{m}$  step was 1028 and showed repeatability greater than the resolution of the gauge in one direction. When the direction was changed, a 300 step discrepancy was seen resulting in a back lash of around 3  $\mu\text{m}$ , again this phenomena was repeatable down to an accuracy greater than the resolution of the gauge.

## 4.6 The Control System

The functional specification set out a number of guide lines for the control system with the key points being;

- **Architecture** – The system should be modular and of PIC based construction with a programmable master controller
- **Interface** – Interface with existing printer system and LCD status indicator
- **Programming** – The system was required to include control firmware which was easily adaptable for future development.

The prototype's hardware, incorporated within the four sub-systems, relied on highly synchronous control in order to function correctly. The necessary control was implemented using microprocessor controlled sensors and actuators following predetermined firmware programs. The control of the laser engine and associated RIP was undertaken by Samsung's original microcontrollers. This section will discuss the electronic design and will conclude with a breakdown of the firmware development.

### 4.6.1 Electronic Design

The circuit designs were drawn up using Eagle circuit design software from CadSoft, which allowed the production of Gerber files for PCB production. Microchip's PIC Microprocessors could not multitask and have limited PWM pins which were needed for the control of a number of the actuator processes within the prototype. To allow several processes to be undertaken at the same time, multiple microcontrollers were employed to control peripheral functions such as motor/position control and sensor manipulation. Microchip's PIC16f88 microcontrollers were used as ancillary controllers interfaced with a central PIC16F887, adopting single wire communications. The ancillary subroutines, master program and communications interrupts will be discussed in detail later in this chapter. The schematic of the electronic control system, in Figure 4.25, was broken down into four ancillary controller sections: Master controller (1), unipolar motor controller (2), and two bipolar controllers (3) & (4), as well as an LCD display and driver (not shown). Splitting of the control system, gave the advantage of modular freedom, allowing controllers to be mounted in close proximity

to actuators linked only by power and one additional communication wire. This reduced the complexity of the wiring harness and reduced the hardware debugging time. The modular design also gave additional flexibility when choosing actuators, as differing technologies could be substituted for existing actuators with only the replacement of the ancillary control board.

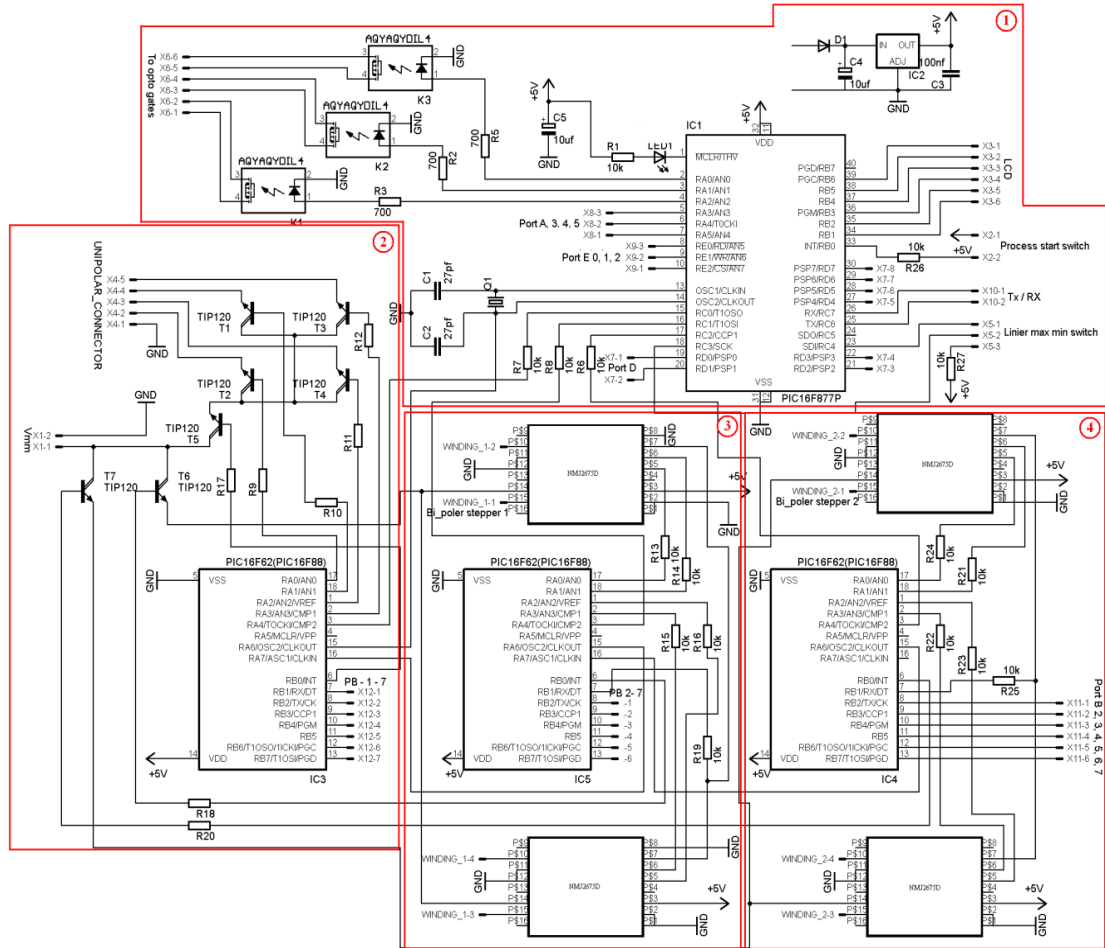
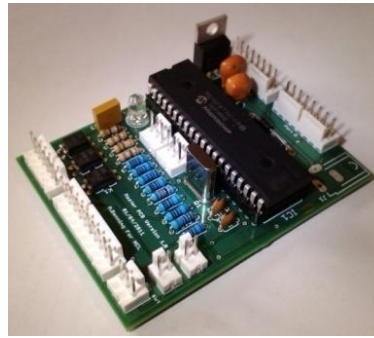


Figure 4.25 A schematic of the main control system broken down in to the four areas consisting of the; (1) Master controller, and the three ancillary controllers; (2) unipolar controller and (3)&(4) Bipolar controllers.

### The Master Controller

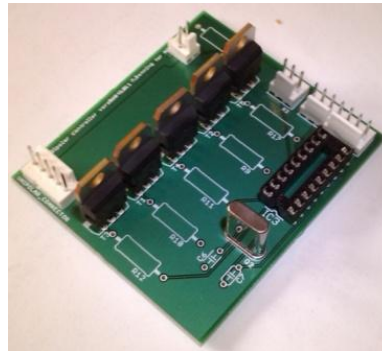
The master controller (Fig 4.25) was responsible for the synchronisation of the ALM process. The controller interfaced directly with both sensors and actuators and communicated with peripheral ancillary control boards.



**Figure 4.26** The assembled Master PCB

### *Unipolar Controller*

The unipolar controller was designed as a module board to integrate with the master controller. The controller incorporated Microchip's small PIC16F88 microcontroller to provide current limited control of a four winding unipolar stepper motor.



**Figure 4.27** The assembled unipolar controller PCB

The circuit (Fig 4.27) contained all the necessary additional components to run the board at 20MHz, apart from the power supply, which was on a common rail from the master controller. For the prototype application it was not necessary to opt for a closed loop current regulated system, such as a chopper circuit, as the maximum motor torque was not required. The PWM allowed for accurate control of current relative to voltage which enabled higher voltages to be used at high rpm, to give better torque characteristics.

Testing showed that an error had been made during the design of the unipolar board, placing the motor load on the emitter side of the Darlington pair transistors. Due to the voltage drop across the transistors the motor did not produce the required torque.

To overcome this issue the stepper load was incorporated upstream of the transistors between power source and collector.

### *Bipolar Controller*

As with the unipolar controller, the bipolar controller was a module designed to drive a stepper motor independently of the master controller, however due to the use of additional ICs the bipolar circuit was significantly more complex. The controller consisted of two H-bridge drivers (one for each winding) a PIC16F88 microprocessor, 20MHz crystal oscillator, a Darlington transistor pair for PWM control, and various other passive components. A picture of the two PCBs can be seen in Figure 4.28.

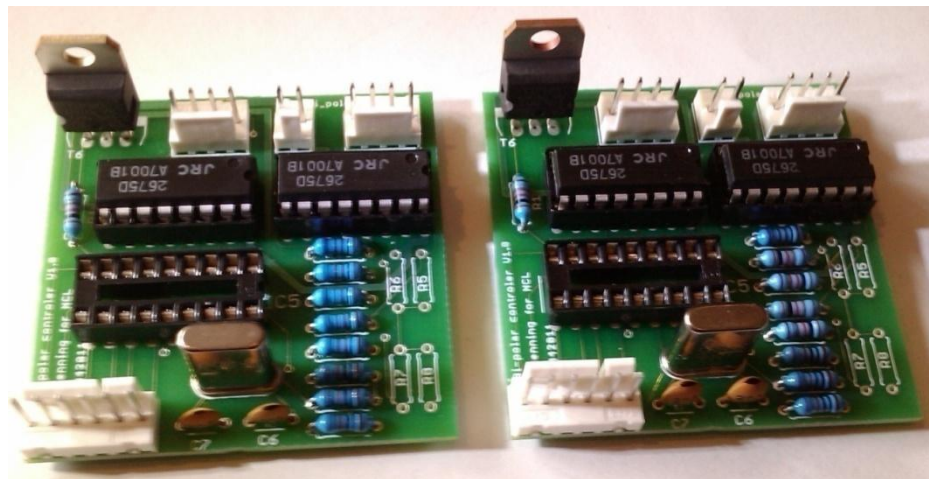


Figure 4.28 The assembled bipolar controller PCB

Testing showed that neither of the assembled boards was functioning as expected. After reviewing the pre-PCB prototype bread board it was found that the H-bridge that was included in the schematic software, although labelled the same, was internally wired incorrectly. All of the 16 pins were incorrectly wired and so a second circuit design was produced and issued to the board house for manufacture. The second set of PCBs worked as expected.

### *Electronics Assembly*

The ancillary PCBs were adhered to the outside of the prototype and wired to central terminal blocks where they were joined to a communications wire leading to the

master PCB. The unipolar and two bipolar PCB's can be seen installed in figures 4.29 and 4.30 respectively.

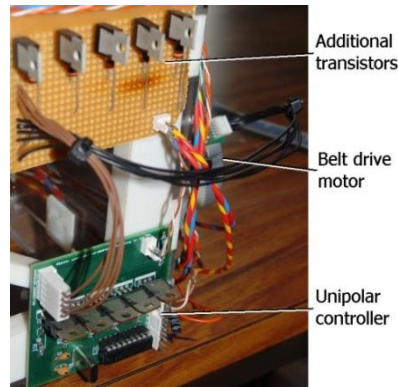


Figure 4.29 The installed unipolar PCB with additional transistors to remedy the low voltage motor supply issues

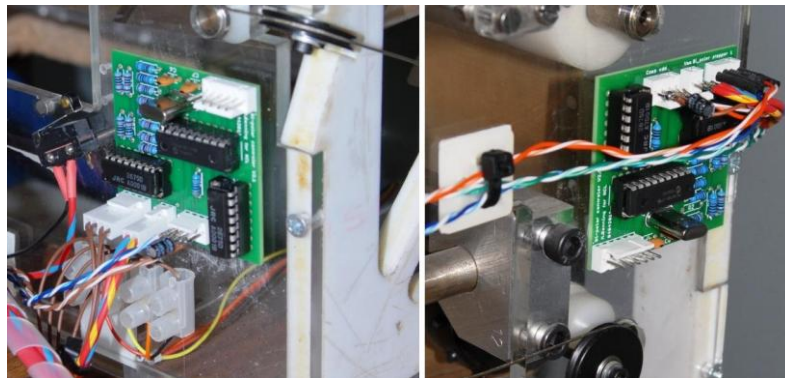


Figure 4.30 The installed bipolar PCB's (mark 2) held in place by adhesive. Left: carriage controller, Right: OPC and deposition roller controller.

Following brief testing of the individual circuits they were assembled into the final control system. During testing it was found that interference from the motor supply cable would affect the PCB communications wire which ran in close proximity. The interference caused unstable motion of the belt and consolidation carriage. An adequate solution was to integrate small capacitors between ground and the communications wire. This buffered voltage spikes as a result of transient current induced within the control wires.

#### ***4.6.2 Firmware Programming***

In addition to the hardware systems, ALM machines need comprehensive firmware programming to ensure synchronous and repeatable operation. With respect to the

system developed within this work, this required the development of programming for four PIC microcontrollers and their interconnecting communications. To produce the PIC firmware a hierarchical software development framework was used. Programming started with a high level flow diagram which represented key operations as 'program macros'. Program macros consisted of a number of functional blocks such as 'component macros' which were high level representations of pre defined C code (C). Once a flow diagram was completed it was compiled to C and a second operation compiled the program to a PIC microcontroller. An example of a flow diagram is illustrated in Figure 4.31, the main program contains a low level calculation block, a mid level component macro and a high level program macro.

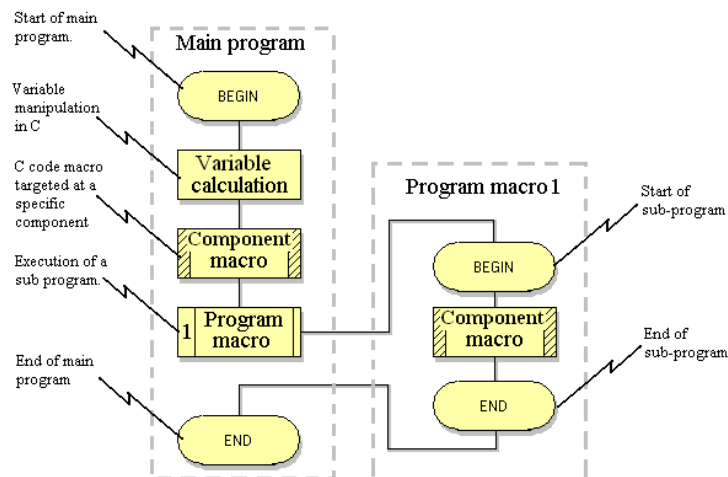


Figure 4.31 The implementation of low, mid and high level macros and their effect on the program flow

### *Low Level Functional Blocks*

Low level blocks such as calculations, delays and C code inputs were the direct manipulation of C code within the block diagram. Low level blocks were avoided as they produced large flow diagrams which were hard to use. Where possible a pre coded mid level block was used.

### *Mid Level Functional Blocks*

Mid level blocks such as component macros, decisions, loops and interrupts were functional blocks which held latent C code which could be indirectly manipulated by adjustment of variables within the block. For example Figure 4.32 shows a short



program which increments a stepper motor 100 steps. The three functional blocks; program loop, motor enable macro and increment step macro contain all the information necessary to drive a stepper motor 100 full steps. However if it was necessary to change the step sequence to half stepping instead of full stepping, only a change of a single variable would be necessary, not a rewrite of the stepper motor code.

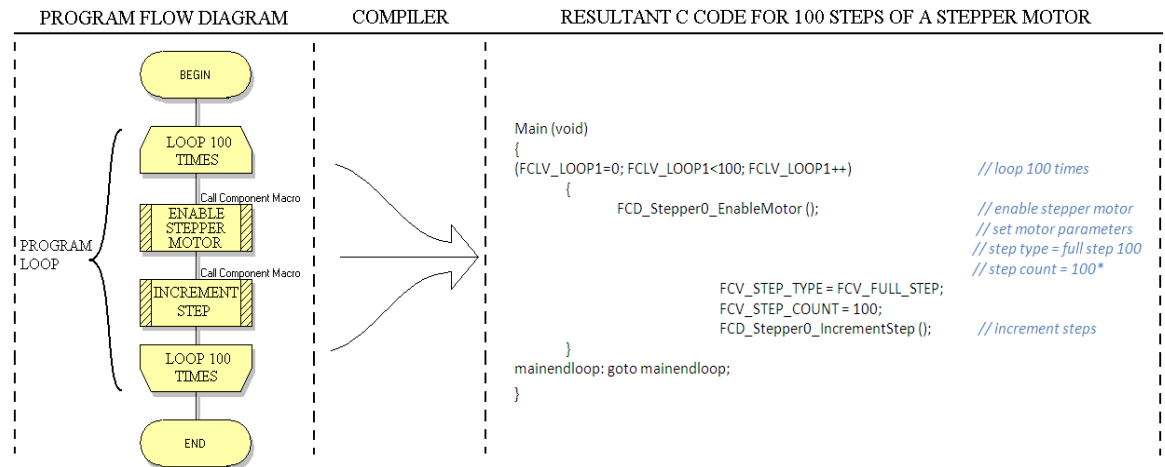

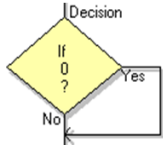
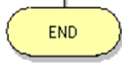
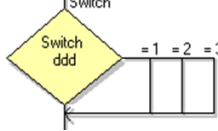
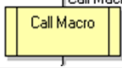
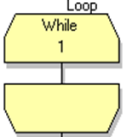
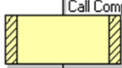

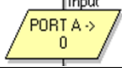

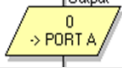
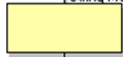
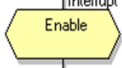
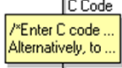
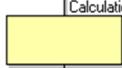


Figure 4.32 An illustrative demonstration of latent code within mid level functional blocks compiled to produce a C code program.

### High Level Functional Blocks

At the highest level was the program macro block. This block was a sub-routine within a main program which allowed the compilation of large complex programs, represented by a number of smaller less complicated sub-programs. The program macros were designed and debugged individually and brought together to form the main controller programs. The macro system allowed the construction of robust programs which, although a little longer than they needed to be, worked reliably. The extra length of the program code was a due to the inclusion of the entire variable set for every component whether they were implemented or not. A program called Flowcode, by Matrix Multimedia, was used to produce and compile the macros, the advantage of this software was that it allowed visual debugging of programs using virtual hardware. There were a number of different blocks used to create the program

flow diagrams all of which are detailed in Table 4.2 with a short description highlighting their use.

	'Begin' denotes the start of a program routine		A decision represents a single Boolean operation with a true or false output
	'End' denotes the termination of a program routine		A switch block represents a Boolean operation tested with multiple outcomes
	The Program macro is a High level representation of a sub-routine		A loop represents looped code which can be infinite, looped a predefined number of times, or terminated by a Boolean operation
	The component macro is a mid level representation of C code to run a hardware function		Go to block represents a jump from one block of code to another
	An 'Input' is expected data input from a specific port		A connection block represents the point at which a 'Go to' command is terminated
	An 'output' is an output from the microcontroller on a specific port		String manipulation blocks represent a low level editing of string variables
	An interrupt brakes the program flow to execute a program macro. The program then returns to the program flow. Interrupts can be set to a clock or port input		
	A C code block represents the low level insertion of program code. For example the insertion of code only used once in the program		
	The calculation block represents a low level operation performed on a variable. For example the addition of one layer unit to a 'CURRENT_LAYER' variable		

**Table 4.2 The key blocks implemented in the program flow diagrams**

The following section will describe the developed firmware for the four imbedded microcontrollers. The programs were designed progressively through the development of early prototype versions. The start of this section looks at programs designed to test the operation of the PCBs before describing the final control programs. As some of the programs are large, a number of the flow diagrams describing lower level program macros are included in the appendices of this thesis.

### *Test Programs*

The first programs compiled onto the microcontrollers were designed to test the PCBs. The initial set tested communications between master and peripheral controllers, before the independent board functions, culminating in an entire program test.

### *Master Controller*

A user interface, in the form of a backlit LCD display with a HD44780 type controller, was integrated within the master controller to visually feedback system status. The

first program written, illustrated by the flow diagram in Figure 4.33, simply tested the LCD port by printing the ASCII message “HERRO WORLD”. The second program enabled the peripheral communication output pins in a pattern which was then detected using an oscilloscope. The sensor inputs were tested by applying a logic voltage to the input pins and then referring to the LCD for visual conformation that the microcontroller received the signal.

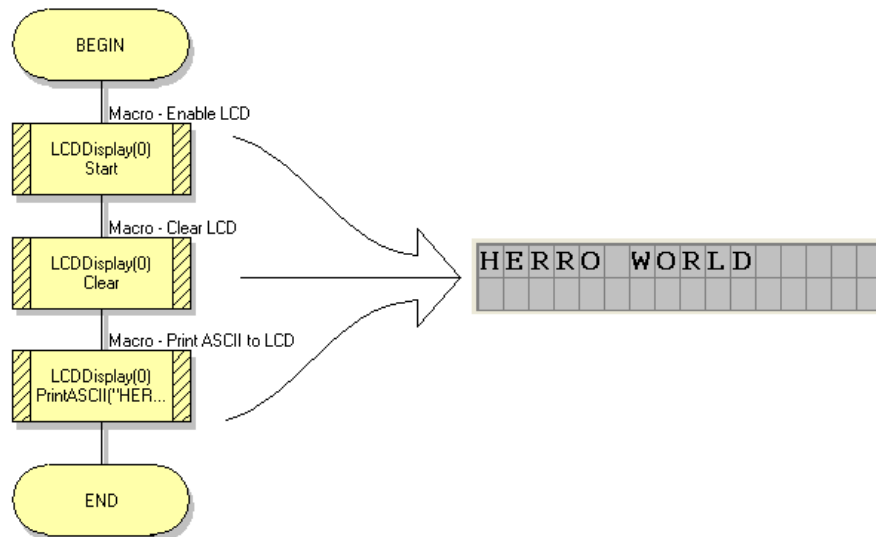


Figure 4.33 The LCD test program

### *Peripheral Boards*

The individual testing of the ancillary stepper motor control boards was undertaken using a program designed to produce a continual stepper drive output in a single direction. This testing time was also used to verify the resultant belt velocity at a given step/min drive and the number of steps for a full belt revolution.

Once individual testing of the boards had been performed it was necessary to link the boards to test their synchronous function. Communications were tested between the Master PCB and the three ancillary control boards by ‘pinging’ (issuing an output from a microcontroller for the purposes of requesting data from an intelligent sensor or microcontroller) the ancillary microcontrollers. These controllers, if functioning correctly would ‘answer’ with an output on the same port they were pinged. The master controller was programmed to send the ping and then wait for a response for

2.5 seconds. If a response was not received from the pinged ancillary controller within this time the ancillary controller and the port by which its communications were connected was flagged as defective. The flow diagram in Figure 4.34 show the high level communications testing program executed by the master controller, while the lower level flow diagrams can be found in Appendix B.

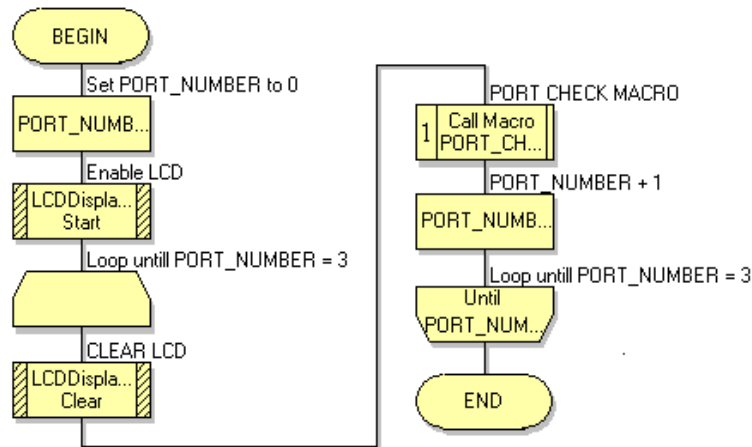


Figure 4.34 A high level flow diagram representing Test program 1 - a program for testing microcontroller communications between three peripheral boards. The ports are tested in order and an LCD outputs the results.

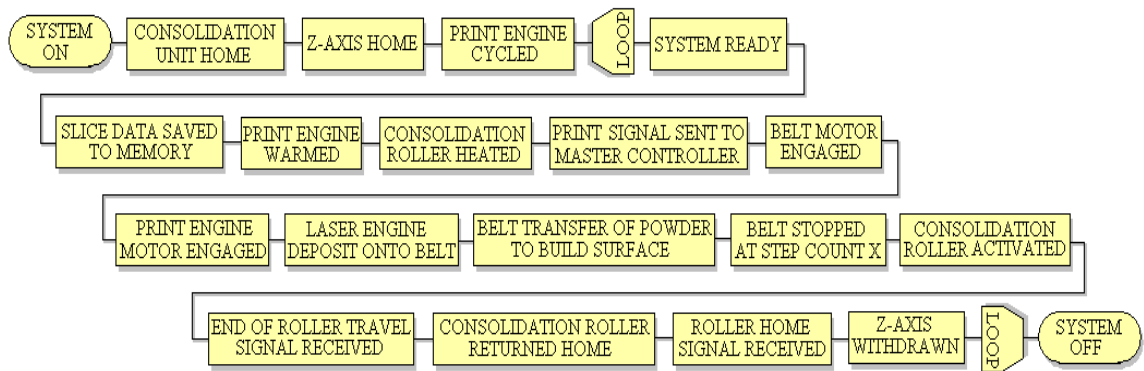
The results from the master controller’s ancillary communications testing were displayed on the LCD, referencing the port, the port bite on which communications were tested and the type of board connected. The port response was either displayed as ‘READY’ or ‘\*\*ERROR\*\*’ depending on the results of the communications test. Figure 4.35 show two pictures of the LCD display, one with the type of ancillary board and its ‘READY’ status, the other showing an example of a communications ‘\*\*ERROR\*\*’ after the ancillary board was remove from the port.



Figure 4.35 Upper image: A successful communications test. Lower image: A communications error as no board was detected

*Control Programs*

Following communications testing, the master and peripheral boards were programmed with their final control firmware, and a number of simulated layer print process were run. The simulations followed a relatively straight forward program but with the additional complexity of multiple controller synchronicity. A high level flow diagram description of the systems key tasks, undertaken in the printing of a single layer, can be seen in Figure 4.36. The following sections will describe the function and development of the individual firmware for each the systems four PIC microcontrollers. Each program will start with a high-level flow diagram with program macros numbered as they were likely to be executed.



**Figure 4.36** A high-level flow diagram describing the milestone program blocks used to complete the deposition of one build layer.

*The Master Controller*

The master controllers program synchronised the actuation of the ALM system’s actuators with the firmware imbedded within the print engine. While the master controller was not needed to perform raster image or laser scanning processing, it did interface with the existing hardware / firmware to facilitate layer printing onto a belt opposed to a paper source, as the printer controller was designed.

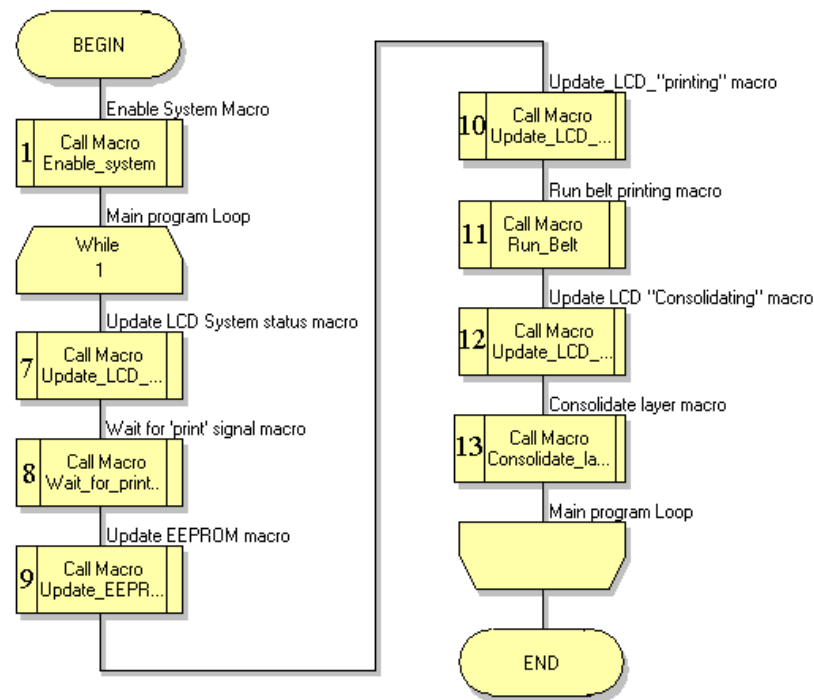


Figure 4.37 The master controller's main program loop. The program macros are numbered in the sequence they were likely to be executed.

The master control program can be described as a set of eight high level program macros executed as described in the flow diagram Figure 4.37. Including the eight high level program macros used to describe the master controller's firmware program, there were a total of thirteen program macros used. All but one of the high level program macros were incorporated within the main program loop which, contained all the program information needed to successfully print and consolidate multiple layers. The full break down of each macro is offered in appendix C.

#### *Bipolar Consolidation Roller and Print Engine Controller Program*

There were two ancillary bipolar stepper motor drivers; one was employed to revolve the print engine in a single direction (unidirectional) whereas the other was expected to move the consolidation carriage in two directions (bidirectional). The flow diagrams in Figure 4.38 describe the programming of the bidirectional controller showing the three program macros which formed the bipolar controller firmware. The unidirectional controller had the same coding as the bidirectional controller, but was instructed to rotate in a single direction only by the master controller.

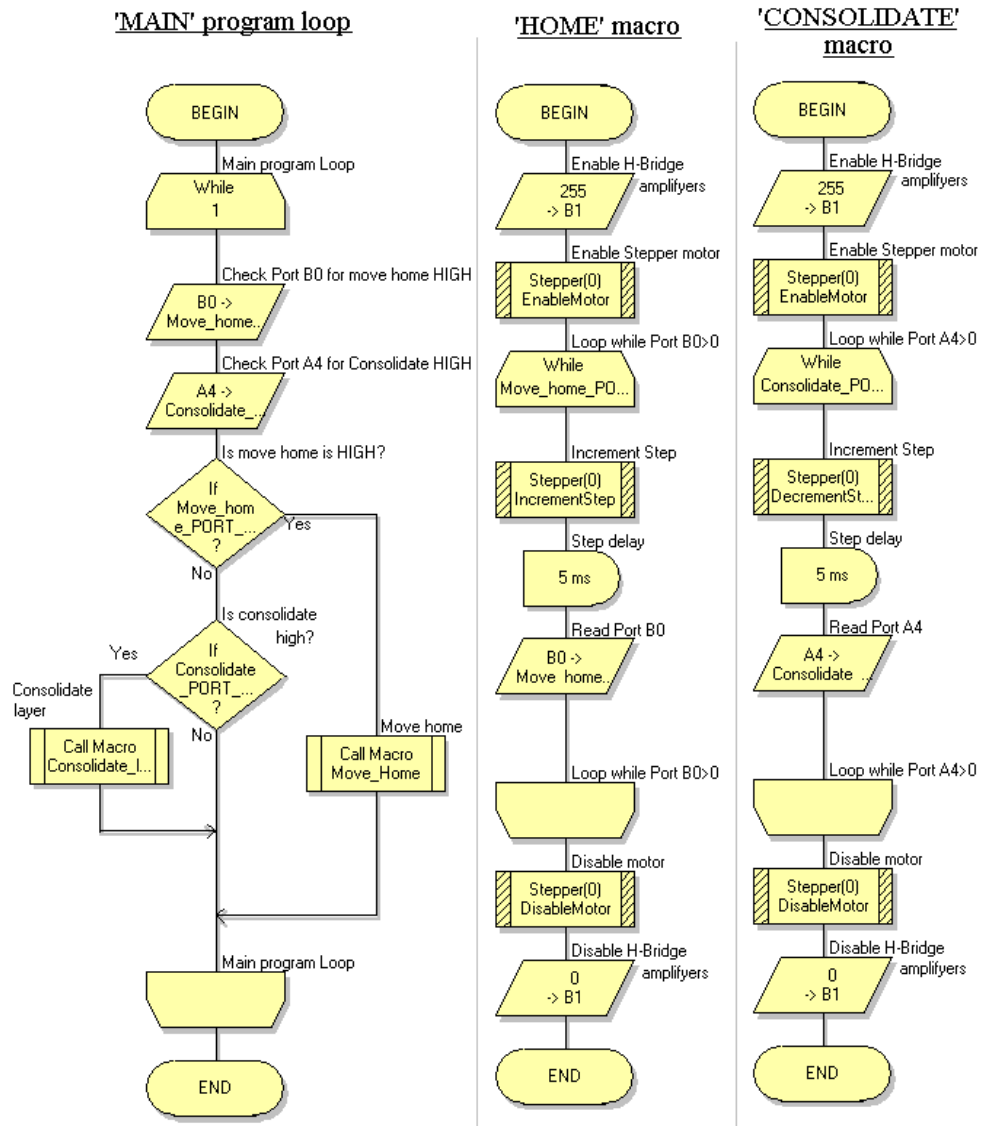


Figure 4.38 Three flow diagrams illustrating the program flow of firmware controlling the stepper motor movements of the consolidation roller/carriage. Left: the main program loop dictating the direction of motor rotation, Middle: Clockwise rotation program macro Right: Counter clockwise rotation program macro.

### Unipolar Controller Program

The ancillary unipolar controller was programmed to rotate the transfer belt in a single direction. Its function was similar to that of the unidirectional stepper motor as controlled by the ancillary bipolar controller. However the underlying C code describing the sequence of outputs sent to the stepper to increment a step was entirely different. Figure 4.39 is a flow diagram illustration of the two program macros used to execute the desired transfer belt motion.

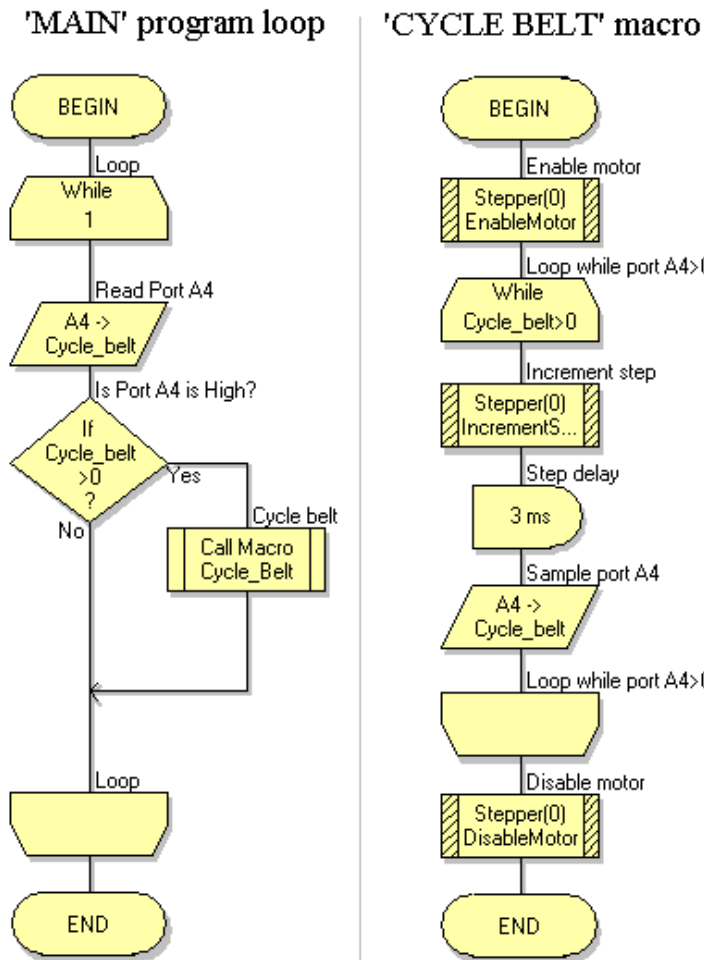


Figure 4.39 Two flow diagrams illustrating the program flow of firmware controlling the stepper motor movements of the transfer belt. Left: The main program loop continually reading port A4 for the start command Right: the program macro used to cycle the transfer belt when instructed to do so by the master controller.

### *Z-axis Controller Programming*

Between sequential print layers, the Z-axis was required to index a layer depth down in the Z direction to allow the next layer to be consolidated. As the z-axis was a third party device it used its own programming syntax. The master controller communicated through RS232 with the z-axis, issuing a single command to cycle the pre-programmed controller. The Z-axis's controller, the DMC-1010, command set was strait forward and the short program necessary to execute the aforementioned routine was written:



```

RS // Reset Z-axis, return to home position,
MTZ = 1 // Set axis as a servo motor
SB 1 // Set bit 1 – (releases axis brake)
PRZ 1553664 // Position relative (1553664 encoder counts ≈ 155.37mm)
SP 20000 // Set speed (20000 counts/min)
BGZ // Begin motion in Z-axis (155.37mm to contact consolidation
roller)
ED // Begin program editor
{
000 # Zprogram // Name program (Zprogram)
001 PRZ -50000
002 BGZ
003 AM // After motion
004 WT 500 // Wait (500 milliseconds)
005 PRZ 49500
006 BGZ
007 EN // End program
}
XQ # Zprogram // Execute program (Zprogram)

```

#### 4.7 POC Prototype Final Assembly

The final assembly of the POC prototype (Fig 4.40) was mounted on a pre machined desktop which allowed the Z-axis build platform to have access to the belt and consolidation roller through an aperture.

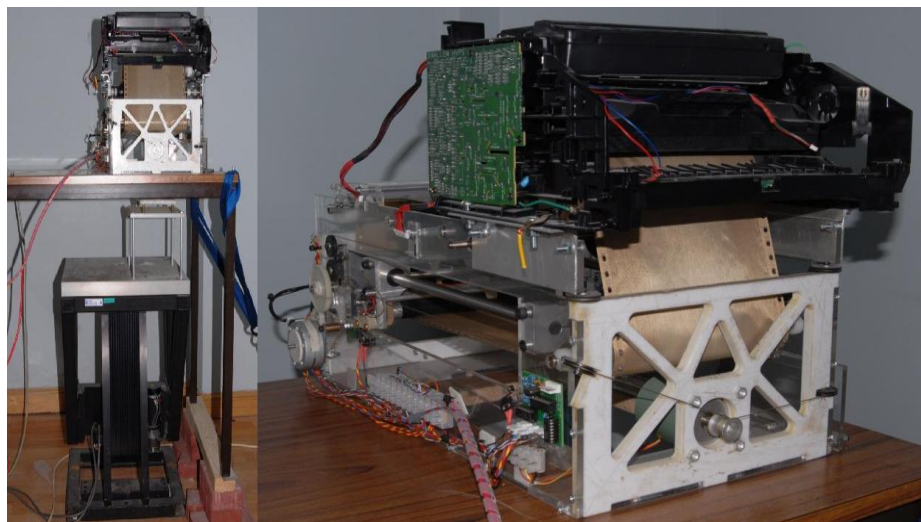
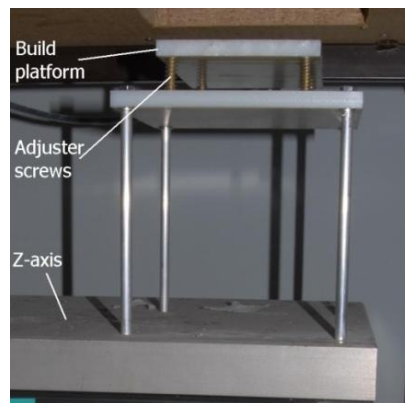


Figure 4.40 The assembled POC prototype and associated control hardware ready for testing. Left: A Prototype unit mounted on a bench with Z-axis below. Right: A view of the POC prototype consolidation and deposition

units

The z-axis was fitted with an extension platform (Fig 4.41) which was adjusted to sit true across the consolidation rollers movement. Following trimming, the Table was coated with an air drying polymer based modelling clay, rolled out by the consolidation roller. The resultant surface was flat and parallel to the movement of the consolidation roller. Printed artefacts were consolidated onto the surface of a sacrificial acrylic sheet which was temporarily adhered to the trued surface, with adhesive tape.



**Figure 4.39** The z-axis platform used to trim the orientation of the build surface relative to the consolidation roller

# Chapter 5: Prototype Trials

Initial testing was undertaken to determine the nominal operating parameters of the prototype before testing to fulfil the objectives set out during the introductory pages of this thesis. Table 5.1 describes the experimental agenda.

Experiment	Description	Objective
1	A series of tests undertaken to deposit material onto the transfer belt, adjusting the belt velocity until it matches the print velocity	To determine the correct belt velocity to synchronise with the print velocity
2	A series of tests where roller temperature was adjusted until consolidation occurred and the z-axis flatness was calibrated	To ascertain the correct roller velocity / temperature ratio as well as Z-axis alignment to ensure consolidation
3	A multi layer artefact consisting of over 20 layers was printed onto a substrate	To demonstrate the system's ability to print without the fringing phenomena
4	The set up and use of the system to produce an artefact of 3.5mm in z-axis height	To demonstrate the system's ability to print without height limitation

Table 5.1 A list of experiments carried out to test the POC prototype in order to realise the research objectives.

## 5.1 Experiment Set 1: Belt Velocity and System Setup

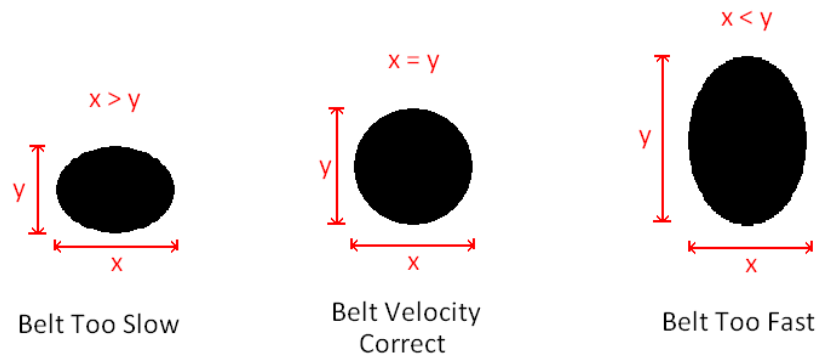
There were a number of variables which needed determining in order for the system to run autonomously before testing to fulfil the objectives could be undertaken:

- Belt velocity
- Belt tension
- Belt position
- Z-axis height
- Z-axis step size

### 5.1.1 Experiment 1.1: Belt Setup

An experiment was undertaken to determine the velocity at which the belt should be driven in order to synchronise with the feed of the deposition system. The belt drive's stepper motor was driven in half step commutation to reduce noticeable. The belt velocity was measured as a factor of steps per minute, set by the 'step\_delay' variable within the controller firmware. An arbitrary velocity of 12k full steps per minute (24k half steps per minute) was used as a starting point for testing. A layer deposition cycle was run, the results analysed and the belt velocity adjusted iteratively until the correct velocity of 15k steps was obtained. The correct belt velocity was known when the

ratio between the length and the width of a printed circle was equal to one. A schematic of the visual velocity identification can be seen in Figure 5.1.

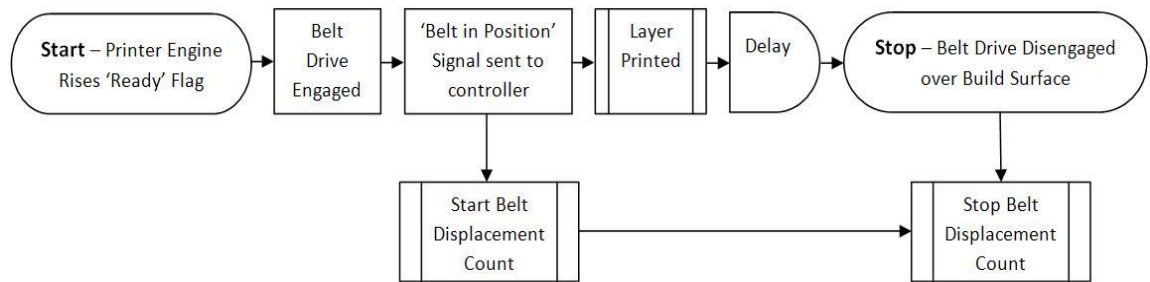


**Figure 5.1** The indicative deposition of a circular geometry dependent on relative belt/OPC velocity

It was clear from the functional testing that, in order to maintain accuracy, the belt must be under tension to prevent sagging. The belt was tensioned through the use of a spring loaded accumulator roller. While the tension necessary to prevent belt sag was quickly determined, the experiment identified an issue with the print quality. The additional tension applied to the transfer belt had a negative impact on the quality of a deposited layer. The deposition system's transfer roller was sprung to allow the passing of the transfer belt, while maintaining the contact interface between the OPC and the belt surface. However, as the belt tension was increased, the backing roller was retracted, allowing the transfer belt to be pulled out of contact with the OPC. The solution was to constrain the transfer roller by substituting its sprung mounting for aluminium spacers, whilst spring mounting the OPC and LSU to allow the passing of the transfer belt. Following the immobilisation of the transfer roller, it was noted that the OPC did not maintain contact with the belt's surface, but rather the belt's reinforced edges. To remedy the issue, the transfer roller was profiled at either edge to allow the passing of the reinforced belt edges while supporting the area of the belt to be printed upon.

After a powder layer was deposited, the belt revolved until the powder image was in the correct position over the build platform for consolidation. It was important that the distance revolved was identical to that of the previous layers, to ensure alignment

of each artefact layer. The sequence of control events is shown in Figure 5.2 and indicates between which events the belt displacement was measured.



**Figure 5.2** The control sequence implemented during the transport of a layer from deposition system to Z-axis build platform.

The belt displacement, from the initiation of layer deposition to the correct location for consolidation, was calculated to be 2k full steps of the drive stepper motor.

### **5.1.2 Experiment 1.2: Z-Axis Setup**

Following the levelling of the Z-axis table, relative to the inclination of the consolidation roller's path, the axis step size was investigated. During the conceptual testing phase of this research, the Z-axis step size was set to 10 microns. A number of consolidation test runs were undertaken to ensure the Z-axis was in the correct position. For the purposes of this experiment, the heated roller was set to a working temperature of 180°C and the roller carriage was propelled at 75 mms<sup>-1</sup> (in common with the fuser temperature and working velocity of the donor printer). The deposited layers were consolidated onto the build platform under fully automated control. It was observed that only the first layer of each build was being consolidated onto the surface of the build platform. Preceding layers remained on the surface of the belt, before being removed by the belt cleaning unit. Following the finalisation of the consolidation unit design, the belt thickness was amended to 0.115 mm, in an effort to reduce the surface texture imparted by the belt's reinforcing. The increased dielectric thickness of the thicker belt material was concluded to have an adverse effect on the deposition density. Initial trials were undertaken to increase the OPC / transfer roller potential, but at the higher voltages needed, spark discharge between the two roller elements occurred. The solution tested and ultimately accepted, for initial testing, was

to accept the thinner layer thickness and reduce the Z-axis step size to  $\mu\text{m}$ . The trials showed that the decrease in step size allowed full layers to remain on the build surface and provided acceptable definition at the artefact's edges.

### 5.2 Experiment Set 2: Consolidation Assembly Setup

Initially the consolidation roller's velocity and temperature were set to emulate that of the fixing apparatus of the donor printer. However, with the additional belt thickness and the necessity to consolidate and bond a new layer to the build volume, it was assumed there would be an optimum temperature/velocity relationship. Within the scope of this research, the empirical modelling of this relationship was not essential; however, ensuring adequate consolidation of artefacts built for prototype testing was of priority. Building on the results of the experiments undertaken for the set up of the Z-axis, testing began with the visual analysis of a five layer artefact consolidated by a roller temperature of  $180^{\circ}\text{C}$  and a velocity of  $75\text{ mms}^{-1}$  (Fig 5.3). With these variables, each layer was lightly sintered and bonded to the build volume. The temperature of the roller was then kept constant while its speed was varied. A constant temperature of  $180^{\circ}\text{C}$  was used as it was significantly above the melting temperature of the toner material used ( $90^{\circ}\text{C}$ ) and was within the maximum working temperatures of the belt and machine materials. The resultant roller velocity for full consolidation was  $25\text{ mms}^{-1}$ , one third of the intended roller velocity as set out within the functional specification.

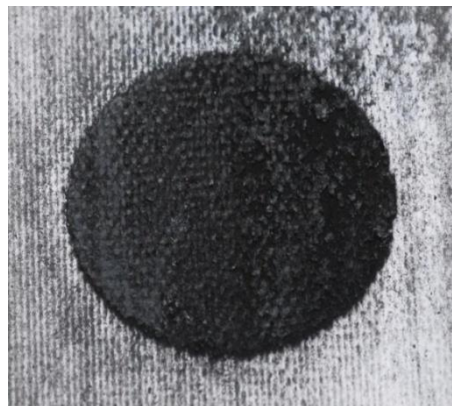


Figure 5.3 A fully consolidated five layer artefact of 25mm diameter, consolidated at a roller temperature of  $180^{\circ}\text{C}$  and a velocity of  $25\text{ mms}^{-1}$

### 5.3 Experiment Set 3: Fringe Analysis

An important part of the POC testing was the demonstration of the system's ability to produce artefacts without a fringe. The concept testing showed that the phenomenon of fringing was initially seen on an artefact's surface after 10 layers, and explicitly observed after 20 layer deposits as a bulge around the periphery or as unconsolidated material in the centre of the artefact. The first experiment undertaken, following machine setup, was the printing of a 20 layer artefact (Fig 5.4). The build platform mounted on the Z-axis was lined with a 120mm x 120mm x 3mm Polymethyl methacrylate (PMMA) sheet which was intended to tackify and retain the first layer of the built artefact through adhesion. The experiment printed and consolidated 20, 5 $\mu$ m layers of the same dimensions, creating an artefact of  $0.1\pm 0.005$ mm. The Z build height and therefore average layer thickness was verified using an LDVT at a number of random points across the artefact. Figure 5.5 shows the surface of the printed artefact showing no sign of fringing. The photograph however, clearly shows the impression imparted by the glass reinforcing within the belt material during consolidation. As previously discussed, the belt material was thickened after the initial designs were completed in an effort to reduce the surface marking produced by the belt.

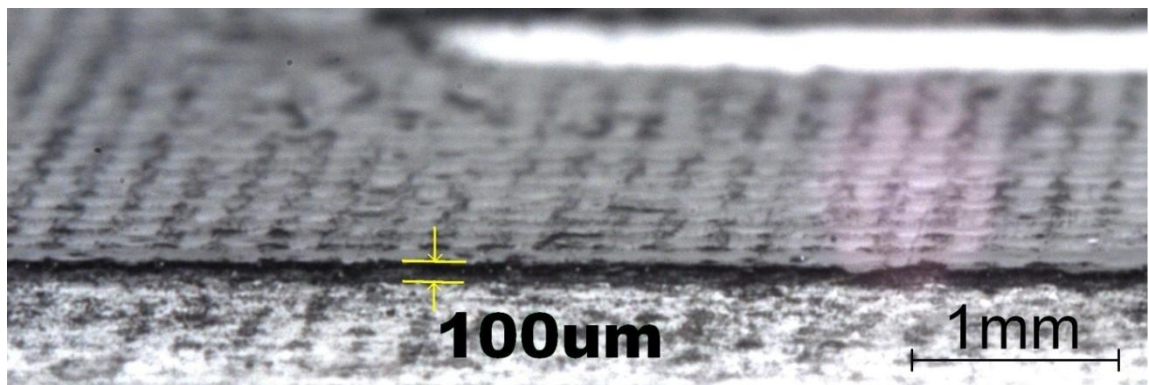


Figure 5.4 The surface of a 20 layer artefact showing no sign of edge fringing

The results from the formation of the 20 layer artefact show that the consolidation and mechanical transfer mechanisms used within the POC prototype have overcome the phenomena of part fringing.



### ***5.3.1 Substrate Testing***

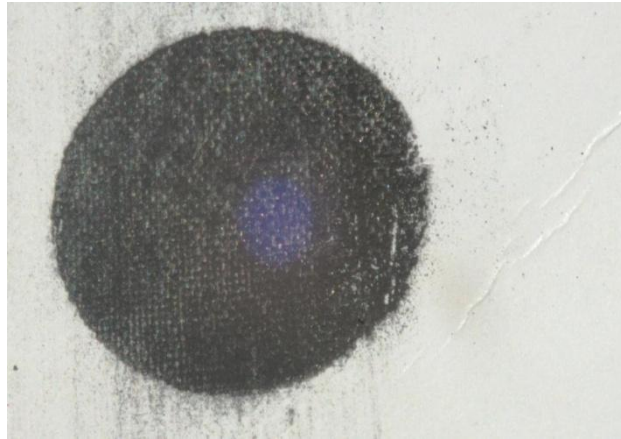
A slight warping of the substrate was observed during initial printing trials. Further tests were performed on the consolidation of powder layers onto the surface of an acrylic substrate to try and identify the cause of the surface disparity seen in former testing. In order to exacerbate the phenomena, the roller velocity was slowed to increase the thermal energy transfer into the substrate. The results of an experiment to print and consolidate 5 layers onto the surface of an acrylic substrate can be seen in Figure 5.5. The 25mm diameter circular layers have been distorted by the melting and warping of the acrylic substrate.



**Figure 5.5** The results of substrate melting on a deposited five layer cylindrical artefact of 25mm in diameter.

A solution considered was to increase the consolidation velocity and limiting the energy transferred into the substrate. The limitation being that, with less thermal input, the powder layer would not fully consolidate. An experiment to print on to a card substrate was undertaken with the same process variables as the PMMA testing. The results in Figure 5.6, show the card with no visible distortion other than a crease to the right hand side where it was removed from the build platform. The picture shows that while no distortion of the substrate occurred, the substrate did not accept the layers in their entirety, as the card substrate was unable to takify. The material which was not transferred remained consolidated on the transfer belt's surface.



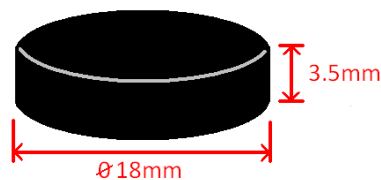


**Figure 5.6 Five layers of a 25mm diameter artefact consolidated onto a card substrate, showing no substrate distortion, but instead showing incomplete layer transfer**

The solution was found by looking at the mechanism used by laser printer fusers to fix toner to paper. The application of both heat and pressure forced the molten toner into the paper substrate thus permanently fusing the materials. An experiment was performed where eight layers were deposited in total. The first three layers were deposited with no Z-axis relief. I.e. the layers experienced both heat and pressure during consolidation, producing a flat takifiable surface from which build layers could be consolidated. The results showed that the pre-treating of a card substrate with fused material was a viable solution to the problems encountered.

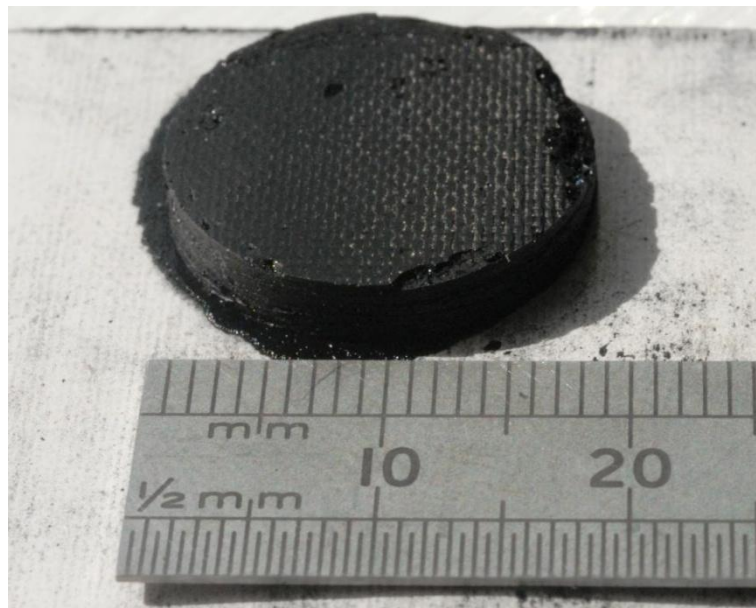
#### **5.4 Experiment Set 4: Z-Axis Height Limitation**

Probably the most significant hurdle to overcome in order to implement an electrophotographic process into an ALM system was the issue of a build height limitation. Building on the findings from the previously conducted experiments, a concluding experiment to satisfy the final research objective was designed (Fig 5.7).



**Figure 5.7 The geometry of an artefact intended to be produced in order to demonstrate unconstrained build height**

A card substrate was applied to the Z-axis and was pre-treated with a tackifying layer through the deposition of three layers without a Z-axis step down. The consolidation roller temperature and velocity were set to 180°C and 25mm<sup>s</sup><sup>-1</sup> respectively, as per the optimum settings recommended by previous testing. A cylinder of 18mm in diameter and 3.5mm in height (Fig 5.8) consisting of 700, 5 micron layers was produced. The part took six hours to produce, averaging one consolidated layer every thirty seconds. The resulting geometry can be seen in Figure 5.8.



**Figure 5.8** The resulting 3.5mm high geometry of a 700 layer artefact. The build direction was from right to left.

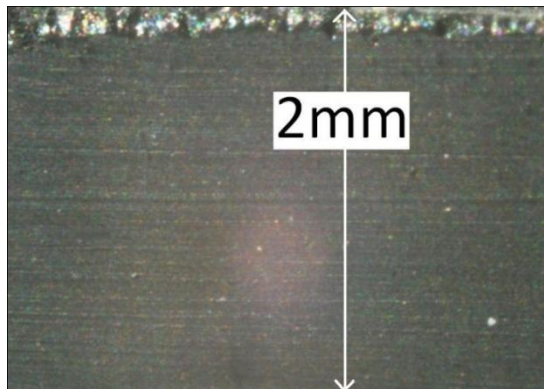
The resultant artefact measured 18.1mm in diameter and 3.5mm in height. There was no evidence of a build height limitation, experienced in the initial research conducted into electrophotographic ALM. There were a number of surface irregularities present on the finished artefact, a number of which were present due to layers 581 to 602 printing incorrectly. The layers in question were not printed in their entirety due to a lack of material present on the developer roller of the laser engine. The printer was paused and the cartridge replaced where upon standard printing and consolidation was resumed. Due to the printing of incomplete layers, the proceeding layers had no underlying support in a number of areas and therefore disparities formed and continued to grow with the artefact. Figure 5.9 illustrates the poor surface finish imparted by the transfer belt during consolidation, but supports the research

objectives of the production of an artefact without a height limitation or the occurrence of fringing.



**Figure 5.9** The surface finish of a 700 layer artefact.

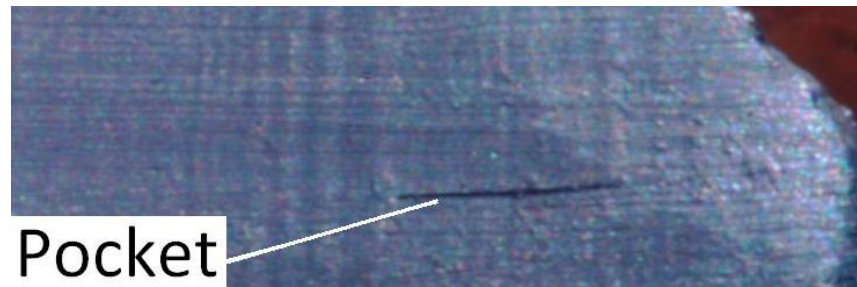
In order to investigate the effectiveness of the consolidation process, the part was removed from the card substrate through the application of heat on the underside of the card. Once released from the card substrate the artefact was sectioned using a micro saw. After preparation and cleaning the surface showed a fully consolidated and dense structure (Fig 5.10).



**Figure 5.10** The bisected and polished surface of the 3.5mm artefact showing fully dense consolidation.

A cross-sectional view of a fractured surface of the built artefact, as seen in Figure 5.11, shows evidence of the unsupported bridging of a void within the volume. This phenomenon occurred only over small areas, small enough for a five-micron layer to support itself and exhibit enough strength to be released from the transfer belt. This

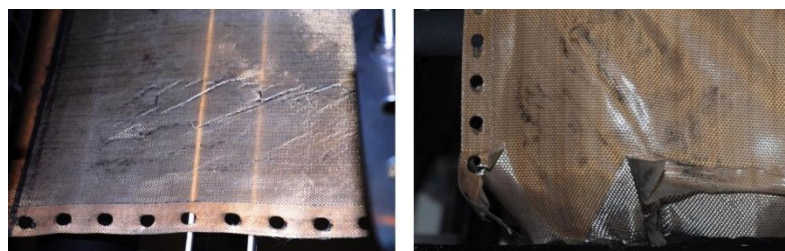
effect was a result of the printed layer forming a consolidated wafer while still on the belts surface. The wafer was subsequently adhered to the surface of the build platform before the belt was peeled away. It was apparent that voids which formed on the leading edge of an artefact were unlikely to be bridged, as the layer wafers were unsupported and thus removed by the peeling action of the peel roller. Damage to the right hand edge of the Figure in 5.9 illustrates the problem described.



**Figure 5.11** The fractured surface of a 3.5mm built artefact showing a 1mm long pocket formed between layers which was then bridged by subsequent layers.

### 5.5 Further Testing

Following the experiments undertaken to satisfy the research objectives, a number of experiments were planned to optimise the printing system and increase the dimensional accuracy of a built artefact. Following the printing of the 700 layers, the belt used had started to show signs of wrinkling and fatigue, due to an uneven applied tension and continuous heating and cooling cycles. To remedy the problem, the belt tension was increased and distributed over the belt more evenly. Shortly after the restarting of the testing agenda the belt catastrophically failed at its seam (Fig 5.12). Due to time constraints and as the necessary testing had already been performed; a new belt was not installed.



**Figure 5.12** (left) The fatigued belt prior to failure. (right) The failed belt along its seam.

## Chapter 6: Discussion

---

The aim of this research was to create an ALM system which was truly 'desktop friendly'. This research was intended to nucleate the development of a commercial system which was acceptable in both office and home environments, much in the same way as a desktop printer.

In order to achieve this aim, structured research was undertaken within the constraints of two proposals. The first:

*"A technology can be identified for development and integration, to form a low-cost desktop ALM system capable of rapidly producing accurate artefacts from engineering materials"*

generated three objectives:

- i. Research current ALM technologies to provide benchmark targets, representative of state-of-the-art ALM systems, which could be used to develop a new system.

The first objective led to the review of current ALM systems in order to identify an existing technology which could have been miniaturised for use within a desktop machine. Initially the review failed to generate a suitable subject for development, but did highlight the market deficit of ALM systems exhibiting truly desk top physical properties. This finding led to the formation of a high level standard for the physical and consumable maxima of a desktop system. This standard was then subsequently used as a benchmark from which to justify the prototype machine's functional specification.

- ii. Identify a suitable technology to take forward to develop into a desktop ALM system, exhibiting the characteristics of high resolution, high productivity and low-cost.

Inspiration was taken from the use of formally 'two dimensional' inkjet printing technologies that had been adapted for use in ALM systems. Laser printing was

identified as a robust powder deposition system which had seemingly lain unexploited within the ALM industry.

- iii. Identify former research papers and patents on the identified technology, highlighting methods and known limitations.

It was identified that a number of researchers had looked into the potential for laser printing or electrophotography for the deposition of layers in a layer based manufacturing process (Bynum, 1992; Grender, 2001; Kumar, 1999, 2000; Kumar, and Dutta, 2003, 2004; Kumar and Zhang, 1999; Kumar et al, 2004; Cormier et al, 2000, 2002; Banerjee and Wimpenny, 2006, 2008; Wimpenny and Banerjee, 2008; Wimpenny, et al, 2009; Jones, et al,2010). However, it was soon apparent that there were a number of technological barriers to electrophotographic ALM implementation which had previously hindered its commercial potential. Both a build height limitation and a fringing effect were discussed in former research and subsequently highlighted as the key problems to solve in order to produce a functional electrophotographic ALM system. Eight patents of interest were reviewed and their key innovations tabulated. The satisfaction of proposal one's objectives paved the way for the generation of the second research proposal.

*“An electrophotographic deposition system of the kind found in a modern laser printer can be utilised to produce a low-cost, high definition, high productivity, additive layer manufacturing system. More specifically, a Desktop Three Dimensional Printer prototype can be produced, which demonstrates no electrostatic build limits in the Z-axis and is capable of producing parts without fringing”*

The formation of the second proposal demanded the resolution of the identified barriers to implementation and generated four research objectives.

- i. Produce a prototype system with the ability to create simple laminate artefacts.

The formation of a prototype to produce simple artefacts was achieved in the first part by developing a physical and theoretical understanding of the limitations highlighted in former research. Following this, a solution concept was generated and a number of its fundamental components tested and developed. The resultant prototype was able to generate simple laminate artefacts consisting of a plurality of deposited and consolidated layers.

- ii. Develop an electronic and firmware control system to facilitate the development of current and future objectives.

The prototype developed in this work was intended to be the first development step in the testing and generation of new materials and process concepts. As such the electronic hardware and firmware were designed to be easily updated. The modular architecture of the control system allowed for simple system debugging, as well as providing a robust system for future machine development.

- iii. Develop and demonstrate a solution to the fringing effect by producing an artefact consisting of a plurality of layers without exhibiting fringe build up.

The work undertaken in the concept phase identified that fringing was visible after ten layer deposits. In the first instance, before considering the testing of build height, the prototype produced an artefact of 20 layers without the presence of fringing. Further testing to demonstrate the build high capabilities of the prototype reinforced this result.

- iv. Develop and demonstrate a solution to the Z-axis height limitation by producing an artefact of over 3mm in build height

The most significant limitation noted in prior works, and then reinforced within testing undertaken in the conceptual development phase of this research, was the physical limit to build height due to electrostatic field depletion. The largest part known to be built was 3mm (Kumar and Dutta, 2004). Testing conducted on the prototype developed within this research demonstrated the unrestricted building of an artefact up to 3.5mm in height.

## 6.1 Prototype Performance

The prototype's success was measurable against the predefined functional specification generated following the development of a concept. The specification applied governance for four distinct development considerations:

- i. Provide a solution to the build height limitation.
- ii. Provide a solution to the fringing phenomenon.
- iii. Produce a system with desktop characteristics.
- iv. Produce a low-cost system.

The following section will analyse the prototype's performance against these headings and discuss the implications of testing.

### *Build Height*

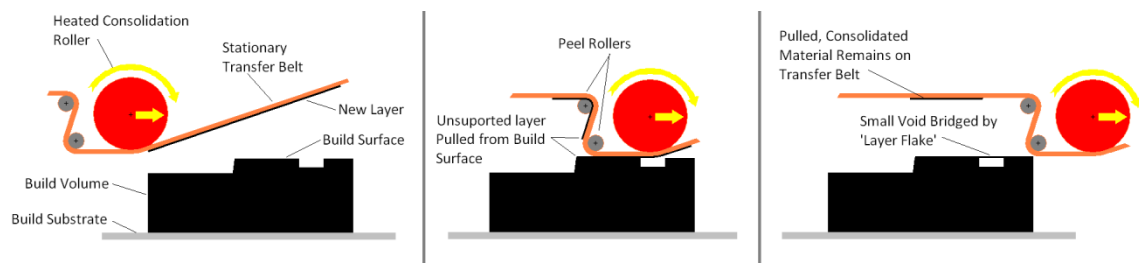
The prototype within this work created an artefact of 3.5mm in height, consisting of 700 layers of uniform thickness, the tallest known part produced in the Z axis of any electrophotographic ALM system to date. The specification highlighted that in order to satisfy the research objective of demonstrating a solution to the build height problem; a part of over 3mm in high had to be built while showing no layer thickness degradation. The 3mm minimum height was specified as a result of the maximum published build height of an ALM system employing electrophotography (Kumar and Dutta, 2004). The 3.5mm artefact exhibited a number of surface irregularities. A number of the pockets were as a result of layers 581 to 602 printing with parts of the layer images missing. The reason for the incomplete image development was found to be a low material volume within the toner cartridge. A second surface irregularity as seen in Figure 6.1 was the absence of a number of layers on the leading edge of a built part.





**Figure 6.1** An artefact produced by the Electrophotographic based ALM prototype with a layer deficit on the leading edge.

It was observed that during printing the image would develop on the transfer belt and consolidate into a 'layer flake' on the surface of the belt through the application of heat. When the layer flake was transferred to the build surface through the application of heat and pressure, it was found it would transfer very much like a 'transfer sticker'. The layer would bridge small voids providing it had a suitable bond to the preceding build surface, in order to initiate peeling. If the leading edge of the build surface was unable to provide a surface for the layer flake to bond to, the layer would be retained on the belt and the peel roller would create a moment force which would fracture the layer flake along a line created by the next point of layer bonding. A graphical representation of this explanation is offered in Figure 6.2.



**Figure 6.2** The process by which improper consolidation of the leading edge of a part can form if the leading edge of the build surface cannot provide a bonding surface to the following layer.

The initial degradation of the leading edge can be formed in a number of ways including: insufficient consolidation of previous layers, improper transfer or image development of the previous layer, or movement of the machine. In the case of the artefact seen in Figure 6.1, it was as a result of an incomplete image development. The incomplete image resulted in a section of the artefact being unable to provide a bonding surface for subsequent layers. One of the benefits seen with 'layer flake' formation is that it is able to bridge small (typically 1mm or less) gaps with no underlying support. At thin layer thicknesses of around 5 $\mu$ m the bridgeable gap is quite small but at higher layer thicknesses and optimised peel rollers, the size of a bridgeable gap should increase. A solution to minimise the occurrence of this effect would be to print a second solid support material which could takify to accept a toner layer. Such materials could be PVOH powders or a lower cost material could be powdered household sugar.

The apparent build height limitation was one of the two most significant limitations to the implementation of electrophotography within an ALM system and was discussed over the course of the research headed by Kumar at the University of Florida (Kumar, 1999, 2000; Kumar and Zhang, 1999; Kumar and Dutta, 2003, 2004; Kumar et al, 2004). The work was then referenced and solutions offered within Wimpenny and Banerjee's work (Wimpenny and Banerjee, 2008). In order to study the problem, the phenomenon was recreated using an adapted printer to print onto a substrate with a transfer field induced by a conductive build plate. It was seen that the layer thickness deposited reduced exponentially with the build surface's increased displacement from the build plate. The layers were observed to be thick to begin with but then became thinner until around 80 prints at which point no noticeable deposits were recorded for a further 10 deposits to 90 prints in total. These results were in support of Kumar and Dutta's findings (Kumar and Dutta, 2003). The degradation in measured electric field was a function of displacement from the field source and was modelled by Kumar and Dutta (2004) in equation 2.12. An expression for the voltage of a field relative to the displacement was derived (Equ. 3.4) and the resultant increasing voltage necessary to maintain a constant electric field on a build surface was plotted. The relationship was

found to be linear and increased at around 5kV/mm. This was significant as it demonstrated that the electric field at the build plate could not be simply increased to maintain a constant electric field at the build surface as the voltages necessary to build artefacts of over one mm were large. An example given was of the 5MV potential difference needed to build an artefact of 100mm. Wimpenny and Banerjee (2008) provided a solution to the problem through the charging of the build surface between layer deposits or the repulsion transfer of powder onto an uncharged build surface. As no experimental evidence was available to demonstrate the effectiveness of these offered solutions, two experiments were undertaken. Initial results for the charging of the surface between layer deposits was promising, as an artefact could be produced with no apparent degradation in layer thickness over the course of 90 layers. Upon further investigation however, it was noted that the centre of the artefact was poorly consolidated due to a 3mm wide fringe build up (fringing will be discussed in the next section). It was concluded that due to the excessive fringing the surface charging method was not a successful solution. The results from the repulsion transfer technique, where the powder image was repelled from the OPC/Transfer medium, again demonstrated promising results. It was shown that while significantly better than a base plate generated charge, the repulsion transfer techniques still demonstrated layer thinning over 90 layers. It was hypothesised that residual charge, left on the surface of the part after layer transfer/consolidation, affected the deposition of further layers. An additional experiment was undertaken to eradicate the surface charge present upon the build surface prior to layer transfer. This was shown to further improve the layer thickness stability but overall a 30% reduction in layer thickness over the 90 layers was observed. Unlike the results from initial base plate generated field experimentation where layer thickness dropped off exponentially with build height, the repulsion results showed a slowly increasing decay of layer thickness. It was apparent however, that the reduction of layer thickness was non-linear and the rate of change increased as the build height increased. With the increase in part height, also came the increase in artefact volume. It is assumed that, while the surface charge present on the build surface is eradicated between layer deposits, an internal volumetric charge grows with the artefact. This charge then

served to hinder subsequent deposits, becoming more significant as the artefact volume increased. The assumption of cumulative volumetric charge was not investigated further as it was concluded that, regardless of the cause of layer thickness decay, repulsion transfer was not a suitable solution to the build height problem as fringing would occur.

The physical mechanisms generating the problems seen during build height investigations were purely electrostatic in nature. The solution conceptualised and tested within this work was that of mechanical layer transfer. The concept saw a powder layer heated to form a layer on the surface of a transfer belt while simultaneously applying heat and a small amount of pressure. As a result of heat applied through the belt, the image present on the belt surface conglomerated to form a layer flake. When applied to the top of the build platform, this layer flake peeled and bonded with the previous layer. A heated roller was used for the consolidation of layers, the velocity and temperature of which were determined empirically to ensure full consolidation. Tackification of a cardboard substrate prior to printing was necessary as without this tackifiable layer, the roller applied image exhibited insufficient bonding to fully transfer. The main problem discovered when bonding the artefact to a card substrate was that its post-process removal from the card substrate was difficult. The test artefact examined in the results chapter of this thesis was removed through heating the card substrate to the softening/melting temperature of the toner material. This process however, damaged the lower surface of the artefact. A solution could have been to use a similar soluble PVOH plastic substrate to print on and then dissolve the substrate away as Cormier et al (2000) did during their experiments.

### *Fringing*

The second most significant objective, to demonstrate the function of the electrophotography based ALM system, was the demonstration of a solution to fringing. In addition to the 700 layer artefact built without evidence of fringing, a pre-emptive 20 layer artefact was created resulting in no fringing. During the conceptual development a number of tests on electrostatic transfer demonstrated the fringing

effect. It was identified that with a  $10\mu\text{m}$  layer thickness, fringing could be clearly seen after 10 layers, and was obvious on an artefact of 20 layers in thickness. An initial prototype test of 20 layers was deemed appropriate to assess whether the system was capable of printing without fringing. A 20 layer artefact was not large enough to satisfy the objective governing the abolition of the height limit, but it was large enough to satisfy the fringe field objective without demanding a 700 layer artefact from an untested prototype. Kumar et al (2004) noted the effects of fringing and suggested it could be overcome by the printing of two powders, a build and a support material. Upon reflection this may have worked using the deposition system within this work. It is apparent however, that the expectation within this work was that fringing not only occurred due to non-uniform fields present on the build surface, but also during development due to the large charge gradient present at the edges of a latent electrostatic image upon a photoreceptor. Pai and Springett (1993) showed with equations 2.4 and 2.5 that the average electric field above the photoreceptor, which directly affects development, is dependent on the dielectric displacement of a developer electrode. The diagram in Figure 6.3 represents the ML4500 development process assuming the ‘worst case scenario’ where the developer roller is at its largest displacement in order to produce a fully dense layer following consolidation of  $l_t$ .

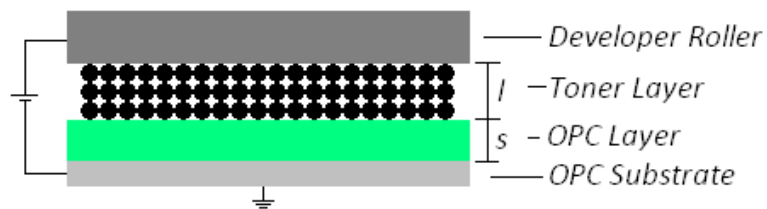


Figure 6.3 The development system within a Samsung ML4500, single component, and non-magnetic laser printer.

Developing the two models originally representing IMB (Equ. 2.4) and CMB (Equ. 2.5) development, and assuming displacement of the developer electrode is equal to the layer thickness  $l$  present on the developer roller (assuming  $\sim 100\%$  transfer efficiency) (Yagi et al, 2001):

$$l \approx \frac{l_t D_T^2}{0.25\pi D_T^2} \quad (6.1)$$

Where  $D_T$  is the average diameter of the toner particles. The average electric field present on the surface of the OPC with respect to the displacement can be given by,

$$E_{ave} = \frac{V_0}{s/K_s + l/K_l} \quad (6.2)$$

Assuming ( $V_0$ ) stays constant, regardless of the developing method, and using the variables given in Table 6.1, the relative  $E_{ave}$  ratios of the IMB, CMB and contact developing methods can be compared:

For IMB:

$$E_{ave} = \frac{V_0}{2.6 \times 10^{-4}} \quad (6.3)$$

For CMB:

$$E_{ave} = \frac{V_0}{9.33 \times 10^{-5}} \quad (6.4)$$

For Contact:

$$E_{ave} = \frac{V_0}{1.14 \times 10^{-5}} \quad (6.5)$$

Variable	Value	Units	Description	Source
$s$	3.0E-05	$m$	Thickness of OPC layer	Pai, Springett, 1993
$K_s$	3	-	OPC Dielectric Constant	Pai, Springett, 1993
$d$	1.5E-03	$m$	Developer Roller to OPC Displacement	Pai, Springett, 1993
$K_d$	6	-	Developer to OPC Dielectric Const. (IMB)	Pai, Springett, 1993
$D$	8.3E-06	$m$	Toner Diameter	Vijayendran, 1975
$R$	1.5E-04	$m$	Average CMB Bead Radius	Pai, Springett, 1993
$l$	6.4E-06	$m$	Developer Roller Layer Thickness	Calculated
$K_l$	4.5	-	Developer to OPC Dielectric Const.	Vijayendran, 1975
$l_t$	5.0E-06	$m$	Resultant Consolidated Layer Thickness	Obtained Empirically

Table 6.1 Variables and their sources.

As expected, the CMB development system shows a significant increase in average electric field strength in the air gap above the OPC over that of the IMB development system. This is both due to the decrease in apparent development electrode displacement and the conducting carrier particles. It is given that a reduction in the displacement of the development electrode to a charged OPC image will generate a greater electric field in the air gap over solid areas and therefore reduce fringe field formation (Thourson, 1972; Pai and Springett, 1993; Kao, 1973). The significantly larger (>8 times) electric field present in the solid areas above the OPC in contact development over that of CMB, supports the lack of a fringing present on prints by the ML-4500 printer. In order to reinforce this conclusion, the OPC system was modelled in QuickField 5.8. The results seen in Figure 6.4 illustrate a cross section of the field above an OPC with a 2mm wide latent charge on its surface. The model is of charged area development type with an OPC thickness of 60 $\mu$ m, a relative OPC dielectric permeability of 3, a surface charge of 1kV, an OPC to developer relative dielectric permeability of 6 and an OPC substrate of 0V potential. Figure 6.4a shows the magnitude and relative X axis position of the applied surface charge. The charge was assumed to be of infinite length perpendicular to the x/y axis presented and is symmetrical about the x axis. Figure 6.4b shows a model of the system with a 0V potential (developer electrode) over 6mm above the OPC surface, demonstrating the relative field intensity without the influence of the developer electrode. Figure 6.4c, d, e and f illustrate the effects of a 0V potential developer electrode approaching the surface of the OPC. The displacement of the electrodes in Figure 6.4c, e, and f, are

representative of the electrode displacement in IMB, powder cloud and CMB development systems respectively (Pai and Springett, 1993). Contact development is not shown, as at a displacement of 6.4 microns, the detail of the graphical model is incomprehensible. The model shows clear evidence of an elevated fringe field and a deterioration of field strength towards the centre of the latent charge (the origin of the x axis) in the absence of a developer electrode (Fig 6.4b). As a developer electrode of 0V potential is introduced at 1mm above the OPC surface (Fig 6.4c) the field in the centre of the latent charge increases but has little effect on the relative magnitude of the fringe fields. The presence of fringe fields at an electrode displacement of 1mm supports the notion that IMB development systems produce significant fringing during OPC development. As the OPC/developer electrode displacement is reduced (Fig 6.4), the significance of the fringe field relative to the increasing field across the charge pattern decreases. At powder cloud development electrode displacements (Fig 6.4e) the relative fringe field is reduced significantly, however small fringe fields still remain. At a developer electrode displacement of 85 $\mu$ m (Fig 6.4f) the fringe fields are unremarkable, supporting evidence of little or no fringing formed on images developed by some CMB and contact development systems with small electrode displacements. The fringe formation seen on the edges of a test print produced on an HP 2055DN printer suggest the use of a developer electrode with a significant displacement. The HP toner used was of mono-component magnetic type which forms brushes much like the IMB type development system but requires no large carrier beads, as the toner has a ferrous core. It is concluded that the Samsung ML4500 with mono-component, non-magnetic toner has a developer electrode of minimal displacement from the OPC and thus minimises fringing. While the previously discussed model supports the findings during concept development, it is a demonstration of one potential factor eliminating the fringing fields. It is also most likely that other factors specifically designed by the printer manufacturer to reduce fringing are at play, such as voltage frequencies and exposure patterns (Neugebauer, 1969). Further work needs to be carried out to determine why fringing did not occur in the printing system used, in order to properly understand the design implications for further work..



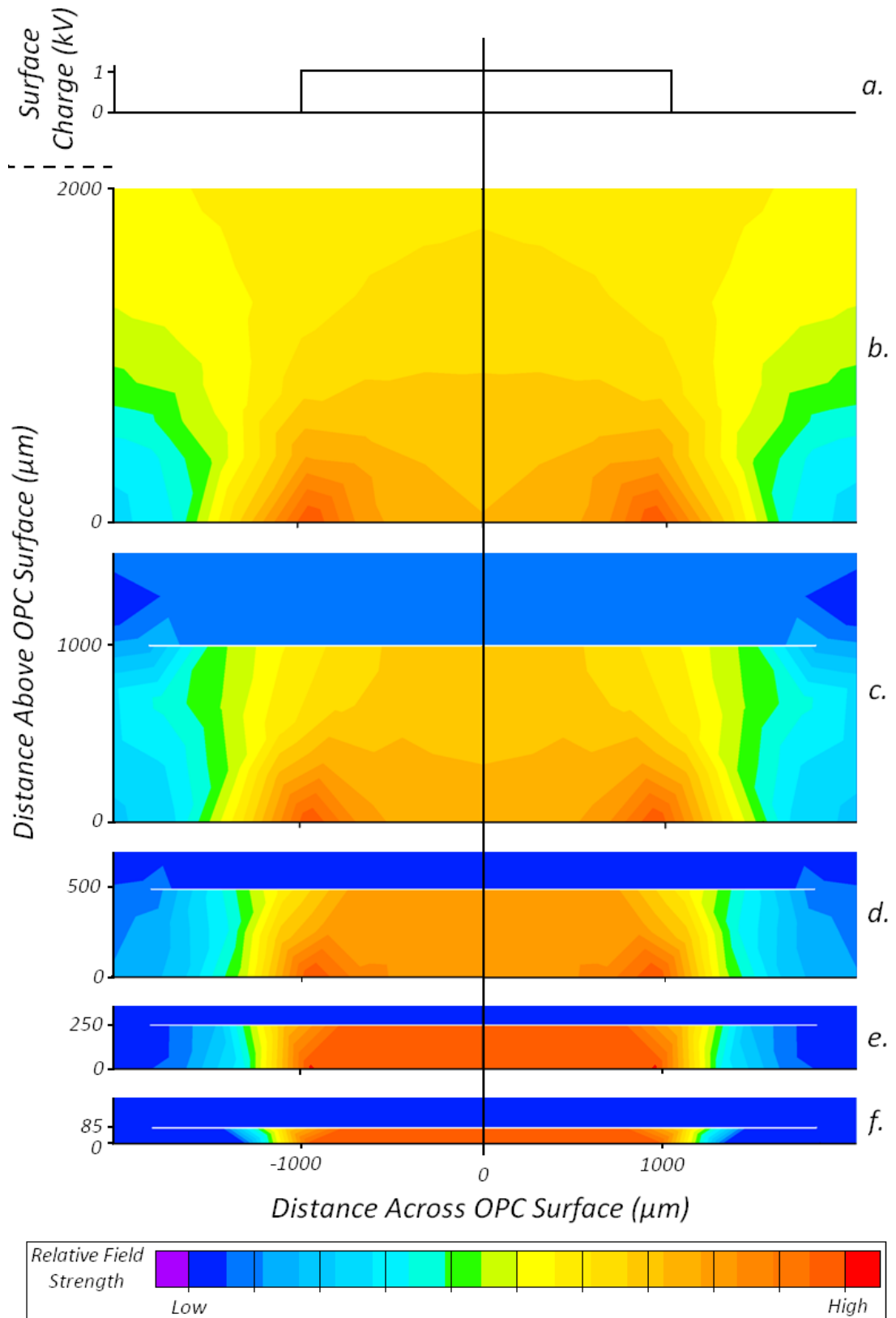


Figure 6.4 The relative field strength present above an OPC with the charge pattern seen in (a) and with: (b) No electrode, (c) An electrode displacement of 1mm, (d) An electrode displacement of 0.5mm, (e) An electrode displacement of 0.25mm and (f) An electrode displacement of 85 $\mu\text{m}$ .

### *Physical Characteristics*

The functional specification highlighted two primary physical characteristics that the prototype as a complete assembly was governed by:

- **Dimensions** - The prototype should have dimensions less than 733 x 600 x 840mm in the X, Y and Z axis respectively
- **Mass** - The prototype should have a mass less than 44kg

Due to the implementation of a technology that was commercially untested in an ALM embodiment and with known barriers to implementation, the physical characteristics were sidelined within the research objectives of proposal two, in order to concentrate on demonstrating that the problems associated with electrophotographic ALM implementation could be overcome. The functional specification however maintained the desktop spirit of the research and demanded that while at 'first prototype' stage every component did not have to be physically optimised, there should be a viable low mass and compact alternative for components uncharacteristic of a desktop product.

The final dimensions of the prototype design were 600 x 300 x 950mm, 110mm larger in height than allowable by the functional specification. In addition to this, further development employed a third party Z-axis which increased the prototype height by 500mm. Although the height of the final prototype was 610mm out of specification, it was understood that a number of components were designed with significant working volume. The working volumes, such as the additional space between the lower and upper portion of the belt loop, allow ease of adjustment and visual monitoring of the system during testing. The additional machine height gained from a floor mounted Z-axis was the most significant component of machine height. A Z-axis was an intrinsic part of all ALM systems and as such is a well known and widely used apparatus. With the substantial task load of objectives covering new ground, the use of a third party Z-axis allowed an area of development and a potential failure mode to be eradicated. The DMC-1010 controlled Z-axis was implemented with the understanding that a number of reduced dimension Z-axis designs were ubiquitously used within low-cost ALM machines such as the Fab@Home or Bits from Bytes systems. Neglecting the Z-

axis dimensions, the deposition and consolidation systems were of desktop dimensions and were not out of place mounted on a bench top.

The resultant mass of the prototype system was 83kg however, over 70% of this mass was contributed by the third-party Z-axis. The remaining 23kg was contributed by the deposition and consolidation systems, which theoretically left 21kg, within the mass specification, for future Z-axis development. As the machine at that point was not designed with optimised mass characteristics it was testament to the compact nature of the electrophotographic deposition system that a machine (neglecting Z-axis mass) of under the specified maximum mass was produced.

### *Cost*

The design specification provided no absolute cost constraints at this stage, rather suggested that all the components used within the system should be implementable at low-cost. The design of the prototype was based on low-cost technology found in a number of commercial desktop laser printers for under £100. Many of the key components used in the prototype, from the donor Samsung ML4500 printer such as the OPC or developer rollers, are widely available from third party manufacturers as service components. For instance, the halogen heat source used in the consolidation roller was a widely available mass-produced component available at a retail cost of around £8. A number of the components within the prototype were 'off the shelf', implemented for their adaptability but with the knowledge that low-cost (high volume) custom designed parts could be integrated within any mass-produced product. For example, the consolidation carriage's linear guide ball bearings were a costly component set when compared to the cost of other components within the system. The cost however was associated with an over-engineered modular bearing system, and was not indicative of future purpose designed bearing system costs. Polymer bearings and extruded guides would have proven to be a more cost efficient but less flexible solution, and at prototype stage would have required an unnecessary additional system design. Accurate control hardware is often an expense in automated machinery. Stepper motors and associated controllers were a relatively expensive motion device when compared to brushed DC motors. However, the ability to be

accurately positioned and their high, low speed, torque proved invaluable as complete actuator/position control systems. While the cost to produce the prototype is not known precisely, all the components were of low-cost or were otherwise implementable at lower cost in future systems. The literature review discussed several low-cost filament extrusion type ALM systems ranging from £800-£2000 and highlighted FDM as the cost benchmark. Functionally the FDM and electrophotographic deposition systems are very different; however, the machines in which they are embodied are very similar. Both require a Z-axis, actuator drive hardware, a PC interface and a desktop housing. While the FDM machines require an X/Y stage for the mounting of extrusion hardware, the electrophotographic system requires a Y actuating consolidation roller and a revolving belt. Both require thermal control apparatus and various other control sensors. The Z-axis actuator within an electrophotographic system would need to be of higher resolution than in an FDM type system. With the similarities and differences of the two systems taken into consideration, a reasonable estimate of the cost of a desktop electrophotographic system, derived from the prototype generated within this work, would be £2000 - £3000.

### ***6.2 Sub-System Novelty***

This section will highlight the novel aspects of this work and how they differ from what is currently in the field.

#### *Consolidation Sub-System*

Despite the identification of a number of patents, only two functioning electrostatic based ALM systems (Kumar, 1999; Jones et al, 2010) are known to have been produced. The consolidation system was a proprietary system developed over the course of this research with the primary intention to demonstrate solutions to former electrophotographic barriers to ALM implementation.

### *Direct Contact Consolidation and Mechanical Transfer*

The consolidation apparatuses developed within this work utilised an inexpensive quartz-halogen heating means to heat an aluminium consolidation roller within a transfer belt. The use of ‘through belt conduction heating’ using a roller to affect consolidation is unique to this work. The advantages of using a roller have been demonstrated through testing, allowing a layer to be consolidated and solidified before removal from the transfer belt. This work produced a means of layer transfer which used mechanical adhesion between layers to transfer each sequential layer onto the build platform. This differs significantly from the former research machines which used electrostatic transfer, as it eliminated the fringing and build height limitations associated with electrostatic transfer.

### *Peel rollers*

The use of peel rollers was an innovation designed to allow the solidification of newly consolidated layers prior to removal from the belt. The layers, once heated, formed a thin flake on the surface of the belt which, with the use of a high shear force created by the peel roller, was removed from the belt. Rollers designed to peel the belt from the part-surface imparted significantly less force on the system than the vertical pull release systems as seen in a number of patents (Liu and Jang, 2002, 2004; Grenda, 2001; Kumar, 2000; Bynum, 1992)

### *Transfer Belt*

Although 5 out of the 6 electrostatic ALM patents reviewed noted the use of a transfer belt in at least one of their embodiments, there was no evidence of any physical machine or prototype being developed. As such, this work is the first example of an electrophotographic ALM system successfully employing such a device. In addition, work undertaken to characterise the electrostatic image acceptance and drive solutions are all novel steps taken with respect to the development of a working prototype. The transfer belt’s seam was a limiting factor in the overall efficiency of the prototype as the deposition system was not able to print on all parts of the belt. It is also apparent that the belt was ultimately the failure mode for the prototype due to

seam failure. Further work must be undertaken to determine the correct belt parameters.

### *Belt Cleaning*

Belt cleaning was performed using an innovative polyurethane wiper design which used tribocharging to repel, attract and retain debris from the belt. The tested system worked well for loose powders; consolidated material, however, was not able to be fully lifted using this cleaning method and so an additional series of cleaning apparatuses were used.

### *Productivity*

Based on the results of the prototype testing, the maximum productivity for the prototype system was around  $450\text{mm}^3/\text{min}$  equivalent to  $2.7 \times 10^{-5} \text{ m}^3/\text{hour}$ , based on a maximum layer area of  $150 \times 300\text{mm}$  and a layer thickness of  $0.005\text{mm}$ . This Figure is over forty times less productive than the  $1.2 \times 10^{-3} \text{ m}^3/\text{hour}$  benchmark offered by the current productivity leading commercial system. While a number of patents had identified a transfer belt as a component in the electrophotographic ALM patents they were either continuously revolving or 'stop-start' in function. As continuous printing was the most productive and a reciprocating Z-axis had a number of limitations, the concept of belt accumulation was derived. The novel concepts saw the continuous layer printing on one portion of a moving belt and the consolidation of a layer onto the build platform on a stationary part of the same belt. An accumulator fed and gathered belt material as and when necessary. The systems were modelled and their productivity against layer volume compared. It was apparent that the system would be most cost effectively implemented with a slower low-cost system over that of a high-cost stop-start. However, if the printing speed exceeds the consolidation speed, the efficiency of the system is reduced. The system needs prototyping to draw conclusions, and it is likely that the consolidation speed will be the limiting factor. Based on the empirically derived consolidation velocity of  $25\text{mm}/\text{second}$  and the intended build volume of  $200 \times 300 \text{ mm}$ , a single layer would take 12 seconds to consolidate; 8 seconds longer than originally anticipated. Future work will look to optimise this consolidation variable. Assuming an optimised system, where the

consolidate time is within specification (75mm/second), the layer thickness is comparable with the resolution benchmark (0.028 mm), the build volume is true to specification (200 x 300 mm), and the deposition technology from a low-cost 12ppm laser printer is used, the resultant productivity of an accumulator system can be estimated to be  $1.2 \times 10^{-3} \text{ m}^3 / \text{hour}$  - equal to the productivity benchmark. This calculated productivity is reliant on two main developments, an increased layer thickness and an increased consolidation rate. With further work it is believed that neither of these two requirements is unobtainable. It is worth noting that while the estimated productivity does not exceed that of the current market leaders, it does possess a 3.6 times higher resolution at an estimated one eighth the price of the productivity benchmark system. Table 6.2 compares the productivity achieved by the prototype, the maximum productivity of one of the least productive commercial systems (FDM), the maximum productivity of the bench mark 3DP system and the theoretical productivity of a developed electrophotographic system.

Process	Manufacturer	Productivity ( $\text{m}^3/\text{hour}$ )	Relative Productivity
Electrophotographic Prototype	N/A	$2.7 \times 10^{-5}$	0.02
Fused Deposition Modelling	Stratasys	$1.89 \times 10^{-4}$	0.16
Three Dimensional Printing (Benchmark)	Z-Corporation	$1.2 \times 10^{-3}$	1
Electrophotographic Potential	N/A	$1.2 \times 10^{-3}$	1

\* FDM productivity assumed to be equivalent to volume extruded per hour, calculation data taken from (Han et al. 2003)

**Table 6.2 The productivity of two commercial systems to that of the prototype and theoretical electrophotographic ALM system.**

### *Fully Adjustable Printing Engine*

While the design of the deposition system was not formally acknowledged within the design section of this thesis, it was included in Appendix A. The deposition system concept saw the design of an electrophotographic printing engine that was fully adjustable with the intention that it could be set up to test a number of powder materials of differing physical properties. While the prototype system did not function as intended due to insufficient manufacturing tolerances, the concept still retains novel value and should be investigated further in future work.

*Materials*

Widely available household powders were printed with varying success. No evidence of the printing of a number of these powders had been seen in former research. There is specific interest in the continued development of low-cost powders being printed in this way. Powdered sugar has been identified within this work as a candidate for further research into a possible low-cost soluble support material.



## 7.0 Conclusion

---

The following conclusions can be drawn from this work:

### *Low-cost Desktop Technology*

- Electrophotography as embodied within desktop laser printers is a suitable technology to be developed into a low-cost desktop ALM system.
- It is possible to print a number of common household powdered materials (powdered sugar, white flower and table salt) from a non-magnetic mono-component developer system; however, the layer density is poor and favourable printing is seen with powders containing additional flow control additives (powdered sugar).
- Generally electropositive materials such as carbohydrates do not print well in a negative charge OPC developer system.
- Mica will not print in the high aspect ratio form tested within this work as it has a tendency to cake.
- Nylon 12 in the form of 3D systems Duraform will print from a non-magnetic mono-component development system if it is sieved to a particle size less than 30 $\mu$ m. However a large particle size distribution will lead to image streaking.
- The productivity demonstrated within this work is comparably poor when considering some commercial ALM systems, but a system incorporating an accumulator should increase productivity by up to 73% over a stop-start belt system.

### *Former Electrostatic ALM Limitations*

- The build high limitation is purely electrostatic in cause.
- Mechanical adhesion was successfully demonstrated as a solution to the build height limitation.
- Fringe development is an electrostatic effect which occurs during image transfer onto a charged build surface and can also occur on the OPC during image development.

- The presence of a developer electrode has a significant effect on the forming of fringing on an OPC during development.
- Using a printer employing conductive magnetic brush or contact development significantly reduces or eliminates the fringing effect.
- A solution to the fringing effect was demonstrated through the use of a deposition system which produced powder images without fringing and the subsequent mechanical adhesive consolidation of layer flakes onto the build surface.
- Using a mechanical adhesive layer transfer mechanism, small unsupported gaps can be bridged.

### *Transfer Belt*

- The transfer belt is an intrinsic part of the system developed within this work; influencing accuracy, deposition, consolidation and ultimately prototype functional life expectancy.
- Glass reinforced PTFE belt materials are highly electronegative and build up internal negative charge within the reinforcing if not adequately discharged, adversely affecting electronegative powder deposition.
- Glass reinforced PTFE belt materials with a reduced dielectric thickness accept a printed image of greater density.
- The thinner ( $\leq 0.115\text{mm}$ ) glass reinforced PTFE belt materials produce poor surface finishes on built artefacts.
- AC corona discharge is the optimal belt surface discharge device to use within an electrophotographic ALM system.
- The belt seam is a limiting factor in terms of machine reliability and productivity within the developed machine.

## 8.0 Further Work

---

Following the work undertaken within this research a system generation model was formed which described the further milestone development of a new ALM system, from initial concept to commercial proposition. The model split the development of the technology down into four prototypes, the current prototype, two more additional research prototypes and one commercial, all with individual milestones.

- **Prototype Phase Two:** The second phase is intended to build upon the first system prototype formally generated, with the objectives of:
  - i. The development of productivity, exploiting the full potential of electrophotography using an accumulator system.
  - ii. The development of a robust, repeatable and reliable system with specific attention paid to laminate alignment and dimensional accuracy, through the further development of belt materials.
  - iii. The demonstration of the system's ability to print simple 3D artefacts rapidly and accurately.
  - iv. The development of a proprietary print engine capable of printing a number of test materials
- **Prototype Phase Three:** The final research prototyping phase would generate a further prototype made with the objectives of:
  - i. The integration of multiple print engines to accommodate a plurality of materials.
  - ii. The study and experimentation of a number of materials, developing deposition and consolidation characteristics.
  - iii. A study of support structures and their implementation.
  - iv. The demonstration of the system's ability to create complex multi-material artefacts using system generated support structures, demonstrating functional mechanical properties.

- **Commercial Prototype:** The final phase of the development model is intended to bring together the findings of the first three phases, generating a commercial prototype with the objectives of:
  - i. The combination of previous developments to generate a reliable product that is designed for service and manufacturing.
  - ii. The generation of an aesthetic embodiment.
  - iii. The development of a proprietary software interface.
  - iv. The demonstration of the system's ability to be integrated within a desktop environment and provided a user-friendly interface
  - v. The creation of accurate and cost-effective artefacts with usable mechanical properties, at high speed.

3dscanningservices.net. (2011) Website accessed 02/05/2011

Additive3d.com. (2011) Website accessed 16/08/2011.

Ahn, S; Montero, M; Odell, D; Roundy, S; Wright, P. K. (2002) "*Anisotropic Material Properties of Fused Deposition Modelling ABS*", Rapid Prototyping Journal, Volume 8, Issue 4, Page 248 – 257.

Allan, R, A. (2001) "*A History of the Personal Computer: The People and the Technology*" Allan Publishing, London, UK, ISBN 0968910807.

Amtekcompany.com. (2011) Website accessed 16/08/2011.

Arptech. (2011) "*Duraform (Nylon) PA Data sheet*" [www.Arptech.com.au/specs/sls-duraform.pdf](http://www.Arptech.com.au/specs/sls-duraform.pdf), document downloaded 03/02/2011.

ASTM. (2011) "*New Specification for Data Exchange Format for Additive Manufacturing*" ASTM International, Standard WK27506.

Banerjee, S and Wimpenny, D.I. (2006) "*Laser Printing of Polymeric Materials*" Seventh Proceedings from the Solid Freeform Fabrication Symposium Austin, Texas, Page 366-374.

Banerjee, S and Wimpenny, D.I. (2008) "*Laser Printing of Soluble Toner for Rapid Manufacturing*" Proceedings from the 2nd International Conference on Additive Technologies, Slovenia.

BitsfromBytes.com. (2011) Website accessed 16/08/2011

Blanther, J. E. (1892) "*Manufacture of Contour Relief Maps*" US Patent 4739901.

Bondi, S, N; Lackey, W, J; Johnson, Wang, R, W, X, Wang, Z, L. (2006) "*Laser Assisted Chemical Vapour Deposition Synthesis of Carbon Nanotubes and Their Characterization*" Carbon, Volume 44, Issue 8, Pages 1393-1403.

BotMill.com. (2011) Website accessed 16/08/2011

Bynum, D, K. (1992) *"Automated Manufacturing System Using Thin Sections"* US Patent 5088047.

Byung, C; Young, H; Jietae, L. (2008) *"Temperature Control of Multizone Heated Rollers"* Conference On Control, Automation And Systems, ICCAS 2008, International, Pages 2876 - 2879

Cahill, V. J. (2011) *"A Short History and Current Development of UV-Curing for Ink Jet Printing"* <https://www.vcesolutions.com/www/library/uvcuring.pdf>, document downloaded 13/05/2011.

Calwell, C. (2008) *"B Class Halogens and Beyond"* European Council For an Energy Efficient Economy. [ecee.org/press/B\\_Class\\_lamps/index/BClassHalogens\\_and\\_beyond-eceereportDecember12.pdf](http://ecee.org/press/B_Class_lamps/index/BClassHalogens_and_beyond-eceereportDecember12.pdf), document downloaded 01/05/2011.

Carlson, C. F. (1942), *"Electrophotography"* US Patent 2297691.

Chen, C and Chiu, G, T. (2001) *"Banding reduction in electrophotographic process"*, Proceedings, 2001 IEEE/ASME International Conference on Advanced Intelligent Mechatronics, volume 1, Page 81-86.

Chen, I and Tse, M. (2005) *"On Roller Charging of Photoreceptors for Electrophotography"* IS&T's NIP21 International Conference on Digital Printing Technologies, Baltimore, Maryland, USA.

Chockalingam, K; Jawahar, N; Chandrasekhar, U. (2006) *"Influence of layer thickness on mechanical properties in stereolithography"* Rapid Prototyping Journal, Volume 12, Issue 2, Pages 106 – 113.

Choi, S.H; and Kwok, K.T. (2002) *"Hierarchical slice contours for layered-manufacturing"* Computers in Industry, Volume 48, Issue 3, Pages 219-239.

Chua, C. K; Leong, K. F; Lim, C. S. (2010) *"Rapid Prototyping: Principles and Applications"* Third Addition, World Scientific Publishing Co, Singapore.

- CODATA (2011), "*The Permeability of Free Space (Magnetic Constant)*", <http://physics.nist.gov/cuu/Constants/Table/allascii.txt>, document downloaded 01/02/2011.
- Cohen, A. L; Zhang, G; Tseng, F. G; Frodis, U; Mansfeld, F; Will, P. M. (1999) "*EFAB: Rapid, Low-Cost Desktop Micromachining of High Aspect Ratio True 3-D MEMS,*" in Technical Digest, 12<sup>th</sup> IEEE Int. Conference on Microelectromechanical Systems, Page 244–251.
- Cohen A. L. (2001) "*Electrochemical Fabrication (EFAB)*", The MEMS Handbook, MEMGen Corporation, edition 1, section 19.
- Cormier, D; Taylor, J; Unnanon, K; Kulkarni, P; West, H. (2000) "*Experiments In Layered Electro-Photographic Printing*" 2000 Solid Freeform Fabrication Proceedings, August 7-9, Austin, Texas, Page 267 – 274.
- Cormier, D; Taylor, J; West, H. (2002) "*An Investigation of Selective Coloring with 3-D Laser Printing*" Journal of Manufacturing Processes, Volume 4, Issue 2, 2002, Page 148-152.
- Creagh, L.T; and Frost, P.J. (2011) "*Piezoelectric InkJet and Organic Electronic Materials*" Spectra, Inc [tinhoahoc.com/Semiconductor/Inkjet-OLED.pdf](http://tinhoahoc.com/Semiconductor/Inkjet-OLED.pdf), document downloaded 12/03/2011.
- Crump, S.S. (1992<sub>a</sub>) "*Rapid Prototyping Using FDMTM: A Fast, Precise, Safe Technology*", Proceedings of Solid Freeform Fabrication Symposium, University of Texas at Austin, Page 189-195.
- Crump. S.S. (1992<sub>b</sub>) "*Apparatus and Method for Creating Three-Dimensional Objects*", US Patent 5121329.
- Dalgarno, K. (2001) "*Production Grade Tooling via Layer Manufacture*", Rapid Prototyping Journal, Volume 7, Issue 4, Page 203-206.

Daneshmand, S; Ahmadi Nadooshan, A; Aghanajafi, C. (2007) *"Investigation of Layer Thickness and Surface Roughness on Aerodynamic Coefficients of Wind Tunnel RP Models"* Institution of Engineering and Technology, Engineering and Technology, Volume 32, Issue 2, Page 7, <http://www.waset.org/journals/waset/v32/v32-2.pdf>, document downloaded 21/05/2011.

Deckard, C. L. (1989) *"Method and Apparatus for Producing Parts by Selective Sintering"* US Patent 4863538.

Dell. (2011) *"LED Verses Laser Printing"*  
[http://www.dell.com/downloads/global/solutions/LED\\_Laser\\_printing\\_US.pdf](http://www.dell.com/downloads/global/solutions/LED_Laser_printing_US.pdf), document downloaded 01/02/2011.

Dimensionprinting.com. (2011) Website accessed 16/08/2011

Dimitrov, D; Schreve, K; de Beer, N. (2006) *"Advances in three dimensional printing - state of the art and future perspectives"*, Rapid Prototyping Journal, Volume 12, Issue 3, Pages 136 – 147.

Drake, J, A, G. (2003) *"Chemical Technology in Printing and Imaging Systems"* Royal Society of Chemistry, First Edition, USA, ISBN 0851866557.

Dynacept.com. (2011) Website accessed 16/08/2011

Elmqvist, R. (1951) *"Measuring instrument of the recording type"* US Patent 2566443.

Elter, M, R. (1985) *"Controller for a fusing device of an electrophotographic printing machine"* US Patent 4551007.

Feygin, M. (1988) *"Apparatus and Method for Forming an Integral Object from Laminations"* US Patent 4752352.

Ferreira, J, C; Santos, E; Madureira, H; Castro. J. (2006) *"Integration of VP/RP/RT/RE/RM for rapid product and process development"* Rapid Prototyping Journal, Volume 12, Issue 1, Page 18 - 25.



- Folkins, J, J. (1988) *"Intermediate conductivities-the crossover function for insulative and conductive two-component magnetic brush development in electrophotography"* IEEE Transactions on Industry Applications, Volume 24, Issue 2, Page 250-255.
- Furfari, F, A. (2001) *"A different kind of chemistry: a history of tungsten halogen lamps"* IEEE Industry Applications, volume 7, Issue 6, Page 10-17.
- Fusayasu, H; Inoue, H; Komatsu, Y; Sekine, Y. (2001) *"Analysis for Electrophotographic Process on Digital Copier"* IEEE Transactions on Magnetics, Volume 37, Issue 5, Page 3440-3443.
- Gebhardt, A. (2003) *"Rapid Prototyping"* Aachen University of Applied Science, Hanser Gardener publications Inc, ISBN 3-446-21259.
- Giuliani, V; Freiheit, T; Gu, P. (2005) *"Design and Realization of Multi-material and Multi-Process Deposition Method"* The Second CDEN Design Conference, Alberta, Canada.
- Grenda, E. (2001) *"Apparatus of Fabricating 3 Dimensional Objects by Means of Electrophotography, Ionography or a Similar Process"* US Patent 6206672.
- Grenda, E. (1994) *"Apparatus of Fabricating 3-Dimensional Objects by Means of Electrophotography, Ionography or similar process"* US Patent Number 6206672.
- Grenda, E. (2009) *"Printing the Future -The 3D Printing and Rapid Prototyping Source Book"* 3rd edition, Castle Island Co, Massachusetts, USA.
- Grimm, T, A. (2010) *"3D Printer Benchmark: European Edition"* T. A. Grimm & Associates, Inc, Kentucky, USA.
- Gusarov A. V; Laoui. T; Froyen. L; Titov, V, I. (2003) *"Contact thermal conductivity of a powder bed in selective laser sintering"* International Journal of Heat and Mass Transfer Volume 46, Issue 6, Pages 1103-1109.
- Hague, R, J, M; Reeves, P, E. (2000) *"Rapid prototyping, tooling and manufacturing"* Rapra Technology Ltd, UK.

- Halim, F; Barringer, S, A; (2007) "*Electrostatic adhesion in food*" Journal of Electrostatics, Volume 65, Issue 3, Pages 168-173.
- Hayne, T, F. (1976) "*Screen Controlled Corona Device (Scorotron) for Charging in a Xerographic Copier*" Industry Applications, IEEE Transactions, volume IA-12, Issue 1, Pages 63-67.
- Helisys. (1995) "*Laminated object manufacturing apparatus and method*" US Patent Number 5,876,550.
- Hon, K, K, B. (2007) "*Digital Additive Manufacturing: From Rapid Prototyping to Rapid Manufacturing*" Proceedings of the 35<sup>th</sup> International MATADOR Conference, University of Manchester, UK, Pages 337 – 340.
- Houbena, R, J; Brouwersa, L, A, M; Rijfersa, A; Willemse, M, A. (2009) "*Inkjet printing for Rapid Manufacturing: Printing towards the future*" TNO Science and Industry, conference.iproms.org/conference/download/4153/51, Document downloaded 29/08/2010.
- Hudson. (1963) "*Xerographic Fixing Device*" US Patent Number 3256003.
- Hughes, J, F. (1997) "*Electrostatic Particle Charging*" Research Students Press LTD, Somerset, UK.
- Hull, C, W. (1986) "*Apparatus for Production of Three-Dimensional Objects by Stereolithography*" US Patent 4575330.
- Idealab.com. (2009) Website accessed 02/02/2009
- Ikuta K; Maruo, S; Kojima, S. (1998) "*New Micro Stereo Lithography for Freely Movable 3D Micro Structure*" Proceedings of the IEEE, Micro Electro Mechanical Systems, Heidelberg, pp. 290–295.
- Ikuta, K; Ogata, T; Tsubio, M; Kojima, S. (1996<sub>a</sub>) "*Development of mass productive micro stereo lithography (Mass-IH process)*" Micro Electro Mechanical Systems, MEMS '96, Proceedings, California, USA, Pages 301 -306

Ikuta, K; Ogata, T; Tsubio, M; Kojima, S. (1996<sub>b</sub>) *"An Investigation of Micro Structures, Sensors, Actuators, Machines and Systems - Development of mass productive micro stereo lithography (Mass-IH process)"* IEEE, The Ninth Annual International Workshop, Pages 301-306.

Im, Y, G; Chung, S, I; Sonj J, H; Y, D, Jung; Jo, J, G; Jeong, H, D. (2002) *"Functional prototype development: inner visible multi-color prototype fabrication process using stereo lithography"* Journal of Materials Processing Technology, Volumes 130-131, 20 December 2002, Pages 372-377.

ITW, Devcon. (2006) *"Z-Corporation's 'Z-Max' Infiltrant Safety Data Sheet"*, [http://www1.carleton.ca/mae/ccms/wp-content/ccms-files/Z\\_Max\\_Infiltrant\\_Resin.pdf](http://www1.carleton.ca/mae/ccms/wp-content/ccms-files/Z_Max_Infiltrant_Resin.pdf), Document downloaded 01/06/2011.

Iuga, A; Calin, L; Neamtu, V; Mihalcioiu, A; Dascalescu, L. (2005) *"Tribocharging of Plastics granulates in a fluidized bed device"* Journal of Electrostatics, Volume 63, Page 937 - 942.

Isi.edu. (2011) website accessed 28/03/2011.

Jackson, T, R; Liu, H; Patrikalakis, N, M; Sachs, E, M; Cima, M, J. (1999) *"Modelling and designing functionally graded material components for fabrication with local composition control"*, Materials and Design, Volume 20, Pages 63-75.

Jacobs. (1992) *"PF Rapid prototyping & manufacturing – Fundamentals of Stereolithography"*, first edition, Society of Mechanical Engineers, USA.

Ji, B, C; Han, Y, A; Lee, J. (2008) *"Temperature Control of Multizone Heated Rollers"* International conference on Control, Automation and Systems, Seoul, South Korea, Page 2876 - 2879.

Jones, J; Wimpenny, D; Gibbons, G; Sutcliffe, C. (2010) *"Additive Manufacturing by Electrophotography: Challenges and Successes"* International Conference on Digital Printing Technologies and Digital Fabrication, Austin, Texas, Page 549-553.

- Kaiser, L, K. (2006) *"Electrostatic Discharge"*, Taylor & Francis Group, USA, ISBN 084937188.
- Kamada, A; Kato, I. (2000) *"Electrophotographic Apparatus"* US Patent 6157789.
- Kao, C, C. (1973) "Electric field, transfer, and spread functions in xerographic image studies", *Journal of Applied Physics*, Volume 44, Page 1543.
- Karlsen, R. (2007) *"Method and Device for Manufacturing a Powder Layer for in Layer Production of Objects"* World Patent WO/2007/073206.
- Katun.com. (2011) Website accessed 16/08/2011
- Kim, H. (2005) *"laser Scanning Unit"* US Patent 6958838.
- Kinzie, N. (1991) *"Method and Apparatus for Constructing a Three-Dimensional Surface of Predetermined Shape and Color"* US Patent 5015312.
- Kruth, J, P; Leu, M,C; Nakagawa, T. (1998) *"Progress in Additive Manufacturing and Rapid Prototyping"* CIRP Annals, Manufacturing Technology, Volume 47, Issue 2, Pages 525-540.
- Kruth, J, P; Mercelis, P; Vaerenbergh, J, V; Froyen, L; Rombouts, M. (2005) *"Binding mechanisms in selective laser sintering and selective laser melting"* Rapid Prototyping Journal, Volume 11, Issue 1, Page 26 – 36
- Kumar, A,V. (1999) *"Electrophotographic Solid Freeform Fabrication"* Office of Naval Research, Annual Report for grant Number: N00014-98-1-0694.
- Kumar, A, V and Zhang, H. (1999) *"Electrophotographic Powder Deposition for Freeform Fabrication"*, Proceedings of the 10<sup>th</sup> Solid Freeform Fabrication Symposium, Austin, Texas.
- Kumar, A, V. (2000) *"Solid Freeform Fabrication using Power Deposition"* US Patent 6066285.

Kumar, A, V and Dutta, A. (2003) *“Investigation of an Electrophotography Based Rapid Prototyping Technology”* Rapid Prototyping Journal, Volume 9, Issue 2, Page 95 – 103.

Kumar, A, V and Dutta, A. (2004) *“Electrophotographic Layered Manufacturing”* journal of Manufacturing Science and Engineering, Volume 126, Page 571 - 576.

Kumar, A, V; Dutta, A; Fay, J, E. (2004) *“Electrophotographic Printing of Part and Binder Powders”* Rapid Prototyping Journal, Volume 10, Issue 1, Page 7 – 13.

Larsson, R. (2003) *“Method and Device for Manufacturing Three Dimensional Bodies”* US Patent 6531086.

Lasersintering.com. (2011) Website accessed 21/02/2011

Lee, B. (2009) *“Triboelectric table”* AlphaLab, Inc; [www.TriField.com/content/triboelectric-series](http://www.TriField.com/content/triboelectric-series), downloaded 04/2011.

Leu, M, C; Zhang, W; Sui, G. (2000) *“An Experimental and Analytical Study of Ice Part Fabrication with Rapid Freeze Prototyping”* CIRP Annals - Manufacturing Technology, Volume 49, Issue 1, Pages 147-150.

Levy, G; Schindel, R; Kruth, J, P. (2003) *“Rapid Manufacturing and Rapid Tooling with Layer Manufacturing (LM) Technologies, State of The Art and Future Perspectives”* CIRP Annals of Manufacturing Technology, Volume 52, Issue 2, Pages 589-609.

Limaye, A, S and Rosen, D, W. (2007) *“Process Planning Method for Mask Projection Micro-Stereolithography”*, Rapid Prototyping Journal, Volume 13, Issue 3, page 76-84

Liu, H, L and Jang, B, Z. (2002) *“Layer Manufacturing Using Electrostatic Imaging and Lamination”* US Patent 6376148 B1.

Liu, H, L and Jang, B, Z. (2004) *“Layer Manufacturing of a Multi-Material or Multi-Color 3-D Object Using Electrostatic Imaging and Lamination”* US Patent 6780368 B2.

Li, L; Syed, W, U, H; Pinkerton, A, J. (2006) *“Rapid additive manufacturing of functionally graded structures using simultaneous wire and powder laser deposition”* Virtual and Physical Prototyping, Volume 1, Issue 4, Pages 217-225.

- Menzel, C. (2009) *"InkJet History and Continuing Role"* Nanotech2009, Inkjet Symposium, Houston, Texas Pages 1 – 9.
- Merot, C; Graves, A, C; Caltabiano, V. (2006) *"Recoater Blade Reservoir and Adjustment Mechanism for Stereolithography Rapid-Prototyping Systems That Allows Removal and Replacement of the Blade-Reservoir without Adjustment to the Blade Height or Rake Settings"* US Patent publication US2006/0219163 A1.
- Minelco. (2011) *"Mica PW-80/30 Data Sheet"*, Minelco 12/01/2011.
- Moore, A, D. (2007) *"A. D. Moore's Electrostatics – Exploring, Controlling and Using Static Electricity"* 2<sup>nd</sup> edition, Laplacian Press, California, USA.
- Morita, K; Ikeda, Y; Tanaka, Y. (2007) *"Organic Photoconductors for Printers"* Fuji Electrical Technical Journal Paper, Volume 53, Issue 2, Page 58
- Nakamura, Y. (2006) *"Material Technology for Organic Photoconductors"* Fuji Electrical technical journal, Volume 53, Issue 2, page 48.
- Nakamura, Y and Kutsuwanda, N. (1989) *"Direct Measurement of Toner Particle Size"* Industrial Applications Society Annual Meeting, Conference Record of the 1989 Institute of Electrical and Electronics Engineers, Volume 2, Issue 1, Pages 2239 – 2242.
- Narita, M and Obinata, T. (2011) *"Photoconductors: Current Status and Future Outlook"* Fuji Electric Review, Volume 57, issue 1, page 1-28.
- NEMA. (2003) *"Tungsten-halogen lamps (bulbs): Ultraviolet, Rupture and High Temperature Risks"* NEMA lighting division, National Electrical Manufacturers association, volume 2, Issue 4.
- Neugebauer, H, E, J. (1969) *"Fields of Electrostatic Images and Their Effect on Development of Visible Pictures"* Applied Optics, Volume 8, Page 76 - 78.
- Pai, D, M and Springett, B, E. (1993) *"Physics of Electrophotography"* Reviews of Modern Physics, Volume 65, Issue 1.
- Park, C, J. (1997) *"F $\theta$  Lens System in a Laser Scanning Unit"* US patent 5631763.

- Penn, S, M. (1997) "*System, Method & Process for Fabrication of 3-Dimensional Objects by a Static Electrostatic Imaging and Lamination Device*" US Patent 5593531.
- Pham, D, T and Gault, R, S. (1998) "*A comparison of rapid prototyping technologies*" International Journal of Machine Tools and Manufacture, Volume 38, Issues 10-11
- Printin3d.com. (2011) Website accessed 02/02/2011
- Prinz, F, B; et al. (1997<sub>a</sub>) "*Rapid Prototyping in Europe and Japan*" JTEC WTEC Panel Report, Society of Manufacturing Engineers, Volume 1
- Prinz, F, B; et al. (1997<sub>b</sub>) "*Rapid Prototyping in Europe and Japan*" JTEC WTEC Panel Report, Society of Manufacturing Engineers, Volume 2
- Reilly, E, D. (2003) "*Milestones in Computer Science and Information Technology*", Greenwood Press, USA, ISBN 1573565210.
- Rodney, A. (2005) "*Building Printer/Output Profiles, Colour Management for Photographers*" Focal Press, Boston, Pages 185 - 243.
- Sachsa, E and Vezzetti, E. (2005) "*Numerical Simulation of Deposition Process for a New 3DP Printhead Design*" Journal of Materials Processing Technology, Volume 161, Issue 3, Pages 509-515.
- Samsung (2001) "*Samsung ML4500 User Manual*" Downloaded from - [org.downloadcenter.samsung.com/downloadfile/ContentsFile.aspx?CDSite=HQ&CttFileID=33483&CDCttType=UM&ModelType=N&ModelName=ML-4500&VPath=UM/200308/20030830142351296\\_MI4500\\_English.pdf](http://org.downloadcenter.samsung.com/downloadfile/ContentsFile.aspx?CDSite=HQ&CttFileID=33483&CDCttType=UM&ModelType=N&ModelName=ML-4500&VPath=UM/200308/20030830142351296_MI4500_English.pdf), Document downloaded 13/02/2010
- Samsung 2006 "*Toner Material Data Sheet*" Samsung Electronics 19/10/2006
- Scharfe, M. (1984) "*Electrophotography principles and optimization*" Research Study Press Ltd, USA.
- Schein L.B; (1999) "*Recent advances in our understanding of toner charging*", Journal of Electrostatics, Volume 46, Issue 1, Pages 29-36.

- Schindel, L, G, N and Kruth R, J, P; (2003) *"Rapid Manufacturing and Rapid tooling with layer Manufacturing (LM) Technologies, State of the Art and Future Perspectives"* CIRP Annals - Manufacturing Technology, Volume 52, Issue 2, 2003, Pages 589-609
- Seitz, H; Rieder, W; Irsen, S; Leukers, B; Tille, C. (2005), *"Three-dimensional printing of porous ceramic scaffolds for bone tissue engineering"* Journal of Biomedical Materials Research Part B: Applied Biomaterials, Volume 74, Issue B, Pages 782–788.
- Solid-scape.com. (2011) Website accessed 29/04/2011
- Sugihara, et al. (2000) *"Heated Roller"* US Patent Number 6396029.
- Sumawi, H and Barringer, A. (2005) *"Positive vs. Negative Electrostatic Coating Using Food Powders"* Journal of Electrostatics, Volume 63, Page 815-821.
- Swanson, W, K. (1977) *"Method, Medium and Apparatus for Producing Three-Dimensional Figure Product"* US Patent 4041476
- Swanson, W, K; et al. (1978) *"Three Dimensional Systems"* US Patent 4078229
- Swanson, W, K. (1980) *"Method, Medium and Apparatus for Producing Three-Dimensional Figure Product"* US Patent 423840
- Swanson, W, K; et al. (1981) *"Three-Dimensional Systems"* US Patent 4288861
- Tateishi, K and Hoshino, Y. (1984) *"Three-layer photoreceptor (Se-SeTe-Se) with high sensitivity in the long-wavelength region"* IEEE Transactions on Electron Devices, Volume 31, Issue 6, Page 793 - 796.
- Thomson, W. (1867) *"Lord Kelvin's patent for an ink jet "Receiving or Recording Instruments for Electric Telegraphers"* UK Patent Number 109688.
- Thourson, T, L. (1972) *"Xerographic Development processes: A review,"* Electron Devices, IEEE Transactions on , Volume 19, Issue 4, Pages 495- 511.
- Tulagin, V. (1969) *"Imaging Method Based on Photoelectrophoresis"* Journal of the Optical Society of America, Volume 59, Issue 3, Page 328 – 329.



- Urban et al. (1987) *"Fusing roller"* US Patent Number 4810858.
- Voxeljet. (2011) *"3D-Printers Technical Data 2011-03 02.pdf"* voxeljet.de/fileadmin/Voxeljet/Systems/VX\_500/voxeljet\_3d-printers\_technical\_data\_2011-03-02.pdf
- Waters, R, T and Stark, W, B. (1975) *"Characteristics of the stabilized glow discharge in air"* Journal of Physics D: Applied Physics, Volume 8.
- White, D, R. (2003) *"Ultrasonic Consolidation of Aluminium Tooling"* Advanced Materials & Processes, Volume 161, Issue 1, Page 64.
- Wohlers, T. (2008) *"Wohlers Report 2008: State of the Industry"* Wohlers Associates, Colorado, USA.
- Wohlers, T. (2010) *"Wohlers Report 2010: State of the Industry"* Wohlers Associates, Colorado, USA.
- Wimpenny D, I and Banerjee, S. (2008) *"Electrostatic Printing Method and its Use in Rapid Prototyping"* World Patent 2008/096105.
- Wimpenny D, I; Banerjee, S; Jones, J. (2009) *"Laser Printed Elastomeric Parts and Their Properties"* 20th International Solid Freeform Fabrication Symposium, Austin, Texas.
- Yagi, et al. (2001) *"Electrophotographic Photosensitive Body Intermediate Transfer Medium and Electrophotographic Apparatus"* US Patent 6248489.
- Yan, X and Gu, P. (1996) *"A Review of Rapid Prototyping Technologies and Systems"* Computer-Aided Design, Volume 28, Issue 4, Pages 307-318.
- Yang, C, C and Hartmann, G, C. (1976) *"Electrostatic separation of a charged-particle layer between electrodes"* Electron Devices, IEEE Transactions on, volume 23, Issue 3, Pages 308 - 312.
- Yun, Y, H; Kim, J, D; Lee, B, K; Cho, Y, W. (2009) *"Polymer Inkjet Printing: Construction of Three-Dimensional Structures at Micro-Scale by Repeated Lamination"* Macromolecular Research, Volume 17, Issue 3, Page 197-202

## References

---

Zcorp.com. (2011) Website accessed 12/03/2011

Zcorp.com. (2009) Website accessed 04/02/2009

Zimmer, M; et al. (2002) *“Device for Applying Decors and/or Characters on Glass, Glass Ceramics and Ceramic products”* World patent WO00/25182.

## Appendix A: The Design of a Fully Adjustable Deposition System

The functional specification for the development of the deposition unit described the following key design constraints:

- **Resolution** – A 600 x 600 dpi resolution was required.
- **Materials** – The system should be fully adjustable to allow a plurality of materials in differing particle sizes.
- **Layer Thickness** – The deposition system should have been designed to allow the printing of thicker powder layers typically in the 20 – 25 micron thickness range.
- **Transfer Belt Printing** – Layer deposition onto a transfer belt was to be obtained through induction charging.

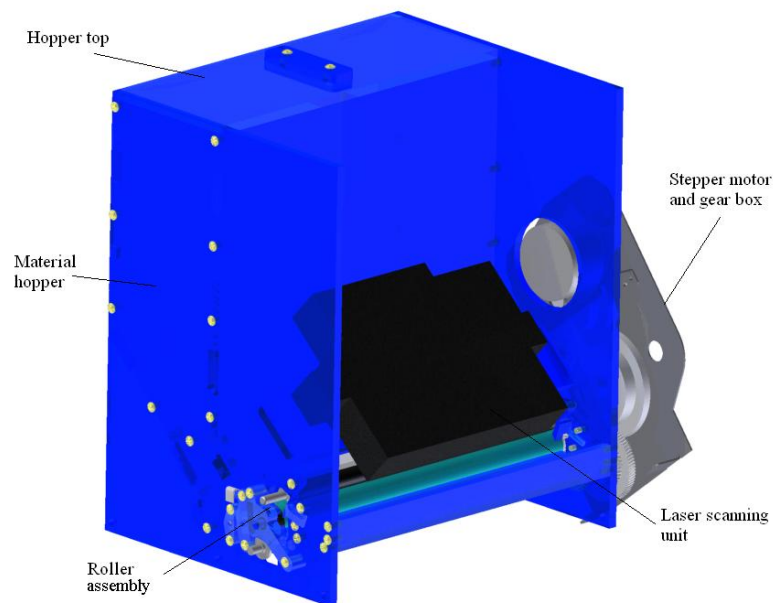


Figure A.1 A CAD render showing the main parts of the deposition unit

The deposition unit, illustrated in Figure A.1, was designed to deposit powdered polymer build materials onto the surface of a revolving transfer belt. The necessity to redesign a 'toner cartridge', an established laser printer part, was realised when attempting to print coarser polymer materials using existing cartridges. The bespoke

deposition unit facilitated the use of a variety of build materials and held a greater powder volume for advance testing. The assembly was based on a reverse engineered Samsung cartridge and a printing engine from the Dell 1120 mono laser printer but incorporated an array of user configurable variables to accommodate the formation of thicker powder layers from courser materials.

### ***A.1 The Rollers***

There were six process rollers used within the adopted design. These are illustrated and labelled in Figure A.2, and shown in their relative positions within the deposition unit in Figure A.3. The rollers worked to sequentially process polymer powder into a uniform layer thickness and distribution in preparation for developing. The sequence and function of rollers in this application can be described as follows:

*The Agitator roller* was made of two polymer fins on a central rotating shaft. The Polyester fins, being of a dissimilar polymer to the build powder, had two main functions:

1. They de-bound the polymer powder within the cartridge to allow free movement of individual particles
2. They provided the kinetic energy to facilitate tribological charging of the powder material.

Predicting the resultant charge of particles after tribological charging is not an exact science. In the Samsung system, using a negative charge OPC, the empirically determined charge for a material was of a negative polarity with respect to ground.

*The pick-up roller* had a tactile textured surface of electrically conductive synthetic rubber over a steel spindle. The function of this roller was to feed an excess of powder material to the developer roller, through both electrostatic attraction and mechanical means, by retaining powder within its tactile surface. The roller was supplied with a DC potential of -600 Volts and, due to the highly negative charge possessed by the powder material ( $\approx kV$ ), the powder was attracted to the roller.

*The developer roller* facilitated the generation and transfer of powder layers of uniform thickness and distribution onto the next roller, the OPC. The surface of the developer roller had a high surface finish and, as with the other rollers, had a potential difference relative to proximal rollers but with an additional multiplexed AC current. The transfer of powdered material from the pick-up roller left an uneven thickness across the surface of the developer roller. A doctor blade created a uniform layer thickness and distribution across the length of the roller before it came into contact with the OPC. The developer roller transferred a charge, relative to ground, of -500Volts (RMS) to the powder, of which enough was transferred to develop the latent image that existed on the surface of the OPC, returning the unused powder to the material hopper.

*The OPC roller* had a charged latent image of 0v and a background image of -1300v relative to ground. When the powder layer present on the developer roller came into close proximity to the OPC, the charged powder particles were attracted to the potential difference of the latent image and repelled by the nil potential difference of the background image. The AC current transposed on the developer roller, allowed it to reacquire stray particles from the background image of the OPC through electrostatic attraction. The developed image was transferred onto the transfer belt where it went on to be consolidated.

*The charge roller* was a conductive rubber roller which was held in contact with the OPC roller. The charge roller was placed before the selective laser discharging apparatus and transferred a charge of -1550v, relative to ground, onto the surface of the OPC.

*The Transfer roller*, in common with the other rollers within the unit, was constructed of an electroconductive rubber. The roller was placed below the OPC drum with the transfer belt run between. In addition to maintaining the transfer belt / OPC interface, the backing roller induced a positive electric field on the surface of the transfer belt, thus attracting the polymer powder.

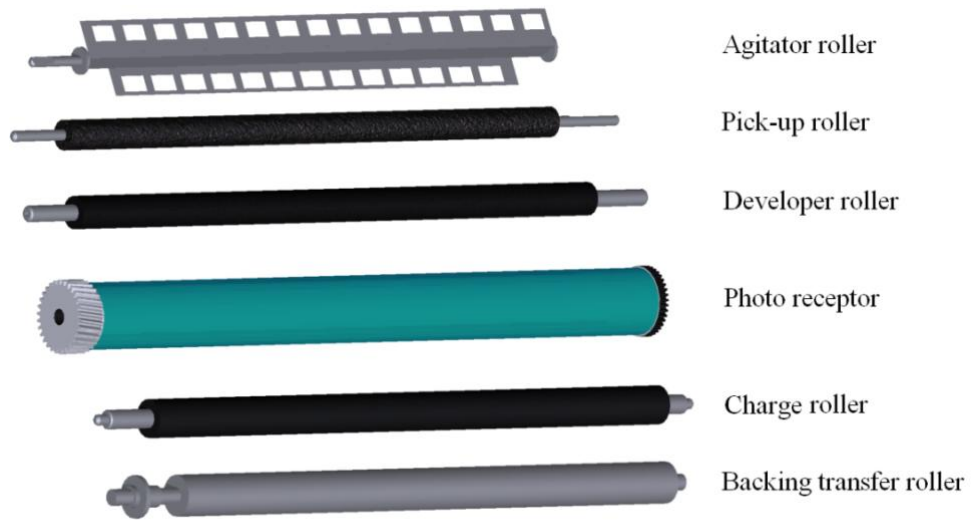


Figure A.2 The six rollers of the deposition system

The rubber rollers were manufactured from a number of rubber materials, for example acrylonitril-butadiene or epichlorohydrin. The electroconductive properties of these rubbers are gained from the addition of conductive additive materials such as carbon black to the rubber mixture prior to vulcanisation. The roller manufacturing process had to be such that there were no parts of greater electrical resistance, nor poor cylindricity, as these may have caused incoherent electric fields, resulting in a poor charge distribution.

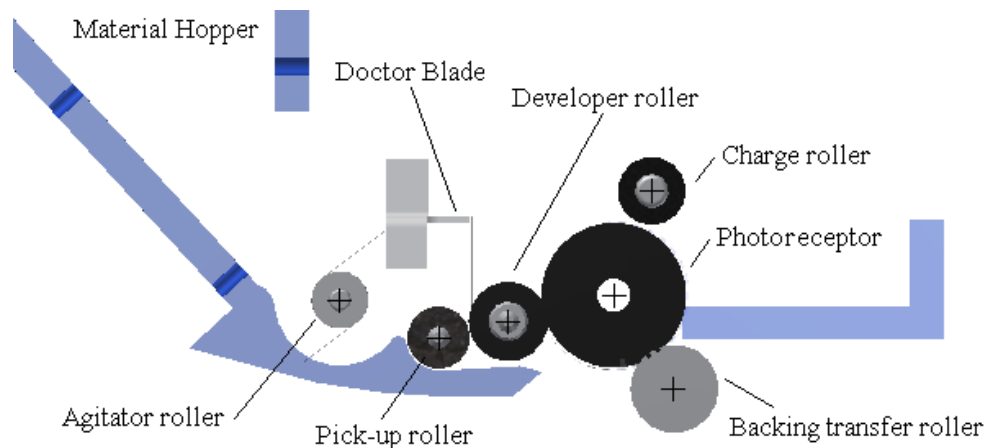


Figure A.3 Deposition roller alignment

## A.2 Construction

A substantial design problem encountered was that of creating enough adjustment within the deposition system to allow the generation of a number of layer thicknesses and the use of a selection of material grades. The solution was to create multiple roller bearing mounts which could be independently adjusted. Figure A.4 shows the multiple mounts, their shape and fixing points. The design allowed the mounts a travel of one millimetre in the X/Z plane from their default position. The exact set-up was to be determined during experimentation. A stepper motor and gearbox was incorporated within the prototype developer unit to provide drive. A CAD illustration of the drive components can be seen in the exploded assembly drawing, Figure A.5. The stepper motor was driven by the prototype's control system, enabling accurate synchronisation with the motion of the transfer belt. The body of the developer unit was constructed from acrylic which was chosen for both its optical clarity, to allow the observation of internal parts during testing, and its tribocharging properties, when in dynamic contact with the polymer build material. The exploded assembly diagram, Figure A.6, illustrates the implementation of novel design concepts which were combined to produce a fully adjustable, multi-material deposition unit.

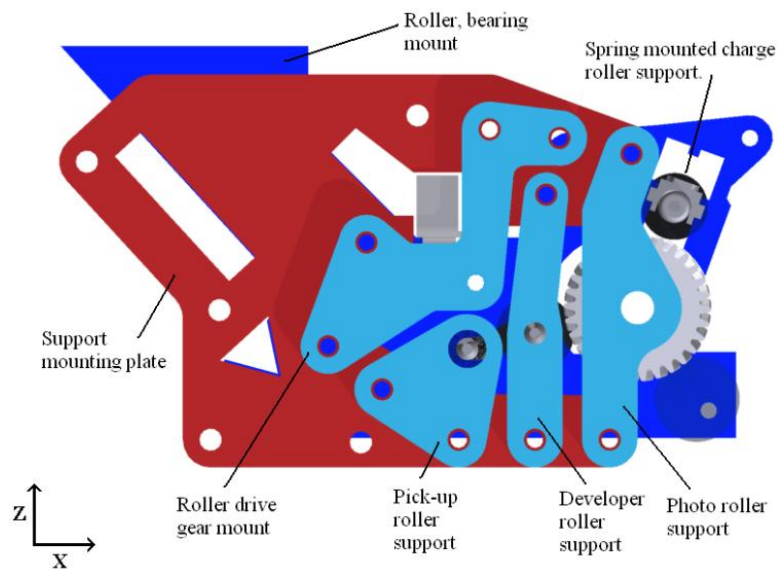


Figure A.4 A CAD illustration of the adjustable roller supports – colours added for clarity

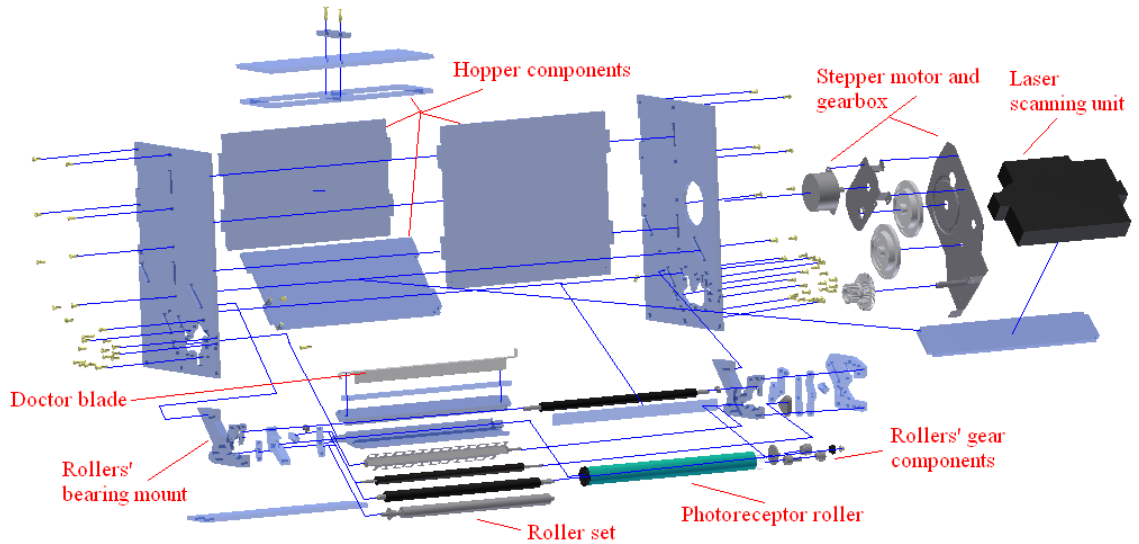


Figure A.5 An exploded diagram of the deposition assembly

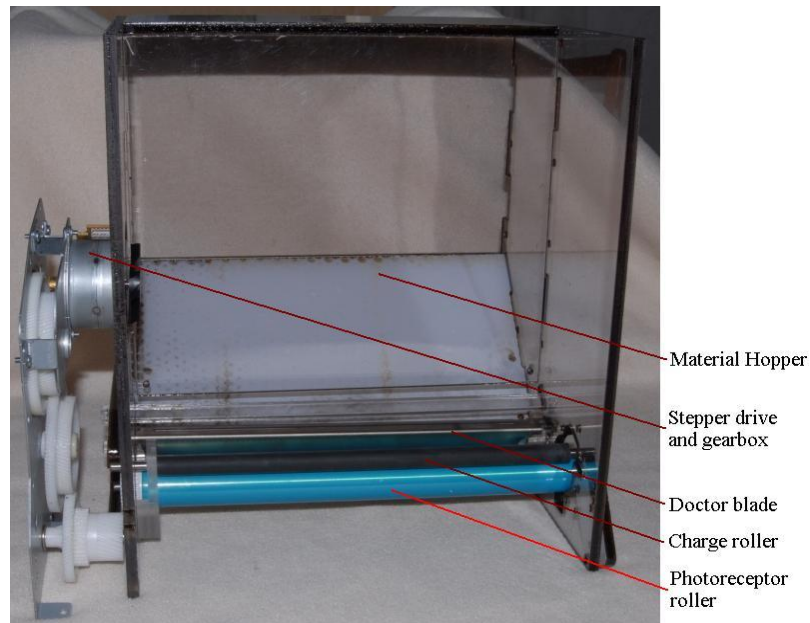


Figure A.6 A picture of the constructed prototype developer unit

### A.3 Testing

The comprehensive adjustment built into the deposition system meant that, while it had great potential for the production of thicker layers and material development, the set up was time consuming. Once assembled and set up, the new system was tested with a standard single component toner material. The cartridge within a standard



ML4500 was removed and the high voltage contacts interfaced with the new deposition assembly. Several print runs, without material, were performed to ensure no error flags were raised within the printer control system. Following the dry run, a number of trial prints with the standard toner material were attempted.

#### ***A.4 Results***

The printing trials with the redesigned printing system failed to deposit any tone powder. There was a range of issues hampering the function of the system, all as a result of improper set up or parts made with poor tolerances. A significant period of time was invested in the iterative set up and of the system which, again failed to print. Following a review of the research objectives, and due to time constraints, the redesign of the deposition system was sidelined and instead the possibility of using a deposition system from a donor printer was investigated. The research objectives, as discussed in the concept chapter, were still acquirable through the implementation of a donor deposition system. However specific lessons for the development of future deposition systems were identified, with consideration paid to:

- Create several deposition prototypes with a limited number of variables. Creating too many adjustable parts caused the setup of the deposition system with this research to be unworkable.
- With the expectation of 20-30 micron layers, the parts must be manufactured with sufficient tolerances to facilitate that level of accuracy. Some of the parts within the deposition system were up to 1mm out of this tolerance, leading to miss alignment issues which resulted in an absence of any development.

### Appendix B: Firmware Test Programming

The flow diagram in figures B.1, B.2, B.3, B.4 and B.5 represent the lower level flow diagrams of the master controller's communications testing program. Figure B.6 is a representative flow diagram of the ancillary controller's response program.

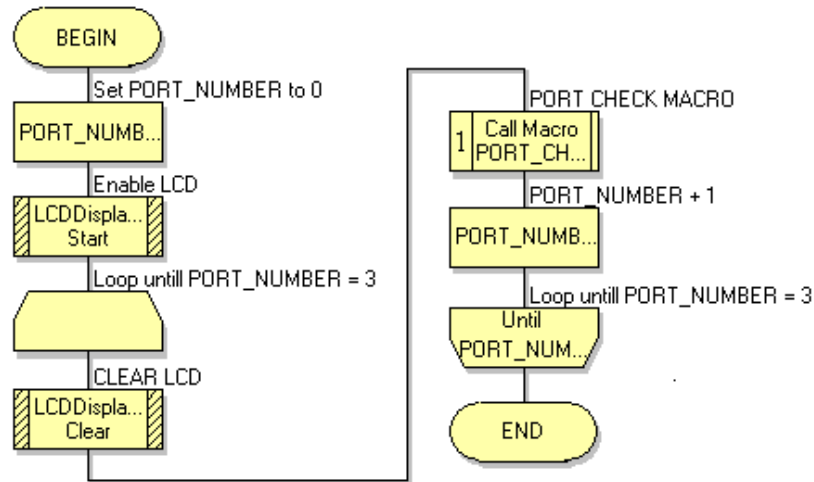


Figure B.1 A high level flow diagram representing Test program 1 - a program for testing microcontroller communications between three peripheral boards. The ports are tested in order with an LCD output of the results.

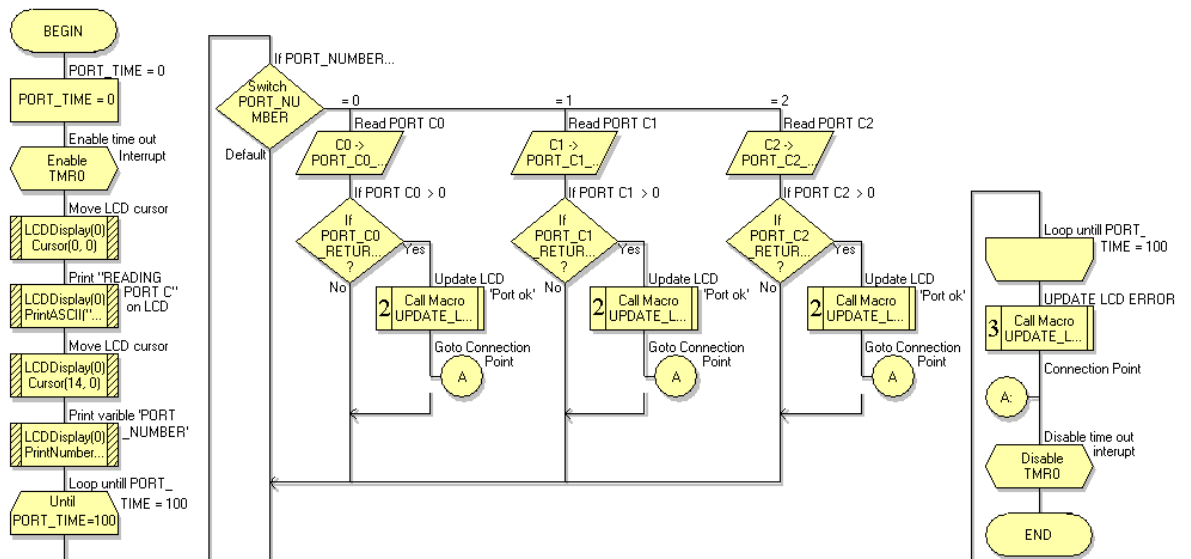


Figure B.2 A flow diagram describing Test Program: macro 1 - 'PORT CHECK' – The master controller ports are pinged and the response read. There was a timeout interrupt which terminates the port read loop in the case that there was no response.

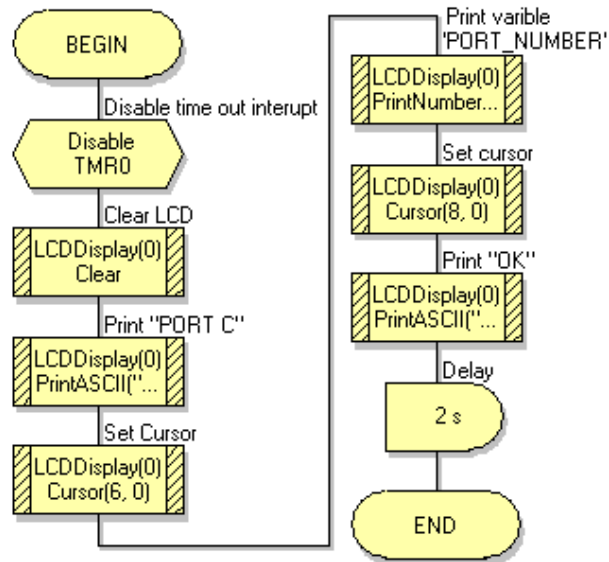


Figure B.3 A flow diagram describing Test Program: macro 2 - 'LCD UPDATE, PORT OK' – A sub routine executed when a satisfactory reply is received from an ancillary controller on a given port.

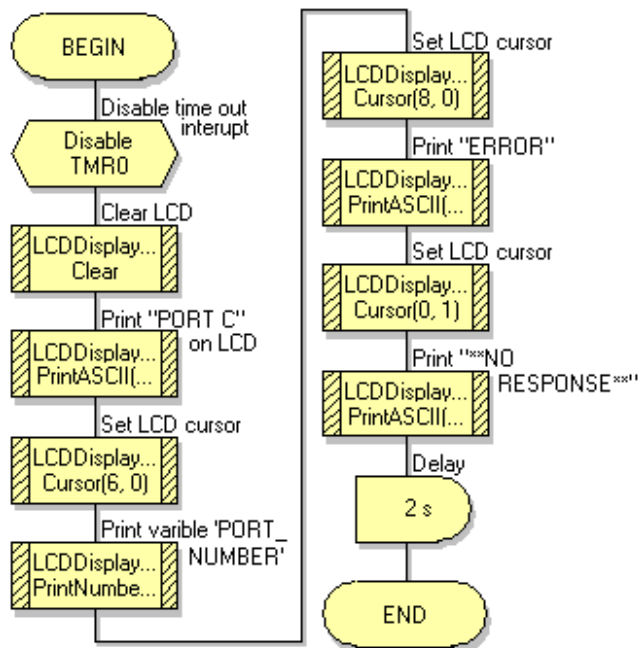


Figure B.4 A flow diagram describing Test Program: macro 3 - 'LCD UPDATE, PORT ERROR' - A sub routine executed when an unsatisfactory reply or no reply has been received from an ancillary controller on a given port.

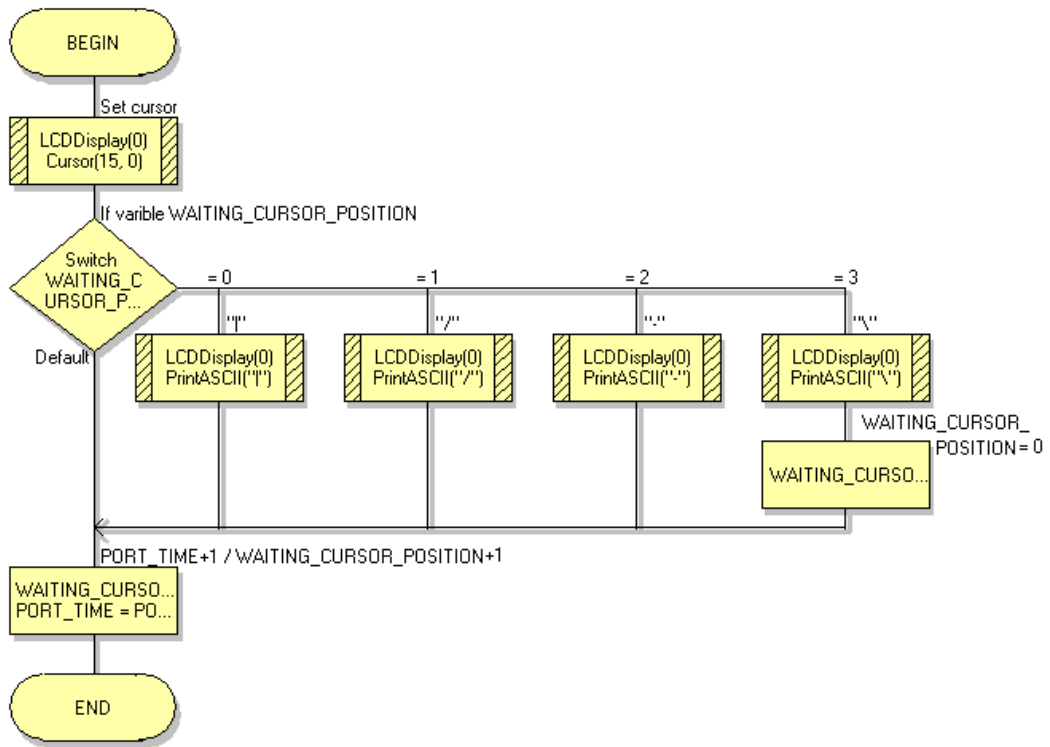


Figure B.5 A flow diagram describing Test Program: macro 4 - 'Interrupt timer and LCD busy Update' – A sub-routine executed on a regular clock pulse to limit the time any given port is tested. The interrupt sub-routine updates the LCD with a rotating “\” to visually ensure the program has not stalled.

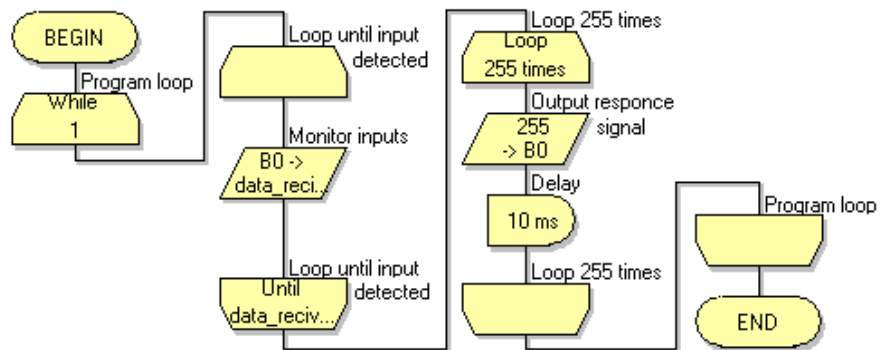


Figure B.6 A flow diagram illustrating the response of an ancillary board's microcontroller when 'pinged' by the master controller. Upon receipt of an input from the master controller the ancillary controller sent a response signal burst lasting 2.5 seconds.

## Appendix C: Control Programs

The following flow diagrams represent the control program for the master controller.

The first program macro 'Enable system' was executed once at start up as a warm up sequence and contained a further five program macros.

### Program macro 1: Enable system

When first powered up, the system undertakes several check and warm up processes which run the system to ascertain if the system is ready to print. The flow diagram in Figure C.1 illustrates the steps which are taken by the master controller during start up.

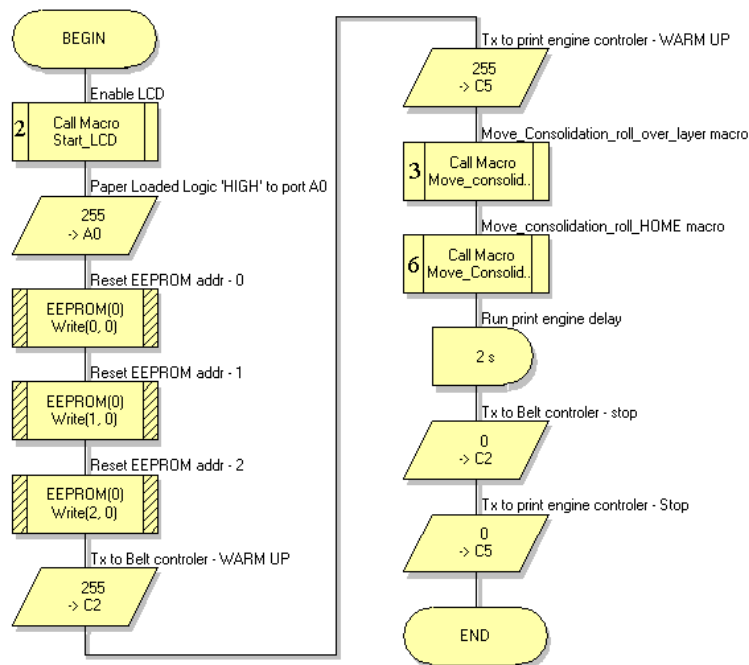


Figure C.1 A flow diagram describing the programming behind the master controller program: Program macro 1 – Enable system.

This macros primary function included;

- Enabling the LCD, to allow the user to track the progress of the warm up cycle.
- Writing to the EEPROM memory, setting all used addresses to a value of 0. This was necessary as the system relied on the EEPROM for layer number calculations and error tracking.

- Cycling the print engine, a process to clean the OPC and distribute build powder within the cartridge and hopper.
- Cycle the transfer belt, undertaken to clean the belt and position it ready for the first layer.
- Cycle the consolidation roller to its extents, returning to home. This checked the free running of the consolidation roller.

**Program macro 2: Enable\_LCD**

The user interface on the POC prototype consisted of a backlit LCD. When the system was powered up, part of the ‘enable system macro’ called for the LCD to be enabled. Figure C.2 illustrates the steps taken to enable the LCD and then post the message “INITIALISING SYSTEM”.

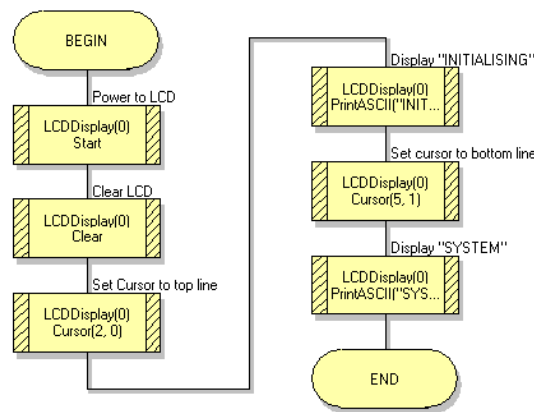


Figure C.2 A flow diagram describing the programming behind the master controller program: Program macro 2 – Enable LCD.

This macros primary function included;

- Power on command to LCD, a command which then allowed other macros to communicate with the LCD module.
- Zero registers, this was necessary to eliminate residual data from the last time the system was active.
- Display the system status, enabling user confirmation of current system status.

**Program macro 3: Move consolidation roll across layer**

Although the consolidation roller’s motor was not directly driven from the master controller, its program did interpret the liner sensors which indicted the consolidation carriage’s position. Figure C.3 shows the flow diagram describing the activation and

termination of the consolidation rollers movement as it consolidated a layer. 'The Move consolidation roll across layer' macro is a general macro which was used through the master controllers program to actuate the consolidation carriage.

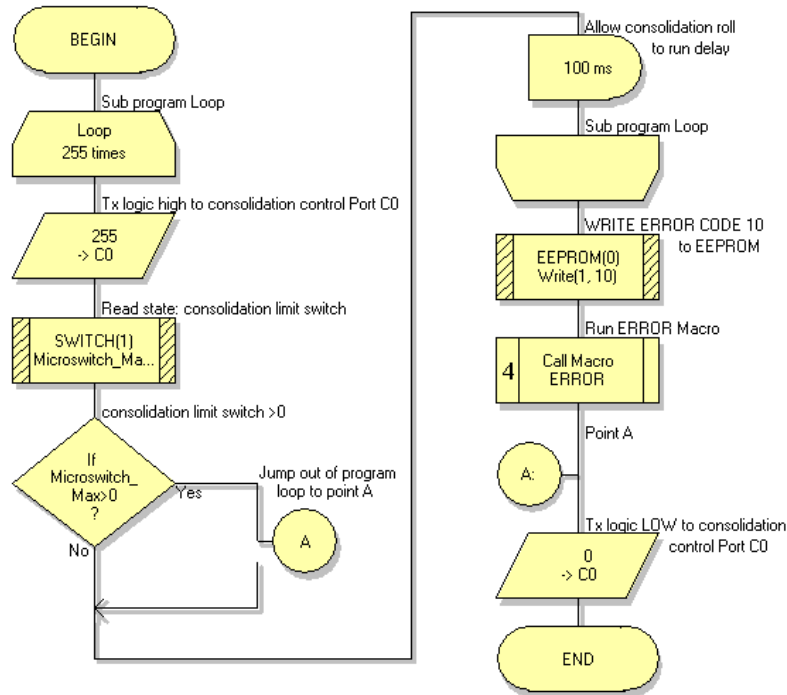


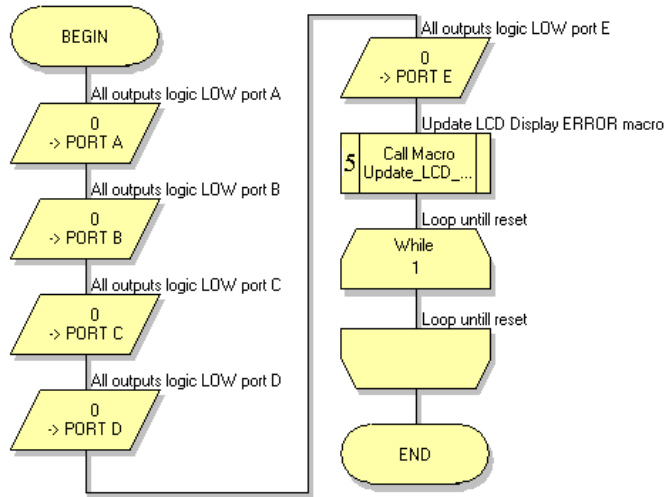
Figure C.3 A flow diagram describing the programming behind the master controller program: Program macro 3 – Move consolidation roller across layer.

This macros primary function included;

- Transmit activate signal to consolidation roller carriage, consisting of a logic high on PORT C0 which when received by the carriage motor controller, commanded it to run its motor cycle program.
- Read the state of the linear limit switch, in order to determine when the consolidation carriage had reached the end of its travel and therefore to establish when to issue a stop command (Logic 0 on PORT C0) to the carriage motor controller.
- Monitoring the carriage cycle time, producing an error return if the carriage took longer than it should to reach its maximum travel.
- Writing a user interpretable error code to EEPROM, allowing user diagnosis if an error occurred due to the consolidation carriage.

**Program macro 4: Error macro**

The error macro was a generic macro which disabled all outputs and called an LCD update to display the error code. Irrelevant of the nature of the error the error macro, if called, would perform the same way and leave the program in an infinite loop containing no executable code, until the user reset the system. Figure C.4 is a flow diagram illustrating the process steps to issue a system error state.



**Figure C.4 A flow diagram describing the programming behind the master controller program: Program macro 4 – Error**

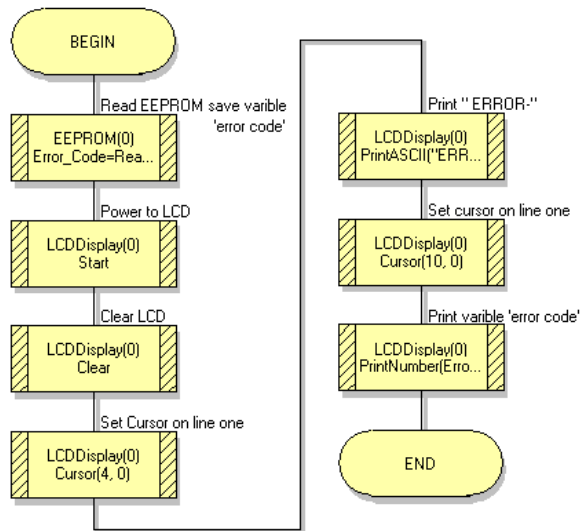
This macros primary function included;

- Sequential shut down of all outputs, a precautionary step to stop damage / further damage occurring to peripheral hardware.
- Call of LCD update, allowing the user to visually interpret the error.
- Execute an infinite loop containing no executable code, allowing the system to stay powered up but without the risk of further errors until the user has acknowledged the primary error.

**Program macro 5: Update LCD – Display ERROR macro**

Following the execution of the error script, an LCD update macro is called to print the error code to the LCD display so that the system user can rapidly diagnose the nature of the error. Figure C.5 illustrates the steps taken by the LCD update macro.





**Figure C.5 A flow diagram describing the programming behind the master controller program: Program macro 5 – Update LCD – display ‘ERROR’**

This macros primary function included;

- Enabling the LCD, a key process as all the ports including the LCD port are disabled in the event of an error occurring.
- Fetching the error code from EEPROM, ready for writing to the LCD.
- Writing the error code to LCD, enabling user error diagnosis

**Program macro 6: Move consolidation roller home macro**

As with the ‘Move consolidation roll across layer’ macro the ‘Move consolidation roller home’ macro interpreted the linear home sensor indicating when the roller carriage was home. Again this macro is a general macro which was used through the master controllers program to actuate the consolidation carriage. Figure C.6 shows the flow diagram describing the activation and termination of the consolidation rollers movement as it returned home.

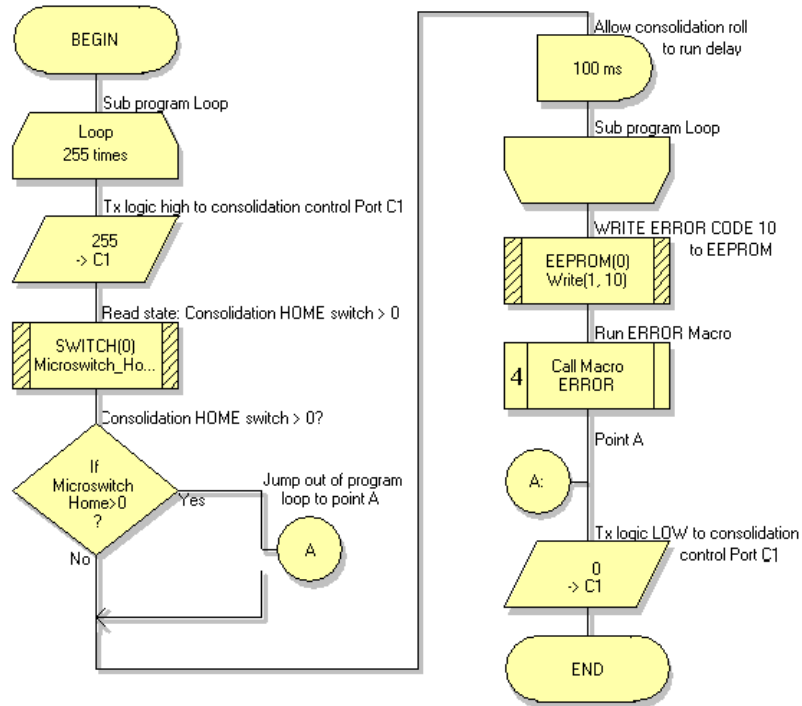


Figure C.6 A flow diagram describing the programming behind the master controller program: Program macro 6 – Move consolidation roller home.

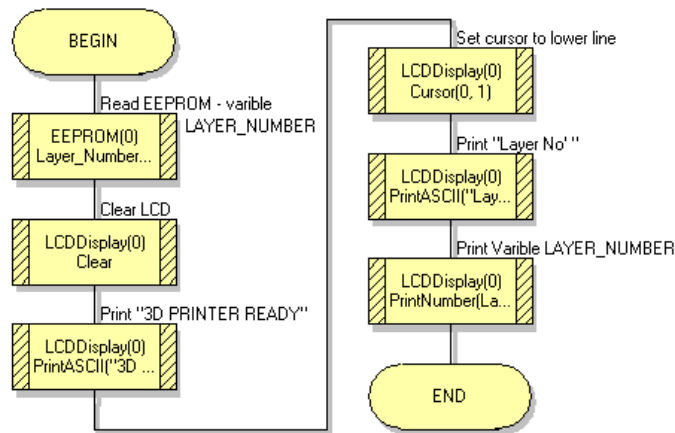
This macros primary function included;

- Transmit activate signal to consolidation roller controller, consisting of a logic high on PORT C1 which when received by the carriage motor controller, commanded it to run its motor cycle return program.
- Read the state of the linear home switch, in order to determine when the consolidation carriage had reached home and therefore to establish when to issue a stop command (Logic 0 on PORT C1) to the carriage motor controller.
- Monitoring the carriage cycle time, producing an error return if the carriage took longer than it should to reach its home position.
- Writing a user interpretable error code to EEPROM, allowing user diagnosis if an error occurred due to the consolidation carriage.

### Program macro 7: Update LDC – System status macro

The system status macro is the seventh program macro to be executed but is the second high level program macro represented by the top level program flow diagram. This program macro is the first in the main program loop and is executed once for every build layer deposited. The macro generates a user interpretable LCD output

from EEPROM saved data indicating the current layer number. Figure C.7 shows the representative flow diagram for the system status macro.



**Figure C.7 A flow diagram describing the programming behind the master controller program: Program macro 7 – Update LCD**

This macros primary function included;

- Access the EEPROM retrieving layer number data, an operation necessary to write the layer information to the LCD
- Write current layer information and system status to LCD, enabling the system user to determine system status.

### **Program macro 8: Wait for print signal macro**

The wait for print signal program macro continuously read the state of PORT B0. In its low logic state the control program was paused, when read as logic 'high' (>0V) the program was allowed to continue to produce a part layer. When logic high was sensed, the macro removed the output on PORT A0, simulating that the printer was out of paper - this stopped the printer engine from depositing an additional layer onto the surface of the transfer belt, before consolidation of the current layer had occurred. Figure C.8 shows the representative flow diagram for the wait for print signal macro.

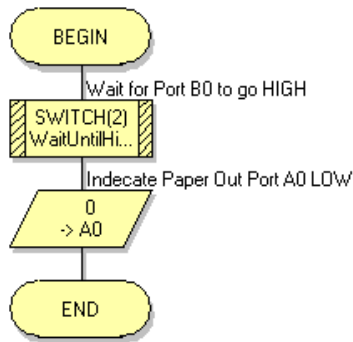


Figure C.8 A flow diagram describing the programming behind the master controller program: Program macro 8 – wait for print signal.

This macros primary function included;

- Pausing of program loop, executed until triggered to stop by an input on PORT A0
- Indicated paper out on PORT A0 upon re-execution of the program loop, thus indicating that the laser printing engine should pause until PORT A0 returned to logic 1.

#### Program macro 9: Update EEPROM

Figure C.9 describes the Update EEPROM macro. Following the input indicating the initiation of a new layer deposition cycle, the new layer number is calculated; new layer number = layer number +1, which was then saved to the EEPROM address 0.

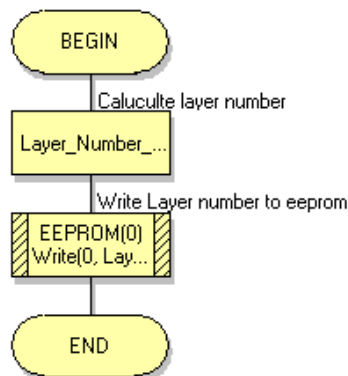


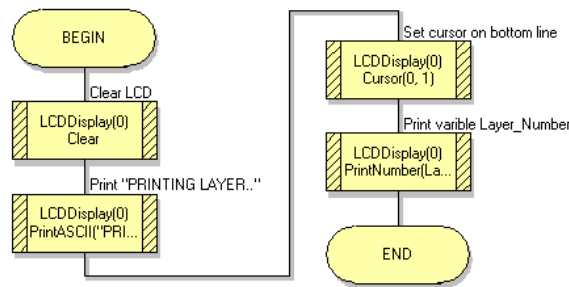
Figure C.9 A flow diagram describing the programming behind the master controller program: Program macro 9 – Update EEPROM.

This macros primary function included;

- Calculating the current layer number and issuing it to EEPROM memory for future reference.

**Program macro 10: Update LCD “PRINTING” macro**

Throughout the layer printing process the LCD was updated so that the system status could be monitored. Figure C.10 describes the update LCD “PRINTING” macro program flow.



**Figure C.10 A flow diagram describing the programming behind the master controller program: Program macro 10 – update LCD ‘Printing’**

This macros primary function included;

- Update LCD to display “Printing LAYER (Variable - Layer\_number)”

**Program macro 11: Run Belt macro**

Macro eleven controlled the cycling of the belt, moving deposited powder layers to the build surface for consolidation. The macro controlled both the manipulation of the printer engine and the run signal to the belt stepper motor controller. The sequential sensor manipulation mimicked the paper passing through the printer developer and fuser units. The flow diagram in Figure C.11 describes the sequence by which these actions were performed.

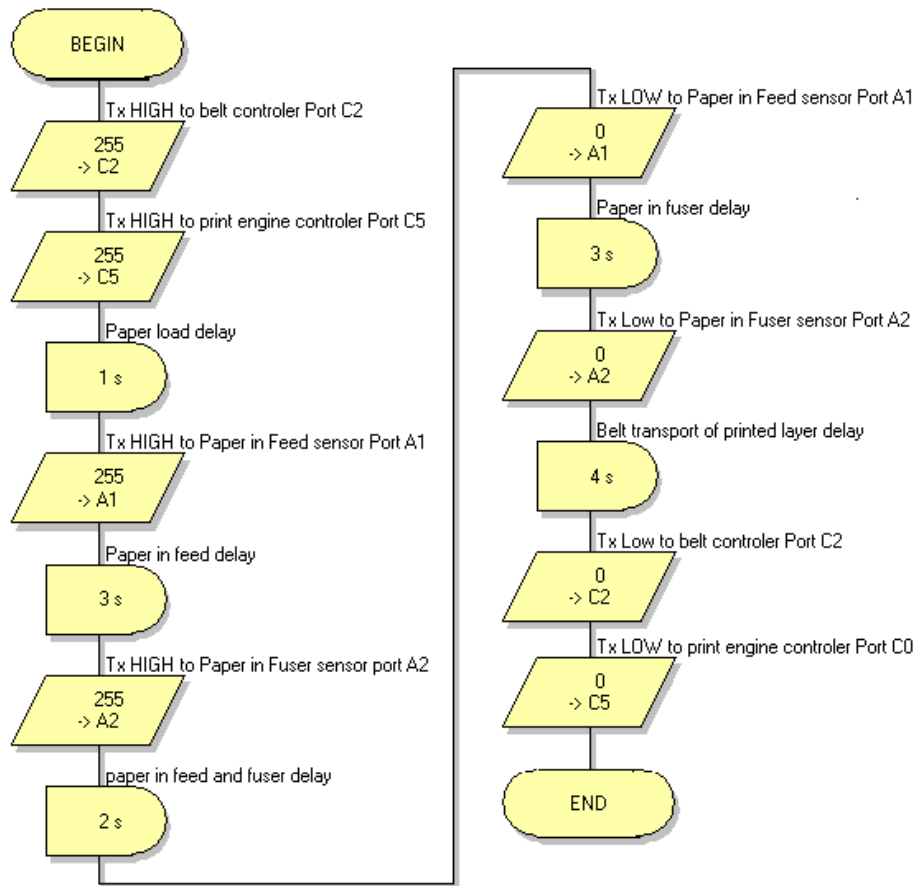


Figure C.11 A flow diagram describing the programming behind the master controller program: Program macro 11 – Run belt.

This macros primary function included;

- Sending logic high/low on PORT C2 to activate and deactivate the belt stepper motor respectively.
- Sending logic high/low on PORT C5 to activate and deactivate the print engine motor respectively.
- Manipulate the sensors on PORTs A1 and A2 simulating the passing of paper media through the print engine and fuser unit.

**Program macro 12: Update LCD “ Consolidating”**

Macro twelve updated the LCD with “consolidating” to confirm consolidation was being performed by the system. Figure C.12 is a flow diagram that describes this sub-routine.

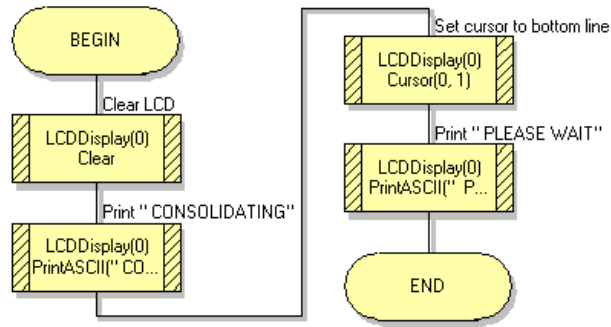


Figure C.12 A flow diagram describing the programming behind the master controller program: Program macro 3 – update LCD ‘Consolidating’.

This macros primary function included;

- Update of the LCD to show consolidation was taking place.

**Program macro 13: Consolidate Layer**

Layer consolidation was executed using two of the existing program macros; macro 3 (move consolidation roller over layer) and macro 4 (move consolidation roller home). The two macros were executed in ascending order with a 100ms pause to allow the mass of the consolidation carriage to come to rest before it was returned to its home position. Figure C.13 is a flow diagram that describes this sub-routine.

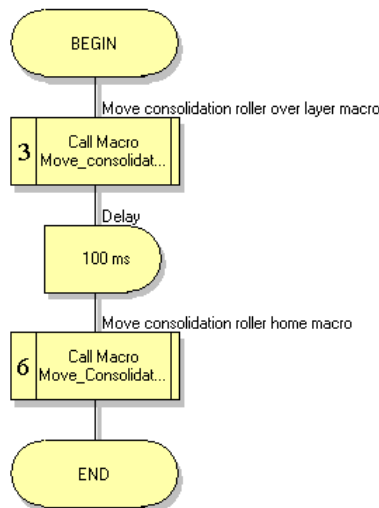


Figure C.13 A flow diagram describing the programming behind the master controller program: Program macro 13 – Consolidate layer.

This macros primary function included;

- Running program macro 3 (move consolidation roller over layer) to consolidate a layer.
- Executing program macro 4 (move consolidation roller home) to return consolidation roll to its home position.

### ***C.1 Bipolar Consolidation Roller and Print Engine Motor Controller Program***

There are two ancillary bipolar stepper motor drivers, one was employed to revolve the print engine in a single direction (unidirectional) where as the other was expected to move the consolidation carriage in two directions (bidirectional). The flow diagrams in Figure C.14 describe the programming of the bidirectional controller showing the three program macros which formed the bipolar controller firmware. The unidirectional controller had the same coding as the bidirectional controller, but was commanded to rotate in a single direction by the master controller.



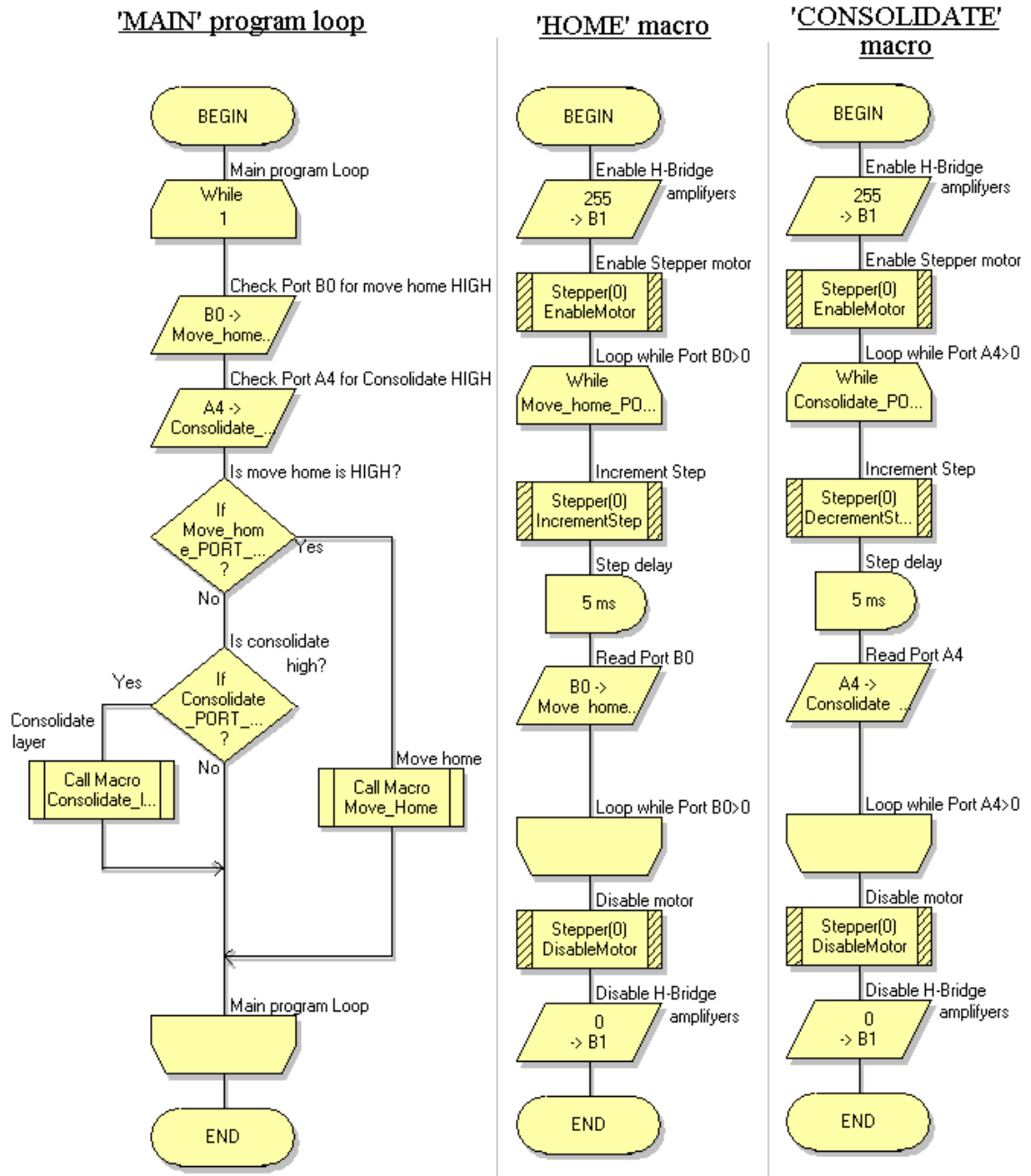


Figure C.14 Three flow diagrams illustrating the program flow of firmware controlling the stepper motor movements of the consolidation roller/carriage. Left: the main program loop dictating the direction of motor rotation, Middle: Clockwise rotation program macro Right: Counter clockwise rotation program macro.

These macros primary functions included;

- The reception of an input from the master controller, sent to start the program.
- Decision to the direction of motor rotation, based on information provided by the master controller.

- Monitor the communications pin, to watch for a stop command from the master controller.
- Enable stepper motor.
- Increment stepper motor.
- Disable stepper motor when not in use.

### C.2 Unipolar Controller Program

The ancillary unipolar controller was programmed to revolve the transfer belt in a single direction. Its function was similar to that of the unidirectional stepper motor as controlled by the ancillary bipolar controller. However the underlying C code describing the sequence of outputs sent to the stepper to increment a step was entirely different. Figure C.15 is a flow diagram illustration of the two program macros used to execute the desired transfer belt motion.

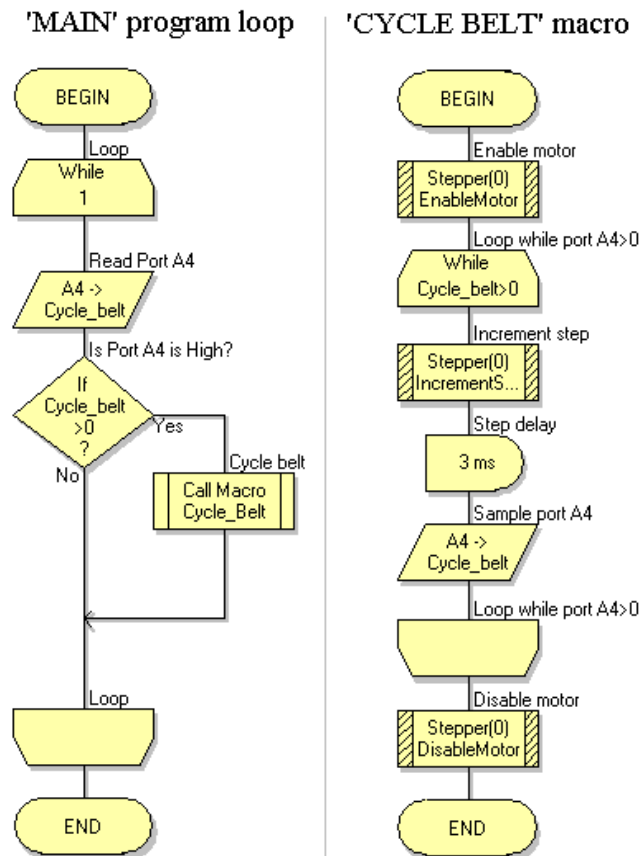


Figure C.15 Two flow diagrams illustrating the program flow of firmware controlling the stepper motor movements of the transfer belt. Left: The main program loop continually reading port A4 for the start command Right: the program macro used to cycle the transfer belt when instructed to do so by the master controller.

These macros primary functions included;

- The reception of an input from the master controller, sent to start the program.
- Monitor the communications pin, to watch for a stop command from the master controller.
- Enable stepper motor.
- Increment stepper motor.
- Disable stepper motor when not in use.

**Appendix D: List of Abbreviations**

3DP	–	Three Dimensional Printing
ABS	–	Acrylonitrile Butadiene Styrene
AC	–	Alternating Current
AFP	–	Advanced Function Printing
ALM	–	Additive Layer Manufacturing
AMF	–	Additive Manufacturing Format
ARM	–	Advanced RISC Machines
C	–	C Programming Language
CAD	–	Computer Aided Design
CAD	–	Charged Area Development
CCA	–	Charge Control Agent
CERP	–	Continuous Electrophotographic Rapid Manufacturing
CGL	–	Charge Generation Layer
CJP	–	Continuous Jet Printing
CMB	–	Conductive Magnetic Brush
CNC	–	Computer Numerically Controlled
CTL	–	Charge Transport Layer
DAD	–	Discharged Area Development
DC	–	Direct Current
DCU	–	Diagnostic Control Unit

DFE	–	Design for Experiments
DLP	–	Digital Light Processor
DMD	–	Digital Micro Mirror
DOD	–	Drop On Demand
DPI	–	Dots Per Inch
DTF	–	Electronic Alto Research Character Generator Scanned Laser Output Terminal
EBM	–	Electron Beam Melting
EEPROM	–	Electrically Erasable Programmable Read-Only Memory
EFAB	–	Electrochemical Fabrication
FCA	–	Flow Control Agents
FDM	–	Fused Deposition Modelling
FEA	–	Finite Element Analysis
FET	–	Field Effect Transistor
HV	–	High Voltage
IC	–	Integrated Circuit
IMB	–	Insulative Magnetic Brush
IR	–	Infrared
KPI	–	Key Performance Indicator
LDPE	–	Low Density Polyethylene
LOM	–	Laminated Object Manufacturing

LSU	–	Laser Scanning Unit
MIT	–	Massachusetts Institute of Technology
OPC	–	Organic Photoconductor
PBT	–	Polybutylene Terephthalate
PCL	–	Printer Command Language
PID	–	Proportional Integral Derivative
PLT	–	Paper Lamination Technology
PMMA	–	Polymethyl methacrylate
POC	–	Proof of Concept
PP	–	Polypropylene
PPM	–	Pages per Minute
PPP	–	Plastic Powder Printing
PS	–	Adobe Postscript
PTFE	–	Polytetrafluoroethylene
PVA	–	Polyvinyl Acetate
PVOH	–	Polyvinyl-Alcohol
PWM	–	Pulse Width Modulation
RIP	–	Raster Image Processor
RISC	–	Reduced Instruction Set Computer
RFP	–	Rapid Freeze Prototyping
RM	–	Rapid Manufacturing

RP	–	Rapid Prototyping
RT	–	Rapid Tooling
RTD	–	Resistive Temperature Device
SEM	–	Scanning Electron Microscope
SGC	–	Solid Ground Curing
SL	–	Stereolithography
SLP	–	Selective Laser Printing
SLA	–	Stereolithographic Apparatus
SLS	–	Selective Laser Sintering
SMD	–	Surface Mounted
SMS	–	Selective Mask Sintering
STL	–	Stereolithographic
UCL	–	Undercoat Layer
UI	–	User Interface
USB	–	Universal Serial Bus
USP	–	Unique Selling Point
UTS	–	Ultimate Tensile Stress
UV	–	Ultraviolet
XPS	–	Microsoft XML Page Specification